

**THEORY AND APPLICATIONS OF  
TRANSPORT IN POROUS MEDIA**

**Percolation Models  
for Transport in  
Porous Media**

With Applications to  
Reservoir Engineering

**V. I. Selyakov  
V. V. Kadet**

## Theory and Applications of Transport in Porous Media

---

*Series Editor:*

Jacob Bear, *Technion – Israel Institute of Technology, Haifa, Israel*

---

Volume 9

*The titles published in this series are listed at the end of this volume.*

# Percolation Models for Transport in Porous Media

With Applications to Reservoir Engineering

by

V. I. Selyakov

*Laboratory of Heterogeneous Media,  
Department of Theoretical Problems,  
Russian Academy of Science,  
Moscow, Russia*

and

V. V. Kadet

*Department of Oil & Gas Hydromechanics,  
State Gubkin Oil & Gas Academy,  
Moscow, Russia*



SPRINGER-SCIENCE+BUSINESS MEDIA, B.V.

A C.I.P. Catalogue record for this book is available from the Library of Congress.

ISBN 978-90-481-4771-7      ISBN 978-94-015-8626-9 (eBook)  
DOI 10.1007/978-94-015-8626-9

ISBN 978-90-481-4771-7      ISBN 978-94-015-8626-9 (eBook)  
DOI 10.1007/978-94-015-8626-9

---

*Printed on acid-free paper*

**All Rights Reserved**

© 1996 Springer Science+Business Media Dordrecht

Originally published by Kluwer Academic Publishers in 1996

Softcover reprint of the hardcover 1st edition 1996

No part of the material protected by this copyright notice may be reproduced or utilized in any form or by any means, electronic or mechanical, including photocopying, recording or by any information storage and retrieval system, without written permission from the copyright owner.

# Contents

<b>Foreword</b>	<b>ix</b>
<b>Abstract</b>	<b>xi</b>
<b>Introduction</b>	<b>1</b>
<b>I Fluid- and Electric Conductivity in Porous Media. Theoretical Analysis</b>	<b>5</b>
<b>1 Percolation Model of Micro Heterogeneous Media</b>	<b>7</b>
1.1 Percolation Theory. Basic Concepts . . . . .	7
1.2 Conductivity of a Network with the Random Distribution of Elements	12
1.3 Effect of Electric Current on Conductivity of Heterogeneous Media	18
<b>2 Percolation Models of One-Phase Flow in Rocks of Different Types</b>	<b>23</b>
2.1 Conductivity of Grained Media . . . . .	23
2.2 "Permeability - Porosity" Correlation . . . . .	26
2.3 Conductivity of Cavernous Media . . . . .	28
2.4 Conductivity of Fractured Media . . . . .	30
2.5 Conductivity As a Function of the Strained State . . . . .	34
<b>3 Percolation Model of Fluid Flow in Heterogeneous Media</b>	<b>41</b>
3.1 Flow at the Micro Level . . . . .	41
3.2 Effect of Pore Space Structure on Laws for Macroscopic Flow . . .	47
3.3 Results of Numerical Calculations and Comparison with Experiment	53
<b>4 Percolation Model of Steady State Multiphase Flow in Porous Media</b>	<b>57</b>
4.1 Steady State Flow of Immiscible Newtonian Fluids . . . . .	57
4.2 Effect of Plastic Properties of Fluids on Phase Permeabilities . . .	64

4.3	Phase Permeabilities of a Medium with Mixed Wettability . . . . .	69
4.4	Three-Phase Steady State Flow of Immiscible Newtonian Fluids . . . . .	79
4.5	Stability of Percolation Methods for Calculation of Phase Permeabilities . . . . .	84
<b>5</b>	<b>Percolation Model of Non-Steady State Two-Phase Flow in Porous Media</b>	<b>89</b>
5.1	Immiscible Displacement of a Viscous Fluid by a Non-Viscous One . . . . .	89
5.2	Effects of Viscosities and Interfacial Tension . . . . .	98
<b>6</b>	<b>Determination of Pore Size Distribution in Grained and Cavernous Rocks</b>	<b>105</b>
6.1	Percolation Model for the Mercury Injection Test . . . . .	106
6.2	Percolation Model for the Electric Porometry Method . . . . .	112
6.3	Percolation Model for the Combined Mercury and Electric Porometry Method . . . . .	119
6.4	Numerical Calculations and Core Data Processing with the Electric Porometry Method . . . . .	122
<b>7</b>	<b>Methods for Determining Parameters of Fractured Rocks</b>	<b>129</b>
7.1	Concentration and Average Length of Fractures Determined from the Core . . . . .	130
7.2	Determination of Fracture Length Distribution from Fracture Traces on the Core . . . . .	132
7.3	Determination of Fracture Parameters from the Core . . . . .	136
<b>II</b>	<b>Effects of Physical Fields on Recovery of Mineral Resources</b>	<b>139</b>
<b>8</b>	<b>Conductivity of a Heterogeneous Medium under Impulse and Alternating Current</b>	<b>143</b>
8.1	Threshold Values for Electric Treatment with Impulse Current . . . . .	143
8.2	Permeability and Electric Conductivity under Impulse Current . . . . .	147
8.3	Determination of Threshold Values for Electric Treatment . . . . .	151
8.4	Permeability and Electric Conductivity after Electric Treatment . . . . .	152
<b>9</b>	<b>Changing Conductivity and Pore Space Structure with Electric Current. Experiments</b>	<b>157</b>
9.1	Conductivity of Sandy-Argillaceous Medium . . . . .	157
9.2	Pore Space Structure of a Sandy-Argillaceous Medium after Electric Treatment . . . . .	160

9.3	Research on Irreversible Change of Conductivities for Sandy-Argillaceous Media after Electric Treatment . . . . .	164
<b>10</b>	<b>Changing Well Production with Electric Treatment</b>	<b>167</b>
10.1	Calculation of Change in Well Production after Electric Treatment	167
10.2	Reversible Change of Permeability. Determination of Optimal Regime for Electric Treatment . . . . .	171
10.3	Results of Field Studies . . . . .	176
<b>11</b>	<b>Gas Colmatation Effect during Electric Action on Saturated Porous Media</b>	<b>181</b>
11.1	Temperature Effects in Capillaries Caused by Electric Current . .	182
11.2	Movement and Growth of Bubbles in Capillaries . . . . .	184
11.3	Permeability Change under Electric Field . . . . .	192
<b>12</b>	<b>Effects of Acoustic Waves on Irreversible Change of Permeability of a Saturated Porous Medium</b>	<b>199</b>
12.1	Dissipation of Energy in Viscous Poiseuille Flow . . . . .	200
12.2	Destruction of Surface Layer in Pore Channels under Tangential Stress . . . . .	202
12.3	Cavitation in Pore Channels under Acoustic Action . . . . .	203
12.4	Dissipation of Acoustic Energy Due to Thermal Slide . . . . .	208
12.5	Gas Colmatation During Acoustic Action on Porous Media . . . .	210
<b>13</b>	<b>Effect of Acoustic Action on Well Production</b>	<b>215</b>
13.1	Laboratory Research on Permeability of Media after Acoustic Treatment . . . . .	216
13.2	Determination of Size for the Acoustic Action Zone . . . . .	220
13.3	Calculation of Well Rate after Acoustic Action and Results of Field Experiments . . . . .	223
13.4	Optimization of Acoustic Treatment of Porous Media . . . . .	225
	<b>Bibliography</b>	<b>229</b>
	<b>Index</b>	<b>239</b>

# Foreword

It is an honour and pleasure to write a foreword to this useful and interesting book. Authors are very well known researchers who pioneered percolation modelling of transport in porous media in Russia from the early 80-th till nowadays.

The main scope of the work presented in the book was developed when bright papers by A. Aharony, H.T. Davis, F.A.L. Dullien, A.A. Heiba, R.G. Larson, R. Lenormand, M.Sahimi, L.E. Scriven, D. Stauffer, M. Yanuka, Y.C.Yortsos were not available at the "other" side of the Iron Curtain.

Nowadays hundreds of works and papers with the "percolation" keywords appear in petroleum and related applied research areas. The book will take a remarkable place in the "petroleum percolation" bibliography.

There are two important features of novelty in the monograph presented.

First of all the authors developed a generalization of percolation clusters theory for grids with varying conductivity. Technique of representation of an infinite cluster as an hierarchial set of trees (so called r-chain model) allows to present conductivity of a stochastic grid in a closed form of explicit formulae.

This method differs from those known in the West, such as effective media theory, solutions for the Bethe-lattice, etc. It has his own area of successful applications.

This technique was applied for modelling of transport of multiphase systems in complex porous media. The majority of cases discussed have been investigated by other authors in the West in more detail using other methods for conductivity calculation (two- and three-phase flows, fractured media); some effects are pretty new (flow of non-Newtonian fluids, deformable porous media).

Quasi static percolation models have been further developed into dynamic ones (so-called model of the forest growth). Theory of non-equilibrium displacement on the pore level in micro heterogeneous media is developed (Chapter 5). This approach could give a hint for solution of a very desirable problem of dynamic transport in fractals.

The second important novelty of the book is percolation modelling of electric current in porous media. The theory provides basics for fast-developing methods



of well stimulation and improved oil recovery by application of different electromagnetic fields to the well drainage areas.

I hope the technique of r-chains and dynamical "forest growth" will be successfully applied and further developed in the area of upscaling of multiphase multicomponent flows in reservoirs with complex heterogeneity.

The book is strong both in theoretical fundamentals and engineering. Wide audience of petroleum engineers, researchers and graduate students will find it useful and informative. Wish them pleasant reading and further inspiration!

Professor Pavel Bedrikovetsky, MSc, PhD, DSc Moscow State Oil and Gas Academy, Russia Presently with PETROBRAS, CENPES CIDADE UNIVERSITARIA Q.7 ILHA DO FUNDAO 21949 - 900 - RIO DE JANEIRO - RJ - BRAZIL  
30th October 1994

# Abstract

Results of theoretical analysis and experimental investigations for transport in porous media are presented. A new approach to modelling of transport in porous media is developed and a number of new percolation models is considered. The models allow to obtain analytical correlations for relative phase permeabilities for different porous media. Different methods of intensification of economic minerals based on new physical effects of reconstruction of the rock's pore space structure, are analysed.

The monograph is of interest for reservoir and chemical engineers, for specialists in reservoir characterization and simulation, for core analysts and researchers, and for post-graduate students in the above-mentioned areas.

# Introduction

Creation of essentially new technologies in the recovery of mineral resources is impossible without a thorough research in fluid transfer phenomena in rocks. However it appears unreasonable to expect discovery of new physical effects in fluid flow in porous media if traditional continuous media models are applied. In these models, the huge variety of rock types is taken account of by varying the coefficients of permeability and porosity in the equations describing fluid flow. With this approach, the coefficient of phase permeability is the only parameter that bears information about pore space structure of rocks; experimental determination of this coefficient, however, is of considerable technical difficulty.

At the same time, it is obvious that the pore space structure has a great influence upon the nature of fluid flow in micro heterogeneous media. Notable pressure gradients during the fluid flow or electric field potential during the electric current flow can emerge at the micro level because of the heterogeneity of the medium; those, in their turn, can bring about more physical effects. For example, as it exceeds a certain threshold value, the high density of energy release in thin capillaries can cause destruction of the cement and result in reconstruction of the pore space structure of the medium. This effect was predicted theoretically and confirmed experimentally in the mid 70s. Based on this effect, an essentially new technology for stimulation of wells was developed, allowing for increase of well rates in recovery of mineral resources (water, oil, metals).

Obviously, to describe a transfer in micro heterogeneous media and related effects, one has to use 3D network models. Solving such problems (both static and dynamic) by means of numerical simulation requires huge amounts of computer time. In this case obtaining approximate analytical solutions using percolation models is of a great interest.

More papers on fluid flow theory, purely computative [1-9] as well as both computative and theoretical [10-16], using methods of percolation theory, began to appear quite frequently in the last years. Experimental investigations in this field come in a series of purely experimental [17-22] or experimental and computative [23, 24] studies, which combine numerical calculations with experimental

measurements of parameters for identical systems with further comparison of the results.

Detailed reports, as well as reviews of works accomplished in this field, are presented in the reviews [25-29, 115-118] and monographs [30-36] of Russian and foreign authors. However the approach used is limited by the framework of standard percolation theory where heterogeneity bears a threshold nature. In other words, within the framework of these approaches, a medium consists of only two types of elements – conducting ones with identical conductivities and non-conducting ones.

This narrows the possibilities for the percolation approach to simulation of fluid flow dramatically, since actual porous media contain a large variety of conducting pore channels. The nature of transfer processes in such media is substantially dependent on the structure of heterogeneity in them (i.e., on pore-space structure of the medium and properties of its surface) and on the way it is filled with fluids.

In the majority of actual porous media, a commensurate contribution to effective conductivity can be made by groups of conducting elements with substantially different intrinsic conductivities. Rocks, with their exclusive variety of pore space structures, represent a typical example of such media. Thus a need for more adequate percolation models arises, so that the latter be able to describe transfer in heterogeneous media when the distribution of conducting elements with respect to values of intrinsic conductivities is known.

The problem of effective conductivity for the media with the stochastic heterogeneity can be effectively solved for the case of a small variation of permeability [104]. In this case perturbation of flow caused by the heterogeneity is small, and the linearized theory is applicable. It allows not only to describe an averaged flow (effective conductivity), but also estimate the covariance. Perturbation method provides exact formulas [104, 105]. The self-consistent approach [104, 106] provides the analytical solution for the highly heterogeneous systems, but under the assumption of self-similarity with the variation of the scale.

It is worth mentioning that simple formulas for the arithmetic average and the geometric average often give reasonable results (for the layer cake reservoir, horizontal and vertical permeabilities, respectively, see [107, 108]). The combined arithmetic/harmonic and harmonic/arithmetic averages give even better estimates [108, 109]. Renormalization method provides further improvement to the accuracy of the estimate of the effective permeability for the media with stochastic heterogeneity [1-4].

Nevertheless analytical models do not give sufficient results in the number of important practical cases, and so numerical models are applied [108, 110].

Calculation of the effective permeability for the two-phase flow in the media with stochastic heterogeneity is more complex and in the general case can be done only numerically [111, 112].

Nevertheless some important cases can be handled analytically. The capillary dominant case of the oil-water flow in porous media with stochastic heterogeneity has been solved analytically using the traditional percolation theory and effective media model [14]. Viscous dominant case of the waterflood in stochastic porous media was solved in [113] using the percolation model proposed in Chapters 1 and 2 of this book. In this study, a new approach to description of transfer processes in stochastically heterogeneous media is presented. The origin of this approach can be found in the series of studies [37-42]. A percolation model of a micro heterogeneous medium is proposed, allowing for obtaining analytical formulas and solutions for problems of the mentioned type. Methods for investigation of pore space structure of different types of rocks are described, allowing for determination of the effective radius probability density function for capillaries. Using this approach, effects of pore space structure of a micro heterogeneous medium upon one- and multi-phase flow are studied. A percolation theory for the two-phase flow developed in Chapter 4 can be used for the generalization of the relative permeabilities model for cases of precipitation of paraffins and for chemical reactions in porous media [114]. Effects of rearrangement of pore space structure resulting from different types of treatment (acoustic, electric) are investigated. Methods for calculating phase permeabilities are proposed, new physical effects due to certain properties of transfer processes in micro heterogeneous media are described. In Part II, some of the technologies based on such effects, are presented.

The examples shown demonstrate that use of percolation models are very promising in investigation of the influence of pore space structure upon transfer phenomena in micro heterogeneous media.

The authors wish to thank their colleagues and students, S.P. Glushko, N.S. Rostovsky, and R.M. Musin, who took part in solving some of the problems reflected in the book. Special thanks are owed to A.J. Greenberg for his great help in preparing the manuscript.

**Part I**

**Fluid- and Electric  
Conductivity in Porous  
Media. Theoretical Analysis**

# Chapter 1

## Percolation Model of Micro Heterogeneous Media

Conductivity of a medium (coefficients of permeability and electric conductivity) depends significantly on the pore space structure. In the case of stochastic distribution of conducting channels in the medium, it is possible to describe the topology of the pore space in terms of the percolation theory [25-27, 29, 30]. However the existing percolation models can be applied only if the conducting structural bonds in the medium are sufficiently homogeneous. This is due to the fact that all the theoretical relationships in percolation theory were obtained under the assumption that there are only two types of structural bonds in the medium, namely the conducting and the non-conducting ones. It is also assumed that the intrinsic conductivities of all conducting bonds are equal. At the same time, in the majority of actual media, a commensurate contribution to effective conductivity can be made by groups of conducting bonds whose intrinsic conductivities are notably different. Rocks, which may have many different types of pore space structure, represent an example of such media.

### 1.1 Percolation Theory. Basic Concepts

Percolation theory and a number of its applications to various problems of mathematical physics are presented in enough detail in the reviews [31-36]. We shall now mention only the basic ideas of percolation theory, those which we will need in the future, as we build models to describe conductivities of media with different types of pore space structure.

Consider specifically the problem of flow through a periodic network (we can consider solid and intersecting spheres, ellipses, covering graphs, or continual flow).

The network consists of sites and conducting bonds between them. Obviously, if all bonds in the network are broken (i.e., do not conduct), then its conductivity vanishes. As the concentration of conducting bonds goes up, the latter begin to merge and form clusters, i.e., conducting unions of bonds. Starting from a certain threshold value of conducting bond concentration, the bonds begin to form an infinite conducting cluster (IC), and the conductivity of the network becomes non-zero. The density of the IC and correspondingly, its conductivity goes up with the further increase of conducting bond concentration. Quantitative description of the threshold value for concentration of bonds for different types of networks, as well as the correlation between the conductivity of a network and the concentration of bonds, is given by percolation theory.

Thus percolation theory studies formation of connected domains (clusters) from elements with certain properties, provided that every bond of each element with another one is arbitrary (though established in a strictly defined way). It is clear that the phenomena described by percolation theory belong to the so-called critical processes which are characterized by a particular critical point each. When this critical point is reached, the principal property of the system, as far as the process in question is concerned, changes fundamentally. Formation of an IC is in essence a phase transition of the second kind, which is quantitatively characterized by a set of universal critical parameters. The universality of these parameters means that they do not depend on the specific model, i.e., on network type, but are determined only by the dimension of the space. This fundamental postulate of percolation theory is based on analysis of results given by numerical modeling of the IC formation in networks of different types. However in the simplest cases, such as that of a two-dimensional square network, analytical solutions can be obtained as well [30]. Percolation theory shows also that although distribution of conducting bonds (sites) in the network is random, there still exists a well-determined threshold conductivity probability for a bond, when the network as a whole acquires conductivity. This threshold value depends only on the network type and the dimension of the problem and does not depend on the specific realization of conducting bonds in the network. In a finite system, however, the percolation threshold does depend on the specific realization of the conducting bond distribution, i.e. is a random variable. As the size of the network increases, the fluctuation of the percolation threshold becomes less, and the value of the percolation threshold approaches the one predicted by percolation theory. In this case,  $\delta$ , the width of the critical region which is most likely (i.e., has overwhelming probability) to contain the value of the percolation threshold for a network of finite size, decreases as  $\delta \cong C/N^{-\nu D}$ . Here  $N$  is the number of sites in the network;  $D$  is the dimension of the problem;  $C$  is a coefficient ( $\approx 1/2$ );  $\nu$  is the critical parameter (the correlation radius) which depends on the dimension of the problem and will be defined later. Since numerical modeling is carried out for net-



Table 1.1:

Network Type	$z$	$P_c^b$	$P_c^b z$
<i>Plane</i>			
Square	4	0.5	2.0
Triangular	6	0.35	2.1
Hexagonal	3	0.75	2.0
<i>Solid</i>			
Simple Cubic	6	0.25	1.5
Body Centered Cubic	8	0.18	1.4
Face-Centered Cubic	12	0.12	1.4
Diamond Type	4	0.39	1.6

works of finite dimensions, the results given by percolation theory are valid only for networks with sufficiently large numbers of sites ( $N \geq 10^4$ ). In this case the size of the network can be considered macroscopic with respect to the size of an elementary cell, and the percolation threshold is defined as the limit of the mean value of the percolation threshold, as the number of sites in the network goes up. We shall now briefly present the major results of percolation theory.

**Percolation threshold.** Let  $P^b$  characterize the probability of conductivity in a bond between any two sites, and  $P^s$ , the probability of conductivity in the sites. Then if  $P^b \geq P_c^b$ , where  $P_c^b$  is the threshold value of the conductivity probability, then an IC is formed in the network. If  $P^b < P_c^b$ , then there is no IC and the conductivity vanishes. The quantity  $P_c^b$  depends on  $z$ , the number of closest neighbors of a site in the network, and on the dimension  $D$  of the network, i.e., it depends on the network type. With good precision, the following invariant can be indicated,

$$P_c^b z = D/(D - 1). \quad (1.1)$$

The values of  $P_c^b z$  for different network types are given in table 1.1.

A similar result is obtained when the conductivity of the network is considered in terms of site percolation. If the probability  $P^s$  of the site conductivity satisfies the condition  $P^s \geq P_c^s$ , where  $P_c^s$  is the threshold conductivity probability of a site, then an IC is formed in the network.

The quantity  $P_c^s$  depends on  $f$ , the charge coefficient, i.e., on the network type. The charge coefficient equals the fraction of the volume covered by a set of balls constructed around each site of the network with radius equal to half the distance

to the closest neighbor. The following invariant holds to within 10 to 15%,

$$P_c^s f = \begin{cases} 0.16 & \text{in the three-dimensional case,} \\ 0.5 & \text{in the two-dimensional case.} \end{cases} \quad (1.2)$$

The values of  $P_c^s f$  for different network types are given in table 1.2.

**Structure of the infinite cluster. Shklovsky - de Gennes model.** The conductivity of the network strongly depends on the IC structure. The regions of an IC consist of the "skeleton" and the "dead ends." A point is said to belong to the "skeleton" of the IC if at least two paths originating from it can be followed to infinity. If there is only one such path, then the point belongs to the "dead end." A model of the IC structure was proposed independently by B. I. Shklovsky and P. de Gennes. According to this model, it is possible to represent the structure of the "skeleton" of an IC as an irregular network with the characteristic period equal to  $R$ , the correlation radius of the IC as determined from the expression

$$R \sim [P^b - P_c^b]^{-\nu}, \quad (1.3)$$

where the correlation radius index

$$\nu = \begin{cases} 0.9 & \text{in the three-dimensional problem,} \\ 1.33 & \text{in the two-dimensional problem.} \end{cases}$$

Numerical experiments show that the relation (1.3) holds for the site percolation as well. In this case, the parameter  $\nu$  is the same as for the bond percolation.

**Electric conductivity near the percolation threshold.** It was shown that within the framework of percolation theory, the electro- or hydroconductivity of the IC increases near the percolation threshold with the increase of either of the probabilities,  $P^b$  or  $P^s$ , as follows

$$\Sigma \sim K \sim [P^b - P_c^b]^d, \quad (1.4)$$

where the quantity  $d$  is determined from the dimension of the problem only:

$$d = \begin{cases} 1.7 \pm 0.02, D = 3, \\ 1.3 \pm 0.02, D = 2. \end{cases}$$

The numerical experiment shows that the relationship (1.4) holds within the interval  $P_c^b \leq P^b \leq P_c^b + \Delta P^b$ , where  $\Delta P^b \leq 0.1$ . In the interval  $P_c^b + \Delta P^b \leq P^b < 1$ , the conductivity of the network can be adequately described by the formula obtained for the model of "effective medium" [29]:

$$K = K_0[1 - (1 - P^b)/(1 - 2/z)],$$

where  $K_0$  is the greatest possible conductivity of a network when there are no broken bonds in it ( $P^b = 1$ ). The same relationship holds for the quantity  $P^s$  in the "site problem."

Table 1.2:

Network Type	$z$	$P_c^s$	$P_s^b f$
<i>Plane</i>			
Square	0.79	0.59	0.47
Triangular	0.91	0.50	0.46
Hexagonal	0.61	0.70	0.43
<i>Solid</i>			
Simple Cubic	0.52	0.31	0.16
Body Centered Cubic	0.68	0.25	0.17
Face-Centered Cubic	0.74	0.20	0.15
Diamond Type	0.34	0.43	0.15

The Shklovsky - de Gennes model allows to relate the quantity  $d$  to the correlation radius index. Since, for instance, the electric current flows only through the "skeleton" of the IC, the electric conductivity of the network is determined only from the conductivities of the parallel capillary chains within the "skeleton" of the IC. The number  $n$  of the capillary chains reaching a unit surface of the cross-section perpendicular to the chosen direction equals  $R^{-(D-1)}$ . The conductivity of the network  $\Sigma \sim n\sigma_1$ , where  $\sigma_1$  is the specific conductivity of a chain. Using the relationship (1.3), we obtain a formula for the specific electric conductivity of the network

$$\Sigma \sim \sigma_0(P^b - P_c^b)^{(D-1)\nu}. \quad (1.5)$$

Here,  $\sigma_0$  is the specific electric conductivity of the network when  $P^b = 1$ . After comparing the relationships (1.4) and (1.5), we find that  $d = \nu$  in the two-dimensional case and  $d = 2\nu$  in the three-dimensional case. This fact supports the validity of the Shklovsky - de Gennes model. In the three-dimensional case, capillary chains can be tortuous. However this feature changes only the formula  $d = 2\nu$  to  $d = \nu + \zeta$ , where  $\zeta = 1$  [26]. In the two-dimensional case this effect does not appear.

Note that the formula (1.5), as well as other percolational relations, was obtained up to a numerical factor of the order of unity.

**Density of an IC.** Research has showed that the value of  $W$ , the number of sites (bonds) which belong to the IC, obeys the exponential law

$$W \sim [P^{s(b)} - P_c^{s(b)}]^\beta. \quad (1.6)$$

The critical parameter found from numerous computational analyses is

$$\beta = \begin{cases} 0.4 & \text{in the three-dimensional case,} \\ 0.14 & \text{in the two-dimensional case.} \end{cases}$$

The contribution to the function  $W$  is made by all the sites which belong to the "skeleton" and the "dead ends" of the IC. Relationships (1.3) and (1.6) imply that near the percolation threshold, the number of sites and bonds of the "skeleton" of the IC are negligible compared to the total number of sites and bonds inside the IC. In other words, the principal part of the IC is concentrated in the "dead ends," which do not affect conductivity.

## 1.2 Conductivity of a Network with the Random Distribution of Elements

The existing percolation models can be applied only if the conducting elements (bonds in the network) are homogeneous. That is, it is assumed in these models that the intrinsic conductivities of all elements in the network are equal. However this approach does not work for many kinds of heterogeneous media, e.g., oil and gas reservoirs. It fails because various groups of structural elements in a medium with intrinsic conductivities differing by several orders can make a commensurate contribution to the effective conductivity of a heterogeneous medium. We suggest a model which allows to describe conductivity of a heterogeneous medium with the given intrinsic conductivity distribution of structure elements. In essence, it is a generalization of the Shklovsky - de Gennes model. Our model is able to describe the case when the network contains conducting elements randomly distributed with respect to values of intrinsic conductivities.

Consider the network model of a heterogeneous medium whose sites are connected with bonds with different conductivities  $\sigma$ . From now on, the general term "conductivity," if not otherwise specified, will be used to describe both the hydroconductivity, or permeability, and the electric conductivity, since the logic behind the construction of models for the two processes is absolutely the same. Let the period of the network equal  $l$ . Suppose that the values of the conductivities (or values of the parameter which determines them, i.e., radius of the section) of the bonds are distributed randomly in the network and are characterized by the distribution function  $f_0(\sigma)$  which satisfies the normalization condition,

$$\int_0^{\infty} f_0(\sigma) d\sigma = 1$$

Since fluid conductivity of a conducting bond is  $\sim r^4$  and its electric conductivity is  $\sim r^2$ , the distribution of bonds with respect to conductivities can also be

characterized by the normalized radius distribution function of conducting bonds  $f(r)$ . From now on, a corresponding form of function  $\sigma(r)$  will be used for specific transfer phenomena, and the function  $f(r)$  will be used to describe heterogeneity of the porous medium. Within this section of the book, for clarity's sake, we shall use  $f_0(\sigma)$  in our reasoning. Let the number of bonds with conductivities  $\sigma > 0$  be characterized by the quantity  $\kappa (0 \leq \kappa \leq 1)$ . Here  $\kappa = 1$  only if all bonds are conducting and  $0 \leq \kappa < 1$  otherwise. Conduct a mental experiment. Suppose that the bond conductivities with values less than  $\sigma_1$  vanish. Then percolation is possible only through those bonds, whose conductivities exceed  $\sigma_1$ . The probability of a bond having conductivity  $\sigma \geq \sigma_1$  is

$$P^b(\sigma_1(r_1)) = \kappa \int_{\sigma_1}^{\infty} f_0(\sigma) d\sigma = \kappa \int_{r_1(\sigma_1)}^{\infty} f(r) dr, \quad (1.7)$$

where  $r_1(\sigma_1)$  is the inverse relation  $\sigma_1(r_1)$ . The infinite cluster and, consequently, percolation appears in the network when  $P^b(\sigma_1) \geq P_c^b$ . Using relationships (1.1) and (1.7), one can find the value  $\sigma_c(r_c)$  of conductivity at the point when the IC is formed. The conductivity of the IC skeleton along the principal axes of the network is generally determined from the conducting chains parallel to these axes and belonging to the IC (see fig. 1). The number  $n(\sigma_1)$  of conducting chains containing the bonds with conductivities  $\sigma \geq \sigma_1$  and reaching a unit surface of a cross-section perpendicular to the chosen direction is equal to  $1/R^2$  in the three-dimensional case and  $1/R$  in the two-dimensional case. From (1.7), (1.1), and (1.3) we obtain that

$$n(\sigma_1) = l^{(1-D)} \left[ \kappa \int_{\sigma_1}^{\sigma_c} f_0(\sigma) d\sigma \right]^{\nu(D-1)}, \quad \int_{\sigma_c}^{\infty} f_0(\sigma) d\sigma = P_c^b, \quad (1.8)$$

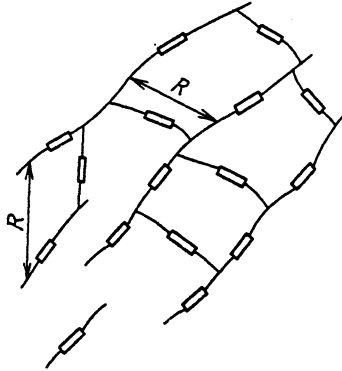


Figure 1: Diagram of the IC skeleton structure in the Shklovsky - de Gennes model

or

$$n(r_1) = l^{(1-D)} \left[ \kappa \int_{r_1}^{r_c} f(r) dr \right]^{\nu(D-1)}, \quad \int_{r_c}^{\infty} f(r) dr = P_c^b. \quad (1.8')$$

The average conductivity of a chain of unit length  $k$  composed from successive bonds is

$$k(\sigma_1) = \left[ \int_{\sigma_1}^{\infty} f(\sigma) \frac{d\sigma}{\sigma} \right]^{-1} \left[ \int_{\sigma_1}^{\infty} f(\sigma) d\sigma \right]. \quad (1.9)$$

If we decrease the threshold value  $\sigma_1 > 0$  further, then  $n$  grows. The new conducting chains which join the ones that were there for the initial value  $\sigma_1$  contain the bonds with conductivities  $\sigma \leq \sigma_1$ . Therefore the new average conductivity is less, but still determined by (1.9), where  $\sigma_1$  denotes the minimum value of conductivity among the bonds contained in the given chain. The average conductivity of the chain is uniquely determined from the quantity  $\sigma_1$ . Knowing the distribution function  $F(\sigma_1)$  of the conducting chains with respect to values of  $\sigma_1$ , one can find the total conductivity of the IC

$$K = \int_0^{\sigma_c} k(\sigma_1) d\sigma_1, \quad (1.10)$$

where  $F(\sigma_1)$  is related to the quantity  $n$  as follows,  $F(\sigma_1) = -dn/d\sigma_1$ . Using this relationship, as well as (1.8), (1.9), and (1.10), we obtain

$$K = \gamma \nu (D-1) l^{(1-D)} \kappa^{\nu(D-1)} \int_0^{\sigma_c} \left[ \int_{\sigma_1}^{\sigma_c} f_0(\sigma) d\sigma \right]^{2\nu-1} f_0(\sigma_1) \frac{d\sigma_1}{I(\sigma_1)} \quad (1.11)$$

where

$$I(\sigma_1) = \left[ \int_{\sigma_1}^{\infty} f_0(\sigma) \frac{d\sigma}{\sigma} \right] \left[ \int_{\sigma_1}^{\infty} f_0(\sigma) d\sigma \right]^{-1}$$

The formula (1.11), as well as other known percolation relations, is obtained under the assumption of no interflows between the conducting parallel chains. This fact is reflected in the formula (1.11) by the numerical factor  $\gamma$  (of the order of unity), which depends on the network type. As was pointed out, in the three-dimensional case the conducting chains of the IC are tortuous. It can be shown that taking account of this property causes the change of the exponent  $2\nu - 1$  in (1.11) to  $\nu + \zeta - 1$ , where  $\zeta = 1$  [26]. In the two-dimensional case, no such effect is observed.

Since the formulas obtained in this work assume no interflows between the parallel conducting chains, the question arises about the accuracy of the results obtained.

Note that in the case of equal conductivities for all conducting channels, formulas of the (1.11) type turn into critical percolation relations  $\Sigma \sim K \sim (P^b - P_c^b)^d$ . It was shown in [29] that relations of this sort describe with good accuracy (10 to 20%) the change of network conductivity near the critical point for the following range of the bond conductivity probability,  $P_c^b \leq P^b \leq P_c^b + \Delta P^b$ , where  $\Delta P^b \leq 0.1$ . For a given distribution of conducting bonds with respect to values of their intrinsic conductivities, verification of formula (1.11) with a numerical experiment is necessary.

**Numerical experiment.** In order to verify the fundamental relationship (1.11) obtained above, its results were compared to those of the following numerical experiment. Consider stationary flow in an arbitrary medium described by the elliptic equation

$$\operatorname{div}(\sigma \nabla \phi) = 0. \quad (1.12)$$

The equation determining the distribution of potential  $\phi$  in a square network with a period  $l$

$$l^{-2}[\sigma_{i+1/2,j}(\phi_{i+1,j} - \phi_{i,j}) - \sigma_{i-1/2,j}(\phi_{i,j} - \phi_{i-1,j})] + \quad (1.13)$$

$$+ l^{-2}[\sigma_{i,j+1/2}(\phi_{i,j+1} - \phi_{i,j}) - \sigma_{i,j-1/2}(\phi_{i,j} - \phi_{i,j-1})] = 0$$

is the difference analog of the relationship (1.12). Here  $i = 1, 2, \dots, N$ ;  $j = 1, 2, \dots, N$  are natural numbers that locate the site in the network;  $\sigma_{i\pm 1/2, j\pm 1/2}$  is the intrinsic conductivity of the bond at the point  $i \pm 1/2, j \pm 1/2$  (set by a random number generator); and  $\phi_{i,j}$  is the value of the potential at the point  $i, j$  (fig. 2). Conductivities of bonds were assigned by a random number generator provided their probability density was determined by a given function  $f_0(\sigma)$ . The boundary conditions were as follows

$$\phi_{0,j} = 1, \phi_{N,j} = 0, \quad (1.14)$$

$$\phi_{i,N} - \phi_{i,N-1} = 0, \phi_{i,1} - \phi_{i,2} = 0. \quad (1.15)$$

The condition (1.15) requires no flow through the boundary of the network in the  $j$ th direction, and the condition (1.14) indicates constancy of the potential on those boundaries of the network, through which the flow comes.

The equation (1.13) has been solved numerically using the relaxation method. To speed up calculations, initial distribution was set to be

$$\phi_{i,j} = 1 - i/N.$$

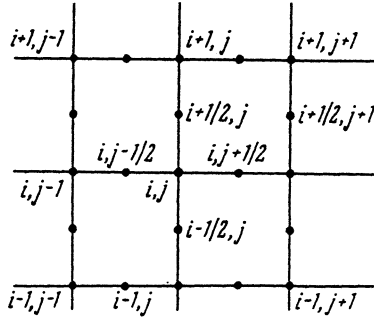


Figure 2: Two-dimensional network built for the numerical solution to the problem of percolation in a network.

For the given potential difference  $\delta\phi = 1$  on the boundaries of the network, the average value of flux between those boundaries was determined by the formula

$$Q = N^{-1} \sum_{j=1}^N \sigma_{N-1/2,j} (\phi_{N-1,j} - \phi_{N,j})$$

Effective conductivity  $\Sigma$  was found from the formula

$$\Sigma = Q/\delta\phi$$

In the course of the numerical experiment, the following types of distribution functions for intrinsic conductivities of the bonds were set,

1.  $f_0(\sigma) = a \exp(-a\sigma), a \gg 0$ ;
2.  $f_0(\sigma) = \kappa\delta(\sigma - 1) + (1 - \kappa)\delta(\sigma - 10^{-1})$ ;
3.  $f_0(\sigma) = \kappa[\eta(\sigma) - \eta(\sigma - 1)]$ ,

where  $\delta(\star)$  and  $\eta(\star)$  are the conventional notations for Dirac's  $\delta$ -function and Heavyside's  $\eta$ -function ( $\delta(\star) = \eta'(\star)$ ). Furthermore, the fraction of conducting bonds in the network  $\kappa$  was also being changed. Sampling was made for each method by calculating the conducting bonds distribution in the network for a fixed function  $f_0(\sigma)$  in different realizations. The quantity  $N$  in different methods of calculation was set to be either 100 or 150. Comparison of results for different distribution functions showed that for  $N = 150$ ,  $\Sigma$  is determined with accuracy of  $\approx 10 - 15\%$ .

The distribution function  $f_0(\sigma) = a \exp(-a\sigma)$  was used to find how accurately the formula (1.11) determines the effective conductivity of a micro heterogeneous medium with a smooth distribution function of its conducting structural elements. This distribution function  $f_0(\sigma)$  is normalized on unity, and its variance can be



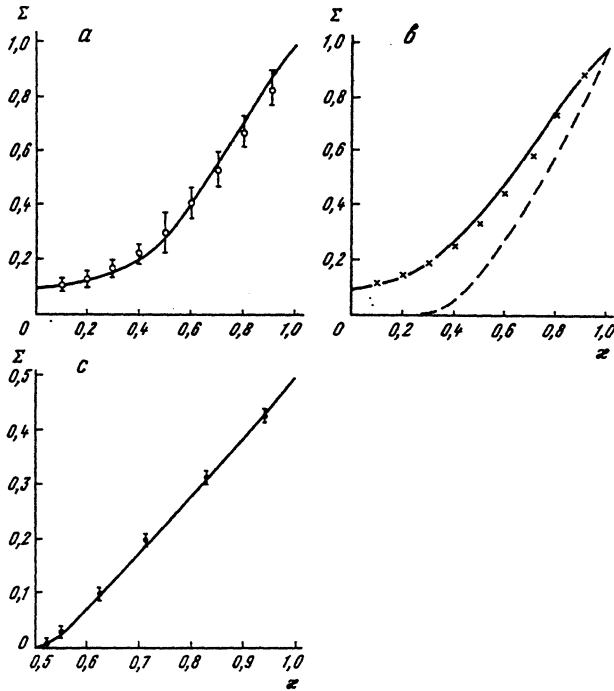


Figure 3: Plot of the effective conductivity against of the parameter  $\kappa$  for the conditions: a -  $D = 2, \nu = 1.33, l = 1$ ; b -  $D = 3, \nu = 0.9, l = 1$  (the dotted line represents the classical curve of percolation theory); c -  $D = 2, \nu = 1.33, l = 1$

altered by varying the quantity  $a$ . This quantity defines the expectation of the function  $f_0(\sigma)$ :  $m_f = \int_0^\infty \sigma f_0(\sigma) d\sigma = a^{-1}$ .

The results of the numerical calculation of the effective conductivity  $\Sigma$  for a micro heterogeneous medium (marked by index  $p$ ) for different values of  $m_f$ , and the theoretical values of  $\Sigma$  (index  $t$ ), found using formula (1.11), with  $\nu = 1.33, D = 2, \gamma = 2.85, l = 1$ , are displayed below:

$m_f$	0.05	0.1	0.5
$\Sigma_p$	0.043	0.089	0.47
$\Sigma_t$	0.043	0.088	0.45

The formula (1.11) describes the effective conductivity of a micro heterogeneous medium with good accuracy in a wide range of  $m_f$ . It is interesting to note that for smooth distribution functions like those considered above, the value of the effective conductivity of the network comes close to the expectation. The latter coincides

with the mean value of the conductivity of the medium  $\Sigma \approx M = \langle \sigma \rangle$ . As for the one-dimensional case, the effective conductivity is determined from the mean value of the inverse conductivity of the medium, i.e., from the average resistance  $\Sigma \approx \langle 1/\sigma \rangle^{-1}$ , and does not coincide with the mean value  $\langle \sigma \rangle$ .

The dependence of the effective conductivity of a medium on the parameter  $\kappa$  defined for the second and third distribution functions by the formula (1.11) is shown in fig. 3. The parameters  $\nu$ ,  $l$ , and  $\gamma$  were the same as in the previous case. Fig. 3, *a*, *b*, shows the results of the calculation for  $f_0(\sigma)$  No. 2, and fig. 3, *c*, shows the results for  $f_0(\sigma)$  No. 3. Values of  $\Sigma$  obtained in the numerical calculation are marked by circles on the same plots.

Distribution function No. 2 differs from the one regularly used in percolation theory only in that the non-conducting bonds are substituted in the network with the bonds with small, but non-zero conductivities. Numerical modeling shows that introduction of the bonds with small conductivities into the network instead of the corresponding "zero" ones changes the nature of the dependence  $\Sigma(\kappa)$  drastically.

Within the framework of classical percolation theory, where the second term in the relation for  $f_0(\sigma)$  No. 2 is of the form  $(1 - \kappa)\delta(\sigma - 0)$ , the given dependence is characterized by a curve resembling the dashed line in fig. 3, *b*. After comparing the curves in fig. 3, *b*, one can notice that although according to the classical theory, in the region  $\kappa \leq P_c^b$ ,  $\Sigma(\kappa) \equiv 0$ , in the considered generalization of this theory,  $\Sigma(\kappa) > 0$  for all  $\kappa$ . Besides, the behavior of the curves  $\Sigma(\kappa)$  in the interval  $P_c^b < \kappa \leq 1$  varies. This is most noticeable near  $\kappa = P_c^b$ . The plots presented in fig. 3 show that satisfactory agreement of the analytical dependence (1.11) with the results of the numerical experiment does take place.

Note that the obtained relation (1.11) includes the limiting case  $(1 - \kappa)\delta(\sigma - 10^{-1}) \rightarrow (1 - \kappa)\delta(\sigma - 0)$ . In this case the calculations using (1.11) yield the classical percolational relation shown on fig. 3, *b*, by the dashed line and described by the formula (1.5).

### 1.3 Effect of Electric Current on Conductivity of Heterogeneous Media

When electrical current passes through successive capillaries of radii  $r_1$  and  $r_2$  the ratio of current densities in them is proportional to  $(r_2/r_1)^2$ , while the ratio of energy discharge densities is  $\sim (r_2/r_1)^4$ . For heterogeneous media, e.g., rocks, the ratio  $(r_2/r_1)$  can be  $\approx 10^3$  and more. This fact shows how far from uniformity can the energy discharge density be in a medium. High densities of energy discharge in thin capillaries can cause changes to the intrinsic conductivities. Specific mechanisms causing such changes can be very different, e.g., the increase of pressure in capillaries, pressure gradients at the micro level, etc. Since in actual

media, capillaries can be bonded not only successively, but also in parallel, correct estimates of the energy discharge density at the micro level must be made using the network model of heterogeneous media (see §1.2). In analyzing current flow through a network of conductors, we will use the more habitual notation for electric conductivity,  $k(\sigma_1)$ , rather than  $\Sigma(\sigma_1)$ .

When electric current flows through a chain of successive resistances, the maximum voltage is achieved on a bond of minimum conductivity  $\sigma_1$  in the chain. The current through the chain is proportional to  $\Sigma(\sigma_1)$ .

Let  $E$  be the gradient of the potential applied to the network. Then the maximum local gradient of the potential in the chain satisfies the relationship

$$(\nabla\phi)_l = \sigma_1^{-1}\Sigma(\sigma_1)E$$

After looking through chains with different  $\sigma_1$ , one can find the maximum gradient of the potential in the network

$$\nabla\phi^*/E = \max_{\sigma_1} \left\{ \sigma_1^{-1} \int_{\sigma_1}^{\infty} f_0(\sigma) d\sigma \left[ \int_{\sigma_1}^{\infty} f_0(\sigma)\sigma^{-1} d\sigma \right]^{-1} \right\} \quad (1.16)$$

Consider a model probability density function of the form

$$f_0(\sigma) = (\sigma_3 - \sigma_2)^{-1}[\eta(\sigma - \sigma_2) - \eta(\sigma - \sigma_3)]. \quad (1.17)$$

After substituting (1.17) into (1.16), we find that

$$\nabla\phi^*/E = (\sigma_3/\sigma_2 - 1)\ln^{-1}(\sigma_3/\sigma_2)$$

It is evident now that with the increase of the variance in the probability density function, the heterogeneity of the local gradient of the potential in the network goes up sharply. The relationship (1.16) allows to determine the conductivity of the first bond in which a change of conductivity has occurred. To determine further change of the conductivity of the bonds in the network, consider a chain characterized by a parameter, say,  $\sigma_1$ . Suppose that the conductivity  $\sigma^1$  of those bonds, whose energy discharge reaches the value  $\epsilon\sigma^1/\sigma_m$ , increases up to the level where it has practically no effect on the conductivity of the chain, i.e.,  $\sigma^1 \gg \Sigma(\sigma_1)$ . Note that the quantity  $\epsilon\sigma_m^{-1}$ , where  $\sigma_m = \text{const}$ , depends only on the physical properties of the material constituting the bonds, and is thus constant for the given medium. The increase in the conductivity of the network results in the increase of the current density in the chains. The latter phenomenon may cause further change in the conductivity of the network.

Suppose that in the network characterized by the parameter  $\sigma_1(0)$ ,  $\sigma_1(t)$  is the conductivity of the bond which changes conductivity at the instant  $t$ . (The bonds

which satisfy the condition  $\sigma_1(0) \leq \sigma \leq \sigma_1(t)$  have already had their conductivities changed.) To obtain the condition for the conductivity change, define the energy discharge  $\epsilon_1$  in the bond  $\sigma_1(t)$  contained in the chain  $\sigma_1(0)$ . After neglecting the effects of heat exchange between the chains and the non-conducting skeleton of the medium, we obtain

$$\epsilon \frac{\sigma_1(t)}{\sigma_m} = \frac{E^2}{\sigma_1(t)} \Sigma^2(\sigma_1(0)) + \frac{E^2}{\sigma_1(t)} \int_{t_0}^t \Sigma^2(\sigma_1(\tau)) d\tau, \quad t_0 \leq t \leq t_k. \quad (1.18)$$

The first term in the right side of the relationship (1.18) corresponds to Joule's heat which has discharged in the bond before the instant  $t_0 = \epsilon \sigma_m^{-1} \times (\nabla \phi^*)^{-2}$ , when the conductivity of the chain began to change. The second term describes the energy discharge during the period when the conductivity of the chain was changing. In this case,  $t_k$  is the time needed for all elements of the chain to acquire infinite conductivity.

Consider the change of the conductivity in the case when the probability density  $f_0(\sigma)$  of the bonds with respect to intrinsic conductivities is described by the model function

$$f_0(\sigma) = (n-1) \sigma_0^{(n-1)} \sigma^n \eta(\sigma - \sigma_0). \quad (1.19)$$

In this case the solution (1.18) can be obtained in the analytical form. As it can be deduced from the relationship (1.16), the value  $\nabla \phi^*/E = n/(n-1)$  is the same for all chains and is assumed at those bonds which have the least conductivity for the given chain.

For an arbitrary chain, (1.18) implies

$$\sigma_1(t) = \sigma_1(0) [1 - (n-1)(t/t_0 - 1)]^{-\lambda_n n}, \quad \lambda_n = \frac{1}{2(n-1)}$$

This means that according to (1.9), the average conductivity of all chains increases in the like fashion, i.e., proportional to  $1 - (n-1)(t/t_0 - 1)^{-\lambda_n n}$ , so that  $t_0$  is the same for all chains. Therefore the effective conductivity of the medium  $\Sigma^0(t) \sim \int_0^{\sigma_1} \Sigma(\sigma(t)) d\sigma$ , and after integrating

$$\Sigma^0(t)/\Sigma^0(0) = [1 - (n-1)(t/t_0 - 1)\eta(t - t_0)]^{-\lambda_n n}$$

If bonds are cylindrical capillaries, then the electric conductivity  $\sigma$  of such a bond is related to its permeability coefficient  $k$  in the following way,  $k \sim \sigma^2$ . Thus we obtain the time dependence of the permeability  $K(t)$  of the medium

$$K(t)/K(0) = [1 - (n-1)(t/t_0 - 1)\eta(t - t_0)]^{-2\lambda_n n}$$

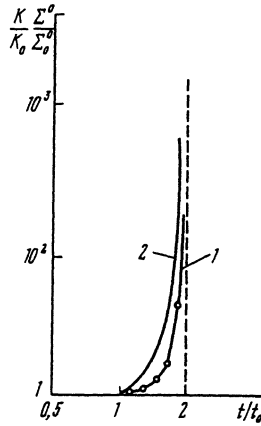


Figure 4: Plots of electric conductivity (1) and permeability (2) of heterogeneous medium against time during electric treatment

It is interesting to observe that when  $t - t_k = t_0 n / (n - 1)$ ,  $\sigma_1(t) \rightarrow \infty$ . In this case, some chains in the network consist only of those elements which changed their conductivities when the electric current passed through them. The dependencies  $\Sigma^0(t)/\Sigma^0(0)$  and  $K(t)/K(0)$  are shown in fig. 4. Also depicted there are the results of numerical modeling of the process in question for a plane square network with the number of sites  $100 \times 100$  and the probability density function of the exponential type (1.19) with  $n = 3$ ,  $\sigma_0 = 1$ . Distribution of the potential in the network was found from the solution of the Laplace equation  $\text{div}(\sigma \nabla \phi) = 0$ , where the values of  $\sigma$  were set by a pseudorandom number generator. For a given probability density function, the solution was found using the relaxation method. When the critical level of the energy discharge was achieved at one of the bonds, its conductivity was set to equal  $10^5$ . Then  $t_0$  was determined. Numerical modeling showed that the values  $t_0$  and  $t_k$  agreed well enough with the values obtained analytically for various probability density functions. It was also showed that the analytical dependencies  $\Sigma^0(t)/\Sigma^0(0)$  and  $K(t)/K(0)$  agreed satisfactorily with the results of numerical modeling.

Thus heterogeneity of a medium at the micro level causes sharp heterogeneity of the density of energy discharge in the conducting elements. Such heterogeneity, in its turn, may cause significant changes in the conductivity of the medium even when relatively small electric fields are applied to the medium. Estimates show that such effects can be observed in rocks with notably heterogeneous pore space. Note that the change of the conductivity predicted by theory is quasi-volumetric, a property which makes this process different from those of the "breakthrough" type, where contraction of the current in the medium takes place. The presence of a threshold, which defines the lower limit of the energy discharge when the rear-

rangement of the pore space structure is still possible, is also of great importance.

Obviously, the described effect can be extensively used to increase the conductivity of media, and consequently, to increase the production rates of wells used for the recovery of minerals (water, oil, productive solutions of underground leaching). Experiments at over 50 places across the territory of the former USSR with different geological structure (clay, gravel, and rock) have shown that production rates of hydrogeological and geotechnological wells increased by factors of 2 to 10 (average 2 -3 ) when their pre-filter parts were treated with electric current. Electric energy consumed in these works did not exceed 300 kilowatt-hours per well.

So the field experiments confirm the possibility of practical application of the effect predicted by the theory.

## Chapter 2

# Percolation Models of One-Phase Flow in Rocks of Different Types

There are many types of pore space structure in natural rocks. We consider oil and gas reservoirs as well as hydrogenous water- and ore-bearing strata. These formations break up in three fundamental groups, namely grained, cavernous, and fractured reservoirs. There also exist rocks of a mixed type, e.g., fractured-cavernous, fractured-porous, etc. Inside each group, it is possible to describe conductivity of the reservoir rocks using the model of a heterogeneous medium (see chapter 1), if the distribution of conducting structural elements with respect to intrinsic conductivities is defined.

### 2.1 Conductivity of Grained Media

Consider a specimen of an infinite grained medium with grain centers arranged in cyclic symmetry and whose grains have equal diameters (see fig. 5). In such a medium fluid can flow only along the thin channels which connect the large pores. The channels between the pores can be partially or entirely trapped by a cementing substance, and therefore channels have different cross-sections. It is possible to characterize conducting properties of each channel by the parameter  $r$ , the effective radius of the channel. Suppose the conducting channels with different  $r$  are distributed randomly with the probability density function  $f(r)$ . Percolation theory treats large pores as sites and the thin channels as bonds between them. When centers of grains are arranged in cyclic symmetry, the system of channels

forms a cubic network. The coefficient of permeability for such a system, which simulates the pore space structure of grained media, can be calculated using the approach discussed in §1.2. This coefficient is determined from (1.11) for the case of hydraulic conductivity  $\sigma = (\pi/8)r^4$ :

$$K = 2\gamma\nu l^{-2}(1 - P_c^b)^{-2\nu} \int_0^{r_c} \left[ \int_{r_1}^{r_c} f(r) dr \right]^\nu \frac{f(r_1)}{I(r_1)} dr_1, \quad (2.1)$$

where  $I(r_1) = 8/\pi \int_{r_1}^{\infty} f(r) (dr/r^4) \left( \int_{r_1}^{\infty} f(r) dr \right)^{-1}$ ,  $r_c$  is the critical radius defined by an expression similar to (1.7)

$$\int_{r_c}^{\infty} f(r) dr = P_c^b. \quad (2.1')$$

Note that in deducing the relationship (2.1), the tortuosity of the elements forming the skeleton of the IC is already taken into account, since this deduction was carried out for a space network.

Now consider electric conductivity of a grained medium when a conducting fluid with specific electric conductivity  $\sigma'$  is contained in the medium. We assume that neither the grains nor the cementing substance conducts electric current. Note that polarization effects can make significant contributions to the current flow through a two-phase medium. Therefore the electric conductivity of the medium is determined not only by  $\sigma'$ , but also by  $\lambda'$ , a parameter which characterizes "surface" electric conductivity induced by the diffuse layer of ions near the phase interface. Detailed research on the effect of polarization on electric conductivity of media was made by S. M. Scheinmann (1969). We shall present here only the final results obtained using the two-phase model.

When the low-frequency current passes through two successive conducting channels, the resistance can be described by the following formula [43],

$$\rho = \Pi\Phi(\omega) + \rho_0, \quad \Phi(\omega) = \tanh(\sqrt{i\omega\tau_i})/\sqrt{i\omega\tau_i}. \quad (2.2)$$

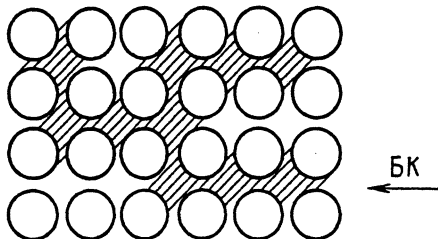


Figure 5: Model of the pore space structure for a grained medium



Here  $\omega$  is the angular frequency ( $0 \leq \omega < 10^5$  radian/s),  $\tau_i$  is the characteristic period of ion diffusion in the channels. The function  $\Phi(\omega)$  characterizes the relation between resistance and frequency:  $\Phi(0) = 1$ ,  $\Phi(\infty) = 0$ . Resistance is determined only by the quantity  $\rho_0$  which characterizes the non-polarized two-component medium

$$\rho_0 = a_1/\sigma_1 + a_2/\sigma_2, \quad i = l_i/l, \quad l = l_1 + l_2, \quad (2.3)$$

where  $l_i$  is the length of the  $i$ -th channel. The conductivity of the  $i$ -th channel is

$$\sigma_i = \frac{\pi r_i^2}{l_i} \sigma' \left( 1 + 2 \frac{\lambda'}{\sigma' r_i} \right).$$

$\Pi$  does not depend on frequency and is a function of the channel parameters and of the equivalent ion transfer numbers  $n_{i\pm}$  in the solution, which depend on the ratio  $\lambda' / (\sigma' r_i)$

$$\Pi = \frac{(n_{1+}n_{2-} - n_{1-}n_{2+})^2}{\sigma_1 n_{1+}n_{1-}/a_1 + \sigma_2 n_{2+}n_{2-}/a_2}.$$

S. M. Scheinmann used the formula (2.2) to calculate the effective conductivity of the medium and its frequency dependence. The conductivity was then averaged with regard to the channel size distribution function. In the discussed approach, the structure of the conducting infinite cluster formed in the medium is determined using this distribution function. Then the effective electric conductivity of the medium is calculated with regard to structure of the conducting chains. As it was showed in §1.2, conductivity of the IC is determined from parallel conducting chains whose distribution with respect to  $r_1$  is described by the function  $F(r_1)$ . Given the mean values  $\langle \sigma(r_1) \rangle$  of electric conductivities for the chains, a formula equivalent to (2.1) can be obtained for calculation of the electric conductivity of the medium

$$\Sigma = 2\gamma\nu l^{-2} (1 - P_c^b)^{-2\nu} \int_0^{r_c} \left[ \int_{r_1}^{r_c} f(r) dr \right]^\nu \langle \sigma(r_1) \rangle f(r_1) dr_1. \quad (2.4)$$

Taking account of the relationship (2.2), one can find  $\langle \sigma(r_1) \rangle$  for a chain of successive resistances

$$\langle \sigma(r_1) \rangle^{-1} = l^{-1} \int_{r_1}^{\infty} [\rho_0(r) + \Pi\Phi(\omega)] f(r) dr \left( \int_{r_1}^{\infty} f(r) dr \right)^{-1}. \quad (2.5)$$

Formulas (2.4) and (2.5) determine the effective electric conductivity of a grained medium. Focus on the calculation of  $\langle \sigma(r_1) \rangle$ . Formula (2.2) was obtained for the case of two cylindrical channels connected to each other. However the geometry of channels in a grained medium can be different. Yet due to

complexity of the electric current flow problem in a two-phase media, no solution for other geometries of channels is available at present. Therefore it is suggested in determining the electric conductivity of a grained medium that parameters of cylindrical channels be chosen correspondingly. Any channel connecting pores in a grained medium can be represented as two cylindrical channels of equal lengths  $l_1 = l_2 = l/2$  but of different effective radii. After setting the radius of the thin channel to equal  $r$  and the radius of the thick one to be of the same order of magnitude as the radius  $l/2$  of the grain and using (2.3), we find the expression for  $\rho_0$  in the explicit form

$$\rho_0 = \frac{1}{\pi\sigma'l} \left[ 1 + \left( \frac{l}{2r} \right) \frac{1}{1 + 2\lambda' / (\sigma'r)} \right]. \quad (2.6)$$

In (2.6), the relationship  $4\lambda' / (\sigma'l) \ll 1$  was taken into account. When radii of channels are large enough ( $2\lambda' / (\sigma'r) \ll 1$ ), the surface conductivity may be neglected and the formula (2.6) reduces to

$$\rho_0 = \frac{1}{\pi\sigma'l} [1 + (l/r)^2].$$

## 2.2 "Permeability - Porosity" Correlation

Since the distribution function of conducting channels with respect to intrinsic conductivities is not always known, finding the correlation between the coefficient of permeability and the porosity of a medium is of a certain practical interest. In this approach, it is certainly impossible to take account of the effects caused by differences in intrinsic conductivities of the channels in a grained medium. However for those grained media, whose permeability is determined primarily by a group of capillaries with approximately equal intrinsic conductivities, such a method is justified. Therefore we shall draw our attention to the model of a grained medium discussed in §2.1 (see fig. 5).

Let  $\Phi_0$  be the porosity of the model structure in question (further called structural porosity of the medium). Structural porosity is related to the coefficient of charge as follows,  $f = 1 - \Phi_0$ . Suppose that some of the sites are trapped with impermeable substance, and thus the porosity of the medium is  $\Phi < \Phi_0$ . If the distribution of trapped sites in the network is random, the probability of a site having non-zero conductivity can be found from the relationship

$$P^s = \Phi / \Phi_0 \quad (2.7)$$

The threshold value of the conductivity probability  $P_c^s$  of a site when an IC is formed is  $P_c^s = 0.16f^{-1}$  in the three-dimensional case. The coefficient

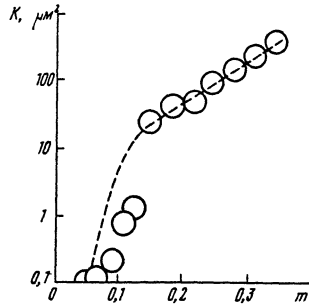


Figure 6: Plot of the coefficient of permeability for a grained medium against porosity

of permeability of the medium near the percolation threshold in the interval  $P_c^s \leq P^s < P_c^s + \Delta P^s$  is determined from the relationship (1.4)

$$K \sim (\Phi/\Phi_0 - P_c^s)^d \eta (\Phi/\Phi_0 - P_c^s). \quad (2.8)$$

Outside this interval, the conductivity of the medium can be adequately described by a linear relation between the conductivity and the quantity  $P^s$ . Moreover when all pores are open ( $P^s = 1$ ) the permeability of the medium is determined from Causeni's formula [44]

$$K_0 = 7 \cdot 10^{-3} l^2 \Phi^3 / (1 - \Phi_0)^2. \quad (2.9)$$

Hence the coefficient in the formula (2.8) can be found approximately by matching the relations (2.8) and (2.9) for  $P^s > P_c^s + \Delta P^s$ . In this case, the formula for the coefficient of permeability becomes

$$K = 7 \cdot 10^{-3} \frac{l^2 \Phi^3}{(1 - \Phi_0)^2} \left( \frac{\Phi}{\Phi_0} - P_c^s \right)^d \eta \left( \frac{\Phi}{\Phi_0} - P_c^s \right). \quad (2.10)$$

Formula (2.10) describes the permeability of the medium in the interval  $P_c^s \leq P^s < P^s + \Delta P^s$  adequately and in the region  $P^s \geq P_c^s + \Delta P^s$ , approximately. The following important fact is implied in by the formula (2.10). The value of the porosity at the point of the IC formation depends on  $\Phi_0$ , a parameter which characterizes the structure of pore space. Structural porosity  $\Phi_0$ , in its turn, depends on the density of packing of the grains and thus can vary within the following limits,  $0.26 \leq \Phi_0 \leq 0.48$ . So the value of the porosity of a grained medium when an IC is formed in it is  $\Phi_c = \Phi_0 P_c^s$  and can vary within the interval  $3.9\% \leq \Phi_c \leq 7.2\%$ . This range defines the lower bound of the permeability for the grained reservoirs, a result that agrees with experimental data [45]. The dotted line in fig. 6 reflects the relation between the coefficient of permeability of a medium

and the porosity. This relation was found from (2.10) with  $f = 0.68, l = 10^{-3}$  m. Experimental data [46] for the permeability of sandstone, which agree satisfactorily with the relationship (2.10), are presented on the same plot for comparison.

The proposed model allows to explain some experimental facts. For example, it is known that for small porosities, a dependence like  $K \sim \Phi^p$  between the coefficient of permeability and porosity takes place, where  $p$  can be as big as 10, while Causeni's formula implies  $p = 3$ . Within the framework of percolation theory for grained media this fact follows naturally, since near the percolation threshold, a sharp dependence of permeability on porosity takes place. If formula (2.10) is approximated by the exponential relation  $K \sim \Phi^p$  then for small  $\Phi$ ,  $p$  becomes just  $\approx 10$ . Note that formula (2.10) implies the lack of a single-valued correlation between the coefficient of permeability and porosity. In order to definitely find the coefficient of permeability for a grained medium, it is necessary to set the value of  $\Phi_0$  which defines the structure of the grain packing. It is therefore possible that the scatter of experimental points near the percolation threshold is caused not by errors of measurement, but by the fact that structural porosities of sandstone cores vary.

### 2.3 Conductivity of Cavernous Media

Consider a medium with the globular pores of equal size and with randomly distributed centers. From the point of view of percolation theory, pores are conducting sites. Bonds between the pores can be formed only when the latter intersect. Consider an arbitrary "reference" point. Other pores can intersect with it if they are no more than  $2R_p$  away, where  $R_p$  is the radius of the pore. If centers of two pores are  $2R_p(1 - \epsilon)$  apart ( $0 \leq \epsilon \leq 1$ ) (see fig. 7), then their intersection forms a channel which connects them, of radius

$$r = R_p \sqrt{1 - (1 - \epsilon)^2} \quad (2.11)$$

In this case, the number of channels whose radii exceed the value  $r_1$  is determined by the number of pore centers inside a sphere of radius  $2R_p(1 - \epsilon)$  (excluding the "reference" pore)

$$N_0 = (4/3)\pi n^0 (2R_p)^3 (1 - \epsilon)^3 - 1, \quad (2.12)$$

where  $n^0$  is the concentration of the pore centers. Using the fact that porosity of the medium  $\Phi \approx (4/3)\pi n^0 R_p^3$  (with no account of the pore overlap), the formula (2.12) can be rewritten as  $N = 8m(1 - \epsilon)^3 - 1$ . The greatest possible number  $z$  of nearest neighbors of the "reference" pore can be estimated taking  $\epsilon = 0$ ,

$\Phi = 1$ . In this case, we find that  $z \simeq 6 \div 7$ . The probability of a channel of radius  $r \geq r_1$  forming between two pores is

$$P^b(r \geq r_1) \cong z^{-1}[8m(1 - \epsilon)^3 - 1]. \quad (2.13)$$

By comparing (2.13) and (1.1) for  $\epsilon = 0$ , one can find the threshold value  $\Phi_c$  of the porosity of the medium at which percolation begins. The corresponding value of the parameter  $\epsilon_c$  can be found from the following condition

$$(4/3)\pi n^0(2R_p)^3(1 - \epsilon_c)^3 = D/(D - 1). \quad (2.14)$$

Using the relation (2.13), in the general approach, it is possible to find the correlation radius of the IC formed from the channels satisfying the condition  $\epsilon \geq \epsilon_1$ ,

$$R = 2R_p\{(4/3)z^{-1}\pi n^0(2R_p)^3[(1 - \epsilon_1)^3 - (1 - \epsilon_c)^3]\}^{-\nu}.$$

Consequently the concentration of parallel conducting chains, which equals  $R^{1-D}$ , is defined by the following relationship

$$n(\epsilon \leq \epsilon_1) = (4R_p)^{(1-D)}\{(4/3)z^{-1}\pi n^0(2R_p)^3[(1 - \epsilon_1)^3 - (1 - \epsilon_c)^3]\}^{\nu(D-1)}. \quad (2.15)$$

The quantity  $\epsilon_1$  characterizes the minimal size of a channel from the chain. The distribution function of the parallel conducting chains with respect to the parameter  $\epsilon_1$  is  $F(\epsilon_1) = -dn/d\epsilon_1$ . Permeability of a cavernous medium is determined from a relationship similar to (1.10)

$$K = \int_0^{\epsilon_c} k(\epsilon_1)F(\epsilon_1) d\epsilon_1. \quad (2.16)$$

Here  $k(\epsilon_1)$  is the average partial conductivity of the chain which contains channels of the minimal radius characterized by  $\epsilon_1$ . Find  $f(\epsilon_1)$ , the probability density

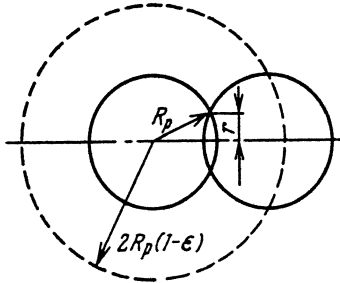


Figure 7: Intersection geometry for spherical pores

for conducting channels as a function of parameter  $\epsilon_1$ . The number of channels formed by those pores whose centers are  $2R_p(1 - \epsilon_1)$  apart is found from formula (2.12). Consequently the probability density  $f(\epsilon_1) = -dN_0/d\epsilon_1$  can be found (up to a normalizing factor) from the relationship

$$f(\epsilon_1) \sim 3(1 - \epsilon_1)^2. \quad (2.17)$$

Given  $f(\epsilon_1)$ , it is possible to find (up to a factor of the order unity)  $k(\epsilon_1)$ , a parameter which characterizes the conductivity of a chain composed of successive channels

$$k(\epsilon_1) \cong \frac{\pi}{8} \int_1^{\epsilon_1} f(\epsilon) d\epsilon \left( \int_{\epsilon_1}^1 \frac{f(\epsilon) d\epsilon}{r_1^4(\epsilon)} \right)^{-1}. \quad (2.18)$$

From (2.18), using (2.17), we can find the dependence  $k(\epsilon_1)$ . After substituting it in (2.16) together with (2.15), we obtain the resultant expression

$$K = \gamma \frac{\pi}{32} R_p^2 \left[ \frac{4\pi n^0}{3z} (2R_p)^3 \right]^{2\nu} \left\{ \frac{1}{4} - \frac{4}{5} (1 - \epsilon_c)^3 + (1 - \epsilon_c)^6 - \frac{9}{20} (1 - \epsilon_c)^8 \right\}. \quad (2.19)$$

Here  $\gamma$  is a numerical factor of the order unity. In evaluating the integral in (2.16),  $\nu$  was set to equal 1. Taking account of the relationship  $\epsilon_c = 1 - (\Phi_c/\Phi)^{\frac{1}{3}}$ , we can use (2.19) to find the dependence near the percolation threshold

$$K(\Phi) \cong R_p^2 \Phi^{2\nu} \left[ \frac{1}{4} - \frac{4}{5} \frac{\Phi_c}{\Phi} + \left( \frac{\Phi_c}{\Phi} \right)^2 - \frac{9}{20} \left( \frac{\Phi_c}{\Phi} \right)^{8/3} \right].$$

## 2.4 Conductivity of Fractured Media

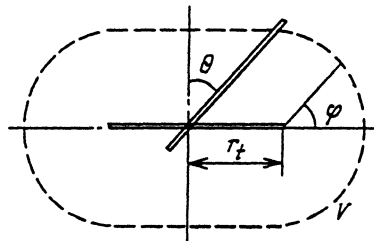


Figure 8: Intersection geometry for circular fractures

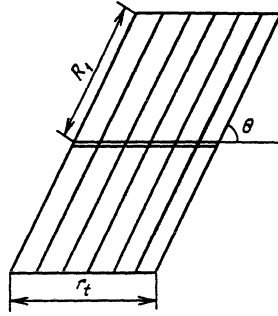


Figure 9: For determining the average number of intersections for circular fractures

Consider a set of randomly distributed circular fractures in an infinite medium. Assume that the fractures are oriented isotropically and all have the same radius  $r_t$  and opening  $b$ . Assume also that the centers of the fractures are sites, and intersections of any two fractures form a bond between the sites. In this case the probability of bonds having a non-zero conductivity is determined from the ratio of two quantities, namely the number of intersections an arbitrary fracture has with other fractures and the number of its nearest neighbors (sites). Consider (fig. 8) an arbitrary "reference" fracture. Among other fractures, only those intersect with it, whose centers lie in the domain  $V$ . The total number of fractures in  $V$  is

$$z_1 = 2\pi n^0 r_t^3 \int_0^{\frac{\pi}{2}} (1 + 2 \cos \phi + \cos^2 \phi) \cos \phi d\phi,$$

where  $n^0$  is the concentration of the fracture centers. The greatest number of sites nearest to the "reference" fracture is

$$z = z_1 - 1 = 2\pi n^0 (1 + \pi/2 + 2/3) r_t^3 - 1.$$

Calculate the average number  $y$  of intersections the "reference" fracture has with its nearest neighbors. Obviously, such an intersection is possible only if the center of the other fracture lies inside  $V$ . En route, consider a more general problem of intersections for those circular fractures which lie in planes forming an angle  $\theta$  between them (fig. 9). The radius of the "reference" fracture equals  $r_t$  and the radii of the fractures intersecting with it are equal to  $R_1$ . Intersection of fractures is possible if the center of the second one lies inside a slanted cylinder whose base has an area equals  $\pi r_t^2$  and whose altitude is  $2R_1 \cos \theta$ . Consequently the number of intersections for such fractures (or, more exactly, the expectation of this number) is

$$y_1 = 2\pi n_1^0 r_t R_1 \cos \theta. \quad (2.20)$$

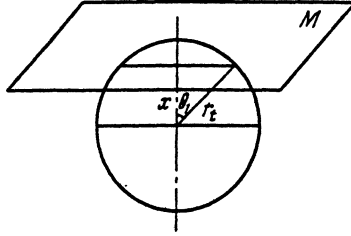


Figure 10: Geometry of intersection of fractures with the plane  $M$

Here  $n_1^0 = n^0 f(\theta, \psi) d\theta$  is the concentration of those fractures oriented at an angle  $\theta$  from the interval  $\theta \div \theta + d\theta$ ;  $f(\theta, \psi)$  is the angle distribution function for the circular fractures. If the fractures are oriented isotropically, then their angular distribution is described in spherical coordinates by the distribution function  $f(\theta, \psi) = (2\pi)^{-1}$  ( $0 \leq \theta \leq \pi/2$ ,  $0 \leq \psi \leq 2\pi$ ). In this case we can average  $y_1$  over the solid angle  $d\Omega = \sin \theta d\theta d\psi$  to obtain the following

$$y = \int y_1 f(\theta, \psi) d\Omega. \quad (2.21)$$

Taking account of the relationship (2.20), we find the average number of intersections from (2.21) to equal

$$y = \pi n^0 r_i^3 R_1. \quad (2.22)$$

If the fractures have equal radii all, then  $y = \pi n^0 r_i^3$ . In accordance with the discussed above, the probability of a bond forming between two sites is

$$P^b = y/z.$$

The threshold value of the probability in the considered bond problem can be estimated using the invariant (1.1) for  $D = 3$

$$P_c^b = 1.5/z. \quad (2.23)$$

In this case the permeability of the medium is determined according to (2.23), i.e., by the following relationship

$$K \cong \gamma(\pi n^0 r_i^3 - 1.5)^d z^{-d} \eta(\pi n^0 r_i^3 - 1.5). \quad (2.24)$$

The coefficient  $\gamma$  can be found by comparing the relationship (2.24) to the relationship for the coefficient of permeability of a medium pierced with infinitely long fractures, oriented isotropically [47]

$$K_0 = 0.5b^3 \Gamma, \quad (2.25)$$



where  $\Gamma$  is the thickness of fractures.

Using the geometry of the problem we can relate the thickness of fractures to their concentration. Consider the cross-section  $M$  (see fig. 10). Intersection of an arbitrary circular fracture with  $M$  is possible only if the distance from the center of the fracture to  $M$  does not exceed  $r_t$ . The intersection probability is determined from the solid angle  $\Omega_1$ . If the fracture lies inside this angle, then it can intersect with the plane  $M$ . It can be seen from fig. 10, that  $\Omega_1 = 2\pi(1 - \cos\theta_1)$ , where  $\cos\theta_1 = x/r_t$  (the segment  $x$  lies in the same plane as the fracture). Taking account of symmetry of the problem, we obtain the formula for the probability of the plane intersecting with the fracture

$$P_1(x) = 1 - x/r_t. \quad (2.26)$$

The number of traces on a unit surface of the cross-section is

$$n_2 = 2n^0 \int_0^{r_t} P_1(x) dx. \quad (2.27)$$

Using (2.26) and (2.27), we find that  $n_2 = n^0 r_t$ . The thickness of fractures, which characterizes the average distance between the fracture traces on the plane, is determined from the relationship

$$\Gamma = \sqrt{n^0 r_t}. \quad (2.28)$$

When  $y \geq 1.5$ , virtually all fractures intersect with each other, and the permeability of the medium can be described by formula (2.25), if  $\Gamma$  is found from (2.28). After comparing the dependence (2.24) for  $\pi n^0 r_t^3 = 1.5$  to the relationship (2.25), we can find  $\gamma$  using (2.28). The resultant expression for the coefficient of permeability of the fractured medium is

$$K \cong 50b^3 \sqrt{n^0 r_t} (\pi n^0 r_t^3 - 1.5)^d (6.5\pi n^0 r_t^3 - 1)^{-d} \eta (\pi n^0 r_t^3 - 1.5).$$

Consider the case when the size distribution of the circular fractures in the medium is described by the function  $f(r_t)$ . Using this distribution and the formula (2.23), we obtain the following expression

$$y = \pi n^0 \langle r_t^2 \rangle \langle r_t \rangle, \quad (2.29)$$

where  $\langle r_t \rangle = \int_0^\infty r_t f(r_t) dr_t$ ,  $\langle r_t^2 \rangle = \int_0^\infty r_t^2 f(r_t) dr_t$ . Consequently the number of adjacent sites is

$$z = 2\pi[(1 + \pi/2) \langle r_t^2 \rangle \langle r_t \rangle + (2/3) \langle r_t^3 \rangle] - 1, \quad (2.30)$$

where  $\langle r_t^3 \rangle = \int_0^\infty r_t^3 f(r_t) dr_t$ .

Let the size distribution of fractures be represented by the following exponential relation

$$f(r_t) = \begin{cases} 0, & r_t > r_1, \\ (1 - e^{-r_1/r_0})^{-1} \exp(-r_t/r_0), & r_t \leq r_1, \end{cases} \quad (2.31)$$

where  $r_1$  is the greatest radius of a circular fracture.

When  $r_0 \ll r_1$ , it follows from (2.29) and (2.30) in accordance with (2.31), that  $y \cong 2\pi n^0 r_0^3$ ,  $z \cong 18\pi n^0 r_0^3 - 1$ . After substituting the found relations into (2.24) and taking account of (2.28) for  $r_t = r_0$ , we obtain the resultant expression for the permeability of the medium for the case of the exponential size distribution of fractures

$$K \cong 3 \cdot 10^2 b^3 \sqrt{n^0 r_0} (2\pi n^0 r_0^3 - 1.5)^d (18\pi n^0 r_0^3 - 1)^{-d} \eta (2\pi n^0 r_0^3 - 1.5). \quad (2.32)$$

(2.32) implies that when the variance of the size distribution function of fractures increases, a substantial drop of the percolation threshold follows. This phenomenon is caused primarily by the increase of the number of the nearest neighbors, and consequently by the increase of the probability of fractures intersecting with each other. It is quite interesting to compare the sizes of the pores and the fractures which correspond to the percolation threshold for a given concentration  $n^0$  in porous and fractured media. It follows from formulas (2.14) and (2.24) that  $R_p \approx 0.55r_t$ . That is, the presence of circular fractures in a medium is as effective in encouraging formation of an IC, as is the presence of pores with radii equal to exactly half the radius of a circular fracture. This fact implies that the conductivity of a medium is primarily affected not by the form of the conducting cut-ins, but by their maximal size.

## 2.5 Conductivity As a Function of the Strained State

Experimental data [48] show that the variation of the strained state of a medium can notably affect its conductivity. Relationships (2.1) and (2.4) obtained in §2.1 allow to find the change of the conductivity in the medium caused by external factors (pressure, temperature, etc.), if the nature of the effect which these parameters have on the distribution function  $f(r)$ , is known. Thus the problem of finding the correlation between the conductivity and the strained state of a medium reduces to that of determining the dependence of the intrinsic conductivity distribution for channels on the strained state of the medium. That is, the problem reduces to the study of the change in the effective capillary radii under external pressure. The problem of the correlation between the capillary size and the value of the strain tensor was discussed in [49] using the model of a nonlinearly

elastic fractured capillary porous medium. It is assumed in this model that the size of a conducting channel depends linearly on  $\epsilon_n$ , the component of the strain tensor which is normal to the channel. The value of  $\epsilon_n$  is calculated using the model of a nonlinearly elastic grained medium which takes account of the contact compressibility of the grains.

Note that generally the correlation between the size of the channels and the strain tensor can be more complex, especially for those media which have a plastic (clay) component. At the same time, as long as elastic deformations of grained media are considered, the assumption of a linear dependence of the channel size on the value of the strain tensor appears reasonable. Under this assumption, find the change of the distribution function  $f(r)$  caused by the stress tensor  $\sigma_i$  applied to the medium. In the case of a uniform comprehensive contraction of the medium, the correlation between the radius  $r'$  of a channel in the loaded medium and the initial radius  $r$  can be described as follows

$$r' = r + 0.5l\epsilon_n. \quad (2.33)$$

Here  $\epsilon_n = \epsilon^0/3$ , where  $\epsilon^0$  is the volumetric deformation, and  $l$  is the grain diameter.  $\epsilon^0$  depends not only on the stress applied, but also on Young's modulus which is a function of the stress. If the discussed medium is isotropic with respect to elastic properties, then the correlation between the small changes of deformations and stresses can be expressed by Hooke's law in the differential form

$$d\epsilon_i = \sum_{j=1}^3 \theta_{ij} \frac{d\sigma_j}{E(\sigma_j)}, \quad (2.34)$$

where

$$\theta_{ij} = \begin{cases} -1 & \text{when } i \neq j, \\ \mu_p, & \text{when } i = j; \end{cases}$$

$\mu_p$  is Poisson's modulus.

According to experimental data [49], the dependence of Young's modulus  $E$  of a grained medium on the principal stress  $\sigma_i$  applied along the  $x_i$ -axis can be written in the following form

$$E(\sigma_i) = A[1 - \exp(-B\sigma_i)] + C \quad (i = 1, 2, 3). \quad (2.35)$$

Here  $(A + C)$  and  $C$  are the maximum and the minimum values of Young's modulus,  $B$  is a constant. By "stress" we mean the "effective" stress, equal to the difference between the external load and the interior pressure in the pores. After integrating (2.34) using (2.35), we obtain the following ([49])

$$\epsilon_i = (A + C)^{-1} \sum_{j=1}^3 \theta_{ij} \{ \sigma_j + B^{-1} \log[E(\sigma_j)/C] \}. \quad (2.36)$$

If stress is relatively small ( $\sigma_j < 10^8 \text{ Pa}$ ) formula (2.35) can be simplified

$$E(\sigma_i) = C + AB\sigma_i.$$

In this case the expression (2.36) becomes

$$\epsilon_i = (1/g^0) \sum_{j=1}^3 \theta_{ij} \log(1 + g^0 \sigma_j / C), \quad g^0 = AB. \quad (2.37)$$

In the case of uniform comprehensive contraction,  $\sigma_j = \sigma^0$  and

$$\epsilon_n = \epsilon^0 / 3 = -[(1 - 2\mu_p) / g^0] \log(1 + g^0 \sigma^0 / C). \quad (2.38)$$

Thus, using formulas (2.33) and (2.38), one can find the distribution function of conducting channels in a medium subject to uniform contraction

$$f(r) = f[r + 0.5(l/g^0)(1 - 2\mu_p) \log(1 + g^0 \sigma^0 / C)]. \quad (2.39)$$

By substituting this function into formulas (2.1) and (2.4), one can find the change of the permeability and the electric conductivity of the medium. Formula (2.39) implies that within the framework of the model of the linear correlation between  $r$  and  $\epsilon_n$ , uniform comprehensive contraction of the medium does not change the shape of the distribution function but only causes its shift by  $0.5l\epsilon_n$ . The variation of the distribution function may change the parameter  $r_c$  as well as the average conductivity of the chains in the skeleton of the IC. We shall present here the resultant expression which determines how the coefficient of permeability of the medium depends on pressure  $P = \sigma^0$  (through the dependence (2.38))

$$K = 2\gamma\mu l^{-2} 2 \left( 1 - \int_0^{\Delta} f(r) dr \right)^{2\nu} \int_{\Delta}^{r_c} \left[ \int_{r_1}^{r_c} f(r) dr \right]^{\nu} \frac{f(r_1) dr_1}{I(r_1)} \quad (2.40)$$

$$\text{where } I(r_1) = (8/\pi) \int_{r_1}^{\infty} f(r)(r - \Delta)^{-4} dr \left( \int_{r_1}^{\infty} f(r) dr \right)^{-1}, \quad \Delta = 0.5l\epsilon_n.$$

The specific electric conductivity of the medium in this case is also found from formula (2.40), but with

$$I(r_1) = l^{-1} \int_{r_1}^{\infty} f(r)[\rho_0(r - \Delta) + \Pi\Phi(\omega)] dr \left( \int_{r_1}^{\infty} f(r) dr \right)^{-1}.$$

When contraction of the medium under the stress tensor  $\sigma_i$  is not monoaxial, the components of the strain tensor  $\epsilon_i$  are found from the formula (2.36).

Consider, for instance, a channel oriented parallel to the principal axis  $i = 1$ . The change of its cross-section is determined from the values of  $\epsilon_2$  and  $\epsilon_3$ , i.e., by those components of the strain tensor, which are perpendicular to the axis of the channel. Assuming that the cross-section  $s_i$  of a channel is proportional to the product of its dimensions along the directions perpendicular to its axis, we obtain that  $s_i \sim (r + 0.5l\epsilon_2)(r + 0.5l\epsilon_3)$ . Consequently the effective channel radius is  $r_{eff} = s_i^{\frac{1}{2}}$ . If the condition  $0.5l\epsilon_{2,3} \gg r_{eff}$  is satisfied, then the change in the effective radius of the channel in the first approximation is

$$\Delta r_{eff} \cong (l/4)(\epsilon_2 + \epsilon_3).$$

Using (2.36) we get

$$\Delta r_{eff} = l/(4g^0) \sum_{j=1}^3 (\theta_{2j} + \theta_{3j}) \log(1 + g^0 \sigma_j / C). \quad (2.41)$$

Similar dependencies take place for the channels oriented in directions  $i = 2, 3$ . Note that if the condition  $\Delta r_{eff} < r_{eff}$  is satisfied, then the channels do not close under the applied load, the value of  $\kappa$  does not change, and the structure of the IC is preserved. Therefore the change of the conductivity in the medium for this case is caused only by the change in the conductivities of the chains. If the tortuosity of the chains is not taken into account, then the average conductivity of a unit length of chains is described by (1.9). In this case the distribution function  $f(r')$  is of the following form,  $f(r') = f(r + \Delta r)$ , where  $f(r)$  is the distribution function for  $\sigma_i = 0$  and  $\Delta r = \Delta r_{eff}$  found from (2.41). When deformation of the medium happens at a constant pressure  $p = (1/3)(\sigma_1 + \sigma_2 + \sigma_3)$  and the condition  $\Delta\sigma_1 = 0.5\sigma_2 = 0.5\sigma_3$  is satisfied, a case which is of practical importance, the expression (2.41) appears in a less complicated form

$$\Delta r_{eff} = l/(2g^0) \{ (\mu_p - 1) \log[1 - g^0(p - 0.5\Delta\sigma_1)/C] + \mu_p \log[1 + g^0(p + \Delta\sigma_1)/C] \}. \quad (2.42)$$

Formulas (1.9), (1.11), (2.20), and (2.41) define the values of the corresponding components of the permeability tensor. Similar relationships take place for the specific electric conductivity of the medium.

The relationships presented allow to calculate the change of the coefficients of permeability in the medium given the distribution function of pore channels with respect to values of intrinsic conductivities. The problem of determining  $f(r)$  will be studied in detail in further sections of this book. Now we shall use the most common approximation of the porometric curves obtained from experiment [48]

$$f(r) = a_*/r^2 \cdot \eta(r - a_*), \quad (2.43)$$

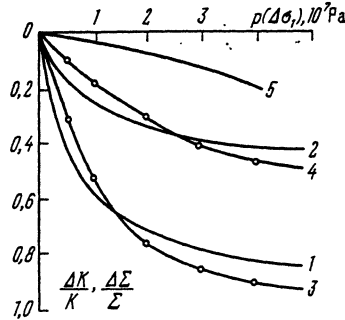


Figure 11: Plots of the conductivity of the medium against its strained state

where  $a_*$  is the minimal radius of a conducting capillary.

Since in the three-dimensional case  $\nu = 0.9 \pm 0.1$ , it is possible to find  $K$  for an exponential function analytically, using formula (2.1), if  $\nu$  is set to equal 1. In this case we get  $r_c = 4a_*$ ,  $K = 2.8\pi\gamma a_*^4/l^2$ . Setting  $\gamma = 2.85$ ,  $l = 0.5 \cdot 10^{-3}$  m,  $a_* = 0.5 \cdot 10^{-5}$  m, we find  $K = 18 \mu\text{m}^2$ . Using the relationships (2.39), (2.40), and (2.43) we can find the coefficient of permeability as a function of pressure  $P$

$$K(p) = \gamma' l^{-2} [a_* - 0.5l(g^0)^{-1} \log(1 + g^0 p/C)]^4.$$

Usually actual experiments measure the quantity  $\Delta K/K$ , where  $\Delta K = K(p) - K(0)$ . The theoretical relationship  $\Delta K/K$  calculated for  $g^0 = 10^3$ ,  $C = 15 \cdot 10^8$  Pa is presented in fig. 11 (curve 1). The plots of  $\Delta K/K$  and  $\Delta \Sigma/\Sigma$  against pressure, measured experimentally for a sandstone core in [48] (curves 3 and 4). are also presented in this figure. The theoretical dependence  $\Delta \Sigma/\Sigma$  (curve 2) has been calculated using formulas (2.4) - (2.6) for  $\lambda'/\sigma' = 7 \cdot 10^{-6}$  m,  $\Pi = 0$ , other parameters the same. Curve 5 corresponds to the difference  $\Delta K_1/K_1$  calculated using formulas (2.42), (1.9), and (1.11) for the case of anisotropic loading of a grained medium under constant pressure  $p = 200 \cdot 10^5$  Pa.

It can be noticed from fig.11 that a satisfactory agreement between theoretical and experimental data takes place for the given set of parameters of the model of a nonlinearly elastic porous medium. Note that the value of Young's modulus  $E \cong 10^3$  MPa differs from its actual characteristic values for typical reservoir rocks of the sandstone type by approximately an order of magnitude. Therefore the presented calculations correspond to strongly contractible rocks with large porosity.

The remarkable phenomenon of high sensitivity of the medium with  $E \cong 10^4$  MPa to relatively low pressures with small deformations can be explained, obviously, by significant impact that a film of a "bounded" fluid has on the flow in thin capillaries. This phenomenon will be studied in detail in the next chapter.

The change of the component of the permeability tensor  $K_1$ , found theoretic-

cally, is also close to the characteristic changes of the permeability tensor yielded by experiment. However, since the full set of experimental data is not available, it does not appear justifiable to compare experimental and theoretical data for the case of anisotropic loading of the medium.

## Chapter 3

# Percolation Model of Fluid Flow in Heterogeneous Media

Numerous cases of violation of the linear Darcy's law, which claims that the value of flux (flow rate) is directly proportional to the pressure gradient, has been observed. For very small flow velocities (pressure gradients) these deviations are caused by the formation of bounded fluid layers on the pore (capillary) surfaces [50, 51]. For relatively large velocities, deviations are caused by turbulence in the flow in pores (capillaries) and by the fluid kinetic energy losses on heterogeneities like capillary junctions, etc. [51, 52]. For sufficiently homogeneous media, it is possible to average the law describing flow at the micro level over the whole volume of the medium to extend it to the macro level [47]. However for some heterogeneous media, such an operation is not valid [52]. Indeed, if  $r_1$  and  $r_2$ , the radii of two successive capillaries, differ by an order of magnitude, then the local pressure gradients in them (for example, in the case of Poiseuille flow through the capillaries) are to one another as  $(r_1/r_2)^4$ , i.e., differ by a factor of  $10^4$ . In such a medium, all types of flow can take place at the micro level, namely the flow with the larger part of the pore space filled with bounded fluid; Poiseuille flow; transient flow from laminar to turbulent; and turbulent flow.

### 3.1 Flow at the Micro Level

Begin with some preliminary remarks and introduce some notations which will make the further presentation easier.



First of all, point out two limiting kinds of porous media, namely the one where the characteristic dimensions of sites (pores) are much greater than the characteristic cross-sections of bonds (capillaries); and the other one where the mentioned dimensions are of the same order of magnitude. Call the first of the described models, model I and the second one, model II.

Second of all, assume the porometric curve  $f(r)$  to be defined on an arbitrary interval  $[a_*, a^*]$  and to vanish outside this interval.

As it was shown in chapter 1, the conductivity of the infinite cluster depends substantially on its structure, or, more precisely, on the structure of its "skeleton" composed of chains formed by the conducting capillaries. To investigate properties of the "skeleton," it is reasonable to build an hierarchy of the conducting chains using the radius  $r_1$  of the thinnest capillary in the chain. We shall call such chains  $r_1$ -chains.

When  $r_1 = r_c$ , the  $r_1$ -chains contain only the largest capillaries ( $r_c \leq r \leq a^*$ ). These will be called the  $r_c$ -chains. When  $r_1 = a_*$ ,  $r_1$ -chains contain capillaries of all possible radii ( $a_* \leq r \leq a^*$ ). These will be called the  $a_*$ -chains.

Finally, for the conductivity  $k(r_1)$  of the chain, as in (1.9), introduce the notation of the mean value of an arbitrary function  $\psi(r)$  over an  $r_1$ -chain as follows

$$\langle r_1, \psi, a \rangle = \int_{r_1}^a \psi(r) f(r) dr \left( \int_{r_1}^{a^*} f(r) dr \right)^{-1}. \quad (3.1)$$

Consider the steady state one-dimensional flow under a given pressure gradient  $G$  with absolute value  $\Delta p L_0^{-1}$ , where  $\Delta p$  is the pressure difference in the medium at a distance  $L_0 \gg l$ . In this case, for an arbitrary  $r_1$ -chain of model II, we have

$$G = L_0^{-1} \left( \sum_i \Delta p_{ci} + \sum_i \Delta p_{ji} \right). \quad (3.2)$$

Here  $\Delta p_{ci}$ ,  $\Delta p_{ji}$  are the pressure differences in the  $i$ -th capillary and the junction of the  $i$ -th and the  $(i+1)$ -st capillaries, respectively. Summation in (3.2) is taken in the direction of the pressure increase, i.e., against the flow. Denote by  $q$  the flow of the fluid through an  $r_1$ -chain. Assume that  $\Delta p_{ji}$  depends only on the radii  $r$  and  $r'$  of the  $i$ -th and the  $(i+1)$ -st capillaries and on the flow  $q$ , while  $\Delta p_{ci}$  can be expressed in terms of the absolute value of the pressure gradient  $g_c(r, q)$  in the  $i$ -th capillary as is customary

$$\Delta p_{ci} = g_c(r, q)l, \quad \Delta p_{ji} = \Delta p_j(r, r', q). \quad (3.3)$$

The average pressure losses on the exit from a capillary of radius  $r$  in an  $r_1$ -chain  $\Delta p_j(r, q)$  are found by means of averaging  $\Delta p_{ji}$  over  $r'$  as in (3.1), using (3.3)

$$\Delta p_j(r, q) = \langle r_1, \Delta p_j(r, r', q), a_* \rangle. \quad (3.4)$$

After changing sums in (3.2) to mean values of the summands in the  $r_1$ -chain for a fixed  $q$ , we obtain the following, using notations in (3.3) and (3.4)

$$G = \alpha' \langle r_1, g_c(r, q), a_* \rangle + \alpha' l^{-1} \langle r_1, \Delta p_j(r, q), a_* \rangle, \quad (3.5)$$

where  $\alpha' = LL_0^{-1} \approx 1.5$ ,  $L$  is the length of the chain.

For model I, as in (3.5), we have

$$G = L_0^{-1} \left[ \sum_k (\Delta p_{ck} + \Delta p_{pk}) + \sum_k (\Delta p_{jk}^i + \Delta p_{jk}^f) \right].$$

Here  $\Delta p_{ck}$  and  $\Delta p_{pk}$  are the pressure drops on the  $k$ -th capillary of length  $l$  and on the pore of size  $l_p$  following this capillary, respectively. Summation is taken in the direction of the pressure increase.  $\Delta p_{jk}^i$  is the pressure drop on the entrance to the  $k$ -th capillary, and  $\Delta p_{jk}^f$  is the pressure drop on its exit. Estimates show that since  $r l_p^{-1} \ll 1$ , the pressure drops  $\Delta p_{pk}$  in the pores, as well as the pore size  $l_p$  dependencies of  $\Delta p_{jk}^f$  and  $\Delta p_{jk}^i$ , are negligible. In this case the pressure drops on the entrance to and the exit from a capillary depend only on its radius  $r$  and flow  $q$ . Denote them by  $\Delta p_j^i(r, q)$  and  $\Delta p_j^f(r, q)$ , respectively. As in (3.5), we have

$$G = \alpha'' \langle r_1, g_c(r, q), a_* \rangle + \alpha'' l^{-1} \langle r_1, (\Delta p_j^i(r, q) + \Delta p_j^f(r, q)), a_* \rangle, \quad (3.6)$$

$$\alpha'' = \alpha' l(l + l_p)^{-1}.$$

Denote the first terms in (3.5) and (3.6), i.e., the average pressure losses per unit length of a capillary, by  $C(r_1, q)$ . The second term in (3.5) and (3.6) (notation:  $J(r_1, q)$ ) describes the average pressure losses per unit length of heterogeneities, such as junctions of capillaries and sites. For model I, it is a capillary - pore junction; for model II, a capillary - capillary junction.

In this case expressions (3.5) and (3.6) can be written in the usual form

$$G(r_1, q) = C(r_1, q) + J(r_1, q). \quad (3.7)$$

The relationship (3.7) is an equation for flow  $q$  through an  $r_1$ -chain with fixed  $G$ , and its solution is  $q(r_1, G)$ . If the number of  $r_1$ -chains is found from (1.8), then the conductivity  $k(r_1, G)$  of the  $r_1$ -chain and the permeability  $K(G)$  of the medium are expressed as follows

$$k(r_1, G) = \mu q(r_1, G) G^{-1}, \quad K(G) = \int_{a_*}^{r_c} k(r_1, G) dn(r_1), \quad (3.8)$$

where  $\mu$  is the dynamic viscosity of the fluid.

After substituting  $q(r_1, G)$  into (3.7) and differentiating the obtained implicit function with respect to  $r_1$  for a fixed  $G$ , we get

$$\frac{\partial G}{\partial r_1} + \frac{\partial G}{\partial q} \frac{\partial q(r_1, G)}{\partial r_1} = 0. \quad (3.9)$$

Let

$$\partial G / \partial r_1 < 0, \quad \partial G / \partial q > 0. \quad (3.10)$$

The first inequality in (3.10) means that the greater the fraction of thin capillaries in a chain (the smaller  $r_1$ , the greater this fraction), the greater the pressure gradient required in the  $r_1$ -chain to let a fixed flow  $q$  pass through this chain. The second inequality in (3.10) means that the greater the flow  $q$  to pass through a fixed  $r_1$ -chain, the greater the average pressure gradient required in the chain. It now follows from (3.9) and (3.10) that  $\partial q(r_1, G) / \partial r_1 > 0$  and from (3.8), that

$$\frac{\partial k(r_1, G)}{\partial r_1} = \mu G^{-1} \frac{\partial q(r_1, G)}{\partial r_1} > 0. \quad (3.11)$$

According to (3.11), the conductivities of the  $r_1$ -chains increase with the increase of  $r_1$ , and therefore for every pressure gradient  $G$ , the hierarchy of  $r_1$ -chains built with respect to the radii  $r_1$  of the thinnest capillaries in the chains is the same as the hierarchy of the chains built with respect to the average conductivities  $k(r_1, F)$ .

The described approach to the construction of the laws describing the fluid flow in porous media holds for gas flow as well, and also allows some modification for other types of media, e.g., fractured and cavernous ones. If additional conditions like (1.10) are satisfied, then (3.11) holds as well.

Thus the considered plan for the construction of the law describing the fluid flow in micro heterogeneous media allows to study the flow of anomalous fluids as well as Newtonian ones, if the laws describing the flow of the former at the micro level are known.

To classify these laws, introduce the Reynolds number  $Re$  and the average velocity  $\nu$  in the capillary of radius  $r$ , when the flow of the fluid with density  $\rho_f$  equals  $q$ , as is customary

$$Re = 2r\nu(r)\rho_f/\mu = q\rho_f/(\pi r\mu), \quad \nu(r) = q/(\pi r^2).$$

Depending on  $Re$ , the conditions of the flow in capillaries can be broken up in three groups. When  $Re < Re_1$  the flow is laminar; when  $Re_1 \leq Re \leq Re_2$  it is transient from laminar to turbulent; when  $Re > Re_2$  it is turbulent. The critical values  $Re_1$  and  $Re_2$  of the Reynolds number for the tubes (capillaries) with circular cross-section lie in the following intervals,  $1500 < Re_1 < 2100$  and  $1900 < Re_2 < 3000$  [53].

**Laminar flow** ( $Re < Re_1$ ). Deviations from the Darcy's law for very small values of the flow rate are usually explained by the formation of the bounded fluid layers on the surfaces of pores (capillaries). These layers can fill a good part of the pore space and can decrease the permeability of the medium significantly, up to the total termination of the flow [50].

Results of a series of experiments on the flow in homogeneous media under small pressure gradients can be found in [54]. Present the empirical dependence that describes these results [50]

$$K = K_0(1 - G_0/G)^2. \quad (3.12)$$

Here  $G_0$  is the minimal pressure gradient, when the flow begins;  $K_0$  is the permeability for pressure gradients  $G \gg G_0$ , where Darcy's law is valid. Assuming that the pore space of a homogeneous medium consists of capillaries with radii  $r$  close to the average radius, after substitutions

$$K_0 = r^2/8, \quad K = \mu\nu g_1^{-1}$$

in (3.12) and some transformations, we can obtain the following correlation between the pressure gradient in the capillary and the value of flow in it

$$g_l(r, q) = g_0 + 0.5q_1^2 r^{-4} (1 + \sqrt{1 + 4g_0 q_1^{-2} r^4}), \quad q_1^2 = 8\mu q/\pi. \quad (3.13)$$

Here  $g_0(r)$  has the meaning of the minimal pressure gradient in a capillary. When  $q_1^2 \gg r^4 g_0(r)$  we get the well-known Poiseuille's formula

$$g_l(r, q) = 8\mu q/(\pi r^4).$$

**Transient regime of flow** ( $Re_1 \leq Re \leq Re_2$ ). The flow in this domain is intermediate from laminar and turbulent (Nikuradze's saddle [12]). It does not depend on the roughness of the capillary and can be described by a certain approximate formula. The latter is obtained after studying the plots of hydraulic resistance against the Reynolds number

$$g_m(r, q) = K_m q^i r^{-j}. \quad (3.14)$$

Here  $i = 2 \div 4$ ,  $j = 4 \div 8$ ,  $K_m$  is a dimensioned constant which depends on  $\rho_f$  and  $\mu$ .

**Turbulent flow** ( $Re > Re_2$ ). For a rough capillary, the following approximate formula can be used

$$g_t(r, q) = K_t q^s r^{-h}. \quad (3.15)$$

Here  $s = 1.8 \div 2.5$ ;  $h = 4 \div 6$ ,  $K_t$  is a dimensioned constant which depends on  $\rho_f$ ,  $\mu$ , and the degree and the type of roughness.

**Energy losses on junctions of the "capillary - capillary" ("capillary - pore") type.** A boundary element of a junction of two successive capillaries in model II or a boundary element between a pore and a capillary in model I can be taken as a local resistance element. Let the radius of the thin capillary at the junction equal  $r$  and the radius of the thick one,  $r'$ . There was a lot of publications dealing with the determination of the energy losses in question in the scientific press. A review of them appears, for instance, in [55] or in [53], where the following semi-empirical formula is proposed

$$\Delta p_j(r, r', q) = 0.5Z(r, r', q) \rho_f \nu^2(r), \quad (3.16)$$

$$Z(r, r', q) = \zeta_\nu(r, r', q) + \zeta_i(r, r', q).$$

Here  $\zeta_\nu(r, r', q)$  is the coefficient of losses caused by viscous forces on the boundary;  $\zeta_i(r, r', q)$  is the coefficient of losses caused by inertial forces.

When  $\text{Re} \gtrsim 300$ ,  $\zeta_i \gg \zeta_\nu$ , and therefore  $Z \approx \zeta_i$ . The following semi-empirical formulas of Borde are valid for  $\zeta_i$ :

$$\zeta_i^f(r, r') = B^f [(r/r')^2 - \epsilon^{-1}(r'/r)]^2, \quad (3.17)$$

$$\zeta_i^i(r, r') = B^i [1 - \epsilon^{-1}(r'/r)]^2,$$

with  $\zeta_i = \zeta_i^f$  when the fluid flows from the capillary of radius  $r$  to the one of radius  $r'$  ( $r < r'$ ), and  $\zeta_i = \zeta_i^i$  when the flow is in the opposite direction. The coefficients  $B^i$  and  $B^f$  are of the order unity. The function  $\epsilon(r'/r)$  in (3.17) characterizes the extent to which the stream is compressed. For  $r'/r \gtrsim 3$  the function  $\epsilon(r'/r)$  is almost constant and equal to  $\epsilon \cong 0.61$ , and as  $r'/r$  goes to unity,  $\epsilon(r'/r)$  also goes to unity.

When  $\text{Re} \lesssim 10 \div 30$ ,  $\zeta_\nu \gg \zeta_i$ , and therefore  $Z \approx \zeta_\nu$ . The function  $\zeta_\nu$  satisfies Wust's formula

$$\zeta_\nu(r, r', q) = A(r, r') R e^{-1}(r, q). \quad (3.18)$$

For  $r'/r \gtrsim 1.3$  the dependence of  $A(r, r')$  in (3.18) on  $r$  and  $r'$  is weak, and the value of this function is  $A \approx 20 \div 40$ . As  $r'/r$  goes to unity ( $r'/r \lesssim 1.1$ ),  $A(r, r')$  goes down to zero very quickly. The relationship (3.18) holds for both directions of flow.

In the interval  $30 \gtrsim \text{Re} \gtrsim 20 \div 40$  the values of  $\Delta p_j(r, r', q)$  can be found with the accuracy good enough for practical calculations by substituting (3.17) and (3.18) into (3.16).

## 3.2 Effect of Pore Space Structure on Laws for Macroscopic Flow

The foregoing relations (3.13), (3.14), (3.15) for flow types in the capillaries and (3.16) for the pressure losses on the junctions allow to specify the form of the equation (3.7) which relates the flow  $q$  through an arbitrary  $r_1$ -chain ( $a_* \leq r_1 \leq r_c$ ) to the pressure gradient  $G$  in the medium.

Consider the second term,  $J(r_1, q)$ , in (3.7). In model I each capillary of radius  $r$  joins with the pore of size  $l_p \gg r$  both at its entrance and exit. After setting  $r' = 0.5l_p$  and passing in (3.17) and (3.18) to  $r' \gg r$  ( $A(r, r'0 \approx A_0$ ,  $\epsilon(r'/r) \approx \epsilon_0$ ), we obtain the following from (3.16) and (3.6)

$$J(r_1, q) = \mu V(r_1)q + 0.5 \rho_f I'(r_1) q^2, \quad (3.19)$$

$$V(r_1) = \gamma_\alpha \langle r_1, r^{-3}, a^* \rangle,$$

$$I'(r_1) = d_\alpha \langle r_1, r^{-4}, a^* \rangle, \quad (3.20)$$

$$\gamma_\alpha = 0.5 \alpha' l^{-1} \pi^{-1} A_0,$$

$$d_\alpha = \alpha' l^{-1} \pi^{-2} \epsilon_0^{-2} [B^j + (1 - \epsilon_0)^2 B^i].$$

For model II, after averaging (3.16) over  $r'$  in accordance with (3.4) with further substitution of the averaged result into the second term of (3.5) (and then averaging the latter with respect to  $r$ ), we shall arrive back at (3.19), but with different functions  $V(r_1)$  and  $I'(r_1)$

$$V(r_1) = \gamma_b \langle r_1, [\langle r_1, A(r, r')/r'^3, r \rangle + r^{-3} \langle r, A(r, r'), a^* \rangle], a^* \rangle,$$

$$I'(r_1) = d_b \langle r_1, [\langle r-1, \zeta_i^f(r, r')/r'^4, r \rangle + r^{-4} \langle r, \zeta_i^f(r, r'), a^* \rangle], a^* \rangle, \quad (3.21)$$

$$\gamma_b = 0.25 \alpha' \pi^{-1} l^{-1}, \quad d_b = \alpha' \pi^{-2} l^{-1}.$$

Introduce the following notations

$$r_m(q) = d_1 q, \quad r_d(q) = d_2 q, \quad (3.22)$$

$$d_i = (0.5 \pi \text{Re}_i \rho_f / \mu)^{-1}, \quad i = 1, 2,$$

$$q_t = a^* d_2^{-1}, \quad q_{tm} = a^* d_1^{-1}, \quad q_{mm} = r_1 d_2^{-1}, \quad qlm = r_1 d_1^{-1}.$$

We shall now specify the form of equation (3.7), taking into account the relationship (3.19) for various pressure gradients, starting with the interval of large  $g$ 's.

**Turbulent flow.** When  $r_d(q) \geq a^*$ ,  $q \geq q_t$ . In this case, according to (3.22) and (3.19),  $\text{Re}(r_1) \geq \text{Re}(r) \geq \text{Re}(a^*) \geq \text{Re}_2$ , and therefore the flow in all capillaries of the  $r_1$ -chain is turbulent.

Equation (3.7) becomes

$$G = \alpha' \langle r_1, g_t(r, q), a^* \rangle + J(r_1, q). \quad (3.23)$$

The least absolute value of the gradient  $G_t(r_1)$  when (3.23) still holds can be found by substituting  $q_t$  into (3.23)

$$G_t(r_1) = \alpha' \langle r_1, g_t(r_1, q_t), a^* \rangle + J(r_1, q_t) G > G_t(r_1). \quad (3.24)$$

Substituting (3.15), (3.19) into (3.23), (3.24) confirms (3.10) and (3.11) and results in the following inequality

$$dG_t(r_1)/dr_1 < 0.$$

Hence, as  $G$  goes up, the first to transfer to turbulent flow are the  $r_c$ -chains and the last are the  $a_*$ -chains. Moreover for heterogeneous media, the interval where  $G_t(a_*) \geq G \geq G_t(r_c)$  can be rather lengthy. If  $G > G_t(a_*)$ , then the flow in all capillaries in the medium is turbulent. After substituting (3.15) with  $s = 2, h = 5$  [53] into (3.23) and neglecting the first term in (3.19), we find from (3.8) that

$$K(G) = \mu G^{-1/2} \int_{a_*}^{r_c} (\alpha' K_t \langle r_1, r^{-5}, a^* \rangle + 0.5 r h o_f I'(r_1))^{-1/2} dn(r_1). \quad (3.25)$$

The relationship (3.25) expresses the well-known quadratic law of fluid flow.

**Turbulent - transient flow.** When  $r_m(q) \geq a^* \geq r_d(q) \geq r_1, q_t \geq q \geq q_{tm}$ , the flow in the capillaries of the  $r_1$ -chain with radii  $r$  from  $r_1 \leq r \leq r_d(q)$  ( $\text{Re}(r_1) \geq \text{Re}(r) \geq \text{Re}_2$ ) is turbulent, and the flow in the capillaries with radii from  $r_d(q) < r \leq a^*$  ( $\text{Re}_2 > \text{Re}(r) \geq \text{Re}_1$ ) is transient. Equation (3.7) becomes

$$G = \alpha' \langle r_1, g_t(r, q), r_d(q) \rangle + \alpha' \langle r_d(q), g_m(r, q), a^* \rangle + J(r_1, q). \quad (3.26)$$

The range of  $G$  where (3.26) is valid can be found by substituting  $q_t$  and  $q_{tm}$  into (3.26)

$$G_t(r_1) \geq G \geq g_{tm}(r_1),$$

$$G_{tm}(r_1) = \alpha' \langle r_1, g_t(r, q_{tm}), z_a \rangle + \alpha' \langle z_a, g_t(r, q_{tm}), a^* \rangle + J(r_1, q_{tm}),$$

$$z_a = d_2 a^* d_1^{-1}.$$

Using (3.14), (3.15), and (3.19), one can confirm the validity of (3.11) and obtain the following inequality,  $dG_{tm}(r_1)/dr_1 < 0$ . Therefore the first to transfer to the turbulent - transient flow with the increase of  $G$  are the  $r_c$ -chains, and the last are the  $a_*$ -chains.

**Transient regime of flow.** When  $r_m(q) \geq a^* \geq r_1 \geq r_d(q)$ ,  $q_{m m} \geq q \geq q_{t m}$

$$(\text{Re}_1 \leq \text{Re}(a^*) \leq \text{Re}(r) \leq \text{Re}(r_1) \leq \text{Re}_2), \quad (3.27)$$

the flow in all capillaries of the  $r_1$ -chain is transient. The inequality (3.27) can be satisfied only for  $a^*r_1^{-1} \leq d_1d_2^{-1} \lesssim 1.5$ , and therefore the transient flow cannot take place in any  $r_1$ -chain of a medium where  $a^*a_*^{-1} > d_1d_2^{-1}$ . The equation (3.7) becomes

$$G = \alpha' < r_1, g_m(r, q), a^* > + J(r_1, q). \quad (3.28)$$

After substituting  $q_{m m}$  and  $q_{t m}$  into (3.28) we find the domain of validity for (3.28) to be

$$\begin{aligned} G''_m(r_1) &\geq G \geq G'_m(r_1), \\ G''_m(r_1) &= \alpha' < r_1, g_m(r, q_{m m}), a^* > + J(r_1, q_{m m}), \\ G'(r_1) &= \alpha' < r_1, g_m(r, q_{t m}), a^* > + J(r_1, q_{t m}). \end{aligned} \quad (3.29)$$

By substituting (3.14), (3.19) into (3.29), one can make sure that conditions (3.10) and (3.11) are satisfied and obtain the inequality  $dG'_m(r_1)/dr_1 < 0$ .

**Turbulent-transient-laminar flow.** When  $a^* \geq r_m(q) \geq r_d(q) \geq r_1$  ( $q_{t m} \geq q \geq q_{m m}$ ), the flow in capillaries with radii  $r_1 \leq r \leq r_d(q)$  ( $\text{Re}(r) \geq \text{Re}_2$ ) in  $r_1$ -chains is turbulent; in those with radii  $r_d(q) < r \leq r_m(q)$  ( $\text{Re}_2 > \text{Re}(r) \geq \text{Re}_1$ ), transient; and in those with radii  $r_m(q) \leq r \leq a^*$  ( $\text{Re}_1 > \text{Re}(r) \geq \text{Re}(a^*)$ ), laminar. In this case the equation (3.7) becomes

$$\begin{aligned} G = \alpha' < r_1, g_t(r, q), r_d(q) > + \alpha' < r_d(q), g_m(r, q), r_m(q) > + \\ &\alpha' < r_m(q), g_l(r, q), a^* > + J(r_1, q). \end{aligned} \quad (3.30)$$

After substituting  $q_{t m}$  and  $q_{l m}$  into (3.30), obtain the range of  $G$  where (3.30) holds

$$\begin{aligned} G_{t m}(r_1) &\geq G \geq G_{l m l}(r_1), \\ G_{t m l}(r_1) &= \alpha' < r_1, g_m(r, q_{m m}), z' > + \alpha' < z', g_l(r, q_{m m}), a^* > + \\ &J(r_1, q_{m m}); \\ z' &= d_1r_1d_2^{-1}. \end{aligned}$$

If  $a^*r_1^{-1} < d_1d_2^{-1}$ , then the turbulent-transient-laminar flow cannot take place in the  $r_1$ -chain. If, moreover,  $a^*a_*^{-1} < d_1d_2^{-1}$ , then the discussed type can take place in no  $r_1$ -chain in the whole medium.

**Transient-laminar flow.** When  $a^* \geq r_m(q) \geq r_1 \geq r_d(q)$ ,  $q_{m m} \geq q \geq q_{l m}$ , transient flow takes place in those capillaries of the  $r_1$ -chain with radii  $r_m(q) \geq$



$r \geq r_1$  ( $\text{Re}_2 \geq \text{Re}(r_1) \geq \text{Re}(r) \geq \text{Re}_1$ ), whereas in those with radii  $a^* \geq r \geq r_m(q)$  ( $\text{Re}_1 > \text{Re}(r) \geq \text{Re}(a^*)$ ) the flow is laminar. Equation (3.7) in this case is

$$G = \alpha' < r_1, g_m(r, q), r_m(q) > + \alpha' < r_m(q), g_l(r, q), a^* > + J(r_1, q). \quad (3.31)$$

After substituting  $q_{m\ m}$  and  $q_{l\ m}$  into (3.31) we find the domain of validity for (3.31) to be

$$G_{t\ m\ l}(r_1) \geq G \geq G_{m\ l}(r_1), G_{m\ l}(r_1) = \alpha' < r_1, g_l(r, q_{l\ m}), a^* > + J(r_1, q_{l\ m}).$$

**Laminar flow.** When  $r_1 \geq r_m(q)$ ,  $q \geq q_{l\ m}$ , laminar flow takes place in all capillaries ( $\text{Re}_1 \geq \text{Re}(r_1) \geq \text{Re}(r) \geq \text{Re}(a^*)$ ) in the  $r_1$ -chain. Equation (3.7) here is

$$G = \alpha' < r_1, g_l(r, q), a^* > + J(r_1, q). \quad (3.32)$$

The validity condition for (3.32) can be obtained after substituting  $q_l$  into (3.32)

$$G_{m\ l}(r_1) \geq G. \quad (3.33)$$

If (3.33) holds for all  $r_1$ -chains ( $a^* \leq r_1 \leq r_c$ ), then the flow is laminar in the whole medium.

**Laminar flow under large pressure gradients.**

If the condition

$$q_{l\ m} \geq q \geq q_l \equiv \max(g_0(r)r^4\mu^{-1}),$$

is satisfied for all capillaries in the  $r_1$ -chain, then the flow in all capillaries is close to Poiseuille. After substituting  $q_l$  into (3.32) we get the boundaries of the domain where Poiseuille flow in an  $r_1$ -chain takes place

$$G_{m\ l} \geq G \geq G_l(r_1); \quad (3.34)$$

$$G_l(r_1) = \alpha' < r_1, g_l(r, q_l), a^* > + J(r_1, q_l).$$

After substituting (3.19) into (3.32) we get the following relations for Poiseuille flow

$$G = \mu(k_0^{-1}(r_1) + V(r_1))q + 0.5\rho_f I'(r_1)q^2, \quad (3.35)$$

$$k_0(r_1) = (\pi/8)(\alpha' < r_1, r^{-4}, a^* >)^{-1}.$$

Here  $k_0(r_1)$  is the conductivity of the  $r_1$ -chain when Poiseuille flow takes place in all of its capillaries if there are no pressure losses on junctions. If (3.34) holds for all  $r_1$ -chains, then it follows from (3.8) that

$$K(G) = \mu G^{-1} \int_{a^*}^{r_c} E(r_1)(\sqrt{1 + GF^{-1}(r_1)} - 1) dn(r_1), \quad (3.36)$$

$$E(r_1) = \rho_f \mu^{-1} I'^{-1}(r_1)(V(r_1) + k_0^{-1}(r_1)),$$

$$F(r_1) = 0.5 \rho_f I'(r_1) E^2(r_1).$$

Define the average radius  $\langle r \rangle$  of a capillary in the medium and the variance  $\sigma_d^2$  of the function  $f(r)$

$$\langle r \rangle = \langle a_*, r, a^* \rangle, \quad \sigma_d^2 = \langle a_*, (r - \langle r \rangle)^2, a^* \rangle.$$

If the medium is described by model II and is sufficiently homogeneous ( $\sigma_d \ll \langle r \rangle^{-1} \lesssim 0.1$ ), then  $k_0 \sim \langle r \rangle^4$ , and according to (3.21),  $V(r_1) \ll \langle r \rangle^4$ ,  $I'(r_1) \ll \langle r \rangle^5 \ll r_1 l^{-1}$ . In this case  $F(r_1) \gg G$ . After expanding the square root in (3.36) in powers of  $GF^{-1}(r_1)$  and taking the first three terms, we obtain the following

$$K(G) = \int_{a_*}^{r_c} k_0(r_1) dn(r_1) - \int_{a_*}^{r_c} V(r_1) k_0^2(r_1) dn(r_1) -$$

$$0.5 \rho_f G \mu^{-2} \int_{a_*}^{r_c} I'(r_1) k_0^3(r_1) dn(r_1). \quad (3.37)$$

The first integral in (3.37) is the permeability of the medium in the case when Poiseuille flow takes place in every capillary, and therefore this term does not depend on  $G$ . The presence of the second and third integrals in (3.37) is due to the decrease in the permeability of the medium because of, respectively, the viscous and the inertial pressure losses on heterogeneities like the capillary junctions. For homogeneous media, the relationship (3.37) is valid in the whole domain described by (3.34). However for heterogeneous media described by models I and II (when  $\sigma_d \ll \langle r \rangle^{-1} \gtrsim 1$ ) the contribution of the third term to (3.35) can become notable; in the domain  $G \lesssim G_{ml}(r_1)$ , where  $\text{Re}(r_1) \lesssim \text{Re}_1$ , the term can even become dominant. Thus in heterogeneous media, permeability can decrease by several times merely because of the inertial pressure losses on the capillary - capillary (capillary - pore) junctions, with no turbulence in capillaries. As for homogeneous media, it is known that any notable decrease in permeability is possible only as a result of turbulence in capillaries.

**Laminar flow under very small pressure gradients.** If the condition

$$q \ll q_0 = \min(g_0(r)r^4 \mu^{-1}) \quad (3.38)$$

is satisfied for all capillaries in an  $r_1$ -chain, then after expanding (3.13) in powers of the small parameter  $q_1^2 g_0^{-1}(r)r^4$ , we get the right side of (3.7) as a series in  $q_1$ . The number of terms to be taken in the series (3.7) depends on the form of  $g_0(r)$ ,  $f(r)$ , the size of the range  $G$  under consideration, and the required accuracy of

calculations. Consider (3.7), taking the first three terms in the expansion

$$\begin{aligned}
 G &= G_0(r_1) + q_1 M(r_1) + q_1^2 N(r_1), \\
 G_0(r_1) &= \alpha' < r_1, g_0(r), a^* >, \\
 M(r_1) &= \alpha' < r_1, g_0^{1/2}(r) r^{-2}, a^* >, \\
 N(r_1) &= \pi/8[2k_0^{-1}(r_1) + V(r_1)].
 \end{aligned} \tag{3.39}$$

In writing out (3.39), we took into account the fact that the contribution of the quadratic term of  $q$  to (3.19) can be neglected in comparison with other terms in the equation (3.39). First negative terms appear in (3.39) only with the term proportional to  $q_1^5$ , and the term proportional to  $q_1^3$  does not appear at all.

The value  $G_0(r_1)$  can be called the minimal pressure gradient of the  $r_1$ -chain, since when  $G < G_0(r_1)$ , the flow in this  $r_1$ -chain stops because the thinnest capillaries get completely filled with the bounded fluid. After differentiating  $G_0(r_1)$  with respect to  $r_1$ , one can verify that  $dG_0(r_1)/dr_1 < 0$ , since  $g_0(r)$  is a monotone decreasing function of  $r$ . Thus if we decrease  $G$ , then at the point when  $G = G_0(a_*)$  the flow stops in the  $a_*$ -chain, and when  $G < G_0(a_*)$ , it stops in the chains with  $r_0(G) \geq r \geq a_*$  as well, where  $r_0(G)$  is found from the equation

$$G_0(r_0) = G. \tag{3.40}$$

If  $r_0 = r_c$ , then the flow stops in the largest  $r_1$ -chain, i.e., the medium becomes impermeable. Therefore  $G_0(r_c)$  can be called the minimal pressure gradient for the given medium. Taking account of the fact that  $q(r_1, G)$  is found from (3.7) for those  $r_1$ -chains with  $r_0(G) \leq r_1 \leq r_c$  and the fact that for the rest of the  $r_1$ -chains,  $a_* \leq r_1 \leq r_0(G)$ , we obtain the following relationship according to (3.8)

$$K(G) = \int_{r_0(G)}^{r_c} k(r_1, G) dn(r_1) \tag{3.41}$$

which is valid in the interval

$$G_0(r_c) \leq G \leq G_0(a_*). \tag{3.42}$$

If  $G > G_0(a_*)$ , then  $r_0(G)$  in (3.41) must be taken equal to  $a_*$ . The relationship (3.34) shows that when  $G$  varies within the domain (3.42) the following process takes place. First of all, the fluid flow begins or stops in the set of  $r_1$ -chains [see (3.40)] and second of all, the permeability  $k(r_1, G)$  of other conducting  $r_1$ -chains changes. These two factors cause strong dependence of the permeability on  $G$ . If the medium is heterogeneous, then the relationship (3.41) can have a rather complicated form, and the domain (3.42) can appear very lengthy, a fact which causes difficulties in determining its boundaries in an experiment. When

$G \geq G_0(a_*)$  the dependence  $K(G)$  becomes weaker. Since the second and the third terms in (3.39) are small if the condition (3.38) is satisfied and the inequality  $V(r_1)k_0(r_1) \ll \langle r \rangle l^{-1}$  is also satisfied, for sufficiently homogeneous media ( $\sigma_d \langle r \rangle^{-1} \ll 0.1$ ) the dependence  $k(r_1, G)$  near the permeability threshold  $G_0(r_c)$  of the medium can be found to have approximately the following form

$$k(r_1, G) \simeq 1/8k_0(r_1)(1 - G_0(r_1)G^{-1})^2GN_m(r_1)[1 - 1/2V(r_1)k_0(r_1) - 1/2GN_m(r_1)(1 - G_0(r_1)G^{-1})], \quad (3.43)$$

$$N_m(r_1) = 4N(r_1)M^{-2}(r_1) \gtrsim G_0^{-1}(r_1).$$

It is evident from (3.43) that the conductivity of an  $r_1$ -chain near  $G_0(r_1)$  is substantially less than its Poiseuille conductivity  $k_0(r_1)$ .

Introduce the Reynolds number for a medium

$$\text{Re} = d^0 \langle \nu \rangle \rho_f \mu^{-1}. \quad (3.44)$$

Here  $\langle \nu \rangle$  is the average flow velocity, and the quantity  $d^0$  is chosen using either the average grain size in the medium, or the average pore diameter. If we substitute  $K(G) = \mu \langle \nu(G) \rangle G^{-1}$  in (3.44), we obtain

$$\text{Re}(G) = K(G)Gd^0 \rho_f \mu^{-2}. \quad (3.45)$$

If we consecutively substitute into (3.45) the above boundary conditions for the pressure gradient for different types of flow and the corresponding values of permeability determined from (3.8), the critical Reynolds numbers for the medium can be obtained.

### 3.3 Results of Numerical Calculations and Comparison with Experiment

The experiment studied the flow of water ( $\rho_f = 10^3 \text{ kg/m}^3$ ,  $\mu/\rho_f = 10^{-6} \text{ m}^2/\text{s}$ ) in a medium whose pore space was simulated by a cubic network ( $P_c^b = 0.25$ ,  $\kappa = 0.5$ ) with pores situated in sites and connected with rough capillaries. The experimental relations found in [53] were used in the construction of the laws to describe the flow in capillaries and in the determination of the pressure losses on the capillary - capillary (capillary - pore) junctions: in (3.14),  $i = 3, j = 6, K_m = 3 \cdot 10^{-7} \rho_f^2 \mu^{-1} = 300 \text{ kg/m}^5$ ; in (3.15),  $s = 2, h = 5, K_t = 10^{-3} \rho_f = 1 \text{ kg/m}^3$ ; in (3.16) and (3.17),  $\alpha' = 1.5, B^i = B^f = 1, A_0 = 30$ .

The dependence  $g_0(r) = C_0 r^{-2}$  was taken from [50], where the value  $C_0 = 10^5 \text{ N/m}$  has been found experimentally [56]. To illustrate the dependence of the function  $K(G)$  on the form of the relationship  $f(r)$ , a numerical experiment was

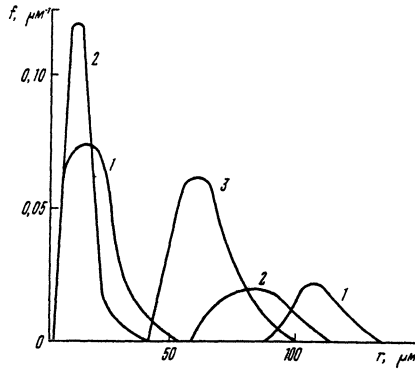


Figure 12: Plots of the density of the radius distribution for capillaries in heterogeneous media 1 - 3

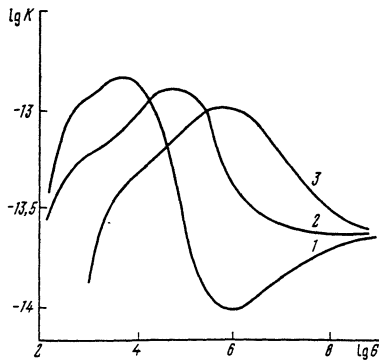


Figure 13: Curves for the permeability as a function of pressure gradients for media with different probability density functions for capillaries

carried out for three media with equal average capillary radii  $\langle r \rangle$  and variances  $\sigma_d$  which differed at least by 15 % ( $l < r >^{-1} = 20$ ,  $l_p = l$ ). The plots of  $f(r)$  are shown in fig.12, and the corresponding  $K(G)$  are shown in fig.13. It can be seen from fig.12 that equal values of  $\langle r \rangle$  and the proximity of  $\sigma_d$ 's for  $f(r)$  do not produce even qualitative similarity in the behavior of  $K(G)$ . Also note that the probability density functions  $f(r)$  having two "domes" can be found in fractured porous media, sandy-argillaceous media, and those media that have block and interblock porosity.

In fig.13 (curve 1), the first maximum and minimum of  $K(G)$  correspond to the passage of all large  $r_1$ -chains ( $r_1 > 110\mu\text{m}$ ) through all flow types consecutively, while in the thin  $r_1$ -chains ( $r_1 < 40\mu\text{m}$ ) separation of the bounded fluid is still in process (the domain described by (3.42)). According to (3.45), for example, some

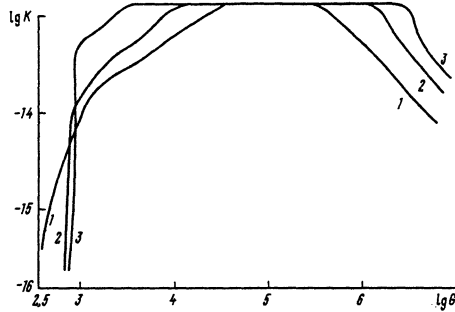


Figure 14: Curves for the permeability as a function of pressure gradients for media with exponential probability density functions for capillaries

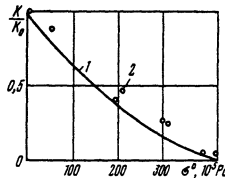


Figure 15: Permeability as a function of squeezing pressure: 1 - calculated curve, 2 - experimental data

critical values of the Reynolds number can be calculated for the relation  $K(G)$  shown on the curve 3:  $Re(G_0(r_c)) = 1.8 \cdot 10^{-6}$  (near the permeability threshold),  $Re(G_0(a_*)) = 3.4 \cdot 10^{-4}$  (flow has started in all  $r_1$ -chains),  $Re(G_t(a_*)) = 0.62$  (flow in all  $r_1$ -chains is Poiseuille),  $Re(G_{m1}(r_c)) = 6.9$  (the beginning of transient flow in the  $r_c$ -chain),  $Re(G_t(a_*)) = 29.3$  (turbulent flow in the whole medium).

The relations  $K(G)$  for the simpler probability density functions

$$f(r) = \text{const} \cdot r^{-i} \tag{3.46}$$

are shown in fig.14.

Curves 1-3 correspond to the values  $i = 2, 6, 10$ . The constant was chosen to satisfy the normalization condition for  $f(r)$  and for the values of  $K(G)$  to be equal in the domain defined by (3.34), where Darcy's law is valid. It can be seen from fig.14 that the values of  $K(G)$  in the domain (3.42) can differ by one to three orders of magnitude, whereas in the domain (3.34) they can differ by several times. The domain (3.34) shrinks with the increase of the variance of  $f(r)$  (with the decrease of  $i$ ), and the rate of the change decreases in the domain (3.42).

Numerical calculations of  $K(G)$  in accordance with (3.41) in the domain (3.42)

for  $g_0(r) = C_0 r^{-h}$  ( $h = 1.5; 2; 2.5; 3$ ) and of  $f(r)$  in the form (3.46) showed that in this range of  $G$ , changes of the permeability are very notable (by tens of times), and the greater  $h$ , the sharper the changes.

Using the experimental distribution function of [48], which corresponds to (3.46) for  $i = 4$  and  $a_* = 25\mu\text{m}$ , numerical calculations were carried out for the change of permeability of the medium when the relative elastic deformation of all capillaries in the conducting  $r_1$ -chains is the same (Hooke's law). The value of Young's modulus was taken as usual for sandstones,  $E = 10^4$  MPa (fig. 15).

Such sensitivity of the specimen's permeability towards its squeezing even with a small pressure (when the majority of deformations is elastic) is due to the fact that a good deal of  $r_1$ -chains, where the thinnest capillaries become completely filled with the bounded fluid, is excluded from the fluid flow. The described sensitivity is higher when the variance of  $f(r)$  is less.

Also note that the calculations carried out for the model in which the pore space of the medium is presented as a body of parallel tubes with constant radii gives a low (several per cent) change of the permeability, if the layers of the bounded fluid in thin tubes are taken into account, and deformations caused by squeezing the specimen are mostly elastic.

Thus the structure of the pore space of the medium can notably affect laws for macroscopic fluid flow, since various types of flow can take place at the micro level in such a medium. Therefore knowledge of merely the macroscopic parameters of a heterogeneous medium (i.e., some average coefficients of permeability and porosity or the average pore size) does not suffice to describe the fluid flow for different pressure gradients.

## Chapter 4

# Percolation Model of Steady State Multiphase Flow in Porous Media

Description of multi-phase transport in actual rocks is based on the determination of the effective macroscopic properties for micro heterogeneous media. In practice these properties are determined mostly through direct experiments which are rather cumbersome and time consuming. At the same time, simple theoretical models, like that of infinite cylindrical pores, are too inaccurate and insufficient to describe and explain many of the experimental data. To develop a more adequate theoretical description of multiphase transport at the micro-level, one should use the network models of the pore space structure and the percolation methods for analysis of these models, including the necessary calculations.

### 4.1 Steady State Flow of Immiscible Newtonian Fluids

Up to a fairly recent period, the majority of theoretical studies of two-phase flow was mostly dedicated to phenomenological models of Buckley - Leverett and Rapoport - Leas [57, 58]. Attempts made towards analyzing the said phenomenon at the micro-level were reduced to the simulation of the medium by a bundle of parallel capillaries with different radii. These attempts, however, bound to fail, since the sum of phase permeabilities for such a model is constant, while all the known experiments indicate otherwise.

Studying two-phase flow in heterogeneous media by means of numerical simu-



lation with network models was first reflected in the works [22, 59, 60, 61]. This approach does not have the drawbacks of the phenomenological and the "one-dimensional" models but neither does it possess the necessary universality of the obtained results, the latter being a typical advantage of analytical methods.

To obtain analytical relations which allow to calculate and analyze the behavior of the coefficients of phase permeability, we use the approach developed in chapter 1. Based on the obtained results, consider the displacement of a wettable fluid by a non-wettable one in a porous medium (we treat both fluids as incompressible and viscous). For clarity, we shall use the model which looks upon the medium as a cubic network whose sites (pores) are connected with bonds (capillaries) of different conductivities. We shall also continue to describe the conductivities of the capillaries by means of the probability density function  $f(r)$ .

Suppose that partial displacement of the phase which saturates the core took place in some macroscopic volume, and the ICG of the displacing fluid (further denoted by ICG) was formed. From now on, we shall mark the quantities relating to the wettable and the non-wettable fluids with indices 1 and 2, respectively. Assume that the fraction of capillaries filled with the wettable fluid exceeds the percolation threshold, and also that the medium contains an infinite cluster ICD of the capillaries containing the displaced phase. Obviously, the wettable fluid can be displaced only from those capillaries that satisfy the following condition

$$p_k(r) \leq \Delta p, \quad p_k(r) = 2\chi \cos \theta / r \quad (4.1)$$

and have contact with the ICG. Here  $\Delta p$  is the pressure difference in the fluids,  $\chi$  is the coefficient of surface tension, and  $\theta$  is the contact angle of the surface. In other words, displacement can take place only in those capillaries that can be reached by the displacing fluid along the chains which belong to the ICG.

By definition, the ICG consists of those capillaries that satisfy the condition (4.1). At the same time, the condition (4.1) can be also satisfied by some capillaries which do not belong to the ICG and are filled with the wettable fluid. However, as it will be shown later, the fraction of such capillaries, excluding a small domain near the percolation threshold, is small. Moreover, such capillaries do not affect the conductivity of the ICG at all, since they are not connected to it. From this point of view, it does not matter whether these capillaries are filled with the wettable or the non-wettable fluid. Thus the radius probability density for those capillaries that are conducting for the ICG, can be represented by the function

$$f_2(r) = \begin{cases} f(r)/\xi(r_k), & r \geq r_k, \\ 0, & r < r_k \end{cases} \quad (4.2)$$

Here  $r_k$  is the minimal radius of a capillary where displacement of the wettable fluid can take place for a given value of  $\Delta p$ .

By substituting  $f_2(r)$  into (2.1), we can find  $K_2$ , the permeability of the macroscopic volume under consideration, to the displacing fluid. Using the relationships for the absolute permeabilities  $K_0$  and  $K_2$  of the medium, one can find the analytical expression for the relative phase permeability  $k_2(r_k)$  of the displacing fluid. Relative phase permeabilities are defined by the relationships  $k_i = K_i/K_0$  ( $i = 1, 2$ ), and therefore can be found from (2.1) and (4.2)

$$k_2(r_k) = \int_{r_k}^{r_c} \left[ \int_r^{r_c} f_2(r) dr \right]^\nu \frac{f_2(r) dr}{I(r)} \left\{ \int_0^{r_c} \left[ \int_r^{r_c} f(r) dr \right]^\nu \frac{f(r) dr}{I(r)} \right\}^{-1} \quad (4.3)$$

Note that the resultant expression for relative phase permeability contains only the radius probability density function for capillaries and the percolation invariant  $\xi_c \equiv P_c^b$  which depends only on the network type and the dimension of the problem. Thus the resultant expression (4.3) is valid not only for a cubic network, but also for networks of other (in fact, any) types and dimensions. The network type affects the value of  $\xi_c$ , while the dimension of the problem affects the value of the exponent  $\nu$ .

To determine the relative phase permeability  $k_1$ , consider the structure of the ICD in a similar fashion. Obviously the ICD contains those capillaries from which the wettable fluid can by no means be displaced for a given value of  $\Delta p$ , i.e., the capillaries of radii  $r < r_k$ . Furthermore the ICD contains the capillaries with no displacing fluid in them whose radii exceed  $r_k$ . The fraction of such capillaries is

$$\alpha(r_k) = \xi - W(\xi), \quad \xi = \kappa \int_{r_k}^{\infty} f(r) dr$$

Here the quantity  $\xi$  defines the fraction of capillaries which satisfy the condition  $r > r_k$ , and the function  $W(\xi)$  defines the fraction of those of such capillaries contained in the ICG.

Near the percolation threshold  $\xi = \xi_c$ , the asymptotics (1.6)  $W(\xi) \sim |\xi - \xi_c|^\beta$  is valid, where  $\beta = 0.4$  when  $D = 3$ . Hence  $\xi - W(\xi) \approx \xi_c \sim (1 \div 2) \cdot 10^{-1}$  when  $|\xi - \xi_c| \ll 1$ . However, starting from the values  $\xi - \xi_c \approx 10^{-1}$  and further, up to  $\xi = 1$ , the dependence  $W(\xi)$  becomes linear ( $W(\xi) = \xi$ ) very quickly. This means that  $\alpha(r_k) = 0$  in the outlined range of  $\xi$ . Thus the coefficient  $\alpha(r_k)$  is of the order of  $10^{-1}$  only in the closest vicinity of the percolation threshold when the ICG is formed, while further on, with the increase of  $\xi$ , it goes to zero very quickly.

Consider equilibrium flow, i.e., the process of the ICG formation when the percolation threshold  $\xi \cong \xi_c$  is crossed, is not being analyzed. The study is carried out under the assumption that the dynamic stage of growth of the chains forming the ICG is finished, and that the cluster is already a sufficiently stable formation in the space. Formally this means that the quantity  $\xi$  is finitely separated from

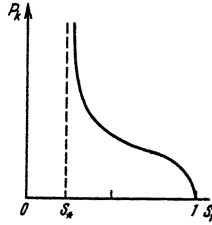


Figure 16: Typical form of the capillary pressure curve (Leverett's function)

the percolation threshold  $\xi_c$ ,  $\xi - \xi_c \sim 10^{-1}$ . In this case we obtain the following estimate for  $\alpha(r_k)$ ,  $\alpha(r_k) \leq 10^{-2}$ . Now we shall set  $\alpha(r_k) = 0$  to make further the computations easier. Taking account of this assumption, we can represent the probability density function  $f_1(r)$  for capillaries, which defines the conductivity of the ICD, in the following form

$$f_1(r) = \begin{cases} 0, & r > r_k, \\ f(r)/(1 - \xi(r_k)), & r \leq r_k \end{cases} \quad (4.4)$$

Using (2.1) and (4.4), we find the formula for the relative phase permeability

$$k_1(r_k) = \int_0^{r'_c} \left[ \int_r^{r'_c} f_1(r) dr \right]^\nu \frac{f_1(r) dr}{I(r)} \left\{ \int_0^{r_c} \left[ \int_r^{r_c} f(r) dr \right]^\nu \frac{f(r) dr}{I(r)} \right\}^{-1} \quad (4.5)$$

Here  $r'_c$  is defined by the relationship

$$\int_{r'_c}^{r_k} f(r) dr = \xi_c. \quad (4.6)$$

It is interesting to obtain the correlation between the found expressions for the relative phase permeabilities and the quantity  $S_1$  which characterizes saturation of the medium with the wettable fluid.

Consider two limiting cases of  $S_1$  calculation. If we use model I, then we can estimate  $S_1$  under the assumption that the number of pores filled with the wettable fluid is proportional to the number of capillaries filled with it. If the sizes of the pores do not differ significantly, then

$$S_1 = \int_0^{r_k} f(r) dr \quad (4.7)$$

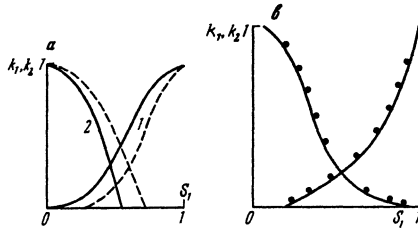


Figure 17: Phase permeability curves calculated using model exponential (a) and log-normal (b) distribution functions

In model II the quantity  $S_1$  is defined by the volume of capillaries which conduct the first fluid. In this case

$$S_1 = \int_0^{r_k} f(r) r^2 dr \left[ \int_0^\infty f(r) r^2 dr \right]^{-1} \tag{4.8}$$

Thus the formulas (4.3) and (1.7) for  $\sigma_1 = r_c$ ,  $P^b = \xi_c$  and (4.5) - (4.8) define parametric dependencies of the relative phase permeabilities on saturation of the medium for the two models mentioned above.

Note that the probability density function for capillaries, together with (4.8) or (4.7), defines Leverett's function  $p_k = (S_1)$ , which sets the correlation between the capillary pressure and the saturation of the specimen during equilibrium flow. The phase permeabilities and Leverett's function make up the complete set of data necessary for calculating the two-phase flow. To define the function  $f(r)$  in the form most convenient for future computations, investigate the behavior of Leverett's function  $p_k = (S_1)$  (its typical form is presented in fig.16). Using the following formula for the derivative,  $dS_1/dr = dS_1/dp_k \cdot dp_k/dr$ , and taking account of the fact that  $p_k \sim r^{-1}$ , we obtain the following estimate from either (4.7) or (4.8)

$$f(r) \sim A' \left| \frac{dS_1(r)}{dp_k} \right| \frac{1}{r^2}$$

where  $A' = r^{-2}$  in the case (4.8) and  $A' = 1$  when  $S_1$  is defined by formula (4.7).

Since today there are virtually no reliable ways of experimental determination of the probability density function for capillaries with respect to values of intrinsic conductivities, it seems reasonable to carry out qualitative analysis of the phase permeabilities for a model probability density function. Since  $f(r) \rightarrow 0$  as  $r \rightarrow \infty$ , in the general case this function can be represented in the form of an expansion

in negative powers of  $r$  (Weierstrass's theorem)

$$f(r) = \sum_{i=1}^{\infty} a_i/r^i$$

where  $a_i$  are the coefficients of the expansion. By choosing the principal term in the sum, which makes the major contribution to  $f(r)$ , and taking it as a model probability density function, we can obtain analytical expressions for the phase permeabilities and the capillary pressure. Take a model probability function as in the empirical dependence (3.46)

$$f(r) = 0, \quad (a_* < r, r > a^*), \quad f(r) = \frac{a_* a^*}{a^* - a_*} \frac{1}{r^2}, \quad (a_* \leq r \leq a^*) \quad (4.9)$$

Here  $a^*$  defines the maximum possible capillary radius; obviously,  $a^*$  cannot exceed the size of a grain in the medium. The quantity  $a_*$  defines the minimum radius of a conducting capillary. The existence of such a limiting radius can be related, for instance, to the fact that each capillary has a double electric layer which hinders fluid flow through thin capillaries because of the exceedingly large viscosity generated there.

After using, for determinedness, the relationship (4.8) in the case (4.9), we find the following correlation between the saturation of the medium with the wettable fluid and the quantity  $r_k$

$$S_1 = (r_k - a_*)/(a^* - a_*) \quad (4.10)$$

The phase permeabilities found from relationships (4.3) - (4.5) and (4.10) are presented in fig.17, *a*, where the curves  $k_1(S_1)$  and  $k_2(S_1)$  are denoted by numbers 1 and 2, respectively. In the same figure, the functions  $k_1(S_1)$  and  $k_2(S_1)$  in the case when saturation is defined by the relationship (4.7) (model I) are drawn in dotted lines. Fig.17, *b*, contains the phase permeability curves obtained in the case when

$$f(r) = (\sqrt{2\pi\sigma_d} r)^{-1} \exp[-(\log r - \mu')^2/(2\sigma_d^2)],$$

a form of the dependence  $f(r)$  used in numerical calculations in [60]. As in [60], the parameters were set as follows,  $\sigma_d = 0.25$ ,  $\mu' = 2$ ,  $z = 6$ . The results of the numerical simulation of the two-phase flow using the network models [60] presented in fig.17, *b*, (dots) show that the outcomes of analytical and numerical calculations for the same function  $f(r)$  coincide satisfactorily. For the limiting cases ( $S_1 \rightarrow 1$  and  $S_1 \rightarrow a_*/a^*$ ), setting  $\nu = 1$ , we can obtain the asymptotic expressions for the relative phase permeabilities by expanding the corresponding relations in powers of the small parameter  $\epsilon_1 = a_*/a^* \ll 1$ . After taking only the first terms in the expansions we obtain the following

$$k_1(S_1) = \begin{cases} 1 - 2\epsilon_1/(\xi_c S_1), & S_1 \rightarrow 1, \\ \xi_c^2 (S_1^2/\epsilon_1^2 - 1), & S_1 \rightarrow \epsilon_1 \end{cases} \quad (4.11)$$

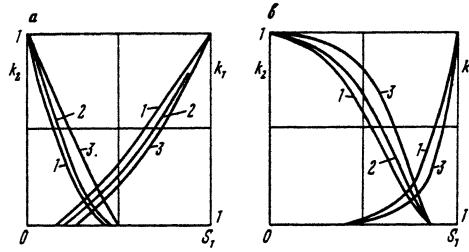


Figure 18: Curves for the phase permeabilities as functions of pressure

$$k_2(S_1) = \begin{cases} 0 & , S_1 > \epsilon_1/\xi_c, \\ 1 - (S_1\xi_c/\epsilon_1)^2 & , S_1 \leq \epsilon_1/\xi_c \end{cases} \quad (4.12)$$

Analysis of relation (4.11) shows that when  $S_1 \rightarrow 1$ , the curve  $k_1(S_1)$  is convex upward, and its slope at the point  $S_1 = 1$  is non-zero. When  $S_1 \rightarrow \epsilon_1$ , the curve is convex downward, and its slope at the point  $S_1 = \epsilon_1$  is close to zero. Similarly it can be seen from relationship (4.12) that the curve  $k_2(S_1)$  is convex upward on the whole range. When  $S_1 \rightarrow \epsilon_1$ , we have  $k_2(S_1) \rightarrow 1$  with almost horizontal slope, while when  $S_1 \rightarrow \epsilon_1/\xi_c$ , we find that  $k_2(S_1)$  tends to zero rather quickly.

The relationship (4.10) also allows to obtain the dependence  $p_k(S_1)$  for the case of the equilibrium flow. Since  $p_k \sim r_k^{-1}$ , we find from (4.10) that

$$p_k(S_1) \sim [a_* + S_1(a^* - a_*)]^{-1}$$

and therefore  $p_k \rightarrow 0$  as  $S_1 \rightarrow 1$  and  $p_k \rightarrow \infty$  when  $S_1 \rightarrow 0 (S_1 \rightarrow \epsilon_1)$ . The qualitative form of the calculated dependence completely coincides with the one presented in fig.16.

The expressions (4.3) and (4.5) also describe the change of phase permeabilities of the medium under exterior factors (such as pressure, temperature, etc.), if their correlation with  $f(r)$  is known. In the case of elastic deformation of a granular medium under the stress tensor  $\sigma_i$ , we find the following correlation between the distribution function and the change of  $\sigma_i$  if the method presented in §2.5 is used,  $f(r) = f_0(r + \epsilon_i r_0)$ . If the distribution function  $f_0(r)$  is known for  $\sigma_i = 0$ , then the changes of the phase permeabilities can be determined from formulas (4.3) and (4.5).

The pressure dependencies of the phase permeabilities are presented in fig. 18, a, b. Calculations were carried out for the function  $f(r)$  defined by (4.9). The curves in fig. 18, a, correspond to the case when saturation is defined by the relationship (4.8), and the ones in fig. 18, b, to the case when it is defined by the relationship (4.7). For calculations, the following values were assigned,  $C = 1.5 \cdot 10^3$

MPa,  $g^0 = 10^3$ ,  $\mu_p = 1/3$ ;  $\tau_0/a_* = 0.2 \cdot 10^2$ . Calculations were performed for three values of pressure  $p = \sigma^0$ : the curves 1 - 3 correspond to the values 1, 7, and  $10^2$  MPa, respectively. It can be seen from fig.18 that the dependence  $k_2(S_1)$  is more sensitive to the pressure changes than is  $k_1(S_1)$ .

In this model, the phase permeabilities are completely determined by the probability density function for conducting capillaries with respect to values of intrinsic conductivities (the effective radius) and the value of the percolation threshold which characterizes the structure of the medium (the network type). Unfortunately today we do not possess reliable experimental data regarding the form of the function  $f(\tau)$ , and therefore it is impossible to calculate the phase permeabilities and compare the experimental and the theoretical dependencies numerically. However the results of the calculations made for the model probability density function demonstrate qualitative agreement of the experimental and the theoretical dependencies of the phase permeabilities. It should be pointed out that within the considered percolation model, dynamic effects [22] are all but not taken into account. At the same time, these effects can cause notable deviation of the flow from the quasi-stationary regime when the flow rate is large enough. In this case an important part can be played by the nature of the pressure distribution in the medium at the micro-level, a property which depends on the flow rate. Special research on this topic will be carried out further.

In conclusion, we want to note that the developed approach demonstrates the presence of the "endpoint effect" very clearly. This effect expresses itself in the trapping of the displacing phase near the surface of the rock until the saturation of the medium by the displaced fluid reaches a value close to the limiting one,  $S_{10} \sim \xi_c$ . Therefore the rock is impermeable for the second fluid practically up to the values of  $S_1 \cong 0.2 \div 0.4$ , and only after the saturation drops below the mentioned value of  $S_1 \approx S_{10}$ , the breakthrough of the displacing fluid occurs.

## 4.2 Effect of Plastic Properties of Fluids on Phase Permeabilities

Determination of the parameters of plastic flow in porous media is based on two principal assumptions. The first one concerns the description of the flow at the micro-level, i.e., through an elementary capillary (pore channel). According to this assumption, a certain analytical dependence of the shear rate  $\dot{\gamma}_s$  on tangent stress  $\tau_s$  is taken as the friction law of the fluid flow in capillaries. The flow of a viscous incompressible fluid through a capillary in this case can be described by

the formula [62]

$$q = \frac{8\pi R_g^3}{\tau_0^3} \int_0^{\tau_0} \tau_s^2 \phi(\tau_s) d\tau_s, \quad \tau_p = R_g \nabla p \quad (4.13)$$

Here  $q$  is the volumetric flow velocity in a capillary;  $\phi(\tau_s)$  is defined by the friction law  $\dot{\gamma}_s = \phi(\tau_s)$ ;  $R_g$  is the hydraulic radius of the capillary (in the case of a circular cylindrical capillary of radius  $r$ ,  $R_g = r/2$ );  $\nabla p$  is the pressure gradient in the capillary;  $\tau_p$  is the maximum shearing stress generated on the surface of the contact between the fluid and the capillary if the traditional condition of "sticking" (i.e., vanishing of the fluid velocity of the fluid) is granted.

Using (4.13), it is possible to express the pressure gradient of the fluid in the capillary as a function of the flow  $q$ ,  $\nabla p = \nabla p(q)$ .

According to the second assumption, the pore space structure is simulated by a regular network with pores situated in its sites and pore channels of circular cylindrical form the edges (bonds) of the network. All the inferences made from this model in the percolation approach, which takes account of the hierarchy in summation of the selected conducting chains, are the same as those outlined in §1.2. Among them, the relationship (1.8) holds for the distribution function  $n(r_1)$  of the  $r_1$ -chains, i.e., for those chains of the conducting capillaries with minimal radius  $r_1$  chosen in the direction of the exterior  $\nabla P$  when capillaries in the network in general are distributed according to some probability density function  $f(r)$ .

During the flow through a selected  $r_1$ -chain with flux  $q$ , a local gradient  $\nabla p$ , defined by (4.13), acts inside each of the capillaries. The macroscopic pressure gradient  $\nabla P$ , averaged over the chain, equals the following

$$\nabla P(r_1) = \int_{r_1}^{\infty} \nabla p(q) f(r) dr \left( \int_{r_1}^{\infty} f(r) dr \right)^{-1} \quad (4.14)$$

which results in the correlation  $q(r_1) = q(\nabla P(r_1))$ .

The total flux

$$Q = \int_0^{r_c} q(\nabla P(r_1)) dn(r_1) \quad (4.15)$$

Since the gradient  $\nabla P$  is the same for all  $r_1$ -chains, (4.15) describes the correlation between the flux  $Q$  through a porous medium and the applied gradient  $\nabla P$  (or some function of this gradient). The coefficient in this relation is naturally set to equal the coefficient of permeability divided by viscosity (perhaps, raised to some power). Thus the suggested plan of calculations (4.13) - (4.15) using (1.8) allows to determine the permeability of the medium if the functions  $f(r)$  and  $\phi(\tau_s)$  and the values of  $z$  and  $l$  are known. In the course of computing the relative phase



permeabilities, the term in (1.8) which appears before the integral cancels out, and therefore the knowledge of  $l$  is not necessary.

**Flow with the initial pressure gradient. The Binghamian plastic.** The friction law with limiting shearing stress in the case of the flow of a visco-plastic fluid is defined by its structure in the field of the surface forces at the points of contact with the solid surface. The most general form of such law was given by Wilkinson

$$\tau_s = \frac{A\dot{\gamma}_s}{B + \dot{\gamma}_s} + \mu\dot{\gamma}_s \quad (4.16)$$

where  $A$  and  $B$  are constants found from experiment. For the calculation of the permeability in accordance with the given algorithm, the specific form in which the law  $\phi(\tau_s)$  is written does not matter. However if  $A$  and  $B$  are arbitrary constants, then after integrating, the expression (4.13) becomes very complicated and inconvenient for further use. Therefore it seems reasonable to consider, for illustration, a rather frequently encountered specific case of (4.16), when  $A = \tau_p$ ,  $B/\dot{\gamma}_s \ll 1$ , i.e., the Binghamian plastic. Similar rheological properties can be found in heavy viscous oils which contain components with high molecular weights.

In the outlined case the function  $\phi(\tau_s)$  has the following form

$$\phi(\tau_s) = [(\tau_s - \tau_p)/\mu]\eta(\tau_s - \tau_p) \quad (4.17)$$

Substitution of (4.17) into (4.14) yields the well-known relation of Bingham

$$q = \frac{\pi r^4}{8\mu} \nabla p \left[ 1 - \frac{4}{3} \left( \frac{\nabla p^*}{\nabla p} \right) + \frac{1}{3} \left( \frac{\nabla p^*}{\nabla p} \right)^4 \right], \quad \nabla p^* = 2\tau_p/r \quad (4.18)$$

(4.18) implies that even in the considered case (i.e.,  $\nabla p^*/\nabla p \sim 1$ ), the ratio of the third term in the square brackets to the second one is  $\sim 0.1$ . Therefore it is possible to neglect the third term in the square brackets and write the following for the local  $\nabla p$

$$\nabla p(q) = \frac{8\mu}{\pi r^4} q + \frac{4}{3} \nabla p^* \quad (4.19)$$

After substituting (4.19) into (4.14) we obtain the value of the macroscopic gradient

$$\nabla p(r_1) = \left[ \frac{8\mu}{\pi} q(r_1) \int_{r_1}^{\infty} f(r) \frac{dr}{r^4} + \frac{8\tau_p}{3} \int_{r_1}^{\infty} f(r) \frac{dr}{r} \right] \left( \int_{r_1}^{\infty} f(r) dr \right)^{-1}$$

and

$$q(r_1) = \frac{\pi}{8\mu} \nabla p(r_1) \int_{r_1}^{\infty} f(r) dr \left( \int_{r_1}^{\infty} f(r) \frac{dr}{r^4} \right)^{-1} -$$

$$\frac{\pi \tau_p}{3\mu} \int_{r_1}^{\infty} f(r) \frac{dr}{r} \left( \int_{r_1}^{\infty} f(r) \frac{dr}{r^4} \right)^{-1} \quad (4.20)$$

In this case it follows from (4.15) and (4.20), in accordance with (1.8), that

$$Q = \frac{2\nu}{l^2} (1 - \xi_c)^{-2\nu} \frac{\pi}{8\mu} \nabla P \int_0^{r_c} \left[ \int_{r_1}^{r_c} f(r) dr \right]^\nu \times \left\{ \left[ \int_{r_1}^{\infty} f(r) dr - \frac{8}{3} \frac{\tau_p}{\nabla P} \int_{r_1}^{\infty} f(r) \frac{dr}{r} \right] \left( \int_{r_1}^{\infty} f(r) \frac{dr}{r^4} \right)^{-1} \right\} f(r_1) dr_1 \quad (4.21)$$

After introducing the notation  $\lambda_0 = (1/4)\nu\pi l^{-2}(1 - \xi_c)^{-2\nu}$  and  $r'_m = 2\tau_p/\nabla p$ , we obtain, due to (4.21), the expression for the absolute permeability of the Binghamian plastic with the limiting shear  $\tau_0$  for a given gradient  $\nabla P$

$$K_0^b = \lambda_0 \int_0^{r_c} \left[ \int_{r_1}^{r_c} f(r) dr \right]^\nu \int_{r_1}^{\infty} f(r) \left(1 - \frac{4}{3} \frac{r'_m}{r}\right) dr \times \left( \int_{r_1}^{\infty} f(r) \frac{dr}{r^4} \right)^{-1} f(r_1) dr_1 \cdot \eta \left(1 - \frac{4}{3} \frac{r'_m}{r}\right) \quad (4.22)$$

If we took all the terms of (4.18) into account, then the  $\eta$ -function in (4.22) would have had  $(1 - r'_m/r)$  as its argument. This would have reflected the obvious fact that the capillaries with radii  $r < r'_m$ , for given  $\tau_p$  and  $\nabla P$ , become impermeable for the Binghamian fluid. However, neglecting the last term in the square brackets in (4.18) results in an error of  $\approx 30\%$  in calculation of  $r'_m$ .

**Flow without the initial pressure gradient. Pseudo-plastic and "dilatant" fluids.** Flow of a number of fluids, such as colloidal solutions, emulsions, or thinly dispersed suspensions, is described by a non-linear friction law without a limiting shearing stress [63]

$$\phi(\tau_s) = (\tau_s/\mu_1)^{1/n} \quad (4.23)$$

where  $\mu_1$  is some sort of analog to viscosity, and  $n$  is an exponent to be found from experiment. It was discovered [63] that the law (4.23) for  $n < 1$  does well enough reflect the behavior of emulsion and polymeric solutions used, for instance, in "polymeric" inundation (pseudo-plastic fluids). For  $n > 1$  this law equally well describes the properties of flowing suspensions, which are widespread in water extraction and in the of underground lixiviation phenomena (dilatant fluids).

We shall not go into realization details of the outlined plan for the calculations here and shall present only the final result of computing the absolute permeability for the discussed type of visco-plastic fluids

$$K_0^d = \frac{2^{3-1/n}}{3 + 1/n} \lambda_0 \int_0^{\tau_c} \left[ \int_{\tau_1}^{\tau_c} f(r) dr / \int_{\tau_1}^{\infty} f(r) \frac{dr}{r^{3n+1}} \right]^{1/n} \left[ \int_{\tau_1}^{\tau_c} f(r) dr \right]^{\nu} f(\tau_1) d\tau_1 \quad (4.24)$$

To calculate the phase permeabilities, address the displacement of a hydrophilic fluid by a hydrophobic one. In accordance with the analysis carried out in §4.1, we select the parts of  $f(r)$  which characterize the distribution of each of the phases in the pore space. This operation is valid for plastic fluids as well, if the plastic resistance ( $\sim \tau_p/R_g$ ) is much less than the capillary resistance ( $\sim \chi/R_g^2$ ). This problem was studied in [64], and it was shown that both the hydrodynamic (viscous) and the plastic forces are small compared to the capillary forces in a common domain of relatively small values of  $\nabla p$ , and therefore, of relatively small local velocities. Since the subject of this part is only steady state flow, i.e., the case of small flow velocities, it follows that the assumption on the nature of the distribution of the fluids in the pore space used in §4.1 may be considered valid for the visco-plastic fluids as well. Consequently the absolute permeabilities for the phases  $K_i^{b,d}$  ( $i = 1, 2$ ) can be calculated using formulas (4.22) and (4.24) as follows. For  $K_2^{b,d}$ , the lower limit of integration is changed to  $\tau_\kappa$ , and the function  $f_2(r)$  acts as  $f(r)$ . For  $K_1^{b,d}$ , relationships (4.22) and (4.24) do not change, only  $f_1(r)$  is used instead of  $f(r)$ , and  $\tau_c$  is found from (4.6) for  $\kappa = 1$ .

Note that the flowing fluids can in fact have different plastic properties, the algorithm of calculating  $K_i^{b,d}$  using (4.22) and (4.24) not being affected by this at all. It is only necessary, when passing to the relative phase permeabilities  $k_i^{b,d} = K_i^{b,d}/K_0^{b,d}$ , to take into account the fact that a specific absolute permeability  $K_0^{b,d}$  of the medium corresponds to each of the fluids. In analyzing the qualitative trends in the behavior of the quantities  $k_i^{b,d}$  we shall confine ourselves to studying the flow of fluids with identical plastic properties. In this case each way of calculations is characterized by a common value of the absolute conductivity of the medium,  $K_0^b$  or  $K_0^d$ .

The choice of a model for the calculation of  $S(\tau_\kappa)$ , naturally, depends on the actual pore space structure of a specific porous medium.

Calculations for a simple cubic network ( $z = 6$ ) with the model function  $f(r) = r_0 r^{-2} \eta(r - r_0)$  will be presented as an illustration. In this model, the saturation  $S_2$  of the medium by the displacing less wettable fluid was used as the saturation variable  $S$ , and the relation  $S(\tau_\kappa)$  was established using model I.

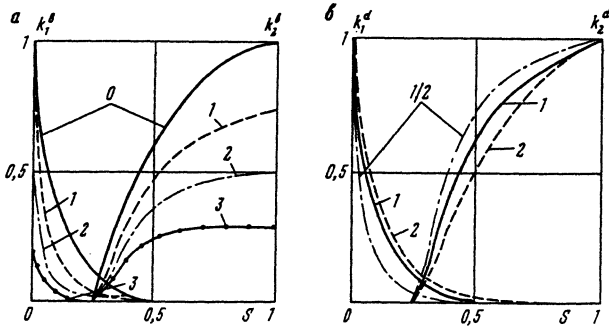


Figure 19: Curves for the calculation of the phase permeabilities for a - flow of the Binghamian plastic (code:  $r'_m/r_0$ ); b - visco-plastic and dilatant liquids (code:  $n$ )

The results of the calculation of  $k_i^b(S)$  for the Binghamian plastic are presented in fig.19, a. As  $\tau_p$  goes up, the phase permeabilities of both the displacing and the displaced fluid drop sharply; therefore, the limiting shear during the extraction of anomalous oils should be made as small as possible.

The obtained results qualitatively agree with the experimental data [65] and with the results of the numerical computations [8] based on the network model, carried out in the development [59] (the agreement is satisfactory). In the latter case, the only non-Newtonian (Binghamian) fluid is oil (water is Newtonian), and it is for oil that the typical transformation of the  $k_2^b(S)$  curve like the one shown in fig. 19, a, is observed.

The plots of the relations  $k_i^d(S)$  for visco-plastic and dilatant fluids are presented in fig.19, b. The case of  $n = 1$  corresponds to the Newtonian fluids;  $n = 2$ , to the dilatant fluids;  $n = 1/2$ , to the pseudo-plastic fluids. When the exponent  $n$  in (4.23) changes, all the more at the transfer from one fluid type to another (from  $n < 1$  to  $n > 1$ ), the phase permeabilities change notably. This phenomenon can be widely used in various applications.

### 4.3 Phase Permeabilities of a Medium with Mixed Wettability

In actual media capillaries often differ not only in size, but also in properties of wettability of their surfaces. The effects of mixed wettability of a porous medium on the relative phase permeabilities of fluids flowing through it has been studied earlier in [9] by means of the numerical simulation of the capillary displacement

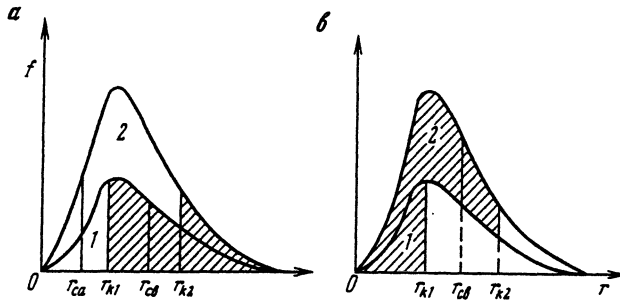


Figure 20: Probability density function for a medium with mixed wettability of the pore space surface, and the conditional breakup of this function

in a two-dimensional network.

Consider a porous medium formed by a regular network of capillaries with the probability density function  $f(r)$  (see fig.20) in an impermeable skeleton. A two-phase equilibrium flow in such a medium is determined by the capillary forces on the phase interface. These forces depend on the coefficient  $\chi$  of surface tension at the phase interface and the contact angle  $\theta$ .

In homogeneous media the parameters  $\chi$  and  $\theta$  are constant. Assume now that the medium is heterogeneous, and  $\chi$  and  $\theta$  can take one of the two values  $\chi_1$  or  $\chi_2$  and  $\theta_1$  and  $\theta_2$  each, with probabilities  $\kappa$  and  $1 - \kappa$  for the first and the second values, respectively. It means that the fraction  $\kappa$  of all capillaries in the network (the conditional region 1 in fig. 20, a) is characterized by values  $\chi_1, \theta_1$ , when they belong to the phase interface, while the remaining fraction  $(1 - \kappa)$  (the conditional region 2 in fig. 20, a) is characterized by values  $\chi_2, \theta_2$ .

For determinedness, consider henceforth the capillary displacement of phase  $a$ , which initially occupies all the capillaries, by phase  $b$  under the increase of the capillary pressure  $p_k = P_a - P_b$  from  $-\infty$  to  $+\infty$ . When the capillary pressure equals  $p_k$  the displacing phase  $b$  can occupy only those capillaries, whose radii are greater than the critical one defined by the Laplace's formula. In the given case we have a specific critical radius for each capillary type

$$r_{ki} = 2\chi_i \cos \theta_i / p_k, \quad i = 1, 2 \quad (4.25)$$

As it follows from (4.25), the parameters  $\chi_i$  and  $\theta_i$  appear only in the product  $\chi_i \cos \theta_i$ . Since  $\chi_i > 0$ , and  $-1 < \cos \theta_i < 1$ , it seems natural to decrease the number of external parameters by setting  $\chi_1 = \chi_2 = \chi$  and considering further only the dependence on  $\cos \theta_i$

An important property of the problem in question is that if  $\cos \theta_1$  and  $\cos \theta_2$  have opposite signs, then the values of  $p_k$  for the two outlined capillary types must have opposite signs, too, since the critical radius ((4.25)) cannot be negative.

Practically the mentioned property means that when  $p_k$  increases from  $-\infty$  to 0 the capillaries with  $\cos \theta < 0$  are filled, and only after this process comes to an end, when  $0 < p_k < \infty$ , are the capillaries of second type ( $\cos \theta > 0$ ) being filled. Moreover for capillaries with  $\cos \theta < 0$ , we have imbibition instead of displacement: in this case the formula (4.25) yields not the least, but the largest radius to be filled by phase  $b$  (the unshaded part of region 1 in fig. 20,  $a$ ). When  $\cos \theta_1 \cos \theta_2 > 0$ , the capillaries of both types are being filled simultaneously, though they have different critical radii as found from (4.25).

Now turn to the calculation of the coefficients of relative phase permeability  $k_a$  and  $k_b$  for such a micro heterogeneous medium. First, study the behavior of the quantity  $k_b$ . We shall begin with the case when  $\cos \theta_1 > 0$ ,  $\cos \theta_2 > 0$ ,  $\cos \theta_1 \leq \cos \theta_2$ . The last condition can always be made valid by means of the simple interchange of the indices 1 and 2. Denote  $\alpha = \cos \theta_1 / \cos \theta_2$ . Then it follows from (4.25) that  $r_{k1} = \alpha r_{k2}$ , where  $0 < \alpha \leq 1$ . The distribution function of capillaries filled with phase  $b$  (the shaded region in fig. 20,  $a$ ) is

$$f_b(r) = \begin{cases} 0, & r < r_{k1}, \\ \kappa f(r)/\Omega_b, & r_{k1} \leq r \leq r_{k2}, \\ f(r)\Omega_b, & r > r_{k2} \end{cases} \quad \Omega_b = \kappa \int_{r_{k1}}^{r_{k2}} f(r) dr + \int_{r_{k2}}^{\infty} f(r) dr \quad (4.26)$$

Now analyze the relation (1.7). When  $p_k$  increases from  $-\infty$  to 0 all capillaries are filled with phase  $a$ , and  $r_{k1}$  and  $r_{k2}$  equal  $\infty$ . When we pass to the domain of  $p_k > 0$ ,  $r_{k1}$  and  $r_{k2}$  are calculated using formula (4.25). As  $p_k$  increases, the radii  $r_{k1}$  and  $r_{k2}$  decrease until they reach the values  $r_{c2}$  and  $r_{c1} = \alpha r_{c2}$  (see fig. 20,  $a$ ), where  $r_{c2}$  is found from the following condition

$$\kappa \int_{\alpha r_{c2}}^{r_{c2}} f(r) dr + \int_{r_{c2}}^{\infty} f(r) dr = \xi_c \quad (4.27)$$

At this point, an infinite cluster of capillaries of both types filled with phase  $b$  (ICB) is formed in the medium for the first time. With the further increase of  $p_k$ ,  $r_{k1}$  and  $r_{k2}$  continue to decrease, and the substitution of  $f_b(r)$  in (1.7) yields the following condition for  $r_{cb}$

$$\kappa \int_{r_{cb}}^{r_{k2}} f(r) dr + \int_{r_{k2}}^{\infty} f(r) dr = \xi_c \quad (4.28)$$

The quantity  $r_{cb}$  is analogous to  $r_c$ . The only difference is in that the former is not a constant but a function of  $r_{k2}$ . It varies in the range  $r_{c1} \leq r_{cb} \leq r_c$ , where  $r_{cb} = r_c$  when  $r_{k2} = r_c$ . Further increase of  $p_k$  causes decrease of the values of  $r_{k2}$  and  $r_{k1}$ , but does not change  $r_{cb} = r_c$ .

Thus from (2.1) we obtain the following, by calculating the values of  $r_{k1}$ ,  $r_{k2}$ , and  $r_{cb}$  and using (4.26)

$$k_b(r_{k2}) = 0, \quad r_{k2} > r_{c2}, \quad -\infty < p_k < p_{c2b} \quad (4.29)$$

$$k_b(r_{k2}) = A'/K_0 \int_{\alpha r_{k2}}^{r_{cb}} \left[ \int_{r'}^{r_{cb}} f_b(r) dr \right]^\nu f_b(r') \\ \times \left( \kappa \int_{r'}^{r_{k2}} f(r) dr + \int_{r_{k2}}^{\infty} f(r) dr \right) \left( \kappa \int_{r'}^{r_{k2}} f(r) \frac{dr}{r^4} + \int_{r_{k2}}^{\infty} f(r) \frac{dr}{r^4} \right)^{-1} dr' \quad (4.30)$$

$$r_c < r_{k2} \leq r_{c2}, \quad p_{c2b} \leq p_k < p_c$$

$$k_b(r_{k2}) = A'/K_0 \left\{ \kappa \int_{\alpha r_{k2}}^{r_{k2}} \left[ \kappa \int_{r'}^{r_{k2}} f(r) dr + \int_{r_{k2}}^{r_c} f(r) dr \right]^\nu \right. \\ \times f_b(r') \left( \kappa \int_{r'}^{r_{k2}} f(r) dr + \int_{r_{k2}}^{\infty} f(r) dr \right) \left( \kappa \int_{r'}^{r_{k2}} f(r) \frac{dr}{r^4} + \int_{r_{k2}}^{\infty} f(r) \frac{dr}{r^4} \right)^{-1} dr' \\ \left. + \int_{r_{k2}}^{r_c} \left[ \int_{r'}^{r_c} f_b(r) dr \right]^\nu f_b(r') \int_{r'}^{\infty} f(r) dr \left( \int_{r'}^{\infty} f(r) \frac{dr}{r^4} \right)^{-1} dr' \right\}, \quad (4.31)$$

$$0 < r_{k2} \leq r_c, \quad p_c \leq p_k < \infty$$

Here  $A'$  is the term which appears before the integral in (2.1).

Now consider the case when  $\cos \theta_1 \cos \theta_2 < 0$ , for instance,  $\cos \theta_1 < 0$ ,  $\cos \theta_2 > 0$ . In this case the region 2 will not begin to be filled until the region 1 is completely filled. The filling of the latter region in this case will be directed towards the increase of the capillary radii, as was noted before. Depending on the value of  $\kappa$ , different types of two-phase flow are possible.

If  $\kappa < \xi_c$ , then as  $p_k$  increases from  $-\infty$  to 0, the flow of phase  $b$  cannot begin, since only the capillaries of the first type can be filled with this phase, whereas there is not enough of them to form an ICB. With further growth of  $p_k$ , the instance will come when the ICB is formed from the sum of the capillaries of the first and the second type. In this case (4.27) becomes

$$\kappa + (1 - \kappa) \int_{r_{c2}}^{\infty} f(r) dr = \xi_c,$$

if the lower limit in the first term of (4.27) is set to equal 0 when  $\alpha < 0$ , and the normalizing condition for  $f(r)$  is taken into account. The function  $r_{cb}(r_{k2})$  is still determined from the condition (4.28) and assumes values from 0 to  $r_c$ , as  $r_{k2}$  varies between  $r_{c2}$  and 0. Thus in this case the displacement of phase  $a$  by phase  $b$  is identical to the case described above, with  $\cos\theta_1 > 0$ ,  $\cos\theta_2 > 0$ , and the formulas (4.29) - (4.31) for  $k_b$  remain valid. Note only that since  $\alpha < 0$ , the lower limits of integration in (4.30) and (4.31), formally, are in the domain of  $r < 0$ , where, obviously,  $f(r)$  is defined to vanish.

Now let  $\kappa \geq \xi_c$ . In this case, the ICB formation from the capillaries of the first type is possible as early as the imbibition stage. When  $-\infty < p_k < 0$ ,

$$f_b(r) = \begin{cases} 0, & r < 0, \\ \kappa f(r)/\Omega_b, & 0 \leq r < r_{k1}, \\ 0, & r \geq r_{k1} \end{cases} \quad (4.32)$$

After substituting (4.32) into (1.7) we obtain the following condition for determining  $r_{cb}(r_{k1})$

$$\int_{r_{cb}}^{r_{k1}} f_b(r) dr = \xi_c$$

For  $r_{cb}$  to be greater than zero, it is necessary that  $r_{k1}$  exceed its limiting value  $r_{c1b}$  which is defined by the condition for the start of the flow for phase  $b$  in the capillaries of the first type,

$$\kappa \int_0^{r_{c1b}} f(r) dr = \xi_c$$

Thus when  $p_k < 0$ , it can be found from (4.32) and (2.1) that

$$k_b(r_{k1}) = 0, \quad 0 < r_{k1} < r_{c1b}, \quad -\infty < p_k < p_{c1b},$$

$$k_b(r_{k1}) = A'/K_0 \int_0^{r_{cb}} \left[ \int_{r'}^{r_{cb}} f_b(r) dr \right]^\nu f_b(r') \int_{r'}^{r_{k1}} f(r) dr \left( \int_{r'}^{r_{k1}} f(r) \frac{dr}{r^4} \right)^{-1} dr',$$

$$r_{c1b} \leq r_{k1} < \infty, \quad p_{c1b} \leq p_k < \infty$$

When the capillary pressure exceeds zero some of the capillaries of the second type being filled with phase  $b$  associate with the ICB, while all capillaries of the first type are by that time filled with this phase. The technique of the further calculations of the change of  $k_b(r_{k2})$  is identical to the one used for the case when  $\kappa > \xi_c$ . It is still described by formulas (4.30) and (4.31), where  $r_{c2} = \infty$  and  $r_{cb}$  is found from the condition (4.28).

We shall use the same scheme to study the quantity  $k_a$ . Let  $\cos\theta_1 > 0$ ,  $\cos\theta_2 > 0$ ,  $\cos\theta_2 \geq \cos\theta_1$ . The distribution function for phase  $a$  (the shaded



region in fig. 20, b), with  $r_{k1} = \alpha r_{k2}$  is

$$f_a(r) = \begin{cases} 0, & r \leq 0, \\ f(r)/\Omega_a, & 0 < r < \alpha r_{k2}, \\ (1 - \kappa)f(r)/\Omega_a, & \alpha r_{k2} \leq r \leq r_{k2} \end{cases}$$

$$\Omega_a = \int_0^{r_{k1}} f(r) dr + (1 - \kappa) \int_{r_{k1}}^{r_{k2}} f(r) dr \quad (4.33)$$

After substituting (4.33) into (2.1') we obtain the condition when the function  $r_{ca}(r_{k2})$  can be found. This function plays in the analysis of the ICA formation the same part as the function  $r_{cb}(r_{k2})$  does in the case of the ICB. Also, depending on the correlation between the quantities  $r_{ca}$  and  $\alpha r_{k2}$ , two forms of the discussed condition can be written

$$\int_{r_{ca}}^{\alpha r_{k2}} f(r) dr + (1 - \kappa) \int_{\alpha r_{k2}}^{r_{k2}} f(r) dr = \xi_c, \quad r_{ca} < \alpha r_{k2} \quad (4.34)$$

$$(1 - \kappa) \int_{r_{ca}}^{r_{k2}} f(r) dr = \xi_c, \quad r_{ca} \geq \alpha r_{k2} \quad (4.35)$$

The case (4.34) is presented in fig.20, b, and the case (4.35), in fig.20, a. The function  $r_{ca}(r_{k2})$  varies between  $r_c$ , when  $r_{k2} = \infty$  ( $-\infty < p_k < 0$ ), and 0 at some minimal value  $r_{k2} = r_{c2a}$  determined from the following condition

$$\int_0^{\alpha r_{c2a}} f(r) dr + (1 - \kappa) \int_{\alpha r_{c2a}}^{r_{c2a}} f(r) dr = \xi_c \quad (4.36)$$

When  $-\infty < p_k < 0$   $r_{k2} = r_{k1} = \infty$  and  $k_a(r_{k2}) = 1$ . In the case described by (4.34), the substitution of (4.33) into (2.1) gives the following

$$k_a(r_{k2}) = K_0^{-1} \int_0^{r_{ca}} \left[ \int_{r'}^{r_{ca}} f_a(r) dr \right]^\nu f_a(r')$$

$$\times \left( \int_{r'}^{\alpha r_{k2}} f(r) dr + (1 - \kappa) \int_{\alpha r_{k2}}^{r_{k2}} f(r) dr \right)$$

$$\times \left( \int_{r'}^{\alpha r_{k2}} f(r) \frac{dr}{r^4} + (1 - \kappa) \int_{\alpha r_{k2}}^{r_{k2}} f(r) \frac{dr}{r^4} \right)^{-1} dr',$$

$$r_{c2a} < r_{k2} < \infty, \quad 0 < p_k < p_{c2a}$$

In the case described by (4.35) we have

$$\begin{aligned}
 k_a(r_{k2}) = & K_0^{-1} \left\{ \int_0^{\alpha r_{k2}} \left[ \int_{r'}^{\alpha r_{k2}} f_a(r) dr \right]^\nu f_a(r') \left( \int_{r'}^{\alpha r_{k2}} f(r) dr + (1 - \kappa) \right. \right. \\
 & \times \left. \int_{\alpha r_{k2}}^{r_{k2}} f(r) dr \right) \left( \int_{r'}^{\alpha r_{k2}} f(r) \frac{dr}{r^4} + (1 - \kappa) \int_{\alpha r_{k2}}^{r_{k2}} f(r) \frac{dr}{r^4} \right)^{-1} dr' + (1 - \kappa)^2 \\
 & \times \left. \int_{\alpha r_{k2}}^{r_{ca}} \left[ \int_{r'}^{r_{ca}} f_a(r) dr \right]^\nu f_a(r') \int_{r'}^{r_{k2}} f(r) dr \left( \int_{r'}^{r_{k2}} f(r) \frac{dr}{r^4} \right)^{-1} dr' \right\}, \quad (4.37)
 \end{aligned}$$

$r_{c2a} < r_{k2} < \infty, \quad 0 < p_k < p_{c2a}$

Note that the cases (4.34) and (4.35) are not necessarily realized separately in the whole range  $0 < p_k < \infty$ . Certain values of  $\alpha$  and  $\kappa$  can be found, such that these cases can pass to one another as the capillary pressure changes.

Let now  $\cos \theta_1 \cos \theta_2 < 0$ ,  $\cos \theta_1 < 0$ ,  $\cos \theta_2 > 0$ . As  $p_k$  increases from  $-\infty$  to 0, the fraction of capillaries of the first type in the ICA decreases. The probability density function for these capillaries is

$$f_a(r) = \begin{cases} 0, & r < 0, \\ (1 - \kappa)f(r)/\Omega_a, & 0 \leq r < r_{k1}, \\ f(r)/\Omega_a, & r \geq r_{k1}, \end{cases} \quad (4.38)$$

where  $r_{k1}$  is determined from (4.25). If  $r_{k1} < r_c$ , then the substitution of (4.38) into (1.7) yields  $r_{ca}(r_{k1}) = r_c$ , while for  $k_a$  we have

$$\begin{aligned}
 k_a(r_{k1}) = & A'(1 - \kappa)K_0^{-1} \left\{ \int_0^{r_{k1}} \left[ (1 - \kappa) \int_{r'}^{r_{k1}} f(r) dr + \int_{r_{k1}}^{r_c} f(r) dr \right]^\nu f_a(r') \right. \\
 & \times \left( \int_{r'}^\infty f(r) dr - \kappa \int_{r'}^{r_{k1}} f(r) dr \right) \left[ (1 - \kappa) \int_{r'}^{r_{k1}} f(r) \frac{dr}{r^4} + \int_{r_{k1}}^\infty f(r) \frac{dr}{r^4} \right]^{-1} dr' \\
 & \left. + \int_{r_{k1}}^{r_c} \left[ \int_{r'}^{r_c} f_a(r) dr \right]^\nu f_a(r') \int_{r'}^\infty f(r) dr \left( \int_{r'}^\infty f(r) \frac{dr}{r^4} \right)^{-1} dr' \right\}, \\
 & 0 < r_{k1} < r_c, \quad -\infty < p_k < p_{c1}
 \end{aligned}$$

When  $r_c < r_{k1} < \infty$  from (4.38) and (1.7), we obtain the dependence  $r_{ca}(r_{k1})$  in the following form

$$(1 - \kappa) \int_{r_{ca}}^{r_{k1}} f(r) dr + \int_{r_{k1}}^\infty f(r) dr = \xi_c$$

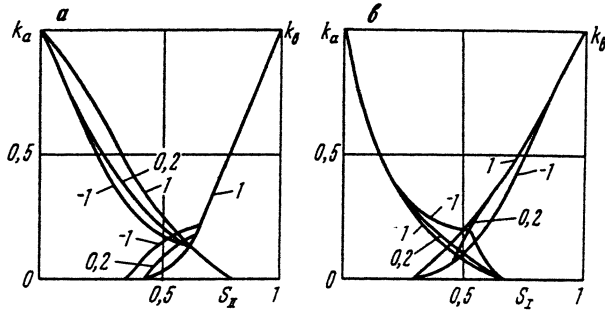


Figure 21: Curves for the phase permeabilities calculated for models I (b) and II(a). Code:  $\alpha$

If  $(1 - \kappa) < \xi_c$ , then as  $p_k < 0$  increases, for some  $p_k = p_{ca} < 0$ , the ICA must cease to exist, since the capillaries of the second type are not sufficient for the ICA formation. If, however,  $(1 - \kappa) > \xi_c$ , then the ICA does not disappear up to  $p_k = 0$  ( $r_{k1} = \infty$ ), and the flow of phase  $a$  stops only when  $p_k > 0$ , i.e., when  $p_{ca} = p_{c2a}$ , and  $r_{c1a} = \infty$ . Thus we obtain the following expression for  $k_a$  in the interval  $r_c < r_{k1} < r_{c1a}$

$$k_a(r_{k1}) = A'(1 - \kappa)^2 K_0^{-1} \int_0^{r_{ca}} \left[ \int_{r'}^{r_{ca}} f_a(r) dr \right]^\nu f_a(r') \left( \int_{r'}^{\infty} f(r) dr - \kappa \int_{r'}^{r_{k1}} f(r) dr \right) \left[ (1 - \kappa) \int_{r'}^{r_{k1}} f(r) \frac{dr}{r^4} + \int_{r_{k1}}^{\infty} f(r) \frac{dr}{r^4} \right]^{-1} dr',$$

$r_c < r_{k1} < r_{c1a}, \quad p_{c1} < p_k < \min\{0, p_{ca}\}$

If  $(1 - \kappa) > \xi_c$ , then in the case when  $p_k > 0$ , only those of the capillaries of the second type are filled with phase  $a$ , whose radii  $r < r_{k2}$ , where  $r_{k2}$  is found from (4.25) if  $p_k$  is known. As  $p_k$  increases, the quantity  $k_a(r_{k2})$  keeps falling until it vanishes at the point  $r_{k2} = r_{c2a}$ , where  $r_{c2a}$  is found using formula (4.36). In the interval  $0 < p_k < p_{c2a}$  ( $r_{c2a} < r_{k2} < \infty$ ),  $k_a(r_{k2})$  is defined by the relationship (4.37), and the function  $r_{ca}(r_{k2})$  is defined by (4.35).

Thus the obtained formulas describe the change of  $k_a$  and  $k_b$  for the discussed model of the micro heterogeneous medium in the whole range of the parameters describing micro heterogeneity,  $0 \leq \kappa \leq 1$ ,  $-1 \leq \alpha \leq 1$ .

Calculations of the relative phase permeabilities  $k_a(S_b)$  and  $k_b(S_b)$  were carried out for different probability density functions  $f(r)$  and different values of parameters  $\alpha$  and  $\kappa$ , based on the formulas obtained above. Here saturation with phase  $b$  ( $S_b$ ) was defined as before for the two limiting cases, model I and model II, and

was expressed for  $\alpha > 0$  by the following

$$S_I = \kappa \int_{r_{k1}}^{r_{k2}} f(r) dr + \int_{r_{k2}}^{\infty} f(r) dr \quad (4.39)$$

$$S_{II} = \langle r^2 \rangle^{-1} \left( \kappa \int_{r_{k1}}^{r_{k2}} f(r) r^2 dr + \int_{r_{k2}}^{\infty} f(r) r^2 dr \right); \quad (4.40)$$

and for  $\alpha \leq 0$ , by the following

$$S_I = \kappa \int_0^{r_{k1}} f(r) dr + (1 - \kappa) \int_{r_{k2}}^{\infty} f(r) dr \quad (4.41)$$

$$S_{II} = \langle r^2 \rangle^{-1} \left[ \kappa \int_0^{r_{k1}} f(r) r^2 dr + (1 - \kappa) \int_{r_{k2}}^{\infty} f(r) r^2 dr \right] \quad (4.42)$$

Plots of  $k_a$  and  $k_b$  for  $\kappa = 0.5$  and the model probability density function

$$f^{(1)}(r) = \begin{cases} 0, & r \notin [1, 3], \\ 4.05r^{-5}, & r \in [1, 3] \end{cases}$$

are depicted in fig.21.

It can be seen that as  $\alpha$  decreases, the values of  $k_a$  fall, whereas the values of  $k_b$  grow. The same effect was obtained in [9] as a result of the numerical simulation of the capillary displacement on a two-dimensional network of capillaries. In [9],  $\kappa = 0.5$ ; a log normal distribution was taken as the function  $f(r)$ ; and it was assumed that the lengths of capillaries correlate with their radii,  $l \sim r^k$ , where  $k$  is the varied parameter. Therefore the above-mentioned congruence of tendencies in the changes of  $k_a$  and  $k_b$  caused by change of  $\alpha$  is merely qualitative. Furthermore it takes place only when saturation is calculated according to model II (see fig. 21, a). If  $S = S_I$ , then the nature of variation of  $k_a$  and  $k_b$  with the change of  $\alpha$  shifts to the opposite, as is evident from fig.21, b, where plots of  $k_a(S_I)$  and  $k_b(S_I)$  are presented, calculated for the same function  $f(r)$  and values of  $\alpha$  and  $\kappa$ .

To study the impact the form of  $f(r)$  has on the functions  $k_a$  and  $k_b$ , calculations were performed for  $\kappa = 0.5$ ,  $\alpha = -1$  and 1 and for three model functions,  $f^{(1)}(r)$  and the following two others,

$$f^{(2)}(r) = \begin{cases} 0, & r \notin [1, 3], \\ 1.5r^{-2}, & r \in [1, 3] \end{cases}$$

$$f^{(3)}(r) = \begin{cases} 0, & r \notin [0, 5], \\ 2r \exp(-r^2), & r \in [0, 5] \end{cases}$$

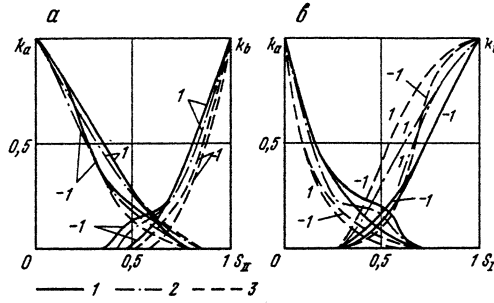


Figure 22: Impact of the form of the function  $f(r)$  on the nature of the dependencies  $k_{a,b}(S)$ :  $\kappa = 0.5$ ; 1 - 3 - curves obtained by calculations using functions  $f^{(1)}(r)$ ,  $f^{(2)}(r)$ ,  $f^{(3)}(r)$ , respectively. Code:  $\alpha$

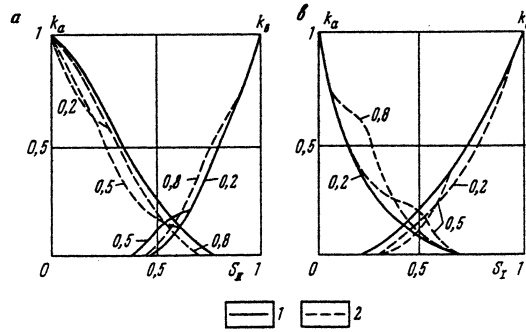


Figure 23: Impact of the parameter  $\kappa$  on the nature of the dependencies  $k_{a,b}(S)$ :  $f(r) = f^{(1)}(r)$ ; 1, 2 - curves for  $\alpha = 1$  and  $\alpha = -1$ , respectively. Code:  $\kappa$

In all cases, the calculations of  $k_a$  and  $k_b$  were carried out for  $\kappa = 0.5$ , using both of the outlined models for computing the saturation  $S$ . The obtained curves are placed beside each other for comparison: those corresponding to model II, in fig.22, a, and those corresponding to model I, in fig. 22, b. It is evident from the plots in fig. 22, a, that as the variance of  $f(r)$  increases ( $\sigma_d^{(1)} < \sigma_d^{(2)} < \sigma_d^{(3)}$ ),  $k_b(S_{II})$  decreases, while the threshold saturation, which determines the beginning of the flow of phase b, increases, both for  $\alpha > 0$  and  $\alpha < 0$ . When  $S$  is calculated using the pore model (fig. 22, b) the same effects are to be found for  $k_a(S_I)$ , i.e., as the variance of  $f(r)$  goes up, the values of  $k_a(S_I)$  go down, and the threshold saturation somewhat increases, though not as notably as in the first case.

The impact of the parameter  $\kappa$  on the forms of functions  $k_a$  and  $k_b$  is reflected in fig.23, where, too, the case a corresponds to model II, and the case b, to model I. The data presented show that when  $\alpha = -1$  for all  $\kappa$ , the  $k_a(S_{II})$  curves lie below the corresponding curves for  $\alpha = 1$ , while the opposite is true for  $k_a(S_I)$ . In this case the fall (or rise) of the curves with respect to  $\alpha = -1$  is steeper when  $\kappa$

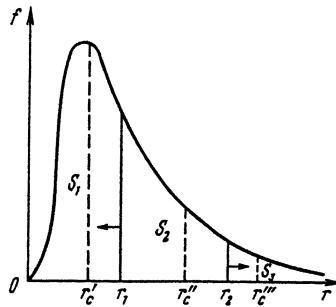


Figure 24: Schematic distribution of phases in the pore space under capillary forces for steady state flow

is greater. The effect is reverse for  $k_b$ . When  $\alpha = -1$  the  $k_b(S_{II})$  curves lie higher and the  $k_b(S_I)$ , lower than the corresponding plot for  $\alpha = 1$ . The characteristic convexities which appear on these curves with the increase of  $\kappa$  go up in the case of  $k_b(S_{II})$  and down in the case of  $k_b(S_I)$ .

## 4.4 Three-Phase Steady State Flow of Immiscible Newtonian Fluids

Due to great technical difficulties encountered in any attempt to determine experimentally the phase permeabilities for three-phase flow, theoretical study of the behavior of the permeabilities is of special importance. The results obtained in research on the equilibrium two-phase flow presented in §4.1 allow to generalize these results to the three-phase flow.

Confine ourselves to the study of flow in those media whose pore space structure is described by model I. Consider equilibrium flow of three different fluids. We shall assign each of them a number from 1 to 3, so that the number is greater when the wettable capacity of the fluid is lower.

In constructing a model for three-phase flow, the requirement for the flow to be equilibrium is significant, just as in §4.1. It means that the flow velocities must be sufficiently small for the distribution of phases in the pore space to be completely determined by the capillary forces. In this case, if initial saturations of the phases are approximately equal (i.e., none of the phases is "trapped"), then any future change of saturations will be accompanied by the rearrangement of the capillaries in the network, so that the more wettable phase inflates the capillaries of smaller radii, and the less wettable one inflates the larger ones.

Estimate the typical saturations ( $S_1, S_2, S_3$ ) of the medium with different phases which admit flows with different numbers of phases. Equilibrium flow of

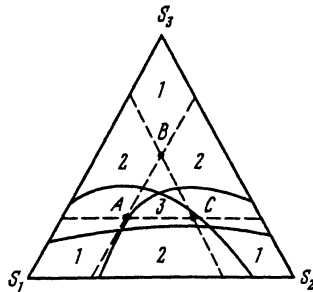


Figure 25: Triangular diagram of the domains where different numbers of phases flow, as a function of the ratio of saturations (the Gibbs - Rosebome triangle)

any phase is possible only in the case when the capillaries filled with this phase form an IC. An IC is formed in the network if and only if the fraction of capillaries containing the given phase exceed a certain threshold value  $\xi_c$ .

Estimate the probability of a capillary containing the  $i$ -th phase. In the course of the equilibrium flow, any phase can access only those capillaries where the capillary pressure does not exceed the pressure  $P_i$  in the phase. Obviously the phase with index 3, whose wettable capacity is least, fills the largest capillaries ( $r > r_2$ , fig.24). The thinnest capillaries ( $r < r_1$ ) contain the phase of index 1, i.e., the most wettable one. Finally, the capillaries of radii  $r_1 < r < r_2$  contain the phase of index 2. The values  $r_1$  and  $r_2$ , which break  $f(r)$  into zones saturated with different phases (see fig. 24), are determined from the phase equilibrium condition

$$r_j = 2\chi_{j,j+1} \cos \theta_{j,j+1} / P_j; \quad j = 1, 2 \quad (4.43)$$

where  $\chi_{j,j+1}$  is the coefficient of surface tension on the interface of the  $j$ -th and the  $(j + 1)$ -th phases;  $\theta_{j,j+1}$  is the contact angle for the  $j$ -th and the  $(j + 1)$ -th fluids.

It was shown in §4.1 that (with a 85% accuracy) the  $i$ -th IC contains all capillaries whose radii satisfy the condition of the  $i$ -th phase penetrating through them. Therefore the probability  $\xi_i$  of the capillary to contain the  $i$ -th phase is defined by the following expressions

$$\xi_1 = \int_0^{r_1} f(r) dr; \quad \xi_2 = \int_{r_1}^{r_2} f(r) dr; \quad \xi_3 = \int_{r_2}^{\infty} f(r) dr \quad (4.44)$$

Consequently the  $i$ -th phase flows if

$$\xi_i \geq \xi_c \quad (4.45)$$

To determine the value of  $\xi_c$  quantitatively, it is necessary to know the network type that simulates the pore space structure most adequately. Actual location

and mutual orientation of the pores and the channels in the medium are random. Random structure of bonds is most easily described by a simple cubic network. Since there are no data at present in favor of any other network type, we shall consider the network to be cubic, as in the previous studies. In this case, from (1.1) we find  $\xi_c = 1/4$ .

It follows from the relationships (4.44) that in model I,  $S_i = \xi_i$ . If we sketch the critical values of saturation obtained in a triangular diagram (fig.25) and draw dotted lines inside the triangle  $S_1S_2S_3$ , we get a series of domains which differ from one another by the number of phases taking part in the flow. The numbers 1 in fig.25 denote the domains of one-phase flow, when two phases out of three are "trapped" (there is no IC for these phases). Given the ratio of the saturations corresponding to domains 1, only the  $i$ -th component flows, where  $i$  is the vertex of the triangle. In the domains marked with number 2, one of the three phases is "trapped," and two-phase flow of fluids  $i$  and  $j$  takes place, where  $i$  and  $j$  are the indices of the sides  $S_iS_j$  of the triangle adjacent to the domains 2. The domain 3, where flow of all three phases is possible, is situated in the center of the triangle.

It is clear from the diagram that three-phase flow is only possible in a small neighborhood of the center of the triangle  $S_1S_2S_3$ . Note that equilibrium four-phase flow is impossible in the case of a cubic network, since conditions like (4.45) cannot be satisfied for four phases simultaneously. One of the phases in this case would have to flow in a disconnected form. However for big coordinational numbers of the network ( $z > 6$ ), the percolation threshold of the system drops and the equilibrium flow of four and more phases is possible, at least in theory.

It appears interesting to compare the obtained theoretical result to the experimental data.

Unfortunately no experimental study of three-phase equilibrium flow for the case of  $\mu_i = \text{const}$  ( $i = 1, 2, 3$ ),  $\chi_1 \cos \theta_1 > \chi_2 \cos \theta_2 > \chi_3 \cos \theta_3$  was carried out before. The only known experiments are those of Leverett (1940) [66], where viscosities of the phases differed substantially ( $\mu_1 \approx \mu_2 \gg \mu_3$ ). The results of these experiments are put on the same triangular diagram of saturations for comparison (continuous lines inside the triangle  $S_1S_2S_3$ ).

It can be seen that the areas of domains 3 are approximately the same both in the theoretical investigation and in the experiment; however, the triangle found experimentally is situated somewhat farther from the vertex  $S_3$ . The domains 2 adjacent to the sides  $S_1S_3$  and  $S_2S_3$  are deformed in the same direction. This can be explained by dynamic effects.

For example, due to its significantly smaller viscosity and consequently, its greater mobility, the third phase can break through the rock on the dynamic stage of flow and thus isolate the "parts" occupied by the less mobile phases 1 and 2. As a result, in a broad range of  $S_3$  ( $1 > S_3 \gtrsim 0.35$ ), one-phase flow of the third fluid takes place. When  $S_3 < 0.35$ , i.e., when the rock contains a sufficiently small



amount of the third phase for the difference in the mobility of the phases to stop determining the nature of their distribution in the pore space, the theoretical and the experimental diagrams of different domains of three-phase flow coincide with accuracy of  $\approx 10\%$ . This fact speaks of a good agreement between theory and experiment for the discussed case of equilibrium three-phase flow.

We shall now present the calculations of the coefficients of relative phase permeability in different domains of the flow. Obviously, in the domains 1 of the triangular diagram, only the relative phase permeabilities of the corresponding  $i$ -th phases do not vanish (they equal 1). In the domains 2, as it was mentioned above, two-phase flow of the  $i$ -th and the  $j$ -th phases takes place. Coefficients of phase permeability for these phases can be found using relationships (4.3) and (4.5). Generalization of these relationships to the case of three-phase flow permits to determine the relative phase permeabilities in the domain 3. Using the conditions (4.43) enables one to cut out the part  $f_i(r)$  of the general probability density function  $f(r)$  corresponding to the fraction of the capillaries containing the  $i$ -th phase. In the case of three-phase flow  $f_i(r)$  have the following form (before normalizing)

$$f_1(r) = \begin{cases} 0, & r > r_1, \\ f(r), & r \leq r_1 \end{cases}, \quad f_2(r) = \begin{cases} 0, & r > r_2, r < r_1, \\ f(r), & r_1 \leq r \leq r_2 \end{cases}, \quad (4.46)$$

$$f_3(r) = \begin{cases} f(r), & r \geq r_2, \\ 0, & r < r_2, \end{cases}$$

After substituting  $f_i(r)$  for  $f(r)$  in (2.1), we find the absolute phase permeabilities  $K_i(r_1, r_2)$  as functions of the quantities  $r_1$  and  $r_2$ , which characterize the domains of saturation of the capillaries with the  $i$ -th phase. Here the saturations of phases are set by the relationships (4.44). Coefficients of relative phase permeability are calculated using the formula

$$k_i(r_1, r_2) = K_i(r_1, r_2)/K_0 \quad (4.47)$$

They are completely defined by the radius probability density function for capillaries and by the percolation threshold of the system, which depends on the network type (coordinational number  $z$ ).

Thus the expressions (4.44), (4.45), (2.1), (4.46), and (4.47) allow to calculate the relative phase permeabilities in the domain 3 using the relationship (4.43). In the special case,  $r_1 = r_2$ , we have  $f_2(r) = 0$ , and two-phase flow is realized directly along the side  $S_1S_3$  of the triangle  $S_1S_2S_3$ . If, however,  $r_1 = r_2$  and some  $\xi_i < \xi_c$ , then two-phase flow takes place in the domains 2 with a trapped  $i$ -th phase. Note that the phase permeabilities  $k_1(r_1 = 0, r_2 = r_1) = k_1(r_1)$  and  $k_3(r_1 = r_2, r_2 = \infty) = k_3(r_2)$  are actually functions of merely  $r_1$  and  $r_2$ , respectively, and are calculated uniformly for all domains on the diagram. The

outlined phenomenon was observed in Leverett's experiments, where it was also noted that the permeability of the most wettable phase (water) depended only on the saturation with this phase and was insensitive to the ratio of other phases.

Find the phase permeabilities for the model probability density function (4.9) when  $a_*/a^* \ll 1$ , i.e.,

$$f(r) = a_* r^{-2} \eta(r - a_*) \quad (4.48)$$

Assume further that  $a_* = 1$ . After substituting (4.48) into (4.44) we find the correlation between  $r_1$  and  $r_2$  and the saturations of the phases,  $S_1 = 1 - r_1^{-1}$ ,  $S_3 = r_2^{-1}$ ,  $S_2 = 1 - S_1 - S_3 = r_1^{-1} - r_2^{-1}$ . Clearly, it is reasonable to find the relation for  $k_2$  right away, since the values of  $k_1$  and  $k_3$  can be obtained from it by means of the corresponding passages to limits. We can find the correlation between the critical radius  $r_c''$  of the function  $f_2(r)$  and  $r_2$  from (1.7), using (4.46) and (4.48). To simplify the calculations, we take  $\nu = 1$  instead of the actual  $\nu \approx 0.9$ . In this case, after substituting  $r_c''$  into (2.1), using (4.46) and (4.47) and neglecting the terms  $\sim (r_c''/r_2)^5$ , we find the coefficient of phase permeability for the second phase,

$$k_2(S_1, S_3) = \frac{2}{27} \frac{1}{(S_3 + \xi_c)^2} \left\{ 1 - \frac{S_3}{2(S_3 + \xi_c)} - 3 \left( \frac{S_3 + \xi_c}{1 - S_1} \right)^2 \right. \\ \left. \times \left[ 1 - \frac{2(2S_3 + \xi_c)}{3(1 - S_3)} + \frac{S_3(S_3 + \xi_c)}{2(1 - S_1)^2} \right] \right\} \eta(1 - S_1 - S_2 - S_3 - \xi_c) \quad (4.49)$$

To determine the phase permeability  $k_2$ , it is necessary to know any two of the three saturations, which are related through the customary relation,  $S_1 + S_2 + S_3 = 1$ .

The values of  $k_1$  and  $k_3$  are obtained from (4.49) by means of the passage to the limit from a three-phase system to the two-phase one. It helps in the case of  $k_1$  to let  $S_1$  approach zero ( $r_1 \rightarrow 0$ ). In this case we obtain a two-phase system, where the part of  $S_1$  is formally played by the saturation  $S_2$ , while the phase "interface," as far as  $f(r)$  is concerned, is  $r_2$ . The quantity  $r_2$  is uniquely determined by the saturation  $S_3$ , which equals  $1 - S_1$  for the considered case. Therefore we find  $k_1(S_1) = k_2(0, 1 - S_1)$ , or

$$k_1(S_1) = \frac{2}{27} \frac{1}{(1 - S_1 + \xi_c)^2} \left\{ 1 - \frac{1 - S_1}{2(1 - S_1 + \xi_c)} - 3(1 - S_1 + \xi_c)^2 \right. \\ \left. \times \left[ 1 - \frac{2}{3}(2 - 2S_1 + \xi_c) + \frac{1}{2}(1 - S_1 + \xi_c)(1 - S_1) \right] \right\} \eta(S_1 - \xi_c)$$

Similarly, in the case of  $k_3$  we let  $S_3$  approach zero ( $r_2 \rightarrow \infty$ ). Now  $S_2$  is formally  $S_3$ , while  $S_1$  should be replaced by  $1 - S_3$ . We thus find that  $k_3(S_3) = k_2(1 - S_3, 0)$ , i.e.,

$$k_3(S_3) = 1/27(32 - 6S_3^{-2} + S_3^{-3}) \eta(S_3 - \xi_c)$$

It is impossible to compare the theoretical calculation of  $k_2(S_1, S_3)$  to the experimental data in the domain  $ABC$  of three-phase flow because there are no experimental data of such kind. However good qualitative and quantitative agreement of theory with experiment in the domains of one- and two-phase flow (domains 1 and 2 on the phase diagram  $S_1S_2S_3$ ) presented in §§1.2 and 4.1, as well as in the case of Leverett's experiments mentioned above, supports the proposed theoretical description of the equilibrium three-phase flow.

## 4.5 Stability of Percolation Methods for Calculation of Phase Permeabilities

The essential characteristic of a medium in the developed approach to determination of the phase permeabilities, as well as other coefficients of transfer, is the radius probability density function  $f(r)$  of capillaries. For actual media, this function is determined by one of the existing porometric methods [47, 48] and is always known up to a certain error. Therefore it is important to estimate the effect that the error in establishing the function  $f(r)$  has on the results of the phase permeability calculations.

The expressions for calculating the phase permeabilities  $K_1$  and  $K_2$  for two-phase flow obtained in §4.1 have similar structure, and therefore it suffices to study the behavior of any one of them, e.g.,  $K_2$ , when  $f(r)$  varies.

$$K_2(r_k) = A' \int_{r_k}^{r_c} \left[ \int_r^{r_c} f(r) dr \right]^\nu \left[ \int_r^\infty f(r) \frac{dr}{r^4} \right]^{-1} \int_r^\infty f(r) dr f(r) dr \quad (4.50)$$

Here  $A'$  is a pre-integral term which does not affect stability of (4.50). In the three-dimensional case the correlation radius index  $\nu = 0.9 \pm 0.1$ . In this interval  $K_2$  is a continuous function of the given parameter with a continuous derivative. Therefore, without loss of generality, we can investigate stability of this function for any of the values  $0.8 \leq \nu \leq 1.0$ , for instance,  $\nu = 1$ .

Take two functions  $f^+(r), f^-(r) \in C[a_*, a^*]$ , where  $C[a_*, a^*]$  is the class of continuous functions on  $[a_*, a^*]$  normalized on unity. We shall mark the values corresponding to these two functions by the same signs. Introduce the norm  $\| \cdot \| = \left[ \int_{a_*}^{a^*} (\cdot)^2 dr \right]^{1/2}$ . Using Cauchy-Bunyakovsky inequality, we can write the following estimate for  $\omega(r) = f^+(r) - f^-(r)$

$$\left| \int_{a_*}^{a^*} \omega(r) dr \right| \leq \int_{a_*}^{a^*} |\omega(r)| dr \leq \left( \int_{a_*}^{a^*} \omega^2(r) dr \int_{a_*}^{a^*} 1 \cdot dr \right)^{1/2}$$

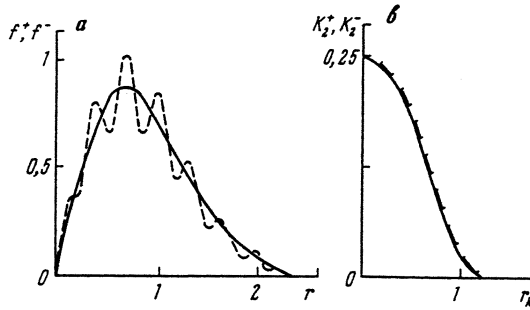


Figure 26: Effect of the oscillatory perturbation of the function  $f(r)$  (a) on the permeability change (b)

$$= (a^* - a_*)^{1/2} \|\omega(r)\| \tag{4.51}$$

Introduce the notations,  $K_0 = K_2(r_k = 0)$ ;  $\phi_0 = (K_0^+ - K_0^-)/A'$ ,

$$\phi_1 = (K_2^+ - K_2^-)/A'; S_+ = \int_{r_c^+}^{a^*} f^+(r) \frac{dr}{r^4}, S_- = \int_{r_c^-}^{a^*} f^-(r) \frac{dr}{r^4}$$

$$S_-^+ = \int_{r_c^-}^{a^*} f^+(r) \frac{dr}{r^4}; \epsilon_* = \int_{a_*}^{a^*} |\omega(r)| dr$$

After substituting the critical radii  $r_c^+$  and  $r_c^-$  into (1.7) we can write the following

$$\left| \int_{r_c^-}^{r_c^+} f^+(r) dr \right| \leq (a^* - a_*)^{1/2} \|\omega(r)\|, \left| \int_{r_c^-}^{r_c^+} f^-(r) dr \right| \leq (a^* - a_*)^{1/2} \|\omega(r)\| \tag{4.52}$$

Suppose  $r_c^+ \geq r_c^-$ . Then the following estimate can be written using (4.51) and (4.52) for  $r_k < r_c^-$  (the intervening computations are left out)

$$|\phi_1| \leq \Lambda_0 \epsilon_* \tag{4.53}$$

where  $\Lambda_0 = S_+^{-1} + 4(S_-^+)^{-1} + a_*^{-4}(S_- S_-^+)^{-1}$ .

When  $r_k \geq r_c^-$   $K_2^- \equiv 0$  and

$$|\phi_1| \leq \Lambda_1 \epsilon_* \tag{4.54}$$

where  $\Lambda_1 = S_+^{-1}$ . In the case of  $r_c^- > r_c^+$  (4.53) and (4.54) remain valid up to the interchange of the indices "+" and "-" in the expressions for  $\Lambda_0$  and  $\Lambda_1$ . Thus (4.53) holds for all  $r_k$  and we finally obtain the following

$$\|K_2^+ - K_2^-\| \leq A' \Lambda_0 (a^* - a_*)^{3/2} \|\omega(r)\| \tag{4.55}$$

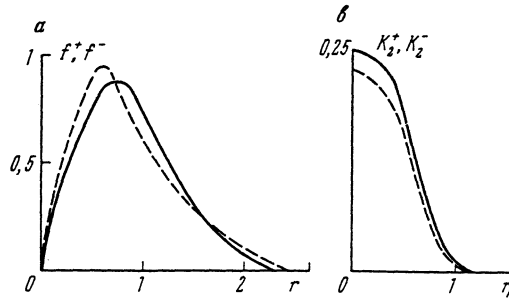


Figure 27: Effect of the shift of  $\langle r \rangle$  for the function  $f(r)$  (a) on the permeability change (b)

Therefore as  $\|\omega(r)\| \rightarrow 0$ ,  $\|K_2^+ - K_2^-\| \rightarrow 0$ , i.e., the phase permeabilities are stable with respect to small perturbations of  $f(r)$ . Obviously the relative phase permeability  $k_2 = K_2/K_0$  is also stable. Indeed, we can follow the same line used in deriving the relationship (4.53) for  $r_k = 0$  to obtain

$$\phi_0 \leq \Lambda_0 \epsilon_*$$

and then

$$|k_2^+ - k_2^-| \leq (2A'/K_0^+) \Lambda_0 \epsilon_* = \lambda_* \epsilon_*$$

and finally

$$\|k_2^+ - k_2^-\| \leq \lambda_* (a^* - a_*^{3/2}) \|\omega(r)\|$$

which proves the stability of the relative phase permeabilities with respect to small variations of  $f(r)$ .

To illustrate the analysis presented above, a series of calculations of  $K_2(r_k)$  was carried out for different  $f(r)$ 's. Two examples from this series are presented in figs.26 and 27. Shown in figs.26, a, and 27, a, is the nature of the perturbations (dotted lines correspond to  $f^-(r)$ ) of the original function  $f^+(r) = 2r \exp(-r^2)$  defined on  $[0, 3]$ . In the first case the perturbation is oscillatory, but does not change the average radius  $\langle r \rangle$  of capillaries and the variance  $\sigma_d$  of the distribution  $f(r)$ . In the second case, a shift of  $\langle r \rangle$  takes place. However in both cases the total deviation on the whole range of  $f(r)$  is the same,  $\epsilon_* \cong 0.1$ . Presented in figs.26, b, and 27, b, are the corresponding plots of  $K_2(r_k)$ . They imply that in the first case  $K_2(r_k)$  does not really change, whereas in the second case a notable difference between  $K_2^+$  and  $K_2^-$  appears. Calculations show that the phase permeability is as sensitive to changes in the variance of  $f(r)$ .

In the outlined cases the numerical value of the coefficient  $A' \Lambda_0 (a^* - a_*)^{3/2}$ , which appears in the estimate (4.55), is virtually always greater than its exact

calculated value by several orders of magnitude. This is due to the fact that the estimates in (4.53) and (4.55) are majorants, and therefore are rather overstated. The closest proximity of the estimated and the exact values of the discussed coefficient is observed in the case when the principal difference of  $f^+(r)$  from  $f^-(r)$  takes place in the neighborhood of the minimal radius  $r = a_*$  when  $a_* \rightarrow 0$ .

Concluding the topic, we would like to remind that other macro properties of a porous medium can be calculated using a given  $f(r)$ , just like the phase permeabilities. The specific electric conductivity  $\Sigma$  of the medium in the case when it is saturated by a conducting fluid, is an example of such a property. Since the expression (1.11) for  $\Sigma$  is akin to (4.50) for  $r_k = 0$ , if the numerical factor  $A'$  is replaced in the latter and  $r^4$  in its denominator is replaced by  $r^2$ , it follows that all estimates presented above remain valid up to the numerical values of the majorizing constants  $S_-, S_+, S_-^+$ .

Thus it turns out that the calculation of the effective macro properties of porous media, carried out in the percolation approach, is stable with respect to errors in determining  $f(r)$ .

## Chapter 5

# Percolation Model of Non-Steady State Two-Phase Flow in Porous Media

### 5.1 Immiscible Displacement of a Viscous Fluid by a Non-Viscous One

At present, the description of non-steady state flow of immiscible fluids is carried out using equilibrium phase permeabilities and a capillary pressure curve. The mentioned functions are determined by the saturation of porous media with any of the phases and do not depend on time and space coordinates. In this case the phase permeabilities are determined by the results of laboratory experiments on steady state two-phase flow, and the Leverett's function is found from the porometric curve.

However experimental data [14, 23] indicate the relaxational nature of inter-phase equilibrium attainment in non-steady state fluid flow. Considering this effect, a phenomenological model was suggested in [24] for the description of two-phase flow. This model includes time-dependent phase permeability with characteristic time of relaxation towards the equilibrium value. However, experimental determination of these dependencies encounters great technical difficulties.

In this study, for the description of two-phase flow in micro heterogeneous porous media a model of "forest growth" was proposed. It is a percolation model which permits to take into account the non-equilibrium effects of such fluid flow.

**Physical premises.** In the network model of heterogeneous media [25], capillaries form an IC, whose conductivity is determined by the capillary chains oriented in the direction of the flow and composing the skeleton of the IC. These chains communicate with each other through analogous capillary chains, providing flow in the transverse direction. Some of these chains create a network of an irregular form. As it is shown in [25], there exists an hierarchy of chains according to their average conductivity; therefore, the phase flow velocities, including the case of displacement of one phase by another, are different. At two-phase flow the injected phase enters the chains (later called "tree trunks") oriented in the direction of the applied pressure gradient, and through them enters the "branches of trees" – the capillary chains which provide flow in the transverse direction. As a result, growth of the tree formed by a trunk and branches takes place during the injection of the displacing phase.

In their turn, the branches provide inflow of the displacing phase into the "leaves," the capillary chains oriented parallel to the trunk. Leaves may have a complicated arborescent form, too. In Fig.28, two interrelated trees are presented schematically. The number 1 indicates trunks of growing trees, the number 2, branches, and the number 3, leaves.

Thus the same chains of capillaries oriented in the direction of flow may take part in the formation of both trunks and leaves, depending on how the displacing phase enters them. We shall consider leaves belonging to a given tree if the displacing phase enters them through branches of this tree. During the flow in the medium, trees grow at different rates. As a result, rapidly growing trees outrun in growth the slower-growing ones and block their further growth; this results in the decrease in the concentration of the latter. A similar situation is observed during the growth of leaves, which grow until the capillary chains forming IC them intersect with the next tier of branches. As a result, the displacing phase is trapped in these chains. This effect is caused by the dynamic nature of the displacement, and the fraction of the trapped phase is determined by the ratio between the rates of growth of the trunk and leaves.

Residual saturation of the displaced phase, trapped at the dynamic stage, may relax to the equilibrium value. This can happen if the IC of the displaced phase exists in the macro-volume, and the capillary forces prevent the invasion of the displacing phase into the IC. If the pressure  $P$  of the displacing phase is greater than the threshold pressure  $P_t$  at which the capillaries filled with the displaced phase form an IC, then the maximum possible fraction of the displaced phase is dynamically trapped. The above-mentioned mechanism allows to explain the increase of the fraction of the trapped phase with the increase of the flow velocity.

Below, we consider the approach which allows to get a quantitative description of two-phase flow in porous media using the forest growth model, where the "forest" is understood as the sum of trees (or one "banyan tree") formed by the



displacing phase.

It is obvious that taking into account all peculiarities of the interaction between the trees in a three-dimensional case will require an extremely cumbersome mathematical apparatus for its description. At the same time, considering the plane case of this problem will allow to simplify mathematical models, but will all the same reflect the main features of the phenomenon.

**Model of the medium.** We shall consider the network model of a heterogeneous medium. Conducting bonds (capillaries) of the network are distributed chaotically in it and their distribution according to the value of effective hydraulic radius is described by an arbitrary normalized probability density function  $f(r)$ . Suppose that before the displacement began the network was completely saturated with the displaced phase, whose viscosity is  $\mu_1$ , and the initial pressure,  $P_0$ . At the time  $t = 0$  the displacing phase, whose viscosity is  $\mu_2$ , is supplied under pressure  $P$  to the network boundary  $x = 0$ , and the displacement begins.

Consider the case when  $(P - P_0) \gg P_k$ , where  $P_k$  is the capillary pressure. During the description of the displacement we shall neglect flow tongues formed at the breakthrough of the displacing phase along a finite sequence of connected "thick" capillaries, since these "tongues" attenuate quickly. The velocity  $x_f$  of the phase interface, beyond which the saturation of the displacing phase is non-zero, is determined by the average conductivity of an infinite capillary chain, composed from the largest capillaries whose concentration is high enough for an infinite cluster to be formed in the medium.

The probability of the radius of a capillary in the network exceeding  $r_1$  is equal to

$$W(r > r_1) = \int_{r_1}^{\infty} f(r) dr.$$

If  $W(r > r_1)$  exceeds the percolation threshold  $W_c$  in the network, an infinite cluster composed of capillaries that satisfy the condition  $r > r_1$  is formed in the network. Thus the capillary chain which determines the location of the front  $x_f$  must consist of those capillaries that satisfy the condition  $r > r_c$ , where  $r_c$  is found from the condition of the formation of an infinite cluster

$$\int_{r_c}^{\infty} f(r) dr = W_c. \quad (5.1)$$

The chains containing capillaries with  $r > r_1$  form an irregular network, whose characteristic period (correlation radius) is determined by the expression

$$R(r_1) \sim d|W(r_1) - W_c|^{-\nu}, \quad (5.2)$$

where  $d$  is the period of the network,  $\nu$  is the correlation radius index and depends on the dimension of the problem [4]. The concentration of the conducting chains

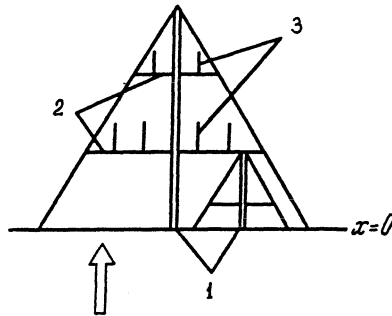


Figure 28: Diagram of the "tree" formation in the "forest growth" model

with  $r > r_1$  (the number of the conducting chains intersecting a unit surface)  $N(r_1)$  equals  $R^{1-z}(r_1)$ , where  $z$  is the dimension of the problem. As for the density of the concentration of  $r_1$ -chains, where  $r_1$  changes from  $r_1$  to  $(r_1 + dr_1)$  equals  $n(r_1) = -dN(r_1)/dr_1$  and, using (5.1), (5.2), is determined by the expression

$$n(r_1) = \nu(1-z)f(r_1) \left[ \int_{r_1}^{r_c} f(r) dr \right]^{\nu(z-1)-1} d^{1-z} \quad (5.3)$$

**"Forest growth" model.** Consider the interaction between trees during their growth in more detail. At the micro level the average flow velocity along an  $r$ -chain under the conditions  $\mu_1 \gg \mu_2$  and  $x_f \ll l$ , where  $l$  is the characteristic size of the region of the applied pressure difference, is determined from the Hagen-Poiseuille formula

$$V = r^2 \Delta P (8\mu_1 l)^{-1}. \quad (5.4)$$

This chain joins two opposite ends of the specimen, and therefore in order of magnitude its length coincides with that of the specimen, and the pressure difference applied to the ends equals the pressure difference applied to the given specimen. As is evident from (5.4), the maximum average displacement velocity in an  $r_c$ -chain is

$$V_m = r_c^2 \Delta P (8\mu_1 l)^{-1}. \quad (5.5)$$

Knowing the flow velocity along an  $r_c$ -chain (5.5), we can determine the position of the phase interface at any instant  $t$ ; behind it, saturation of the displacing phase is non-zero

$$x_f = V_m t.$$

Since the average flow velocity along the chain for a given pressure gradient is uniquely related to its effective radius, it is possible to go over from the capillary

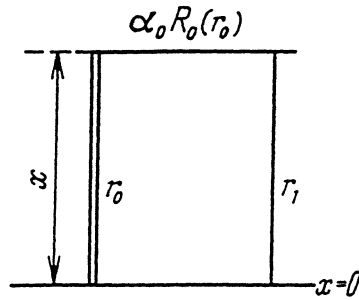


Figure 29: Blocking of the movement of the displacing fluid along the adjacent thinner capillary

radius distribution function  $f(r)$  to the fluid velocity distribution function for  $r$ -chains  $\phi(V)$ . For example, in the case  $f(r) = Ar^{-3}\eta(r - r_n)$ , we have  $\phi(V) = BV^{-2}\eta(V_m - V)\eta(V - V_n)$ , where  $\eta(*)$  is the stepwise Heaviside function, and the coefficients  $A$  and  $B$  are determined from the normalization conditions

$$\int_0^{\infty} f(r) dr = 1; \quad \int_0^{\infty} \phi(V) dV = 1.$$

In this case it should be taken into account that the "cutting-off" of the function  $\phi(V)$  in the region of large  $V$  will occur at the point  $V = V_m$ , determined not only by the properties of the medium, but also by the nature of the phenomenon.

Consider the interaction between trees growing with different rates behind the displacement front, and first of all obtain the condition for the blocking of a trunk by branches of other, faster-growing trees. Two competing factors influence this process: on the one hand, more slowly growing trees must be restrained by the more quickly growing trees; on the other hand, the characteristic distance between such trees is great, a property that decreases the restraint probability.

Blocking may take place if along the branches of the tree formed by a  $V_0$ -chain the displacing phase reaches the  $V_1$ -chain earlier than along the trunk of the latter (Fig.29). Consequently, the blocking condition has the form

$$\frac{x + \alpha R(V_0)}{V_0} = \frac{x}{V_1}. \quad (5.6)$$

Here  $R(V_0)$  is the correlation radius of the IC formed by the capillaries, where the minimal flow velocity is  $V_0$ ;  $\alpha$  is a coefficient of the order unity introduced as a result of the fact that the condition (5.6) is written for an arbitrary  $V_1$ -chain in the mean. Besides, in writing (5.6) it was supposed that branches grow with the same rate as the trunk.

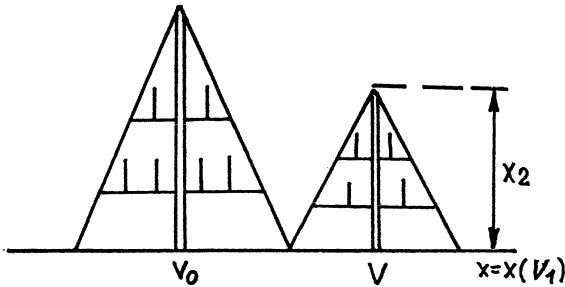


Figure 30: Diagram of the formation of the "crown" of a "tree"

In principle, the rates of the growth of lateral branches are different. To simplify calculations we may average these rates and introduce a certain average rate of growth of the branches for a given tree. It is obvious that the higher the rate of growth of the trunk, the higher the average growth rate of its branches due to the expansion of the range of radii of  $r_1$ -chains forming the branches. Without loss of generality we may take the proportionality factor in the mentioned dependence equal to unity, which means that the average rate of the branches' growth is equal to the rate of the growth of the trunk

If condition (5.6) is satisfied, blocking of all trees formed by  $V$ -chains with  $V < V_1$  takes place. The other trees continue their growth. It can be seen from (5.6), that blocking of a  $V_1$ -tree is possible by branches of different trees growing with a higher rate, but will occur at different distances  $x$ . It is obvious that actual blocking of the considered trial tree will be carried out by those trees, whose branches are connected at the minimum value  $x$ , to which corresponds the satisfaction of the following condition

$$dx/dV_0 = 0. \quad (5.7)$$

Thus, taking into account the obvious equality

$$x(V_1) = x_f \frac{V_1}{V_m} \quad (5.8)$$

we obtain a system of three equations for the three unknowns  $V_0$ ,  $V_1$ , and  $x(V_1)$ , it being obvious a priori, that  $V_0 > V_1$ . This system is solvable for any values of  $x_f$ .

Consequently, the considered region may be conventionally divided into three zones. When  $x > x_f$  one-phase flow without changing of saturation occurs. When  $x < x(V_1)$  flow of the displacing phase is observed through surviving tree trunks corresponding to the values  $V > V_1(x)$ . Here  $V_1(x)$  is determined from (5.6)-(5.8) as an inverse function to  $x(V_1)$ . The permeability of the displacing phase in this

zone is equal to zero. Finally, when  $x_f > x > x(V_1)$  we have the dynamic stage of the flow.

Now estimate the values of saturation for the porous medium in these zones. When  $x < x(V_1)$  the fraction of the displacing phase in the  $V$ -chain at the moment of blocking of the  $V_1$ -chain by the  $V_0$ -chain is  $\epsilon = V/V_1$ , and therefore the fraction of the trapped displaced phase in this chain is  $1 - \epsilon$ .

After averaging over the region of characteristic size  $R(V_0)$ , using (5.1)-(5.3), we have

$$S_0(x) = \frac{\int_0^{V_1} (1 - V/V_1) n(V) B(V) dV}{\int_0^{V_m} n(V) B(V) dV}, \quad (5.9)$$

where  $B(V) = 1$  in the pore model, and  $B(V) = V$  in the capillary model [26].

In the region  $x > x(V_1)$  trees grow practically without interaction. Around each trunk a "crown" is formed, i.e., a zone where the first phase has already been displaced from (Fig.30). Assuming that crowns have a triangular form and grow around the tree trunks with constant rates, we find the distribution of the saturation of the medium with the displacing phase in this region. The displacement zone begins to form around a  $V$ -chain after the length of the tree trunk in the course of its growth exceeds the considered coordinate  $x(V_1)$ . The transverse dimension of the region is proportional to the quantity

$$l(V) = x_f(V/V_m) - x,$$

which characterizes the distance between the tree top and the plane with coordinate  $x$ . Therefore the saturation by the displaced phase in the region  $x_f > x > x(V_1)$  equals

$$S = 1 - \beta \int_{V(x_2)}^{V_m} n(V) l(V) B(V) dV \quad (5.10)$$

Here the coefficient  $\beta$  is determined from the condition of matching solutions (5.9) and (5.10) for  $x = x(V_1)$ ;  $x_2$  is the current coordinate, measured from the level  $x = x(V_1)$  (Fig.30), and  $V(x_2)$  is the velocity of the phase interface in the chain, where it manages to move up to the level  $x_2$ . The velocity is determined from relationship (5.8)

$$V(x_2) = V_m(x_2 + x(V_1))x_f^{-1}. \quad (5.11)$$

Thus, the system (5.6) - (5.11) allows to determine the distribution of the saturation of the displaced phase for an arbitrary position of the front  $x_f$ , if the probability density function  $\phi(V)$  is known.

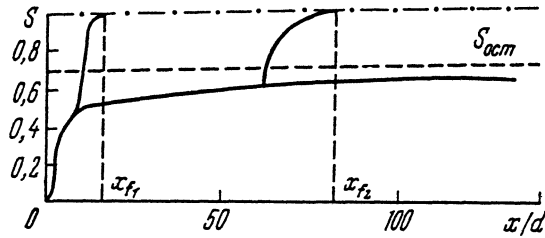


Figure 31: The displaced phase saturation distribution behind the displacement front

In this model it is also possible to estimate the characteristic size of stagnation zones for the displaced phase  $D$ , which corresponds to the value  $R(V_0)$ . As the front advances further, evermore rapidly growing trees are included in the restraint, and therefore the size of the stagnation zones grows with the increase of  $x$ . The quantity  $D(V_0) \sim R(V_0)$  can be estimated from (5.2), using the value  $V_0(x)$  determined from (5.6) - (5.8).

**Analysis of results.** The qualitative picture of the  $S_0$  and  $D(x)$  distribution behind the displacement front may be obtained from (5.6)-(5.11), after assigning the most characteristic form of the velocity probability density function, such as

$$\phi(V) = AV^{-2}\eta(V - V_n)\eta(V_m - V),$$

where  $A = V_m V_n / (V_m - V_n)$ . In the case  $V_n / V_m \ll 1$  we have  $A \approx V_n$ .

As a result, for  $x < x(V_1)$  we obtain

$$S(x, x_f) = \left[ \frac{V_m(V_1 - V_n)}{V_1 V_n} - \ln \frac{V_1}{V_n} - \frac{V_m}{V_1} \ln \frac{V_1}{V_n} + \frac{V_1 - V_n}{V_1} \right] \times \left[ \frac{V_m - V_n}{V_n} - \ln \frac{V_m}{V_n} \right]^{-1} \quad (5.12)$$

and for  $x > x(V_1)$ ,

$$S(x_2, x_f) = 1 - \frac{\beta}{V_m} \left[ (x_f + x) \ln \frac{V_m}{V_n} - (V_m - V_n) \left( \frac{x_f}{V_m} + \frac{x}{V_n} \right) - x_2 \frac{V_m - V_n}{V_n} + x_2 \ln \frac{V_m}{V_n} \right] \quad (5.13)$$

$$D(x) = x \left[ 2 \left( \frac{\alpha x V_n}{dV_m} \right)^{1/2} + \alpha \right]^{-1}. \quad (5.14)$$

The relations (5.12) - (5.14) are represented in graphical form on Figs. 31,32. From the diagram in Fig.31 it is clear that the asymptotic value of residual saturation obtained in the given model is a quantity of the order of 0.6-0.7, a fact that is

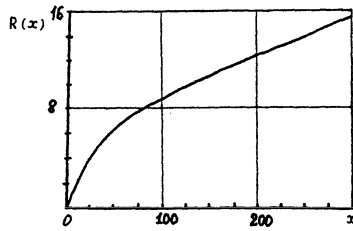


Figure 32: Characteristic dimension of the stagnation zones of the displaced phase as a function of the coordinate  $x$

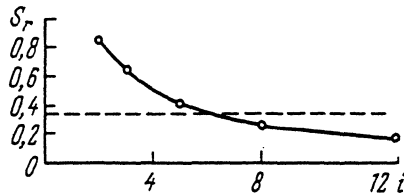


Figure 33: The dependence of the residual saturation on the form of the probability density function

consistent with the results of laboratory experiments [18]. This value substantially exceeds that of residual saturation of water corresponding to stable displacement, when the displacing phase flow is possible up to the breakdown of the IC, i.e., up to the values of the order of 0.2-0.3. The diagram in Fig.31 shows that  $S(x, x_f)$  tends to the asymptotic value at  $x/d > 100$ . This means that numerical simulation of non-steady state fluid flow presents great technical difficulties, since in order to obtain stable reliable results it is necessary to use in the two-dimensional case a calculation grid (capillary network simulating the pore space) of the size not less than  $200 \times 200$ . It is clear that in the three-dimensional case, for calculation one should use a network with the number of elements around  $10^7$ .

In the given model it is also possible to estimate relaxation times  $\tau$  for different distances behind the displacement front. They will correspond to characteristic closure times of the cells with size  $D \sim R(V_0)$ , i.e.  $\tau \sim D(x)/V_0(x)$ , where  $V_0(x)$  is determined from (5.6) - (5.8), and  $D(x)$ , from the relationship (5.14). For the model function  $\phi(V) = V_n V^{-2} \eta(V - V_n)$  in dimensionless units we obtain  $\tau \approx 1$ .

It is of great interest to analyze the influence of the form of the porometric curve  $f(r)$  and the corresponding  $\phi(V)$  on the quantity  $S_0$ . Calculations of the residual saturation dependence on the exponent  $n$  in the probability density function  $\phi(V) \sim V^{-n}$  are represented in Fig.33. As can be seen from the diagram, the quantity  $S_0$  for dynamic displacement may be less than in the case of steady state two-phase flow, and in the limit as  $n \rightarrow \infty$  asymptotically tends to zero.

This effect is explained by the fact that as  $n \rightarrow \infty$ , the function  $\phi(V)$  approaches the  $\delta$ -function in form. Then the displacement velocities in all chains are equal, as a result of which the trapping of the displacing phase turns out to be impossible.

We note that all the above-mentioned arguments are also true for the three-dimensional case. The forms of the corresponding analytical expressions for the three-dimensional problem are different, but the obtained relationships are qualitatively the same.

## 5.2 Effects of Viscosities and Interfacial Tension

A great impact of the flow velocity, interfacial tension, and viscosities of fluids on the IC structure was observed [18, 27, 28]. From these quantities, one can make up two dimensionless parameters, namely the capillary number  $C = (Q\mu_1)/\sigma$  (the ratio of the viscous forces to the capillary forces), and the viscosity ratio  $M = \mu_1/\mu_2$ . Here  $Q$  is the flow velocity,  $\mu_1$  is the viscosity of the injected fluid,  $\mu_2$  is the viscosity of the displaced fluid,  $\sigma$  is the coefficient of interfacial tension. When  $M \gg 1$  a stable interphase border is formed in the medium, and the displacement has a piston-type nature. When  $M \ll 1$  the displacement front turns out to be unstable: so-called "fingers," formed by the largest pores and pore channels along which displacing phase breaks through, develop.

It is natural to take into account the influence of the pore space structure, where the displacement takes place, in the form of the capillary function  $f(r)$ . It is interesting to observe the effects of the above-mentioned factors on the structure of the IC of the displacing phase during the displacement, because knowledge of the structure allows for qualitative estimates of saturation of the porous medium with each fluid for non-stable two-phase flow.

In §5.1 the "forest growth" model is suggested and its calculation is carried out for the simplest limiting case  $M = 0$ ,  $C \rightarrow \infty$ . The main attention was paid to the investigation of residual saturation of the medium with the displaced phase behind the displacement front, while the difference in phase permeabilities for steady state and non-steady state fluid flows was not analyzed at all. However, the approach suggested in §5.1 allows to consider non-steady state two-phase flow in the general case  $M \neq 0$ ,  $C < \infty$ , as well as to calculate the relative phase permeabilities  $k_i(S)$  for it ( $i = 1, 2$ ; 1 is the index of the displacing phase, and 2, the index of the displaced phase,  $S = S_1$ ).

Invoke the famous solution of the Buckley-Leverett problem [14], where for the saturation front velocity we have

$$V_f = QF(S)S^{-1}m^{-1}$$

Here  $V_f$  is the velocity of the phase interface averaged over an elementary physical volume,  $F(S) = [k_1(S)/\mu_1 + k_2(S)/\mu_2]^{-1}$ ,  $\Phi$  is the porosity. From the



microscopic point of view,  $V_f$  is the velocity averaged over the  $r$ -chains [14] with  $r > r_1$ , where  $r_1$  is the minimum radius capable of admitting the displacing phase. Using the technique of the effective radius distribution for chains, we can calculate the concentration of  $r$ -chains in the direction of the flow  $n(r)$  [25] and after summing up over all chains, we obtain

$$S = (1 - S_0) \int_{r_1}^{r_c} n(r) r^2 dr \left( \int_0^{r_c} n(r) r^2 dr \right)^{-1} + S_0, \quad \int_{r_c}^{\infty} f(r) dr = S_0$$

During the flow of the front, in some vicinity, the formation of "traps" is observed, i.e., the restraint of a displacing phase in the chains, where flow runs at a velocity less than the speed of overlapping of the chains with "branches" of rapidly growing "trees" (Figs. 28,29). In essence, this is the process of infinite cluster formation. The skeleton of this cluster, according to the Shklovsky-de Gennes model is a network of irregular form with the characteristic period (correlation radius)

$$R(r_1) \sim d \left( \int_{r_1}^{r_c} f(r) dr \right)^{-\nu}$$

The correlation radius represents the characteristic size of traps, and the characteristic time of their closure is

$$\tau \sim R(r_1)/V_f(r_1) \quad (5.15)$$

Here two processes compete. The maximum velocity of the interphase movement is realized in the thickest chains (the  $r_c$ - chains). At the same time  $R(r_c) \rightarrow \infty$ ; therefore, they cannot interact with forming of traps. It is obvious that physically the situation which is realized corresponds to the minimal time of restraint  $\tau = \tau_*$ , whereas from the condition of achieving the minimum value,  $d\tau/dr = 0$ , the corresponding minimum radius of chains  $r_*$  in the skeleton of the IC of the displacing fluid at the moment of the trap formation can be determined.

In the chains with  $r < r_*$  the ratio of the volume occupied by the displacing fluid to the total volume of the chains at the moment of restraint is

$$\epsilon = V(r)/V(r_*) = r^2/r_*^2,$$

where  $V(r)$  is the flow velocity in the  $r$ -chain. In this case the mass of the IC of the displacing phase is

$$S = (1 - S_0) \left[ \int_{r_*}^{r_c} n(r) r^2 dr + \int_0^{r_*} n(r) \epsilon r^2 dr \right]$$

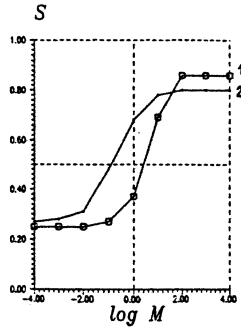


Figure 34: The dependence of the residual saturation of the displacing phase on the viscosity ratio (for a fixed capillary number:  $\log C = 3.5$ )

$$\times \left( \int_0^{r_c} n(r) r^2 dr \right)^{-1} + S_0 \quad (5.16)$$

The nature of the relation  $S(M)$  obtained for the case of the model probability density function  $f(r) = (10/9)r^{-2}$ ,  $1 < r < 10$  is represented in Fig.34 by line 1. It can be seen that in the limiting cases  $M \gg 1$  and  $M \ll 1$ , theoretical calculations give the maximum (the case of piston-type displacement) and the minimum (the case of viscous fingering) saturation and correlate well quantitatively with the results of numerical experiments [18], represented in Fig.34 by curve 2. These relations  $S(M)$  are obtained for the case  $C \rightarrow \infty$  (in the numerical experiment  $C$  was set to equal 3.5).

Draw our attention to the investigation of the effect that parameter  $C$  has on the nature of the displacement. The minimum radius of a capillary which can be reached by the displacing fluid for the given pressure difference is determined from the condition of the equality between the hydrodynamic and the capillary pressure differences

$$\Delta P_g / \Delta P_c = 1 \quad (5.17)$$

From Darcy's law we have  $\nabla P_g = Q\mu_1 / (k_0 k_1)$ . The characteristic sizes in this problem are pore sizes (for example, the average radius  $\langle r \rangle$ ) and the size  $L$  of the specimen. It is obvious that using the hydrodynamic pressure difference on pore size is physically unjustified since the action of mass forces is not taken into account. Therefore in (5.17) it is necessary to use the estimate of the value  $\Delta P_g$  over the size  $L$ :  $\Delta P_g = \nabla P_g L$ . From Laplace's formula we have  $\Delta P_c = 2\sigma/r$ . In this case, after substituting these relations in (5.17), we have

$$C = k_0 k_1 / (rL) \quad (5.18)$$

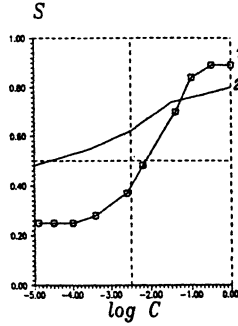


Figure 35: The dependence of the residual saturation of the displacing phase on the capillary number (for a fixed viscosity ratio:  $\log M = 2.9$ )

Thus, using (5.18) we can determine from the capillary number the minimal radius of capillaries  $r_k$  accessible for the non-wetting fluid. Two situations are possible. In the first case  $r_* < r_k$ . Then the capillary pressure does not allow the non-wetting fluid to enter the capillaries with radii  $r < r_k$ , and traps are formed by the  $r_k$ -chains. At the closure of these traps, restraint does not occur since other chains, being the more rapidly growing ones, have managed to grow beyond the region formed by this conditional trap. For such formation of an IC, equilibrium fluid flow takes place. To take into account the influence of the surface tension forces on the structure of the IC, it is necessary to substitute  $r_k$  for  $r_*$  in (5.16).

For the model function  $f(r)$  used above, calculations of the relation  $S(C)$  were carried out for a fixed  $M$  ( $\ln M = 2.9$ ). The obtained theoretical relation is shown in Fig.35 by line 1. Line 2 in this Figure corresponds to the results of the numerical experiment [18] for  $\ln M = 4.0$ . A good consistency of transfer regions from capillary fingering to stable piston-type displacement in theoretical and calculated data can be noticed from the figure. Some difference may be explained by the corresponding differences in the values of  $M$  and in the forms of functions  $f(r)$  used in the calculations.

The second situation occurs when  $r_* > r_k$ . In this case the process is essentially non-steady state. When the fore front of the displacement passes, there appear traps where the displaced phase is retained, the fraction of the trapped phase being greater than the critical value necessary for forming an IC of the displaced phase. Therefore the phase retained in the traps does not lose connectedness and flows away through its IC, accompanied by the replacement of phase 2 by phase 1 in  $r$ -chains with  $r_k < r < r_*$ . This means that the skeleton of IC 2 remains as it was (IC 2 only loses its "dead ends"), whereas new chains are added to the skeleton of IC 1 to increase its conductivity.

We may suggest the following model of relaxation. Fluid 2 is displaced from the capillary chains retained in the trap starting from  $r_*$ , up to  $r_k$ . When fluid 2 is

completely displaced from the  $r_i$ - chain it will become part of the skeleton of IC 1. The other chains with  $r_k < r < r_i$  will remain for the moment dead ends without any contribution to the conductivity of IC 1. Therefore, for the conductivity of IC 1 at the given instant, taking into account [26], we have

$$k_1 = \left( \int_{r_i}^{r_c} n(r) I(r) dr \right) \left( \int_0^{r_c} n(r) I(r) dr \right)^{-1}, \quad I(r) = \int_r^{\infty} f(r_1) dr_1 \\ \times \left[ \int_r^{\infty} f(r_1) r_1^{-4} dr_1 \right]^{-1} \quad (5.19)$$

and for its mass, taking account of the dead ends, we have

$$S = (1 - S_0) \left[ \int_{r_i}^{r_c} n(r) r^2 dr + \int_{r_k}^{r_i} n(r) \epsilon r^2 dr \right] \\ \times \left[ \int_0^{r_c} n(r) r^2 dr \right]^{-1} + S_0 \quad (5.20)$$

Relations (5.19), (5.20) represent the non-steady state phase permeability of phase 1 in a parametric form through the parameter  $r_i$  ( $r_k < r_i < r_*$ ).

Consider the conductivity of IC 2. At the closure of traps, some part of fluid 2 will be retained in them. At the same time, there is IC 2 in the medium, which consists of the capillaries with  $r < r_k$ . Along this IC, relaxation of the trapped phase to the equilibrium value of its saturation in the medium takes place. As new channels for moving of fluid 2 are not formed at that moment, the conductivity of the IC does not change in the course of relaxation and is equal to

$$k_2 = \left( \int_0^{r'_c} n(r) I(r) dr \right) \left( \int_0^{r'_c} n(r) I(r) dr \right)^{-1}, \quad \int_{r'_c}^{r_k} f(r) dr = S_0 \quad (5.21)$$

As relaxation takes place, the current value  $r_i$  approaches the equilibrium value  $r_k$ , while the phase permeabilities approach theirs. Time of relaxation to the equilibrium value depends on the values of parameters  $C$  and  $M$ . The non-steady state phase permeabilities represented in Fig.36 are calculated using the mentioned model function  $f(r)$ , for the case  $\ln M = 0$  and  $\ln C = -1.1$ . It is clear from the above-mentioned data that there are two characteristic flow regions.

1.  $S(r_*) < S < S(r_k)$ . In this region, traps are formed, fluid flow is essentially non-equilibrium, and therefore for the calculation of  $k_1(S)$ , it is necessary to

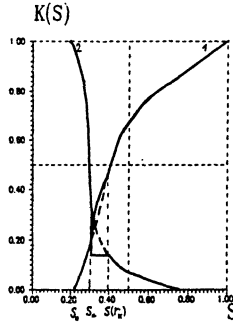


Figure 36: Unsteady phase permeabilities of phases 1 (curve 1) and 2 (2) for the model distribution function  $f(r) = A/r^2$  near the displacement front ( $\log M = 0$ ;  $\log C = -1.1$ )

use formulas (5.19), (5.20), and for the calculation of  $k_2(S)$ , relations (5.20), (5.21).

2.  $0 < S < S(r_*)$ ,  $S(r_k) < S < 1$ . In these zones either steady state flow before the front without forming of the trapped phase is observed, or the relaxation displacement of the trapped phase at the front has already finished, and the fluid flow becomes equilibrium again. Here the relations from §2.1 are valid for the calculation of  $k_1(S)$  and  $k_2(S)$ .

The presented calculated curves agree qualitatively with the results of experimental investigations [29] which demonstrate the main tendencies in deviation of the dynamic curves of the phase permeabilities from steady state.

Thus obtained non-steady state phase permeabilities may be used for the calculation of the fluid flow based on Buckley-Leverett or Rappoport-Leas equations [14]. The capillary number actually determines residual saturation of the medium with fluid 2 and affects the rate at which saturations reach their limiting values.

It is interesting to consider the region of small values of  $C$  when relaxation in the traps formed is slow. As it is known from laboratory experiments [27, 28], in this case the flow velocity through the trunk and branches of a tree differ substantially. We shall introduce a coefficient which accounts for this anisotropy,  $\alpha = V_c/V_b$ , where  $V_c$  is the rate of growth of the trunk, and  $V_b$  is the average rate of growth of branches. This coefficient may be different for different  $r$ -chains and may also depend on the pressure difference in the specimen. For qualitative analysis, we can set the form of the relation  $\alpha(r)$  to be linear, and consider the slope of the line proportional to the applied pressure difference, as in [27].

By analogy with (5.15), introduce the time of restraint  $t_b$  of the traps formed by branches of  $r$ -chains,  $t_b = R(r)/V_b(r)$ . Under the assumption of  $\mu_1 \ll \mu_2$  and

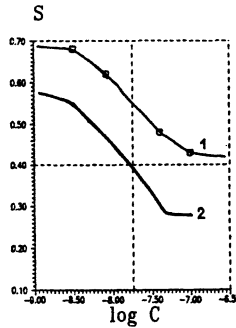


Figure 37: The dependence of the phase saturation on the capillary number for the distribution function  $f(r) = A/r^2$

$x_f \ll L$ , for the rate of growth of the trunk we have [30]  $V_c(r) = \Delta P r^2 (\mu_2 L)^{-1}$ . Consequently  $V_b(r) = \alpha(r)V_c(r)$ . In order to determine the radius of the chains forming the traps let us again require the minimality of time of their joining,  $dt_b/dr = 0$ . Having determined from this condition  $r_b^*(\Delta P)$ , we can calculate the dependence  $S(\Delta P)$  from (5.16). Furthermore, by taking into consideration Darcy's law, we may obtain from (5.18) the dependence  $C(\Delta P)$  and determine the correlation  $S(C)$ . The results of calculations for the above-mentioned model function  $f(r)$  are represented by curve 1 in Fig.37, where curve 2 corresponds to the data of the numerical experiment [18].

Thus the model proposed in this chapter allows not only to explain qualitatively the results of laboratory experiments on the investigation of non-steady state displacement for immiscible fluids in porous media, but also to calculate quantitatively the main parameters of the process, namely the saturation of the medium with each phase and the conductivities of the formed IC's. To perform theoretical calculations within the framework of the suggested "forest growth" model, it is necessary to know the capillary function and the critical percolation indices. The results of the calculations performed for the model function  $f(r)$  and the typical value of the correlation radius index  $\nu$  for an IC demonstrates a good quantitative agreement with experimental data [27, 29] and the results of direct numerical modeling in two-dimensional networks [18].

## Chapter 6

# Determination of Pore Size Distribution in Grained and Cavernous Rocks

It follows from the results presented above that the quantities  $\Sigma$ ,  $K$ ,  $k_i$  are determined primarily by the function  $f(r)$ . Therefore the first thing to know for the calculation of permeabilities is the size probability density function (PDF) for the pore channels.

At present practical determination of the coefficients of permeability is carried out mainly by means of direct experiments [72]. These, however, are too complicated and cumbersome. An alternative approach suggests the development of indirect methods for the determination of transfer coefficients, the most important of which are  $K$  and  $k_i$ . These methods should be based on model theoretical perceptions of the pore space of the medium and the fluid flow. Information about the pore space structure required by these methods can be obtained using one of the known porometric methods for the chosen model of the medium.

The purpose of the porometric methods is to determine the size probability density function (PDF) for the pores. The meaning of this function depends on the model of the pore space structure used to interpret the porometric data. The model of infinite cylindrical pores (ICP), which the majority of the contemporary schemes of the porometric data interpretation is based upon, is too inaccurate and can bring about considerable errors [73]. To take account of specific properties of the pore space structure of actual media more adequately, it is necessary to use network models and percolation models to interpret the porometric data.

Many actual media (e.g., grained or cavernous ones) have twofold porosity, i.e., large-scale, or porous, and small-scale, or capillary [47]. Volumetric proper-

ties (such as saturation) of such media are mainly determined by the volumes of the pores, while their conducting characteristics depend primarily on the capillary subsystem of the pore space. Usage of the conventional porometric methods permits to study only the large-scale pore subsystem [73]. To determine the parameters of a capillary subsystem, it is necessary to gather information about the subsystem using a quantity that does not depend strongly on sizes of the pores. Electric conductivity is an example of such a quantity. Parameters can be found based on electric surface measurements using electro-porometric methods in a core partially saturated with a conducting electrolyte [74]. This method suggests that the measurements of the specific electric conductivities for different parts of the core saturated with a wetting electrolyte in the gravitational field be taken instead of the measurements in the non-wetting mercury volume. The described approach allows to get rid of the influence from the subsystem of the site pores. It is also possible to determine the PDF for capillaries based on direct use of the percolational formula for electric conductivity. This method suggests a combined scheme of mercury and standard porometry.

## 6.1 Percolation Model for the Mercury Injection Test

During the mercury injection test the displacement of gas from the core by a non-wetting phase (mercury) takes place. As it fills the capillaries, the non-wetting phase overcomes the capillary pressure

$$p_k = \Delta p = p_1 - p_2 = 2\chi \cos \theta / r_k. \quad (6.1)$$

For small pressure differences at the initial stage of the process, pores with radii greater than  $r_k$  do not form a connected system. They form finite clusters, only those of which can be reached by mercury, that are adjacent to the outer cross-section of the specimen. When the pressure difference reaches the breakthrough value, large enough for mercury to appear in the outer cross-section of the core, the pores filled with mercury form a connected system, i.e., an infinite cluster.

At the intervening stage of the process, as  $\Delta p$  increases further, the density of the infinite cluster of the pores filled with mercury goes up. When saturation  $S$  reaches the second threshold value the connected system of the gas-saturated pores breaks.

From this instant, during the final stage of the process, the gas stops coming out of the core. Trapped in the finite clusters, the gas compresses as the pressure in the non-wetting phase goes up.

Take a periodic network of cylindrical capillaries as a geometrical model of the pore space and consider the outlined stages for the filling of the core with



mercury [75].

**The initial stage of displacement.** Suppose that at the initial stage displacement takes place along non-intersecting tortuous paths. In this case the fraction of the super-critical capillaries being filled with mercury is

$$X(r_k) = 1 - F(r_k) = \int_{r_k}^{\infty} f(r) dr. \quad (6.2)$$

The probability  $\xi_i$  of the first  $i$  capillaries being super-critical and the  $(i+1)$ -th capillary having radius  $r_k$  (i.e., subcritical) is  $X^i(r_k) F(r_k)$ .

The average volume  $\nu'(r_k)$  of a super-critical capillary is found as the conditional expectation of the random variable  $\pi r^2 l$  (capillary volume) when  $r_k \leq r < \infty$ . The volume of mercury that has reached the first  $i$  super-critical capillaries in a chain equals  $i\nu'(r_k)$ . After averaging this volume with regard to the expression for probability  $\xi_i$ , we obtain the mean volume  $V(r_k)$  of mercury which has passed into the chain of total volume  $V = V(r_k = 0)$ . Since at the considered stage the saturation of the pore space with mercury is  $S = V(r_k)/V$ , using (6.2) we obtain the following correlation

$$S(r_k) = \frac{\pi l}{VF(r_k)} \int_{r_k}^{\infty} r^2 f(r) dr. \quad (6.3)$$

After using (6.1) to pass to the variable  $r_k$ , in the dependence  $S(\Delta P)$ , which has been measured by means of the mercury porometry method, we obtain the experimentally determined dependence  $S(r_k)$ .

After integrating the right side of (6.3) by parts using (6.2) and then differentiating both sides of the obtained equation with respect to  $r_k$ , we obtain

$$\frac{d}{dr_k} g(r_k, X) - r_k^2 \frac{dX}{dr_k} = 0; \quad g(r_k, X) = \frac{V(1-X)S}{\pi l} \quad (6.4)$$

After passing in (6.4) to the new independent variable  $S$  we obtain an ordinary differential equation for the function  $X(S)$  with the initial condition  $X(S=0) = 0$ . Its solution is

$$X(S) = 1 - \exp \left[ - \int_0^S \frac{V dS'}{V S' + \pi l r_k^2(S')} \right] \quad (6.5)$$

From (6.5) and (6.2) we obtain the desired dependence  $f(r_k) = -(1-X)V(VS + \pi l r_k^2)^{-1}(dS/dr_k)$ .

At the instant when mercury appears in the outer cross-section, the fraction  $X$  of the super-critical pores equals the percolation threshold  $X_c$ , and an infinite cluster of the super-critical pores is formed. The value  $X_c$  is determined from the relationship (1.1).

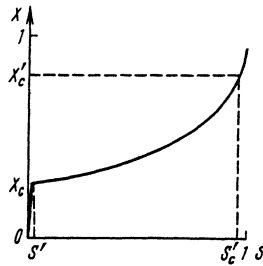


Figure 38: Dependence of the fraction of super-critical capillaries filled with mercury on the saturation of the medium with it

After substituting the value  $S_c$  of saturation at the time of the breakthrough as measured in the experiment and the value  $X_c = X(S_c)$  from (1.1) in (6.5), we obtain the following relationship for the constants  $z$ ,  $V$ , and  $l$  of the network,

$$\frac{D}{z(D-1)} = 1 - \exp \left[ - \int_0^{S_c} \frac{V dS'}{V S' + \pi l r_k^2(S')} \right] \quad (6.6)$$

**Simulation of the intervening stage.** At the second stage of mercury injection, the non-wetting phase fills the infinite cluster of the super-critical capillaries. Concentration  $N(r_k)$  of such capillaries per unit volume of the specimen is  $0.5 z \mu_z l^{-3} W(X)$ , where  $\mu_z$  is the correction due to the geometry of the network and  $W(X)$  is the density of the infinite cluster. Saturation  $S(r_k)$  at this stage is equal to  $N(r_k) \nu'(r_k) / \Phi$ , where  $\Phi$  is the porosity of the medium, or, taking account of (6.1),

$$S(r_k) = \frac{\pi z \mu_z W(X)}{2 m l^2 X} \int_{r_k}^{\infty} r^2 f(r) dr \quad (6.7)$$

After integrating by parts in (6.7) using (6.2) and differentiating both sides of the obtained relation with respect to  $r_k$ , we obtain the equation (6.4) for the function  $X(r_k)$  again, where now  $g(r_k, X) = 2 S m l^2 X [\pi z \mu_z W(X)]^{-1}$ .

It is also possible, as at the first stage, to pass to the new independent variable  $S$  in this equation:

$$\frac{dX}{dS} = 2X \left[ \frac{r_k^2(S)}{m l^2} \pi z \mu_z W(X) + 2S \left( \frac{X}{W(X)} \frac{dW}{dX} - 1 \right) \right]^{-1} \quad (6.8)$$

Since when  $X$  is equal to the threshold value  $X_c$ , the density  $W(X)$  of the infinite cluster vanishes, it follows from the equation (6.7) that  $S(X_c) = 0$ . This

relationship is the initial condition for the equation (6.8). However in the experiment, at the end of the first stage the value of saturation is  $S_c > 0$ . The obtained "discrepancy" in data at the transition from the first to the second stage is due to the fact that the model (6.8) does not take into account the volume of the super-critical pores filled with mercury and adjacent to the entrance cross-section. To take this volume into consideration, we shall use the formula (6.5) to calculate  $X(S)$  in the interval  $0 < S \leq S'$  and the solution of the Cauchy problem (6.8) to calculate it for  $S > S'$ . It is natural to choose the point  $S'$  at the intersection of the plots of these two relations in the  $(S, X)$ -plane (see fig. 38).

At the instant when the displaced phase stops coming out of the core, the infinite cluster of the gas-containing capillaries breaks up. The value  $X(S'_c)$  equal to the percolation threshold for the gas cluster  $X'_c = 1 - X_c$  corresponds to the value of saturation  $S'_c$  measured at the said instant. The expression

$$X(S'_c) = 1 - X_c \quad (6.9)$$

gives the correlation between the constants  $z$  and  $l$  of the network.

**The final stage of displacement.** At the third stage of the experiment, the non-wetting phase still occupies the infinite cluster of the super-critical pores. Therefore the equation (6.8) remains valid. Nevertheless at this stage the relation  $r_k(S)$  has to be found anew, since the pressure  $p_2$  in the formula (6.1) becomes the pressure in the trapped compressing clusters, and is therefore unknown. Suppose that trapping of air takes place simultaneously throughout the whole core at the instant when the cluster of the gas-containing capillaries breaks up. Consider the gas ideal and let all finite clusters filled with the trapped gas compress according to the law

$$dV_k/V_k = -dS/(1 - S), \quad (6.10)$$

where  $V_k$  is the volume of the cluster.

Due to the low heat conductance of an actual porous medium it is possible to consider compression to be isentropic. When heat conductance is high a polytropic process is considered similarly. After differentiating the law of isentropic compression  $p_2 V_k = \text{const}$  and using the relationship (6.10), we obtain

$$dp_2 = \gamma_0 \frac{dS}{1 - S} p_2, \quad (6.11)$$

where  $\gamma_0$  is the isentropic exponent.

The quantity  $p_2$  can be expressed in terms of the known value of pressure  $p_1$  from the formula (6.1) for the capillary pressure as follows,  $p_2 = p_1 - 2\chi \cos \theta / r_k$ .

After substituting this expression for  $p_2$  as well as its differential  $dp_2$  in (6.11) and some algebraic transformations, we obtain

$$\frac{dr_k(S)}{dS} = \frac{r_k^2(S)}{2\chi \cos \theta} \left( \gamma_0 \frac{p_1(S) - 2\chi \cos \theta / r_k}{1 - S} - \frac{dp_1(S)}{dS} \right) \quad (6.12)$$

The desired dependence  $r_k(S)$  can be found from this equation, if the experimental dependence  $p_1(S)$  is known. At the time of trapping, the pressure in the gas phase coincides with the pressure  $p_0$  in the outer cross-section of the core; therefore, the initial condition for the equation (6.12) is

$$r_k(S'_c) = \frac{2\chi \cos \theta}{p_1(S'_c) - p_0}$$

When the displacement is over, the value of porosity  $\Phi$  can be found as the ratio of the volume of mercury that has entered the pores to the volume of the core. This quantity can be also calculated as the product of the average capillary volume and the concentration of the edges of the network

$$\Phi = \frac{\pi z \mu_z}{2l^2} \int_0^{\infty} r^2 f(r) dr \quad (6.13)$$

The last expression represents another correlation between the constants  $z$  and  $l$  of the network.

Thus the formulas (6.5), (6.8), (6.12) permit to find the dependencies  $X(r_k)$  and  $f(r_k)$  for the given  $l$  and  $z$ . To determine the constants  $z$  and  $l$  from the relationships (6.9) and (6.13), an iterative procedure is set up with respect to these parameters. Once this is done, the quantity  $V$  is found from the relationship (6.6), and the dependencies  $X(r_k)$  and  $f(r_k)$  are determined in the domain of the macro-pores using this quantity at the first stage of displacement.

The presented algorithm of data interpretation in mercury porometry was obtained for model II. Without drawing close attention to it, we note that the equations describing the sequence of stages for mercury injection in a porous medium for model I can be derived in a similar fashion.

**Results of the calculations using experimental data.** To demonstrate the efficiency of the outlined method for the experimental data interpretation, we shall present the calculations for the experiment on the displacement of air by mercury from a core extracted from the East-Poltavian layer (data given by N. V. Savchenko). The plot of the  $X(S)$  relationship for this core appears in fig. 38. The obtained dependence proved to be stable with respect to small changes of the initial conditions. The value of  $S_c$  close to zero and the value of  $S'_c$  close to unity are characteristic of this dependence. For the specimen under consideration,  $S_c = 6.5 \cdot 10^{-4}$ ,  $S'_c = 0.964$ .

The curve  $I$  in fig. 39 corresponds to the initial experimental data. The curve  $II$  is obtained, if a relative error of 0.05 is allowed in determining the quantity  $S$ . The greatest difference between the two curves is achieved at the values of  $r_k$  corresponding to the third stage of the experiment and makes 15%. For the first two stages this difference does not exceed 5%. As the relative error goes down,

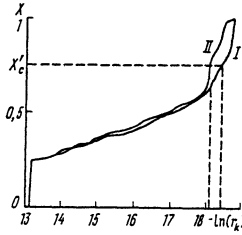


Figure 39: Results of the study on stability of the dependence  $X(\eta_k)$  with respect to small changes of initial values

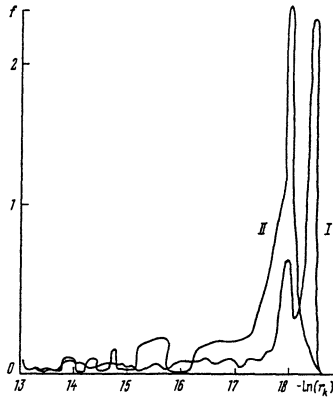


Figure 40: Plots of the function  $f(-\log r_k)$  obtained for curves  $I$  and  $II$  (see fig. 39)

the curves  $I$  and  $II$  are observed to approach each other. This fact confirms the conclusion about the stability of the dependence  $X(r_k)$  with respect to the small changes of the initial conditions based on (6.5) and (6.8).

The plots of  $f(-\ln r_k)$  relations for the cases  $I$  and  $II$  shown in fig. 39 are presented in fig. 40. These curves diverge by more than 100% almost everywhere, a fact that speaks of the essential unstability of the dependence  $f(r_k)$  with respect to the small changes of the initial conditions.

Stability of the dependence  $X(r_k)$  and unstability of  $f(r_k)$  are typical not only for percolation models of mercury injection. The problem arises from the fact that obtaining the dependence  $f(r_k)$  requires applying to the dependence  $X(r_k)$  a differential operator which is unstable in the general case. To overcome this unstability, one can use the regularized differential operator [76].

At the same time, the permeability and the electric conductivity of a porous medium are expressed in terms of integrals of the  $\int \phi(r) f(r) dr$  type, where  $\phi(r)$

is a known exact dependence. After integrating by parts we find

$$\int_0^a \phi(r) f(r) dr = \phi(0) - \phi(a) X(a) + \int_0^a \phi'(r) X(r) dr$$

Therefore the integral, which is necessary for the calculation of the coefficients of permeability, is stable towards errors of the experiment.

The obtained pore radii distribution function, together with the constants  $z$  and  $l$  of the network, forms sufficient initial data for the calculation of the coefficients of permeability for a porous medium.

## 6.2 Percolation Model for the Electric Porometry Method

If one of the sides of an initially non-saturated core is immersed in a container with a wetting electrolyte (see fig. 41), a saturation distribution, decreasing with height, is formed there. This phenomenon is due to the fact that a wetting fluid rises in a capillary of radius  $r$  in the gravitational field up to a height

$$L = 2\chi \cos \theta / (\rho_f g r), \quad (6.14)$$

where  $\chi$  is the coefficient of surface tension,  $\theta$  is the contact angle,  $\rho_f$  is the density of the fluid, and  $g$  is the acceleration of gravity. In general, vertical capillary chains are not isolated, but nevertheless the fraction of the saturated pores at the height  $L$  can be considered, up to some proportionality factor, as determined by a critical radius  $r(L)$  which correlates with  $L$  through (6.14). In this case the specific electric conductivity in the vertical direction is a function of saturation, and therefore of height  $L$ , and can serve as a source of information about the size distribution of pores.

Measure the specific electric conductivity at the heights  $\{L_i\}$  in sufficiently thin layers  $\Delta L_i \ll L_i$  (see fig. 41), so that within the portion measured, the specimen can be considered uniformly saturated. Estimate the specific electric conductivity of an arbitrary portion of the specimen and the contributions to it made by the subsystems of the site pores and the bond pores. Let the specific electric conductivity of the electrolyte be  $\sigma_e$  and of the skeleton of the specimen,  $\sigma = 0$ . Obviously, the electric conductivity of the material in the vertical direction is determined by the vertically-oriented chains of pores filled with the electrolyte. Taking account of the transverse bonds between them in the considered case brings coefficients of the order unity into the calculations and does not affect the estimates. Consider a unit cube of an element of the specimen. If  $l$  is the period of the network and  $\kappa$  is the fraction of the vertical chains in a unit volume filled with the

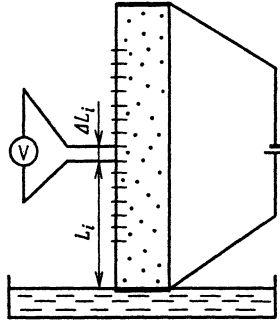


Figure 41: Principal scheme of measurements in the electric porometry method

electrolyte, then the concentration of such chains on an elementary cross-section is  $N_b = \kappa l^{-2}$ . Bonds of each chain are connected successively, and therefore the conductivity of a vertical chain is  $\sigma_i = \left( \sum_{j=1}^{N_1} R_j^i \right)^{-1}$  ( $R_j^i$  is the resistance of the  $j$ -th bond of the  $i$ -th chain,  $N_1 = l^{-1}$  is the number of bonds in a chain).

Estimate the contribution made by each of the subsystems to the value of  $\sigma_i$ . We shall take into account the following facts: characteristic radius of sites is  $r_s = l/4$  and bonds are cylinders with characteristic radii  $r_b \ll l$  and lengths  $\approx l/2$ .

In this case, for the resistances of the bonds in the chains we have  $R_b \sim \sigma_e^{-1}(l/r_b^2)$ ,  $R_s \sim \sigma_e^{-1}l^{-1}$ , and their ratio  $R_s/R_b \sim (r_b/l)^2 \ll 1$ . This implies  $\sigma_i = \left( \sum_{j=1}^{N_1/2} (R_b)_j^i \right)^{-1} \sim \sigma_e r_b^2$ , from which we obtain the following estimate for the specific electric conductivity of the material,

$$\sigma^{(0)} \sim \sum_{j=1}^{N_b} \sigma_i \sim \sigma_e (r_b/l)^2 \quad (6.15)$$

The relationship (6.15) shows that the specific electric conductivity of a specimen made up of the site pore and the bond pore subsystems of different scale depends only on the bond resistances. Therefore it is possible within the proposed electric porometry method (EPM) to pass from the network model (NM) with solid sites to an NM with point sites, where the volumes, electric and fluid flow resistances of the sites vanish. The properties of such network (from the point of view of the EPM) are determined by the radius probability density function (PDF) of the bond pores. Hence radii of different bonds in capillary chains of any orientation are of the same order (unlike the chains with sites, where capillaries of different scale  $r_b \gg r_s \sim l$  connect at each period of the network). This permits to establish the actual correlation between capillaries of variable radii and cylindrical

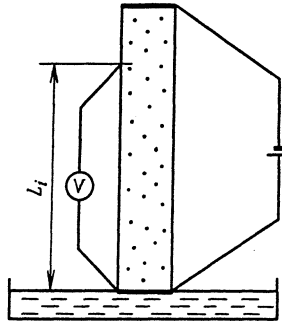


Figure 42: Modified scheme of measurements in the electric porometry method

capillaries of some effective radii.

Introduce some complimentary simplifying assumptions. Consider the network simple cubic and the vector  $E$  of the applied electric field collinear to the vertical edges of the network. For the chosen type and orientation of the network, only vertical capillary chains play an essential part: the transverse bonds affect the general picture of the current flow in the medium rather weakly, since they are perpendicular to the vector  $E$ . In this model we can take the ICP approximation, which proves to be more relevant and justified with EPM than with the mercury porometry method. In this case it is possible, using the ICP model, to analytically solve in the explicit form both the direct and the reverse problems of electric porometry.

Suppose the pore space of the core consists of a system of vertical cylindrical pores distributed with respect to radii with the PDF  $f(r)$ . Establish the correlation between the integral electric conductivity  $\sigma$  of a specimen portion as a function of height  $L$  and the radius PDF for capillaries. (The scheme of measurements is represented in fig. 42.) Taking into account the fact that all pores are connected successively, we obtain

$$\sigma(L) = \sum_{i=1}^{N_L} \frac{1}{R_i} r_i < r(L) = S^* N_b \pi \int_0^{r(L)} f(r) \sigma_e(r^2/l) dr,$$

where  $S^*$  is the cross-section of the specimen,  $N_L$  is the total number of saturated pores in the specimen at the height  $L$ .

Introduce the mean square radius at the height  $L$

$$\langle r^2 \rangle_L = \frac{\sigma(L)L}{\sigma_e \pi S^* N_b} = \int_0^{r(L)} f(r) r^2 dr$$



After passing to the limit  $L \rightarrow 0$  we have

$$\langle r^2 \rangle_{L=0} = \lim_{L \rightarrow 0} \frac{\sigma(L)L}{\sigma_e \pi S^* N_b} = \int_0^\infty f(r) r^2 dr$$

Consider the function  $X = \langle r^2 \rangle_L / \langle r^2 \rangle_{L=0}$  which can be expressed in terms of  $\sigma(L)$  as well as  $f(r)$

$$X = \frac{\sigma(L)L}{\lim_{L \rightarrow 0} [\sigma(L)L]} = \int_0^{r(L)} f(r) r^2 dr / \langle r^2 \rangle_{L=0} \quad (6.16)$$

Obviously  $\lim_{L \rightarrow 0} [\sigma(L)L] = \sigma_0 S^*$  ( $\sigma_0$  is the specific electric conductivity of the completely saturated core). Therefore  $X = \sigma(L)L\sigma_0^{-1}(S^*)^{-1}$  is uniquely related to  $r(L)$  and can be measured experimentally.

On the other hand, after differentiating the equality (6.16) with respect to  $r(L)$  and taking account of the normalization condition  $\int_0^\infty f(r) dr = 1$  we find

$$f(r(L)) = r^{-2}(L)(dX/dr) \left\{ \int_0^\infty r^{-2}(L)(dX/dr) dr(L) \right\}^{-1} \quad (6.17)$$

Taking into account the correlation between  $r$  and  $L$  determined by the expression (6.14) and the correlation between  $X$  and  $\sigma(L)$ , it is possible to pass to the new variable  $L$  in (6.17)

$$(G' = 2\chi \cos \theta / \rho g)$$

$$f\left(\frac{G'}{L}\right) = \frac{L^4}{G'} \frac{d}{dL} [\sigma(L)L] \left\{ \int_0^\infty L^4 \frac{d}{dL} [\sigma(L)L] dL \right\}^{-1} \quad (6.18)$$

Thus upon measuring the integral conductivity  $\sigma(L)$  experimentally for the corresponding sequence of the values of  $L$ , we can determine the radius PDF for capillaries uniquely using the formula (6.18).

If we give up the severe constraints on the network type and orientation and consider these parameters arbitrary, then the ICP approximation proves to be unacceptable, and a percolation model should be used. However the direct and reverse problems of electric porometry in this case become substantially more complex.

One of the possible approaches to the determination of the PDF for capillaries in this more general setting is as follows. The NM is considered in an approximation, admitting an analytical solution of the direct problem, so that the analytical

correlation of the PDF with some macro-characteristics could be later inverted, at least by means of some numerical method.

Realize the first part of the proposed plan, i.e., find an approximate solution of the direct problem of the EPM. Assume that the experimental measurements are taken according to the scheme represented in fig. 41. Also, still assume that only those capillaries are saturated at the height  $L$ , which have a radius less than the critical  $r(L)$  as defined by formula (6.14). Now, considering the radius PDF for capillaries known and the system infinite (since the size of the core is much greater than the period of the network), find the conductivity of such a medium.

The problem just set is one of the classical problems in percolation theory, the problem of the calculation of the conductivity for the bonds in a network. (Conductivity  $q_1$  of a separate capillary correlates with its radius as follows,  $q_1 = \sigma_l \pi r^2 l^{-1}$ .) Solving this problem, but for the case of Bethe's classical network, is possible only in numerical methods [1, 3]. Due to this fact this solution cannot be used further for solving the reverse problem. However the necessary analytical correlation  $\sigma(L)$  with the radius PDF for capillaries can be obtained approximately using the effective medium model (EMM) [29], a model that allows to get approximate results which agree satisfactorily with those of the exact calculations of the percolation problems. Notable deviations ( $\sim 20\%$ ) are observed only near the percolation threshold. Therefore if we consider the measurements of  $\sigma(L)$  being taken not too "high," so that  $\int_0^{r(L)} f(r) dr > 1.2\xi_c$ , the use of the EMM proves to be legal enough.

The main idea of the EMM is to substitute the network of random resistances with a similar network of identical "effective resistances" under the condition for the conductivity of the whole medium not to change. In this case, as is shown in [29], the conductivity  $q_m$  of a single bond in the effective medium is determined from the equation

$$\int_0^{\infty} f_0(q_1)(q_m - q_1)[(z/2 - 1)q_m + q_1]^{-1} dq_1 = 0 \quad (6.19)$$

Here  $f_0(q_1)$  is the conductivity PDF for bonds,  $z$  is the number of the nearest neighbors for the given network type. In the further calculations, it is more convenient to pass from the relationship (6.19) for  $q_m$  to a similar one for  $r_q$ . In doing so, we should take into account the correlation between the conductivity of a capillary and its radius and the equality of random variables when they are functionally dependent  $f_0(q_1) dq_1 = f(r) dr$ . In this case (6.19) can be rewritten as

$$(z/2 - 1)^{-1} \int_{r(L)}^{\infty} f(r) dr + \int_0^{r(L)} f(r) r_q^2 [(z/2 - 1)r_q^2 + r^2] dr = 0$$

Now, taking into account the normalization condition for  $f(r)$ , we obtain the resultant expression for  $r_q$

$$\int_0^{\tau(L)} r^2 [(z/2 - 1)r_q^2 + r^2]^{-1} f(r) dr = 2/z \quad (6.20)$$

We shall further set  $z = 6$ , which corresponds to the simple cubic network. In this case the equation (6.20) becomes

$$\int_0^{\tau(L)} r^2 (2r_q^2 + r^2)^{-1} f(r) dr = 1/3, \quad (6.21)$$

which implies, for instance, that for the given network type the percolation threshold  $\xi_c$  determined in the effective medium model equals  $1/3$ . The value of this quantity found in percolation theory is  $1/4$ . To obtain a reliable criterion of applicability for the EMM take  $\xi_c = 1/3$ . In this case the equation (6.21) can be used for describing the conductivity of the considered NM within the range  $r' < \tau(L) < \infty$ , where  $r'$  is found from the condition

$$\int_0^{r'} f(r) dr = 0.4. \quad (6.22)$$

If the radius PDF for capillaries is known, it is possible to find  $r_q(L)$  from (6.22) using (6.19), and therefore find the conductivity

$$\sigma(L) = \sigma_e \pi [r_q(L)/l] (S^*/\Delta L) \quad (6.23)$$

(we consider the intervals of the measurement of  $\Delta L_i$  equal to  $\Delta L$  all), and thus solve the direct problem of the EPM for the chosen NM.

Now investigate the reverse problem of the EPM for the given NM. Suppose that the values of  $\sigma(L)$  have been measured in the course of the experiment at  $j$  different heights satisfying the condition (6.22) and determine the radius PDF for capillaries according to these data. Using formulas (6.14) and (6.23),  $\sigma(L)$  can be easily recalculated into effective radii  $r_q(r(L))$ . As a result, we obtain a mathematical problem of solving a Volterra integral equation of the first type, which is the relationship (6.21) for the unknown function  $f(r)$ . The difficulty of this problem lies in the fact that the analytical dependence of the kernel of this equation on the upper limit or, more exactly, on  $r_q(r(L))$ , is unknown. Moreover, the function  $r_q(r(L))$ , which is a part of the kernel, has to be found experimentally, and therefore is always known up to a certain error of measurement. Given these conditions, the problem of finding the solution of the integral equation (6.21) is

ill-posed, and classical methods for its solution are not applicable. To find the PDF from (6.21), some kind of a regularized method, stable towards small errors in input data, should be used.

One of the possibilities lies in the reducing the integral equation (6.21) to a system of linear algebraic equations and solving the latter by means of the regularization method. In this study, the method of approximating functions was used for passing to a system of algebraic equations, where the sought PDF was expanded over some system of linearly independent functions. Due to the fact that a priori information about the behavior of the PDF is usually very limited, it is hard to prefer one system of approximating functions to another. In this case we can use Weierstrass's theorem on the expansion of any analytical function in power series

$$f(r) = \sum_{-\infty}^{\infty} a_i r^i \quad (6.24)$$

It can be assumed that  $f(r)$  is non-vanishing only in the interval  $[a_*, a^*]$ . After taking only a finite number of terms in the expansion (6.24) and substituting it in (6.21), we obtain the following

$$\sum_{-n}^n a_i F_{ik} = 1/3 \quad (6.25)$$

where

$$F_{ik} = \int_0^{r(L)} r^{2+i} (r^2 + 2(r_q^2)_k)^{-1} dr.$$

The immediate use of the system (6.25) would have led to a system of equations for an infinite number of unknowns, which does not have a unique solution.

When  $j > 2n + 1$  the relation (6.25) represents an overdetermined system of algebraic equations for the unknown coefficients  $\{a_i\}$  of the expansion and an inaccurately assigned matrix  $F_{ik}$ . Regularization method [76] can be used to find a normal pseudosolution of this system, and the regularization parameter should be chosen consistent with the errors in the input data. However the error caused by using the NM for describing the pore space structure is impossible to estimate quantitatively, and therefore the error of the assignment for the matrix is in fact unknown. Hence the customary condition of the residual cannot be used to choose an optimal regularization parameter. Instead, quasi-optimum criteria or relations [76] that do not require knowledge of the input data errors can be used.

If the condition of obtaining  $f(r)$  as an analytical expression is not necessary and it is sufficient to represent the sought  $f(r)$  as a plot, then the following procedure can be suggested.

Substitute the integral in the left side of the equation (6.21) by an integral sum according to some quadrature formula. For example, if we divide the interval  $[a_*, a^*]$  with the grid  $\{r_i = r_{i-1} + h, h = (a^* - a_*)/(n - 1), i = 1, \dots, n\}$  and use the trapezoid formula, we obtain

$$\sum_{i=1}^n f_i A_{ik} = 1/3 \quad (6.26)$$

where

$$f_i = f(r_i); A_{ik} = \begin{cases} r_i^2/[r_i^2 + 2(r_q)_k], & 1 < i < i_k, \\ r_i^2/2[r_i^2 + 2(r_q)_k], & i = 1, i_k; \end{cases} (r_q)_k = r(L)_k$$

Now the system (6.26) can be solved using the regularization method, as described above. As a result, the values  $\{f(r_i)\}$  of the sought PDF at the chosen set of points are obtained.

### 6.3 Percolation Model for the Combined Mercury and Electric Porometry Method

The method of determining the PDF for capillaries using the data of electric porometry presented in §6.2 is more exact and well-defined than the analytical formula (6.18) based on the model of ICP. However this method, in its turn, carries an error due to the use of the effective medium model, the latter being merely a limiting case of the exact percolation model. The EMM describes the properties of the medium well enough only at some distance from the percolation threshold  $\xi_c$  and brings an error of  $\approx 20\%$  into the calculations of the percolation parameters in the vicinity of  $\xi_c$ . Therefore the interval of radii where  $f(r)$  is determined with due reliability becomes smaller. Also, when a wetting fluid is used as an electrolyte in the electric porometry method according to the scheme in fig. 36, the most significant interval, i.e., that of small radii, is not scanned because the conducting IC breaks up. Furthermore in practice, to obtain representative experimental information about the studied core, its vertical dimension should be big enough (1 - 10 meters), which is much larger than the cores actually studied.

Overcoming of these drawbacks is possible in the development of a combined method, that of mercury electric porometry, which integrates positive features of mercury porometry and the standard electric porometry (see fig. 41). The use of a non-wetting conducting fluid, which is injected in the medium under pressure, takes care of the problem of core size and allows to scan the interval of small radii. It is most natural to use mercury as such a fluid. As for the mathematical methods to be used for processing the experimental data, they may be upgraded with

respect to those presented in §6.2 if the percolation model of transfer phenomena (described in part 1), instead of the approximate effective medium model, is used.

The scheme of the experimental measurement of the specific electric conductivity  $\sigma_y$  for the medium is as follows. A specimen with cross-section  $S^*$  and height  $L$  is placed in a container with mercury, and the latter is injected in the specimen under pressure  $p$ . After making a current  $I$  pass through the specimen and measuring the voltage drop  $U$  on its resistance  $R_0 = U/I$ , the specific electric conductivity  $\sigma_y = L/(S^*R_0)$  is found. After carrying out a series of such measurements for different values  $\{p_i\}$  of pressure and relating them, according to the Laplace formula, to the minimal capillary radius  $r_i = 2\chi \cos\theta/p_i$  where mercury can pass, we obtain the dependence  $\sigma_y(r_i)$ . This correlation can be either represented in the form of an interpolated curve or tabulated for further numerical processing on a computer.

Specific electric conductivity can be calculated using the percolation model of a heterogeneous medium according to (2.4), using the formula

$$\sigma_y(r_i) = A'' \int_{r_i}^{r_c} \left[ \int_r^{r_c} f(r) dr \right]^\nu \left[ \int_r^\infty f(r) \frac{dr}{r^4} \right]^{-1} \int_r^\infty f(r) dr f(r) dr \quad (6.27)$$

where  $A''$  is a numerical factor,  $r_c$  is the critical percolation radius.

If we now consider the function  $\sigma_y(r_i)$  known and the function  $f(r)$  unknown, then (6.27) becomes a nonlinear integral equation for  $f(r)$ . After differentiating it once with respect to  $r_i$  and making some transformations we obtain

$$f(r_i) = -1/A''(d\sigma_y/dr_i) \int_{r_i}^\infty f(r) \frac{dr}{r^2} \left[ \int_{r_i}^{r_c} f(r) dr \right]^{-\nu} \left[ \int_{r_i}^\infty f(r) dr \right]^{-1} \quad (6.28)$$

or, if we introduce the following notations

$$\lambda(r_i) = -1/A''(d\sigma_y/dr_i) \left[ \int_{r_i}^{r_c} f(r) dr \right]^{-\nu} \left[ \int_{r_i}^\infty f(r) dr \right]^{-1}, \quad (6.29)$$

$$z(x) = \int_x^\infty f(r) \frac{dr}{r^2}, \quad z_c = z(r_c), \quad \phi(r_i) = z_c \lambda(r_i),$$

a nonlinear inhomogeneous Volterra equation of the second type in the standard form

$$f(r_i) = \lambda(r_i) \int_{r_i}^{r_c} f(r) \frac{dr}{r^2} + \phi(r_i) \quad (6.30)$$

It easily follows both from the physical meaning of the percolation model of transfer phenomena in a heterogeneous medium and from the immediate analysis of the relation (6.28) that the latter expression, as well as (6.30), is valid within the interval  $0 < r_i < r_c$ .

In measuring  $\sigma_y(r_i)$  some intervals  $r_i < r < r_i + \Delta_i$  can be obtained where electric conductivity of the medium does not change, i.e.,  $d\sigma_y(r_i)/dr_i = 0$ . If  $\Delta_i$  do not contain  $r_c$ , then in these intervals  $\lambda(r_i) = \phi(r_i) = 0$ , and from (6.30),  $f(r_i) = 0$  when  $r_i < r < r_i + \Delta_i$ . This means that there are no capillaries with  $r_i \in \Delta_i$  in the medium. If, however, some  $\Delta_i$  contains an  $r_c$  together with its neighborhood, then after substituting  $\lambda(r_i) = \phi(r_i) = 0$  in (6.30), we also obtain  $f(r_i) = 0$ . In this case, the fact that the integral of  $f(r)$  is in the denominator of (6.29) formally causes a zero-over-zero indeterminacy. However the equality  $d\sigma_y/dr_i = f(r_i) = 0$  near the initially introduced  $r_c$  simply means that there are no capillaries with  $r_i$  close to  $r_c$ . Therefore it suffices to decrease  $r_c$  up to the closest  $r_i$ 's, for which  $d\sigma_y/dr_i \neq 0$ , and take it as the new  $r_c$ . This changes neither the meaning nor the contents of all formulas, but allows to get rid of the formal indeterminacy. These cases can be encountered only in those media which possess an  $f(r)$  function with two global maximums, i.e., in those having two different types of porosities (e.g., porous and capillary or block and interblock) described by the same  $f(r)$ .

Taking account of the new definition of  $r_c$ , estimate  $\lambda(r_i)$  and  $\phi(r_i)$ . It follows from (6.27) and (6.29), noting that  $0 \leq f(r) \leq M_0 < \infty$ , that

$$\begin{aligned} |d\sigma_y(r_i)/dr_i| &\leq A''(1 - \xi_c)^\nu M_0/z_c, & (6.31) \\ |\lambda(r_i)| &\leq \frac{M_0}{z_c \xi_c} \left( \frac{1 - \xi_c}{N_c \delta'} \right)^\nu, \quad |\phi(r_i)| \leq \frac{M_0}{\xi_c} \left( \frac{1 - \xi_c}{N_c \delta'} \right)^\nu \end{aligned}$$

Here  $N_c$  is the average value of  $f(r)$  in the first segment  $r_1 \leq r \leq r_c$  ( $r_c - r_1 = \delta'$ ).

Since the contraction mappings principle is valid for the Volterra integral equation of the second type for every finite  $\lambda(r_i)$  and  $\phi(r_i)$  [77, 78], the relationships (6.31) speak in favor of the existence and the uniqueness of the solution to the equation (6.30) and justify the use of the method of successive approximations with an arbitrary initial function  $f^{(0)}(r)$  for solving this equation.

In this case, once we have a normalized function  $f^{(n)}(r)$  as the  $n$ -th approximation, to obtain the next approximation according to (6.30), we first calculate its non-normalized value

$$\tilde{f}^{(n+1)}(r_i) = \lambda^{(n)}(r_i) \int_{r_i}^{r_c} f^{(n)}(r) \frac{dr}{r^2} + \phi^{(n)}(r_i) \quad (6.32)$$

and then, after normalizing,

$$f^{(n+1)}(r) = [C^{(n+1)}]^{-1} \tilde{f}^{(n+1)}(r), \quad C^{(n+1)} = \int_0^{\infty} \tilde{f}^{(n+1)}(r) dr \quad (6.33)$$

The use of relationships (2.1'), (6.29), (6.32), (6.33), where the function  $\sigma_y(r_i)$  is considered known from the experiment, permits to determine  $f(r)$  in the interval  $0 \leq r \leq r_c - \delta'$ . For  $r > r_c - \delta'$ , the function  $f(r)$  is not determined directly in the given approach, since "pressure scanning" becomes impossible because the IC breaks up. Therefore some a priori suppositions regarding the behavior of  $f(r)$  in this interval are necessary; in the absolute majority of cases  $f(r)$  decreases monotonely in this interval. For  $r > r_c - \delta'$  one can take  $f(r) \sim r^{-j}$ , where  $j > 1$ . In this case, for example, for  $j = 2$ , taking into account (2.1') we have

$$f(r) = \xi_c(r_c - \delta')/r^2, \quad r_c - \delta' < r < \infty \quad (6.34)$$

Consequently the quantity  $z$ , which is also defined in the interval  $r_c - \delta' < f < \infty$ , must be calculated using relationships like (6.34).

In the example given,  $z_c = (\xi_c/3)(r_c - \delta')^{-2}$ .

Thus the relationships (2.1), (6.29), (6.32) - (6.34) represent a closed algorithm for determining  $f(r)$  when the dependence  $\sigma_y(r_i)$  is known from experiment.

## 6.4 Numerical Calculations and Core Data Processing with the Electric Porometry Method

To determine the efficiency of the methods for recovering of the PDF for capillaries (PDFC) using the electric porometry data described in §§6.2 and 6.3, a series of numerical experiments has been carried out. The experiments have been performed in the following order. At first, for the chosen PDFC  $f_{in}(r)$ , the direct problem of electric porometry was solved and the specific electric conductivity of the medium found for different degrees of its saturation with electrolyte. Then a uniformly distributed random error  $\delta_s$  was introduced into the obtained data, and the determination of the PDFC was carried out using one of the known methods. The functions  $f_{out}(r)$  thus obtained were then compared to the original  $f_{in}(r)$ . To find out the properties of the outlined procedures for determination and eliminating additional systematic errors, introduced by the use of different models (the effective medium model and the percolation model), solutions of the direct and the reverse problems were carried out for the same model.

The method for determining the PDFC based on the use of the effective medium



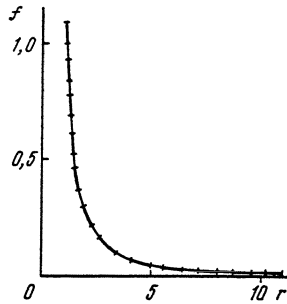


Figure 43: Result of establishing the model function  $f_{in}(r)$  by means of solving the reverse problem with exact output data

model and described in §6.2 was tried for the following initial model PDFC

$$f_1(r) = \begin{cases} \frac{a_* a^*}{a^* - a_*} \frac{1}{r^2}, & a_* \leq r \leq a^*, \\ 0, & r < a_*, r > a^*. \end{cases} \quad (a_* = 1, a^* = 11) \quad (6.35)$$

In the direct problem with a given function  $f_{in}(r)$  and a chosen set of limits superior  $\{(r(L))_k\}$ , the transcendental equation (6.21) was solved using the Newton - Ruthson method and  $\{(r_q(L))_k\}$  were found. Also, the validity threshold  $r'$  of the effective medium model was found previously from the condition (6.22), and all  $(r(L))_k$  were chosen from the segment  $[r', a_*]$ .

The obtained dependence  $\{(r_q(L))_k\}$  was used as the initial data for solving the reverse problem of the EPM by means of solving the system (6.25) using the regularization method with the quasi-optimality criterion. The following system of functions, decreasing with the increase of the radius, was chosen as approximating,

$$f_{app}(r) = \begin{cases} \sum_{i=1}^n a_i / r^i, & r \in [a_*, a^*], \\ 0, & r \notin [a_*, a^*]. \end{cases}$$

The following equation, which reflects the normalization condition for the PDF, was added to the system (6.25),

$$\sum_{i=1}^n a_i F_{i,j+1} = 1, \quad F_{i,j+1} = \int_{a_*}^{a^*} \frac{dr}{r^i}$$

The results of solving the reverse problem of determining the model PDF (6.35) are presented in figs. 43, 44 (the dotted line indicates the true curve  $f_{in}(r)$ ). In the first case (fig. 43), exact input data were used for solving the initial problem,

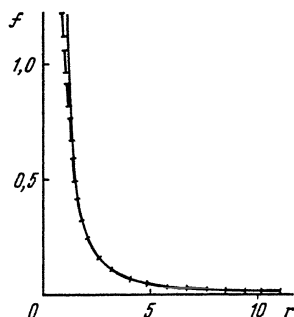


Figure 44: Result of establishing the disturbed model function  $f_{in}(r)$

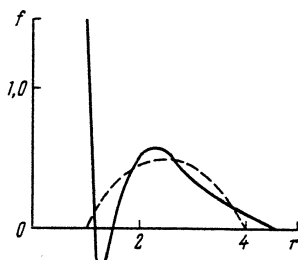


Figure 45: Result of establishing the function  $f_{in}(r)$  in the case of inadequate choice of the system of approximating functions (monotone decreasing exponential functions)

while in the second case (fig. 44), errors of  $\approx 1\%$  were introduced into  $f_{in}(r)$  after solving the direct problem. It can be seen that when the system of approximating functions is chosen adequately and the errors in input data are not too large the desired PDF is recovered with good precision.

To study the influence of errors brought in by inadequate choice of approximating functions, the PDF was determined for the same  $f_{app}(r)$

$$f_2(r) = \frac{6(a^* - r)(r - a_*)}{(a^* - a_*)^3}, \quad a_* = 1, \quad a^* = 4$$

The results are presented in fig. 45 (the dotted line represents the exact PDF for comparison). It is clear that although on the whole the original PDF is recovered approximately correctly, it is altogether impossible to approximate the exact PDF by means of the chosen system of functions with adequate precision. Therefore substantial errors are observed in the vicinities of the endpoints of the range. It follows that in order to adequately choose  $f_{app}(r)$ , additional a priori information concerning the qualitative behavior of  $f(r)$  is necessary. In this case, one can expect a high degree of accuracy in determining  $f(r)$ , and the result can be represented in the analytical form.

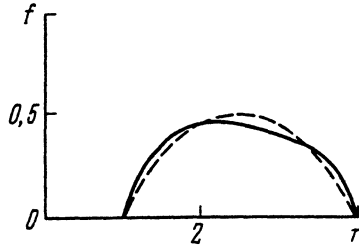


Figure 46: Result of solving the inverse problem of establishing the original function  $f_{in}(r)$  without using the system of approximating functions

If, however, the condition of obtaining the recovered  $f(r)$  as an analytical expression is unnecessary, then a procedure of reducing the integral equation (6.21) to a system of linear algebraic equations, based on substituting the integral with an integral sum according to some quadrature formula, can be used as described in §6.2. When the trapezoid formula is used, the relationship (6.21) is reduced to the system (6.26). After solving this system using the regularization method the values of the desired PDFC at the chosen set of points  $\{r_i\}$  are obtained. The results of solving the reverse problem of the EPM on recovering the original PDFC  $f_2(r)$ , based on the system (6.26), are presented in fig. 46 (the dotted line indicates  $f_2(r)$ ). It can be seen from the figure that the consistency of the original and the recovered functions is good enough. This result was obtained for the errors of the order  $\delta_s \approx 1\%$ .

To define the PDFC properly in the interval of small radii, it is necessary to use the combined mercury electric porometry method and invert the exact percolational dependence  $\sigma_y(r_i)$  according to the iterative procedure described in §6.3. To verify its efficiency, the dependencies  $\sigma_y(r_i)$  obtained by the direct calculations from the formula (6.27) for the given  $f_{in}(r)$  were taken as the initial data. Then these functions were determined by means of the described iterative procedure and the obtained distributions  $f_{out}(r)$  were compared to the original  $f_{in}(r)$ .

In all cases  $f^{(0)}(r) = \text{const}$  was taken as the zero approximation. Calculations showed that the iterative process converges quickly enough, and the number of iterations before relaxation is  $\approx 5 - 10$ . When the nature of the dependence  $f(r)$  in (6.34) is chosen correctly the consistency of the recovered and the original functions is very good ( $\approx 0.1\%$ ). Introduction of a significant error into (6.34) and, consequently, into the quantity  $z_c$  causes the distortion of the behavior of  $f(r)$  near  $r_c$  ( $\approx 50\%$ ). Nevertheless on the whole the function  $f(r)$  is recovered satisfactorily in this case as well, the most precise case being in the interval of small  $r$ . This fact that is crucial for many applications.

Results of recovering for the following original distributions

"one-humped"

$$f_{\text{in}}(r) = (2x/r_0) \exp(-x^2)$$

and "two-humped"

$$f_{\text{in}}(r) = (0.3\sqrt{\pi r_0})^{-1} \{ \exp[-(x - x_1)^2/a] + \exp[-(x - x_2)^2/a] \},$$

$$x = r/r_0; r_0 = 10^{-4} \text{ m}; x_1 = 0.4; x_2 = 0.8; a = 0.15$$

are presented in fig. 47 to illustrate the efficiency of the method. In both cases  $f_{\text{in}}(r)$  are shown by continuous lines and the recovered distributions, by dotted lines. The curves  $f(r)$  are compared in the interval of recovering  $0 \leq r \leq r_c$ . To the right of  $r_c$ , the function  $f(r)$  can be merged with the exponential dependence  $f(r) \sim r^{-j}$ , as it was mentioned in §6.3.

The scheme of the electric porometry method (see fig. 41) was used to recover the PDFC for an actual sandstone rock with different degrees of cementation. These rocks are grained media with twofold (capillary and pore) porosity. Experimental data were processed according to the procedure described in §6.2 (using the effective medium model) by means of solving the system (6.26) using the regularization method. Examples of the recovered PDFC are shown in fig. 48. In the same figure, the functions  $f(r)$ , obtained using the ICP model according to the analytical formula (6.18), are presented. It can be seen that the formula (6.18) permits to correctly estimate the characteristic radii of capillaries and the variance of PDFC, but rather roughly describes the true distribution  $f(r)$ .

Thus the presented results of the numerical simulation and model data processing demonstrate the efficiency of the ways used for interpretation of the experimental data for the recovering of the radius probability density function for capillaries in media with porosity of different scale described in this chapter.

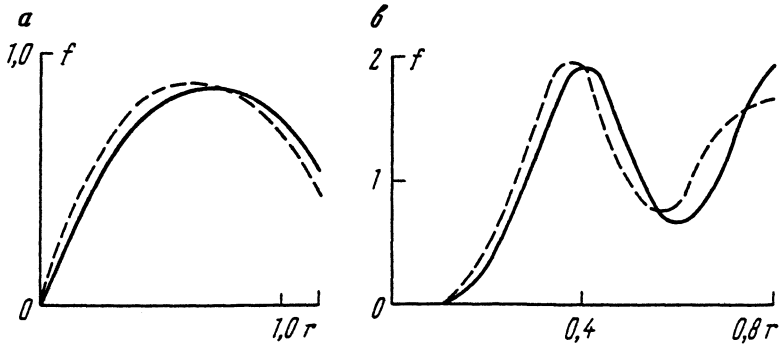


Figure 47: Results of establishing the "one-humped" (a) and the "two-humped" (b) functions of the  $f_{in}(r)$  form by means of the combined mercury and electric porometry method

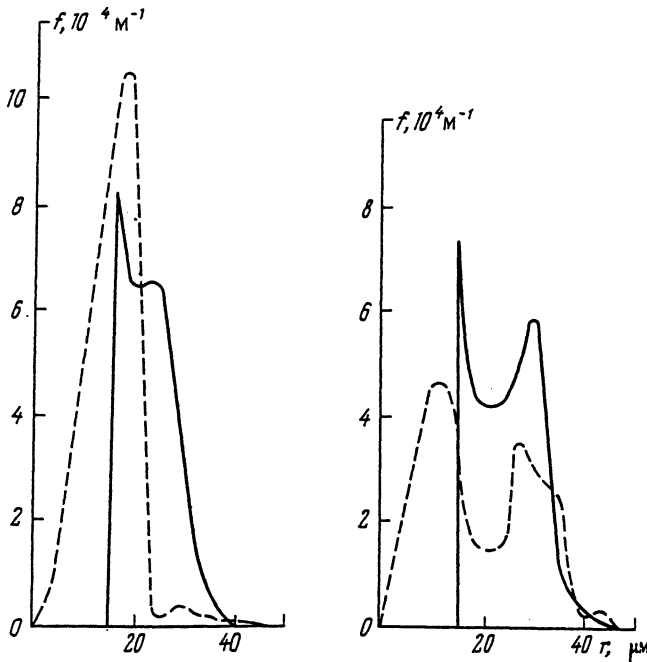


Figure 48: Results of establishing functions of the  $f(r)$  form for actual rocks using experimental data of the electric porometry method

## Chapter 7

# Methods for Determining Parameters of Fractured Rocks

Investigation of the cores brought to the surface is one of the most widespread methods for studying various types of rocks. At present, methods for determining the coefficients of permeability for grained and cavernous reservoir rocks, based on experimental study of cores from the productive layer, are well enough developed. Since in general the sizes of pores or caverns are much less than the dimensions of the core, the latter is in essence a macroscopic volume which can be studied to get information about the rock.

In the case of a fractured medium the lengths of fractures can be commensurate with the characteristic dimension of the core or even exceed this dimension. Therefore the permeability of the core of a fractured reservoir rock cannot be identified with the permeability of the productive layer. Due to this fact there are two possible approaches to the obtaining of reliable information about the permeability of such a reservoir rock. One should either study the coefficient of permeability for the cores with characteristic dimensions much greater than the average length of fractures in the rock, or develop mathematical methods for processing the results of research on the cores of usual dimensions to obtain information about the whole body. Obviously the second approach is preferable from the technological feasibility viewpoint. It must be taken into account, however, that the only piece of information there can be obtained during the study of the core of a fractured reservoir rock is the information about the parameters of the traces left by the fractures on the surface of the core.

## 7.1 Concentration and Average Length of Fractures Determined from the Core

Consider a medium with identical disk fractures distributed chaotically in space and oriented isotropically. Assume that the traces of these fractures on an arbitrary cross-section are identical; let them be line segments of length  $2d_s$ , with concentration of centers  $n_d$ . Calculate  $\nu'$ , the average number of the traces of length  $2d_s$  intersecting the butt surface of the core of radius  $R'$ . The surface of the core can be intersected not only by the segments whose centers lie in the circle of radius  $R'_i$ , but also by the segments whose centers are at a distance of no more than  $(R' + d_s)$  (see fig. 49) from the center 0 of the circle. Here the probability of a fracture trace intersecting the circle depends on the orientation of the fracture and is determined by the angle  $\theta$ . Thus the number of intersections for the traces of length  $2d_s$  and orientation  $\theta$  equals

$$\nu'(d_s) = n_d(\pi R'^2 + 4R'd_s) \quad (7.1)$$

After averaging both sides over the lengths of the traces and over the angles of their orientation and taking account of the fact that the length and angle distribution functions of the traces are normalized, we conclude that in the actual case of arbitrary length distribution of segments the formula (7.1) defines the quantity  $\nu'(< d_s >)$ , where

$$< d_s > = \int_0^{\infty} d_s f(d_s) dd_s$$

is the average value of lengths of the fracture traces distributed with the density  $f(d_s)$ .

If we define  $\nu'_i(< d_s >)$  for circles of different radii  $R'_i$ , then from the system of equations

$$\nu'_i(< d_s >) = n_d(\pi R'^2_i + 4R'_i < d_s >) \quad (7.2)$$

it is possible to find the quantities we are seeking, namely the concentration  $n_d$  of the fracture traces on the cross-section and the average length  $< d_s >$  of a fracture trace on the cross-section. Knowing the quantity  $n_d$ , we can find the concentration of disk fracture centers  $n^*$  and the average radius of a disk fracture  $< r_t >$ . The latter is easy to relate to the average length of a fracture trace on the cross-section, by taking into account the fact that the distribution of fractures is homogeneous. The probability of the length of the trace left on the core surface by a fracture to belong to the interval  $2d_s \div 2(d_s + \Delta d_s)$  does not depend on the distance  $x$  from the center of the fracture to its intersection with the cross-section in the fracture plane. This probability is the same for all distances  $x$  and equal to  $dx / < r_t >$ . Using the correlation between  $d_s$  and  $x$  we obtain the following

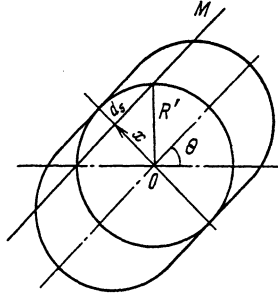


Figure 49: Refers to the determination of the probability of a circle with an arbitrary radius intersecting with a fracture trace on the surface of the core

$$\langle d_s \rangle = \int_0^{\langle r_t \rangle} \sqrt{1 - (x / \langle r_t \rangle)^2} dx \tag{7.3}$$

From (7.3) we find that  $\langle d_s \rangle = \pi/4 \langle r_t \rangle$ . The correlation between the surface concentration  $n_d$  of the fracture traces and the volumetric concentration  $n^*$  of the disk fractures can be found as follows.

Consider the cross-section  $M$  (see fig. 49). Intersection of an arbitrary disk fracture with the cross-section is possible only when the distance from the fracture center to the plane  $M$  does not exceed the quantity  $r_t$ . The probability of intersection is determined by the value of the solid angle  $\Omega$ . If a fracture lies inside this angle, then it intersects with the plane. It can be easily shown that  $\Omega = 2\pi(1 - \cos \theta_1)$ , where  $\cos \theta_1 = x/r_t$ . In this case, when we take into account the symmetry of the problem, we obtain an expression for  $P(x)$ , the probability of the plane intersecting a fracture with the average radius  $\langle r_t \rangle$

$$P(x) = 1 - x / \langle r_t \rangle \tag{7.4}$$

The number of the fracture traces on a unit surface of the cross-section is

$$n_d = 2n^* \int_0^{\langle r_t \rangle} P(x) dx \tag{7.5}$$

Using (7.4) and (7.5) we find  $n_d = n^* \langle r_t \rangle$ . Recall that the density of fractures, which characterizes the average distance between the fracture traces on the plane, is defined by the relationship

$$\Gamma = \sqrt{n^* \langle r_t \rangle}$$

The investigation just carried out shows that the concentration and the average length of the fracture traces on the surface of the core can be found. Knowing



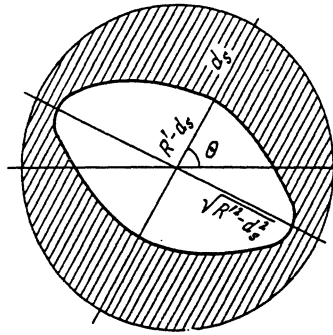


Figure 50: Refers to the determination of the number of fracture traces that fell completely inside the lateral surface of the core

these quantities, one can find the volumetric concentration and the average length of the disk fractures. Finally, upon determining the concentration and the average length of the disk fractures, one can estimate the coefficient of permeability of a fractured medium, for example, for the model presented in the study [79].

## 7.2 Determination of Fracture Length Distribution from Fracture Traces on the Core

Length distribution of fractures is one of the important characteristic properties of a fractured medium. Knowledge of this distribution is necessary both for the calculation of conducting properties of the medium and for the description of its destruction under the impulse loads [80].

In this section, a technique for processing the results obtained from the investigation of fracture traces on the core is proposed, which permits to obtain information about the length distribution for the model of a medium with disk fractures.

Assume that the medium contains disk fractures with arbitrarily distributed centers. Fractures leave traces – line segments of length  $2d_s$  – on some cross-section; distribution of these segments is determined by the function  $n_d(d_s, \theta)$ . In this case  $n_d(d_s, \theta)\Delta d_s\Delta\theta$  is the number of the centers of those fracture traces on a unit area, whose half-lengths lie in the interval  $d_s \div d_s + \Delta d_s$  and which are oriented at an angle from the interval  $\theta \div \theta + \Delta\theta$ . Suppose that a circle of radius  $R'$  corresponds to the surface of the core. Some of the fracture traces with length  $2d_s$  fall within this circle, with some traces lying completely inside the circle and others intersecting with the boundary of the core. The length and location of a fracture center is impossible to determine from the fracture trace

which intersects with the boundary of the core. This is due to the fact that those fracture traces that intersect with the boundary of the core from the inside and from the outside are indistinguishable. Let  $N_d(d_s, \theta)$  be the number of the fracture traces whose half-lengths lie in the interval  $d_s \div d_s + \Delta d_s$ , oriented at an angle from the interval  $\theta \div \theta + \Delta\theta$  and lying completely inside the core. This number is equal to the difference between the total number of all such fractures in the circle and the number of the fracture traces that intersect with the circumference. For the fractures oriented at an angle  $\theta$  (see fig. 50) we have

$$N_d(d_s, \theta) = n_d(d_s, \theta) S_n \quad (7.6)$$

where  $S_n$  is the unshaded part of the circle.

After integrating (7.6) with respect to the angle  $\theta$ , we can find the number of the fracture traces with half-lengths lying in the interval  $d_s \div d_s + \Delta d_s$  and falling completely inside the core

$$N_d(d_s) = \int_0^\pi n_d(d_s, \theta) S_n d\theta \quad (7.7)$$

The area  $S_n$  is equal to twice the area of the section

$$S_n = 2 \left[ R'^2 \cos^{-1}(d_s/R') - d_s \sqrt{R'^2 - d_s^2} \right] \quad (7.8)$$

After substituting (7.8) in (7.7) and taking account of the fact that

$$\int_0^\pi n_d(d_s, \theta) d\theta = n_d(d_s)$$

where  $n_d(d_s)$  is the surface density of the centers of those fracture traces, whose half-lengths lie in the interval  $d_s \div d_s + \Delta d_s$ , we obtain the following expression,

$$N_d(d_s) = n_d(d_s) \left[ 2R'^2 \cos^{-1}(d_s/R') - 2d_s \sqrt{R'^2 - d_s^2} \right]$$

Upon calculating the number of the fracture traces with length  $2d_s$  falling completely inside the core of radius  $R'$ , one can determine the length probability density for fractures

$$n_d(d_s) = 0.5 N_d(d_s) R'^{-2} \left[ \cos^{-1}(d_s/R') - (d_s/R') \sqrt{1 - (d_s/R')^2} \right]^{-1} \quad (7.9)$$

The quantity  $N_d(d_s)$ , where  $d_s$  lies in the interval  $d_s \div d_s + \Delta d_s$ , has to be determined from experiment by gathering the amount of data necessary for statistical analysis. As it can be seen from (7.9), as  $d_s \rightarrow R'$ , the error in determining  $n_d(d_s)$

goes up abruptly. Therefore reliable determination of the function  $n_d(d_s)$  is possible only for those fracture traces whose half-lengths are not too large compared to the radius of the core ( $d_s < R'$ ).

For further calculations, it is convenient to introduce a normalized distribution function

$$f(d_s) = n_d(d_s) \left( \int_0^\infty n_d(d_s) dd_s \right)^{-1} \quad (7.10)$$

Consider a disk fracture of radius  $r_t$  whose mouth is negligible. It is easy to show that by reasons similar to those mentioned in deriving the relationship (7.3), the probability of this fracture leaving on the cross-section a trace of length  $2d_s$  is equal to

$$P(d_s) = \frac{d_s}{r_t \sqrt{r_t^2 - d_s^2}}$$

Let  $F(r_t)$  be the normalized radius probability density function for disk fractures. In this case the probability of the length of a trace on the surface of an arbitrary cross-section to lie in the interval  $2d_s \div 2(d_s + \Delta d_s)$  is determined by the expression

$$f(d_s) = \int_{d_s}^\infty \frac{F(r_t) d_s dr_t}{r_t \sqrt{r_t^2 - d_s^2}} \quad (7.11)$$

In deriving the formula (7.11), it was taken into account that a fracture with radius less than  $d_s$  cannot leave a trace of length  $d_s$  on a plane.

The integral equation of the first type (7.11) establishes the correlation between the experimentally measured function  $f(d_s)$  and the function  $F(r_t)$  which is to be determined. Since such equations represent examples of ill-posed problems, their numerical solutions on computer are unstable. In the special case when the function  $f(d_s)$  and its derivative are continuous and bounded, the solution of the equation (7.10) can be obtained in the explicit form. Aside from the fact that the obtaining of an analytical solution of the equation (7.10) is of separate mathematical interest, it is also very important in the methodological aspect of the considered application. The exact analytical solution, unlike an approximate numerical one, is stable. Since the outlined limitations on the function  $f(d_s)$  are satisfied by the majority of functions obtained in experiment, this solution can be used as a stable technique for the processing of a broad set of probability density functions for traces of fractures on the core.

Make the following change of variables in (7.10),  $r_t^{-1} = t$ . As a result, we obtain

$$f(d_s) = d_s \int_0^{d_s^{-1}} \frac{F(t^{-1}) dt}{\sqrt{1 - d_s^2 t^2}} \quad (7.12)$$

Another change of variables,  $t = \sin \phi / d_s$ , in the equation (7.12) reduces it to

$$f(d_s) = \int_0^{\pi/2} F\left(\frac{d_s}{\sin \phi}\right) d\phi \quad (7.13)$$

The equation (7.13) is one of the Schlömilch integral equations. The solution of this equation can be obtained as follows. After introducing the function  $F_1(\sin \phi / d_s) = F(d_s / \sin \phi)$  into the equation (7.13) and then differentiating it with respect to  $d_s$ , we obtain

$$d_s^2 f'(d_s) = - \int_0^{\pi/2} F_1'(\sin \phi / d_s) \sin \phi d\phi \quad (7.14)$$

By substituting  $x / \sin \psi$  for  $d_s$  in (7.14), integrating it with respect to  $\psi$  from 0 to  $\pi/2$ , and changing the order of integration in the right side, the equation (7.14) can be reduced to

$$\int_0^{\pi/2} \frac{x^2}{\sin^2 \psi} f'\left(\frac{x}{\sin \psi}\right) d\psi = 2 \int_0^{\pi/2} d\phi \int_0^{\pi/2} F_1'\left(\frac{\sin \psi \sin \phi}{x}\right) \sin \phi d\psi \quad (7.15)$$

Having introduced a new variable  $\sin \lambda = \sin \phi \sin \psi$ , after changing the order of integration in the right side, we obtain

$$\int_0^{\pi/2} \frac{x^2}{\sin^2 \psi} f'\left(\frac{x}{\sin \psi}\right) d\psi = - \int_0^{\pi/2} F_1'\left(\frac{\sin \lambda}{x}\right) \cos \lambda d\lambda \int_{\lambda}^{\pi/2} \frac{\sin \phi d\phi}{\sqrt{\cos^2 \lambda - \cos^2 \phi}}$$

Taking account of the fact that

$$\int_{\lambda}^{\pi/2} \frac{\sin \phi d\phi}{\sqrt{\cos^2 \lambda - \cos^2 \phi}} = \frac{\pi}{2},$$

after integrating with respect to  $\lambda$ , we obtain the resultant expression

$$F(r_t) = F(\infty) - \frac{2}{\pi} \int_0^{\pi/2} \frac{r_t}{\sin^2 \psi} f'\left(\frac{r_t}{\sin \psi}\right) d\psi \quad (7.16)$$

Formula (7.16) permits to find the length distribution function  $F(r_t)$  of disk fractures if the length distribution function  $f(d_s)$  of fracture traces is known.

In particular, if the distribution  $f(d_s)$  is defined as an exponential relation

$$f(d_s) = a \exp(-cd_s)$$

then the integral in (7.16) can be easily evaluated. The length distribution of fractures in this case has the following form

$$F(r_t) = 2a\pi^{-1}(ar_t)K_1^m(ar_t)$$

where  $K_1^m(\cdot)$  is Macdonald's function.

### 7.3 Determination of Fracture Parameters from the Core

The techniques for the determination of the fracture parameters for different media were tried on cores of a fractured rock extracted from Well 96 of the condensed gas deposit in Orenburg. Cores were taken from the productive layer of the depositions constructed from organogenic and organogenic-fragmental limestones of the Artine, Sakmarian, and Assel stages of the lower Permian. An interval of dense limestones with low porosities (0.7–3.3%) and minor permeabilities ( $0.001 \cdot 10^{-15}$  -  $0.8 \cdot 10^{-15} \text{m}^2$ ), opened at a depth of 1379–1436.2 m, were chosen for investigations. These are fractured reservoir rocks.

In the studied interval of 57 m thickness, 10 specimen of the core were chosen. The specimen were "cubes" of dimensions  $5 \times 5 \times 5$ .

The method described in [81] was used to detect traces on the lateral faces of each cube. According to this technique, capillary saturation of the rocks with a luminescent solid was carried out, after which they were photographed in the ultra-violet to detect open fractures on the pictures of the faces. On each of the pictures, a pattern with concentric circles  $R'_i = 0.5; 1.5; 2.5$  cm was put and the number of traces inside each of the circles was calculated. After averaging over 60 faces of the studied specimen, the quantities  $\nu'_i$ , average values of the number of the fracture traces inside each circle of radius  $R'_i$ , were found. The constructed histogram  $\nu'_i(R'_i)$  (fig. 51) was processed according to the technique developed based on the results obtained in §7.1. The equation (7.2) is rewritten in the form

$$1/n_d = 4R'_i < d_s > / \nu'_i + \pi R'^2_i / \nu'_i \quad (7.17)$$

By introducing the notations  $Y = n_d^{-1}$ ,  $X = d_s$ ,  $a_i = 4R'_i / \nu'_i$ ,  $b_i = \pi R'^2_i / \nu'_i$ , the system (7.17) can be represented in the form

$$Y = a_i X + b_i \quad (7.18)$$

Formally, this system must be solved by breaking it up in pairs of equations and further averaging of the obtained results. In the averaging of the solutions of the paired systems, their statistical weights determined by the radius  $R'_i$  must

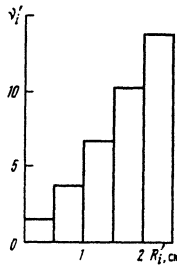


Figure 51: Histogram of the fracture trace concentration on the core surface

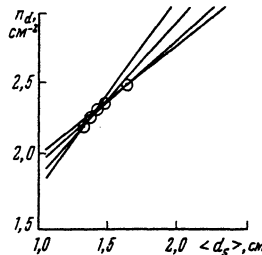


Figure 52: Plot of the graphical solution to a system of algebraic equations for the determination of the concentration and the average size of fracture traces

be taken into account. However in practice it is more convenient to solve the overdetermined systems of linear equations (7.18) graphically.

The linear relations (7.18) constructed for different values of  $a_i$  and  $b_i$  are presented in fig. 52. Intersection points of these lines define the quantities  $n_d^{-1}$  and  $\langle d_s \rangle$ . It can be seen from the plot in fig. 52 that the quantities  $n_d$  and  $\langle d_s \rangle$  are determined up to some error which can be estimated straight from the plot. The following average values were found,  $n_d = 0.4 \text{ cm}^{-3}$ ,  $\langle d_s \rangle = 1.8 \text{ cm}$ . Consequently the volumetric concentration of disk fractures  $n^* = 0.16 \text{ cm}^{-3}$  and their average radius,  $\langle r_t \rangle = 2.3 \text{ cm}$ .

To find the length distribution function of fractures, the number of the traces, from a given length interval, on the surface of the core inside a circle of radius  $R' = 5 \text{ cm}$  was determined. Averaging over 72 faces of the studied specimen yielded the function  $N_d(d_s)$  (fig. 53). Then the distribution  $f(d_s)$  was determined from formula (7.10), taking account of (7.9). The histogram of the half-length distribution of fracture traces is presented in fig. 54, *a*. The approximating relation, which is close to exponential, is marked with a dotted line. The results of determining the probability density function  $F(r_t)$  according to the formula (7.16) are presented in fig. 54, *b*.

Note that the function  $f(d_s)$  and, consequently,  $F(r_t)$  are determined ade-

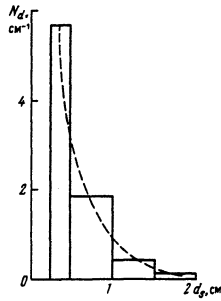


Figure 53: Histogram of density of fracture traces on the surface of the core

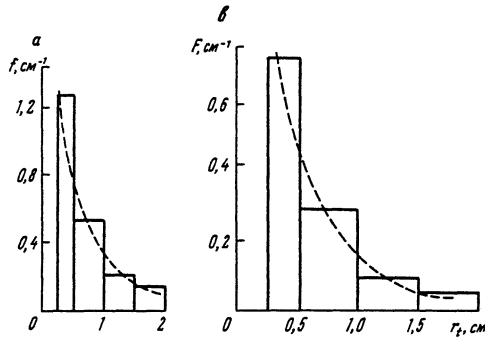


Figure 54: Normalized probability density functions: *a* - of fracture traces with respect to half-lengths; *b* - of circular fractures with respect to dimensions

quately only within certain intervals

$$d_m < d_s < R', \quad d_m < r_t < R'$$

The upper bound of the interval of the reliable determination for the functions  $f(d_s)$  and  $F(r_t)$  is limited by the size of the core, with the error in determination of  $f(d_s)$  going up abruptly when  $d_s \rightarrow R'$ . The lower bound is due to inaccuracy in the determination of the concentration of the fracture centers when  $2d_s < 0.5$  cm. This is due to the imperfection of experimental technique for the calculations in question for small values of  $d_s$ . Therefore nothing definite can be said about the behavior of  $f(d_s)$  as  $d_s \rightarrow 0$  and, consequently, of the behavior of  $F(r_t)$  as  $r_t \rightarrow 0$ . A certain decrease of  $f(d_s)$  observed for  $2d_s < 0.5$  cm might as well be explained by the inaccuracy of the calculations of such fracture traces.

The half-length distribution functions for fractures obtained in this study proved close to the exponential relation that was also observed during the study of the micro fracture half-length distribution in metals [82].

## **Part II**

# **Effects of Physical Fields on Recovery of Mineral Resources**



From the practical point of view, it is vital to find optimal regimes of treatment with various kinds of physical fields applied to reservoir rocks to increase the rate of mineral resources recovery. Theoretical study presented in Part 1 of this book showed that micro heterogeneous structure of the medium can cause sharp intensification of physical effects when they are intensified locally in some group of capillaries. In these cases, weak changes (which are reversible in homogeneous media) in a saturated medium caused by action from physical fields (acoustic and/or electromagnetic) on micro capillaries can transform into irreversible ones. The latter can lead to irreversible changes in macroscopic features of the medium (permeability, porosity, electric conductivity).

## Chapter 8

# Conductivity of a Heterogeneous Medium under Impulse and Alternating Current

Even a preliminary theoretical study allows to assume, with a considerable likelihood, that the use of impulse electric current has certain advantages in applications over other types of electric action. This is due to both the diminishing of the role of dissipative processes (in particular, heat conducting losses) and to the fact that the concentration of energy release in an impulse can bring about the realization of a more effective mechanism for the conductivity change in a medium at the micro level.

### 8.1 Threshold Values for Electric Treatment with Impulse Current

The majority of reservoir rocks consists of a strong skeleton and a far weaker component, cement (clay, biotite, etc.), that conducts electricity and fills mainly the thin capillaries. It was shown in §§1.2 and 1.3 that as the electric current passes through a saturated porous medium, the density of energy release concentrates sharply in thin capillaries, limiting the velocity of the fluid flow in the medium. Such concentration is caused by heterogeneity of the medium and results in the increase of temperature  $T$  and temperature gradients  $T'$  in these capillaries rela-

tive to the average in the medium. Since the fluid flow in cement is hardly ever observed, temperature can fall primarily due to heat conductance of the skeleton of the medium, the fluid, and the cement. When certain threshold values of temperature  $T_c$  ("temperature mechanism") or temperature gradient ("gradient mechanism") are reached, the mechanical tensions developing in the thin capillaries of the cement destroy it. The cement is then ejected entirely or partially into larger cavities. This effect results in a notable increase of the electric conductivity of the medium (by up to several tens of per cent) and to substantial increase of the permeability (by several times).

We shall determine the values of these thresholds for electric treatment with impulse current as functions of the impulse parameters, of the pore space structure and the fraction of the non-conducting capillaries in the medium. Since the electric conductivity of the skeleton is usually negligible, we can suppose that the current flows only through the inter-grain space filled with fluid or cement. Let the average field intensity in the medium  $E(t) = E_0 u(t)$ , where  $E_0$  is the amplitude and  $u(t)$  is a time function that sets the form of the impulse, be given. If the contribution of the high-frequency harmonics (i.e., those with frequencies 100 kHz and more) to the Fourier spectrum of the impulse is small (this is valid for the duration of impulse  $\tau \gtrsim 10^{-5} - 10^{-6}$  s), then the deviations of the form of the current in the medium from  $u(t)$  due to the reactive components of the electric conductivity can be neglected.

If the radii of the capillaries in the medium are sufficiently large  $r > \lambda'/\sigma' \approx 10^{-6}$  m, then the surface conductivity of the capillaries can also be neglected.

For the majority of rocks, the coefficients of temperature conductivity of the fluid, cement, and skeleton differ by no more than 3 to 5 times. Therefore, for clarity, without significant loss of accuracy, the coefficients of temperature conductivity of the fluid, cement, and skeleton can be considered the same, and equal to  $\kappa_t$  ( $\kappa_t \approx 10^{-7}$  m<sup>2</sup>/s).

Since the characteristic size of a grain  $l \approx 10^{-3}$  m and the radii of the capillaries filled with cement  $r \approx 10^{-6} - 10^{-4}$  m, it follows that the characteristic periods of temperature exchange for a capillary  $\tau_k = 1/4r^2\kappa_t^{-1} \approx 2 \cdot 10^{-6} - 2 \cdot 10^{-2}$  s is much less than those for a grain  $\tau_l = 1/4l^2\kappa_t^{-1} \approx 2$  s. Hence for impulse current with the impulse period  $\tau < \tau_l$ , the overlap of the thermal fields of adjacent capillaries can be neglected.

For  $r > 10^{-6}$  m, the current density in a capillary can be considered constant across the cross-section, and the boundary effects at the capillary (or the capillary - pore) junctions can be neglected.

Suppose the electric current  $I(t) = I_0 u(t)$ , where  $I_0$  is the amplitude, flows through two successive capillaries of length  $l$  each and with radii  $r_1$  and  $r_2$ . Assume that  $l \gg r_1, r_2$  and  $r_2 \geq r_1$  and address the determination of the temperature distribution in two semi-infinite capillaries.

Introduce the cylindrical coordinates  $r, \phi, z$  with the origin at the center of the capillaries and with the  $z$ -axis coinciding with the axis of the capillaries. In this case the current density and the energy release density rate (expressed in units of degree per second) vanish outside the capillaries and are determined by the expressions

$$j_{0i}(t) = I(t)\pi^{-1}r_i^{-2}, \quad q_{0i}(t) = j_{0i}^2(t)/(\rho_i c_i \sigma_i') \quad (8.1)$$

inside the capillaries.

Here  $c_i, \rho_i, \sigma_i'$  are, respectively, the specific heat, the density and the electric conductivity of the fluid or cement in a capillary (depending on what it is filled with);  $i = 1, 2$ .

The heat equation, as well as the boundary and initial conditions in the cylindrical coordinates with regard to the independence of temperature and other quantities on the angle  $\phi$  and the fact that there is no fluid flow, for such a complex capillary has the following form,

$$\kappa_t \left( \frac{\partial^2 T}{\partial z^2} + \frac{1}{r} \frac{\partial}{\partial r} \left( r \frac{\partial T}{\partial r} \right) \right) + q(t) = \frac{\partial T}{\partial t}, \quad (8.2)$$

$$T|_{t=0} = \frac{\partial T}{\partial r}|_{r=0} = \frac{\partial T}{\partial z}|_{z=-\infty} = \frac{\partial T}{\partial z}|_{z=\infty} = 0.$$

Here the term that has to do with the source,  $q(t)$ , is determined from the relationship (8.1).

Green's function for the problem (8.2), with regard to (8.1), is [83]

$$G(r', z', t', r, z, t) = \exp \left[ -\frac{(z - z')^2 + r^2 + r'^2}{4\kappa_t(t - t')} \right] \frac{J_0 \left[ \frac{2rr'}{4\kappa_t(t - t')} \right]}{[4\pi\kappa_t(t - t')]^{3/2}}$$

Here  $r', z',$  and  $t'$  are the current values of radius, axial coordinate and time;  $J_0(\cdot)$  is Bessel's function of a purely imaginary argument of the zero order.

Consequently temperature is determined from the expression

$$T(z, t) = \int_0^t dt' q(t') \left[ \int_{-\infty}^0 dz' \int_0^{r_1} dr' 2\pi r' G(r', z', t', r, z, t) \right. \\ \left. + \int_0^{\infty} dz' \int_0^{r_2} dr' 2\pi r' G(r', z', t', r, z, t) \right] \quad (8.3)$$

Distribution of temperature for an infinitely long capillary can be found from (8.3) after setting  $r_1 = r_2 = r$  and integrating with respect to  $z'$  and  $r'$ . The greatest temperature on the capillary axis ( $r = 0$ ) at the moment  $t$  is

$$T(t) = w(I_0, r, t) A(y') A_0^{-1} \quad (8.4)$$

where

$$A(y') = \int_0^1 u^2(x)(1 - \exp(y'^{-1}(1-x)^{-1}))dx,$$

$$y' = 4\kappa_t t r^{-2}, \quad A_0 = A(0)$$

Here  $w(I_0, r, t)$  is the energy (expressed in degrees) per unit volume released in a capillary as the impulse passes through it

$$w(I_0, r, t) = I_0^2 t A_0 H^{-1} r^{-4}, \quad H = \pi^2 c \rho \sigma' \quad (8.5)$$

The  $z$ -component of the temperature gradient (we shall denote it by  $T'$ ) can be obtained by differentiating the expression (8.3) with respect to  $z$  and integrating it with respect to  $z'$  and  $r'$ .  $T'$  assumes its maximal value at the center of the capillary junction ( $r = 0, z = 0$ ). If  $r_2 \approx r_1$  then  $T' \approx 0$ . If  $r_2 \gg r_1$  then the contribution of the second term in (8.3) can be neglected. After denoting  $r_1 \equiv r$ , we find

$$T'(t) = w(I_0, r, t) B(y') A_0^{-1} \theta'^{-1}, \quad \theta' = (4\pi\kappa_t t)^{1/2},$$

$$B(y') = \int_0^1 u^2(x)[1 - \exp(-y'^{-1}(1-x)^{-1})](1-x)^{-1/2} dx \quad (8.6)$$

In this case the conditions of achieving any of the threshold values  $T_c$  or  $T'_c$  can be written in the following form,

$$T(t) = T_c, \quad T'(t) = T'_c \quad (8.7)$$

Consider the dependencies of  $T$  and  $T'$  on the duration  $\tau$  of the impulse for a fixed energy density in the impulse  $w(I_0, r, t) = w_0$ . It follows from (8.4) that for  $\tau \ll \tau_k$ ,

$$T(\tau) \lesssim w_0, \quad T'(\tau) \approx w_0 B_0 A_0^{-1} \theta'^{-1}, \quad B_0 = B(0) \quad (8.8)$$

Evidently, for short impulses, the maximum temperature that can be achieved in a capillary is bounded by the value  $w_0$  of energy density in the impulse. At the same time, the temperature gradient grows proportionally to  $w_0 \tau^{-1/2}$ . In other words, if  $w_0 < T_c$  then the "temperature mechanism" of cement destruction cannot be realized for any  $\tau$ , while the "gradient mechanism" is realized for  $\tau < (w_0 B_0 T_c'^{-1} A_0)^2 / (4\pi\kappa_t)$  according to (8.7) and (8.8).

Using the asymptotics for the functions  $A(y')$  and  $B(y')$  for  $y' \gg 1$  ( $\tau \gg \tau_k$ ), we obtain

$$T(\tau) = C_0 w_0 \left[ \frac{\tau_k}{\tau} \ln \left( \frac{e\tau_k}{\gamma_0 \tau} \right) + \frac{1}{2} \left( \frac{\tau_k}{\tau} \right)^2 - o \left( \frac{\tau_k}{\tau} \right)^3 \right], \quad (8.9)$$

$$T'(\tau) = C'_0 w_0 B_0 A_0^{-1} r^{-1} \left[ \left( \frac{\tau_k}{\tau} \right)^{1/2} - \pi^{-1/2} \left( \frac{\tau_k}{\tau} \right)^{3/2} + o \left( \frac{\tau_k}{\tau} \right)^{5/2} \right]$$

Here  $C_0$  and  $C'_0$  depend on the form of  $u(t)$  and are of the order unity each;  $\gamma_0 \approx 1.780$  is the Euler - Masceroni constant. It can be seen from (8.9) that as  $\tau$  grows,  $T'$  decreases quicker than  $T$ .

Compare the energy density  $w_1$  and amplitude  $I_1$  of a short impulse ( $\tau \ll \tau_k$ ), when  $T'(\tau_1) = T'_c$  and (8.8) holds, to the energy density  $w_2$  and amplitude  $I_2$  of a very long impulse ( $\tau_2 \gg \tau_k$ ), when  $T(\tau) = T_c$  and (8.9) holds,

$$\frac{w_2}{w_1} \approx \frac{T_c \tau_2 \tau_k^{1/2}}{T'_c r \tau_k \tau_1^{1/2}} \ln^{-1} \left( \frac{e \tau_2}{\gamma_0 \tau_k} \right), \quad \frac{I_2}{I_1} \approx \left( \frac{w_2 \tau_1}{w_1 \tau_2} \right)^{1/2}$$

For example, for  $\tau_1 = 10^{-5}$  s,  $\tau_2 = 2$  s,  $\tau_k = 2.5 \cdot 10^{-4}$  s (for  $r = 10^{-5}$  m,  $\kappa_t = 10^{-7}$  m<sup>2</sup>/s and  $T'_c \approx T_c r^{-1}$ ) we obtain  $w_2/w_1 \approx 5 \cdot 10^3$ ,  $I_2/I_1 \approx 0.16$ , i.e., if the "temperature mechanism" is realized, it is possible to decrease the amplitude of the impulse a little (by a factor of 5 to 10). At the same time, energy consumption grows by thousands of times, and the duration of impulse has to be increased by hundreds of thousands of times. Thus impulse current with short impulses and a large amplitude, for which the "gradient" mechanism of cement destruction is realized, is the most effective one.

The dependence of the threshold value of the current amplitude  $I_c$  on the capillary radius  $r$  for a fixed duration  $\tau$  of impulse can be determined from formulas (8.4) - (8.6)

$$I_c(r, \tau) = \begin{cases} A_i y' A^{-1/2}(y'), & A_i = 4\kappa_t (T_c H)^{1/2} \tau^{1/2}, \\ B_i y' B^{-1/2}(y'), & B_i = 4\kappa_t (T'_c H) (4\kappa_t)^{1/4} \tau^{3/4} \end{cases} \quad (8.10)$$

## 8.2 Permeability and Electric Conductivity under Impulse Current

Consider impulse current passing through an element of the medium. Current flows both along "parallel"  $r_1$ -chains of the "skeleton of the infinite cluster" and along bridges that connect the  $r_1$ -chains. However the current flowing along  $r_1$ -chains can be calculated as though there are no bridges, since the allowances to the presence of these bridges, and consequently, the possible rearrangement of the current flow in  $r_1$ -chains, are insignificant according to the results of §1.2.

Let the fraction of capillaries filled with cement be equal to  $\kappa' = 1 - \kappa$ . Furthermore let all these capillaries be thin, i.e.,  $\kappa' = \langle a_*, 1, r_z \rangle$ , where  $r_z$  is the radius of the thickest capillary filled with cement.

All chains with  $a_* \leq r \leq r_z$  do not conduct. We will further mark the quantities relating to the fluid with index 1, and those relating to the cement, with index 2. Using the expressions (3.1), (8.1) for amplitude  $I_0(r_1)$  of the current flowing

through an  $r_1$ -chain during the first impulse, we have

$$I_0(r_1) = E_0 \sigma'_1 \delta_* r_1^2 F_0^{-1}(r_1), \quad \gamma_\sigma = \sigma'_1 / \sigma'_2, \quad (8.11)$$

$$F_0(r_1) = r_1^2 (\langle r_1, r^{-2}, r_z \rangle \gamma_\sigma + \langle r_z, r^{-2}, a_* \rangle) \quad (8.12)$$

Here  $\delta_* \cong 3 \div 4$  for model II and  $\delta_* \cong 6 \div 8$  for model I. By differentiating  $I_0(r_1)$  with respect to  $r_1$ , one can make sure that  $I_0(r_1)$  is a monotone increasing function of  $r_1$  (for fixed  $E_0$ ). The hierarchy of  $r_1$ -chains with respect to the size of the thinnest capillary coincides with the hierarchy of  $r_1$ -chains with respect to the value of their average electric conductivity.

Since  $I_c(r, \tau)$  are monotone increasing functions of  $r$  and  $\tau$  (this can be verified by differentiating (8.10) with respect to  $r$  and  $\tau$ ), it follows that the threshold  $T_c$  or  $T'_c$  will be exceeded in the  $r_1$ -capillary of the  $r_1$ -chain. The minimal field intensity  $E_*(r_1, \tau)$  for which this happens can be found by setting (8.10) equal to (8.12) for  $r = r_1$

$$E_*(r_1, \tau) = I_c(r_1, \tau) F_0(r_1) / (\delta_* \sigma'_1 r_1^2) \quad (8.13)$$

Similarly, the maximal field intensity  $E^*(r_1, \tau)$  for which the threshold (8.10) will be achieved in the thickest non-conducting capillary – the  $r_z$ -capillary of the  $r_1$ -chain – can be found by setting (8.10) for  $r = r_z$  equal to (8.11)

$$E^*(r_1, \tau) = I_c(r_z, \tau) F_0(r_1) / (\delta_* \sigma'_1 r_1^2) \quad (8.14)$$

For  $E_0 < E_*(\tau)$  neither of the thresholds,  $T_c$  and  $T'_c$ , is going to be exceeded in any non-conducting  $r_1$ -chain, and therefore the same holds for all capillaries in the medium that have the same property. Correspondingly, for  $E_0 > E^*(\tau)$  one of the thresholds,  $T_c$  or  $T'_c$ , is going to be exceeded in all non-conducting capillaries of the medium. Thus  $E_*(\tau)$  and  $E^*(\tau)$  can be called, respectively, the minimal and the maximal field intensity for the medium.

Consider the case when the relationship  $E_*(r_1, \tau) < E_0 < E^*(r_1, \tau)$  is valid for an  $r_1$ -chain. Let  $m > 1$  impulses of current have passed through the medium. Denote by  $R(r_1, m)$  the radius of the thickest capillary in the  $r_1$ -chain where the threshold (8.10) was achieved as the  $m$ -th impulse passed through it. Suppose that  $R(r_1, m) < r_z$  (for  $m = 1$ ,  $R(r_1, 1) = r_1$ ). In this case in all capillaries with  $r \leq r_1 \leq R(r_1, m)$  the threshold (8.10) was exceeded and therefore complete or partial destruction and ejection of cement took place in these capillaries. Since  $\sigma'_1 > \sigma'_2$ , the fluid that replaces the cement increases the electric conductivity of the capillary. The cement ejected from the capillary gets into the adjacent pore in model I or a thicker capillary (if filled with fluid) in model II. These phenomena decrease the electric conductivities of the latter a little. Let the electric conductivity of the capillary increase by  $\epsilon(r, m)$  times after the  $m$ -th impulse has passed through it ( $1 \leq \epsilon(r, m) \leq \gamma_\sigma$  if no additional destruction of capillaries happens, and  $\epsilon(r, m) > \gamma_\sigma$  otherwise). The amplitude of the current flowing

through the  $r_1$ -chain when the next,  $(m + 1)$ -th impulse is generated is determined by the expression

$$I(r_1, m) = E_0 \sigma_1' \delta_* r_1^2 F_1^{-1}(r_1, m) \quad (8.15)$$

where

$$F_1(r_1, m) = r_1^2 \langle r_1, r^2 \epsilon(r, m), R(r_1, m) \rangle \\ + \langle R(r_1, m), r^{-2}, r_z \rangle \gamma_\sigma + \langle r_z, r^{-2}, a^* \rangle$$

Therefore the critical radius  $R(r_1, m + 1)$  is determined from the equation

$$I(r_1, m) = I_c(R(r_1, m + 1), \tau) \quad (8.16)$$

Since the amplitude of the current (8.15) increases as  $m$  grows and  $I_c(R, \tau)$  is a monotone increasing function of  $R$ , it follows that  $R(r_1, m + 1) > R(r_1, m)$ .

Thus the considered process is self-supporting. If the sequence  $R(r_1, m)$  converges to  $R_0(r_1) < r_z$ , which is determined from (8.16) by substituting  $R(r_1)$  for  $R(r_1, m)$ , then for the given  $E_0$ , cement is destroyed only in thin capillaries with  $r_1 \leq r < R_0(r_1) < r_z$ , and the  $r_1$ -chain remains non-conducting. If it turns out that for some  $m$ ,  $R(r_1, m + 1) > r_z$ , then in all non-conducting capillaries of the  $r_1$ -chain ( $r_1 \leq r \leq r_z$ ), destruction (perhaps, partial) of cement takes place,  $\epsilon$  falls within the interval  $\gamma_\sigma > \epsilon(r, m) > 1$ , and the  $r_1$ -chain becomes conducting.

We shall now directly calculate how the changes of relative permeability  $K/K_0$  and electric conductivity  $\Sigma/\Sigma_0$  depend on the duration of the treatment with impulse current. ( $K_0$  and  $\Sigma_0$  are the values of the mentioned quantities before electric action was started.)

Suppose the hydraulic conductivity of an  $r$ -capillary after the  $m$ -th impulse have passed through it is determined by the expression

$$(\pi/8)r^4\omega(r, m) \quad (8.17)$$

where  $\omega(r, m) = 1$  for all capillaries with  $r_z \leq r \leq a^*$ ;  $\omega(r, m) = 0$  for the non-conducting capillaries where the threshold (8.10) was not reached; and  $0 < \omega(r, m) \leq 1$  if the threshold was exceeded, and no additional destruction of capillaries took place (otherwise  $\omega(r, m) > 1$ ).

Based on (1.11), we can represent the specific electric conductivity of the medium  $\Sigma(m)$  and its permeability  $K(m)$  in the following form

$$\Sigma(m) = E_0^{-1} \int_{a_*}^{r_c} I_0(r_1, m) dn(r_1); \\ K(m) = \int_{a_*}^{r_c} k(r_1, m) dn(r_1); \quad (8.18)$$

$$k(r_1, m) = (\pi/8) \langle r_1, r^{-4} \omega^{-1}(r, m), a^* \rangle^{-1}$$



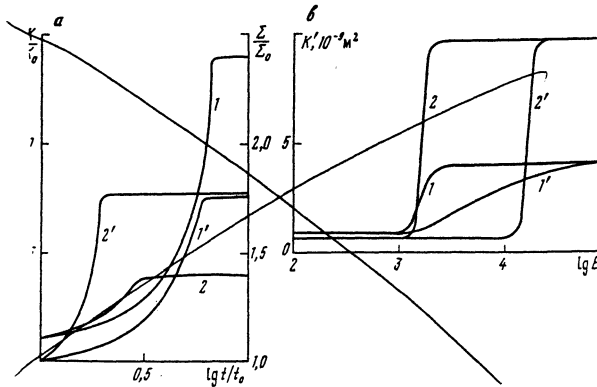


Figure 55: Results of calculations for a model function  $f(r)$ : *a* – dependencies of  $K/K_0$  (1, 2) and  $\Sigma/\Sigma_0$  (1', 2') on the duration  $t$  of treatment with impulse current; *b* – dependence of the greatest possible change of permeability on the amplitude of the field intensity in the impulse

Note that  $k(r_1, m) = 0$  if there is a non-conducting capillary in the  $r_1$ -chain i.e.,  $\omega(r, m) = 0$  for some  $r_1 \leq r \leq r_2$ .

We shall simulate the pore space of the medium by a simple cubic network, as usual. The following characteristic values for the parameters of the medium and the action were used for calculations for model I.  $a_* = 2 \cdot 10^{-6}$  m,  $a^* = l = 10^{-3}$  m,  $\kappa_t = 10^{-7}$  m<sup>2</sup>/s,  $\delta_* = 6$ ,  $\sigma'_1 = 0.05$  cm<sup>-2</sup> · m<sup>-1</sup>,  $\rho_f = 10^3$  kg/m<sup>3</sup>,  $\gamma_\sigma = 1.1$ ,  $\kappa' = 0.6$ ,  $T_c = 0.1$  K,  $T'_c = 10^4$  K/m,  $\epsilon(r, t) = \gamma_\sigma^{-1}$ ,  $\omega(r, t) = 0$  if the threshold (8.7) was not exceeded in the  $r$ -capillary and  $\omega(r, t) = 1$ ,  $\epsilon(r, t) = 1$  if this threshold was exceeded.

In fig.55, the results of the numerical calculations for the function  $f(r)$  of the form

$$f(r) = Cr^i \exp(-Dr^j) \tag{8.19}$$

are presented. The values of  $C$  and  $D$  were chosen so that the normalization condition for  $f(r)$  was fulfilled, and the average capillary radius in the medium was the same for all  $f(r)$  as the exponents  $i$  and  $j$  varied.

Both for  $i = 1, j = 2$  (heterogeneous medium) and for  $i = 5, j = 10$  (homogeneous medium) (marked in the figures by numbers 1 and 2, respectively), for the parameters of the medium and impulse given above, only the "gradient" mechanism of cement destruction is possible.

In fig.55, *a*, the  $t$  dependencies of  $K/K_0$  and  $\Sigma/\Sigma_0$  are presented for  $E = E_0$ ,  $\tau = 0.005$  s,  $\langle r \rangle = 3 \cdot 10^{-4}$  m,  $u(t) \cong 1$ . Here  $E_0 = k\sqrt{(\alpha/\beta)\sigma^*c\rho/(\tau/\sigma)}$ , where  $\alpha$  is the coefficient of volumetric expansion,  $\beta$  is the coefficient of temperature expansion,  $c$ , and  $\rho$  are the specific heat and the density of the fluid,  $\sigma^*$  is the

typical value of the destruction strength for the cementing substance,  $\sigma$  is the electric conductivity of the fluid,  $k$  is the coefficient characterizing the pore space structure of the medium.

In both cases the permeability and the electric conductivity reach saturation values for large  $t$  (we shall denote the limiting values by  $K'$  and  $\Sigma'$ , respectively). These values are less than the permeability  $K''$  and the electric conductivity  $\Sigma''$  of the corresponding media without cement in thin capillaries ( $\kappa' = 0$ ). The greater the quantity  $E_0^2\tau$ , which is proportional to the energy of a single impulse, and the less  $\tau$ , the closer  $K'$  and  $\Sigma'$  to  $K''$  and  $\Sigma''$ . If  $\kappa' < 0.15$ , then  $K$  and  $\Sigma$  stop changing soon and no significant growth of these quantities is observed. If  $\kappa' > 0.15$ , then the permeability can grow by ten and more times and the electric conductivity, by several dozens per cent.

In fig.55, *b*, the  $\ln E_0$  dependencies (for  $\kappa' = 0.6$ ) are presented for a fixed value of the energy in the impulse  $w_0 = 10^5 \text{ V}^2 \text{ s/m}^2$  (curves 1, 2) and for  $w_0 = 1.2 \cdot 10^4 \text{ V}^2 \text{ s/m}^2$  (curves 1', 2'). The presented plots show that the most significant changes of  $K$  and  $K'$  occur for small  $\tau$  and large  $E_0$ . As the medium becomes more homogeneous these changes become more apparent. The more homogeneous the medium, the less  $E_*(\tau)$  and the wider the range

$$E_*(\tau) \div E^*(\tau)$$

### 8.3 Determination of Threshold Values for Electric Treatment

It was shown in §8.1 that impulse electric treatment, i.e., electric treatment by currents with large amplitudes (and consequently with large  $E_0$ ) is most effective. However its realization requires special equipment, and therefore the case of electric treatment by currents with small amplitudes (and consequently with small  $E_0$ ) is more interesting for common practice. This case, however, causes substantial increase to the duration of electric treatment.

Take periodic current. To be able to disregard electro-kinetic phenomena, suppose that the average field intensity for a period vanishes, and the period is no greater than 0.1 second.

If the contribution made by the high-frequency harmonics (those with frequencies greater than 100 kHz) to  $u(t)$  is small, then the effects of the reactive components of the electric conductivity of the medium can be neglected. In this case the current in any capillary can be given in the form  $I(r) = I_0 u(t)$ .

Since, as it was mentioned above, the characteristic heat exchange periods for a capillary are much less than those for the grains, and the heat capacity of a grain is much greater than the heat capacity of a capillary (their ratio is of the order

$l^2 r^{-2} \gg 1$ ), then the superimposition of the thermal fields of adjacent capillaries and the increase of the average temperature in the medium with respect to the increase of the temperature in the capillaries can be neglected.

Under exactly the same assumptions as those made in §8.1, expressions similar to (8.4), (8.6) can be obtained. Taking into account that  $t \gg \tau_k(r)$ , we use the asymptotic expressions for the function  $A(y')$  and  $B(y')$  for  $y' \gg 1$  again. Thus we obtain

$$\begin{aligned} T(t, r) &= A_t I_0^2 r^{-2} \left[ \ln \left( \frac{e\tau_k}{\gamma_0 t} \right) + 1/2 \left( \frac{\tau_k}{t} \right) - o \left( \frac{\tau_k}{t} \right)^2 \right]; \\ T'(t, r) &= B_t I_0^2 r^{-3} \left[ 1 - \left( \frac{\tau_k}{\pi t} \right)^{1/2} + o \left( \frac{\tau_k}{t} \right)^{3/2} \right]; \\ A_t &= (1/4)C_0 A_0 H^{-1} \kappa_t^{-1}, \quad B_t = (1/4)C'_0 B_0 H^{-1} \kappa_t^{-1} \end{aligned} \quad (8.20)$$

The relationship (8.20) shows that  $T$  and  $T'$  are monotone increasing functions of  $t$ . However the temperature gradient  $T'(t, r)$  is upper bounded for  $t \gg \tau_k(r)$ , and therefore for currents with

$$I_0 < I' \cong (T'_c r^3 B_t^{-1})^{1/2}$$

the "gradient mechanism" of cement destruction cannot be realized. It is evident from (8.7) and (8.20) that for

$$t > \theta'' = \gamma_0 e^{-1} \tau(r) \exp[p'T_c/(lT'_c)], \quad p' = C'_0 B_0 / (C_0 A_0)$$

and  $I_0 > I'$  the "temperature mechanism" of cement destruction prevails.

For  $T'_c \approx T_c r^{-1}$  (strong cement), from (8.20) we find that  $\theta''$  is small. But for  $T'_c \approx T_c l^{-1}$  (weak cement),  $\theta'' \approx \tau_k \exp(p'l r^{-1}) \gg \tau_k(r)$ , and the "gradient mechanism" of cement destruction remains the principal one.

## 8.4 Permeability and Electric Conductivity after Electric Treatment

Consider the flow of the electric current through an element of the medium. Since the expressions (8.20) are monotone increasing functions of  $t$  and monotone decreasing functions of  $r$ , it follows that initially the threshold values of temperature  $T_c$  or the temperature gradient  $T'_c$  are assumed in the thinnest  $r_1$ -capillaries of  $r_1$ -chains at a certain instant  $\tau_0(r_1)$ . This instant can be called the minimal starting time of the irreversible changes to the permeability and the electric conductivity of the  $r_1$ -chain.

If we assume that

$$\tau_0(r_1) \gg \tau_k(r_1) \quad (8.21)$$

the following approximate expressions can be obtained based on (8.20)

$$\tau_0(r_1) \cong \begin{cases} \gamma_\sigma e^{-1} \tau_k(r_1) \exp[A_n F_0^2(r_1) r_1^{-2}]; \\ \pi^{-1} \tau_k(r_1) [1 - A'_n r_1 l^{-1} F_0^{-1}(r_1) r_1^{-2}] \end{cases} \quad (8.22)$$

$$\begin{aligned} A_n &= B_n T_c E_0^{-2}; & A'_n &= B_n p'^{-1} T'_c l E_0^{-2}; \\ B_n &= 4\pi^2 c_2 \rho_2 \kappa_t (\sigma_*^* c_0 A_0 \gamma_\sigma \sigma'_1)^{-1} \end{aligned}$$

The condition (8.21) is satisfied when

$$E_0 \ll E_1 = \begin{cases} (B_n T_c)^{1/2} F_0(r_1) r_1^{-1} \\ (B_n p'^{-1} T'_c l)^{1/2} (r_1 l^{-1})^{1/2} F_0(r_1) r_1^{-1} \end{cases} \quad (8.23)$$

The quantity  $E_1$  qualitatively defines the concept of smallness of the current amplitude introduced in §8.3. The upper expressions in (8.22), (8.23) are valid when the "temperature mechanism" of cement destruction is realized ((8.21) is already valid when  $E_0/E_1$  is of the order several times unity). The lower ones are valid when the "gradient mechanism" is realized.

Suppose that for  $t > \tau_k(r_1)$  in all capillaries with  $r_1 \leq r \leq R(r_1, t)$  one of the thresholds (8.7) was exceeded, and therefore partial or complete destruction of cement took place there. Considerations similar to those stated in §8.2 in deriving the relationship (8.15) allow to determine the amplitude of the current that passes through the  $r_1$ -chain at the instant  $t$

$$I_0(r_1, R, t) = E_0 \delta_* \sigma'_1 r_1^2 F_2^{-1}(r_1, R, t) \quad (8.24)$$

where

$$\begin{aligned} F_2(r_1, R, t) &= r_1^2 (\langle r_1, \epsilon^{-1}(r, t) r^{-2}, R \rangle \\ &+ \gamma_\sigma \langle R, r^{-2}, r_z \rangle + \langle r_z, r^{-2}, a^* \rangle) \end{aligned}$$

After substituting (8.24) in (8.20), we obtain  $R(r_1, t)$  as an implicit function of  $r_1$  and  $t$

$$t = t(R, r_1, t) = \begin{cases} \gamma_\sigma e^{-1} \tau_k(R) \exp[A_n \tau_k(R) \tau_k^{-1}(r_1) F_2^2(r_1, R, t) r_1^{-2}], \\ \pi^{-1} \tau_k(R) [1 - A'_n \tau_k(R) \tau_k^{-1} F_2^2(r_1, R, t) r_1^{-2}] \end{cases} \quad (8.25)$$

Obviously, for  $t = \tau_0(r_1)$  we have  $R(r_1, \tau_0(r_1)) = r_1$ , and (8.25) becomes (8.22) and (8.24), (8.11). Denote by  $\tau_q$  the time when the threshold (8.7) is achieved in the thickest capillary of the  $r_1$ -chain, i.e.,  $R(r_1, \tau_q(r_1)) = r_z$ . Suppose that

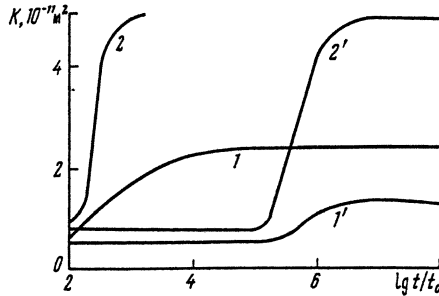


Figure 56: Variation of the permeability of the medium depending on the duration of treatment with periodic current

starting from  $t \geq \tau_q(r_1)$  the  $r_1$ -chain begins to conduct. The function  $F_2(r_1, R, t)$  depends on its argument rather weakly and is close to  $F_0(r_1)$ . Therefore, after setting  $R = r_z$ ,  $t = \tau_0(r_1)$ , we can obtain the following value from (8.25) with good accuracy

$$\tau_q(r_1) \approx t(r_1, r_z, \tau_0(r_1))$$

The relationship (8.22), with regard to the condition (8.21), shows that  $\tau_0(r_1)$  decreases rapidly as  $r_1$  grows (perhaps, with small violations of monotonicity), while  $\tau_q(r_1) > \tau_0(r_1)$  and decreases more rapidly than  $\tau_0(r_1)$  as  $r_1$  grows. Therefore the thick  $r_z$ -chains are the first of all  $r_1$ -chains to become conducting and increase the electric conductivity, and  $a_*$ -chains are the last to do so. This results in the conservation of the initial hierarchy of  $r_1$ -chains with respect to the values of their average electric conductivity during the electric treatment.

It follows from (8.21), (8.25) that for the "temperature mechanism"  $R(r_1, t)$  grows slower than  $\ln t$ , while for the "gradient mechanism"  $R(r_1, t)$  is upper bounded. If we also take into account the fact that large capillaries affect the average hydraulic and electric conductivity of an  $r_1$ -chain to a small degree, we can notice that as time passes,  $K(t)$  and  $\Sigma(t)$  steady. (According to (8.18), the major contribution to the alteration of the specific electric conductivity  $\Sigma(t)$  and the permeability  $K(t)$  of the medium is made by the thick  $r_1$ -chains.)

We shall proceed to determine the starting time  $t'$  for changes of  $\Sigma$  and  $K$  in the medium and the time  $t''$  when these changes stop

$$t'(E_0) = \min(\tau_0(r_1, E_0)), \quad t''(E_0) = \max(\tau_q(r_1, E_0)) \quad (8.26)$$

Here the minimum and maximum are taken over all non-conducting  $r_1$ -chains ( $a_* \leq r_1 \leq r_z$ ).

Results of the numerical calculation of  $K(t)$  for a function of the form (8.19) and the same values of the parameters as in §8.2, are presented in fig. 56.

Calculations show that for  $i = 1, j = 2$  (heterogeneous medium) and for  $i = 5, j = 10$  (homogeneous medium) and for the chosen characteristic values of the parameters of the medium, only the "temperature mechanism" is possible.

Presented in fig. 56 are the curves calculated for the following sets of characteristics of the process and the medium,  $1 - E_0, V/m, i = 5, j = 10$ ;  $2 - E_0, V/m, i = 1, j = 2$ ;  $1' - E_0/2, V/m, i = 5, j = 10$ ;  $2' - E_0/2, V/m, i = 1, j = 2$ . It can be seen from the presented results that the more homogeneous the medium (for fixed  $\langle r \rangle$  and  $\kappa'$ ) and the greater  $E_0$ , the more the relative changes of  $K(t)$  and  $\Sigma(t)$  and the steeper the initial piece of the relation  $K(t)$ .

The quantities  $t'$  and  $t''$  depend most significantly on  $E_0$ , the values of thresholds  $T_c$  and  $T'_c$ , the average radius  $\langle r \rangle$  of capillaries, through  $F_2(r_1, R, t)$  - on the variance of  $f(r)$  and the fraction  $\kappa'$  of non-conducting capillaries. Usually these quantities lie in the following ranges,  $t'$  from several seconds to several hours and  $t''$  from several minutes to many years. This fact implies that for some media the maximal values of  $\Sigma$  and  $K$  cannot be achieved during electric treatment with small current. According to the calculations, the optimal duration of electric treatment (when the most significant changes of  $\Sigma$  and  $K$  occur) is a quantity of the order  $(10^2 - 10^5)t'$ . Here the more homogeneous the medium (for a fixed  $\langle r \rangle$ ), the greater  $t'$  and the smaller the interval between  $t'$  and  $t''$ .

## Chapter 9

# Changing Conductivity and Pore Space Structure with Electric Current. Experiments

### 9.1 Conductivity of Sandy-Argillaceous Medium

We shall analyze the results of laboratory experiments on the electric treatment of a sandy-argillaceous rock by a "small-density" current. These experiments were carried out to study the nature of reversible changes to the permeability and the electric conductivity depending on the value of the electric field intensity, the duration of the electric treatment, and the total energy released per unit mass of the rock.

The experimental set-up completely coincides with the one presented in fig. 41. Voltage is supplied from a source of impulse or alternating current via the power electrodes at the ends of the tube. The electrodes located in the middle part of the tube allow to measure the current and the voltage in the rock with no influence from the surface effects that may take place near the power electrodes.

The study was conducted on sandy-argillaceous rocks whose fractional structure was previously determined (see table 9.1). The average grain size of series I was  $l_1 = 0.203$  mm, and of series II,  $l_2 = 0.186$  mm; the variance for series I,  $\sigma_d^{(1)} = 0.122$ , for series II,  $\sigma_d^{(2)} = 0.117$ ; clay made up 11.07% for series I and 14.5% for series II of the total mass. Thus by the fractional structure, the specified media are averagely homogeneous ( $\sigma_d^{(i)}/l_i \simeq 0.6$ ) and averagely mudded-out.

Table 9.1:

Grain Size, mm	Portion of Fraction in Total Mass of Specimen, %	
	I	II
2.5	0.04	0.02
1.25	0.13	0.20
0.63	1.85	3.15
0.315	31.88	24.04
0.16	44.34	36.57
< 0.16	21.78	36.02

However, since during the fluid flow, clay accumulates in the thin capillaries, it follows that the fraction  $\kappa'$  of the mudded out capillaries is small. This effect sin the low conductivity.

At first, vertical tubes were packed with the rock, with distilled water supplied gradually from the bottom sides of the tubes. This direction of water applying enabled to achieve the maximal displacement of the air from the rock pores, uniform packing and saturation of the rock with the fluid. Three tubes were usually used. Electric treatment with impulse current was carried out in the first tube; electric treatment with alternating current, in the second; and the third one was left for reference. The volume of water used for the saturation of the rock in tubes was measured, and the porosity was determined to equal 18 to 23 % in this series of experiments.

After the tubes have been packed, the flow of distilled water through their cross-section was set up for 15 to 25 days, until the production rates of the tubes steadied. Further, the electric treatment of the rock with alternating current was carried out, with simultaneous measurements of its production rate and electric conductivity taken.

High resistance of the rock did not permit to achieve large values of the current density even for large values of the electric field intensity.

The experiments showed that the electric conductivity of the rock bears a notable dependence on the intensity of the applied electric field. Its permeability increases reversibly by 30 - 40 % for  $E_0$  V/m, and three-fold for  $3E_0$  V/m. After the current was switched off for 5 - 10 minutes, the permeability fell to its original value. In other words, for small current density, in spite of the large values of field intensity, no irreversible changes to the permeability were observed. This confirms the temperature-related nature of the causes for the irreversible changes, which were discussed in chapter 8. Substantial reversible changes in the permeability



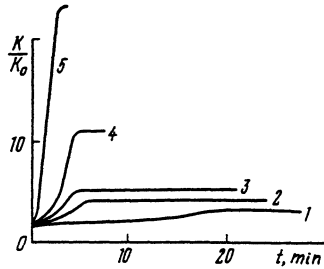


Figure 57: Dependence of the permeability change for a sandy-argillaceous medium (saturated with a leaching solution) on the duration of electric treatment

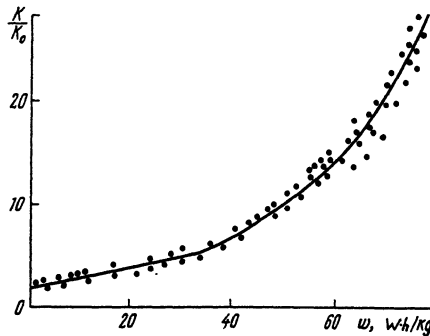


Figure 58: Master scheme of the dependence  $K/K_0 = f(w)$  for a series of experiments

and the electric conductivity with almost no heating (temperatures of the fluids flowing in and out of the tubes were taken) shows that these changes are related to the destruction of layers of bounded fluid. The notable effect of these on the permeability of a medium was shown in chapter 3.

After 30 to 40 days of flow, water was replaced by a leaching solution of low-concentrated (0.01-normal) sulfuric acid. The presence of acid caused intensive ion-saline exchange of suspensions which gradually precipitated on the surface of the capillaries, and after the initial increase of the permeability ( $K/K_0 = 1.5 \div 2.5$ ) decreased the transmission properties of the medium down to  $K/K_0 = 0.5 \div 1.2$ .

During the flow of acid its electric conductivity increased by 40 times, which allowed to substantially augment the current density. However for  $E_0$  V/m no significant reversible decrease of the electric conductivity was observed. At the same time, for  $1.3E_0$  V/m and electric treatment going on for  $t = 20$  minutes, the permeability increased six-fold. When the duration of the treatment was greater, the release of the gas phase took place in the solution, causing the decrease of the permeability and the electric conductivity as time passed.

Presented in fig.57 are several typical dependencies of the permeability upon

the field intensity for a fixed value of total energy used for the electric treatment of a unit mass of the rock

$$w = \frac{1}{2} E_0^2 \int_0^t \Sigma(t) dt$$

Intensities  $E = 0.29E_0, 0.75E_0, 1.2E_0, 2.16E_0,$  and  $2.83E_0$  V/m correspond to the numbers 1 - 5 of curves.

The master schedule of the dependencies  $K/K_0 = f(w)$  for a series of experiments (around 200) is presented in fig.58. It can be seen that for  $w \gtrsim 0.2$  kilowatt-hours per kilogram, after the electric treatment with alternating current, notable irreversible increase of the permeability is observed. Also note that after the electric treatment, a substantial increase (by two to five times) in the concentration of the useful component (metal) in the solution filtered out occurs.

Scattering of the experimental points in the region  $w \leq 40$  kilowatt-hours per kilogram is minor (the relative error is no more than 10 %). For  $w > 40$  kilowatt-hours per kilogram, the relative error can be as big as 30 % (the average error is  $\approx 15\%$ ). This fact is due to water boiling and consequent necessity to take into account the heat emission during its cooling and the energy efflux with the flowing fluid.

Using the plot of the dependence  $K/K_0 = f(w)$  (see fig.58), one can calculate the change of  $K(w)$  (or  $K(T)$ , where  $T$  is the temperature of the medium) as a function of the duration  $t$  of treatment according to the energy  $w$  put in a unit mass of the given ore and the intensity  $E_0$  of the field responsible for the electric treatment. The expected value of the irreversible change to  $K$  can also be calculated using this plot.

## 9.2 Pore Space Structure of a Sandy-Argillaceous Medium after Electric Treatment

In §9.1, the results of studies of both the reversible and the irreversible changes of permeability for different parameters of electric treatment were described. For sufficiently large values of the field intensity, irreversible changes of the permeability are constantly observed. In particular, this phenomenon is accompanied by evident discharge of substance (clay, small sand) with the flow of the fluid. This proves indirectly that the pore space structure of the medium changes.

In this section, experimental data of the research on the irreversible changes of the permeability and the pore space structure of the medium after electric treatment with impulse and periodic current are presented.

Studies were carried out using cores of sandy-argillaceous rocks whose fractional structure was determined beforehand (see table 9.1). To determine the pore space

structure of a medium characterized by a radius probability density function for the capillaries, tubes with length 1 m and diameter 34 mm were used. Along the full length of the vertical tube (see fig.41), electrodes were set at the intervals of 25 - 50 mm.

To exclude the ion exchange between the rock and the solution flowing through it, a weak (0.01-normal) solution of  $\text{CaCl}_2$  was used. Its electric conductivity was determined beforehand, and the electric conductivity of clay taken from a portion of the studied rock and saturated with the same solution (saturation of clay lasted almost 60 days), was measured.

The experiment involved five stages.

**Stage 1.** A volume of the solution greater than the pore volume of the rock was run through the rock. This stage lasted 5 to 15 days depending on the properties of the rock. The column production rate  $Q$  was being measured daily, and the permeability of the medium was determined

$$K = Q\mu(S^0 \rho_f g)^{-1}$$

After a steady value of  $K$  was established, electric current of frequency  $\omega = 5$  kHz and small amplitude (for the current density  $j_0$  to be much less than the critical density  $j_c$ ). This allowed to significantly reduce the error due to the capacitive reactance. For a fixed value of current, the resistance of the whole column was measured by means of the power electrodes. Further, the voltage drop was measured on the sections between adjacent measuring electrodes and between the lowest power electrode and a special measuring electrode (see fig. 42) to get rid of a systematic error due, for example, to the non-uniform density of the packing of the rock. Thus the total resistance of the column  $R_f$  (the  $f$  index designates the fact that the measurements were taken for the steady state flow) and the resistances  $\Delta R_f(L_i)$  of separate sections as functions of height  $L_i$ , counted from the bottom side of the column to the middle of the  $i$ -th section, were determined.

**Stage 2.** Injection of the solution was stopped, and the bottom side of the column was immersed in the solution to a depth of 1 cm. The column was kept in this state for 5 to 15 days until the quantities  $\Delta R_f(L_i)$  steadied. Then the values of the reduced specific resistances  $\rho_y(L_i) = \sigma_y^{-1}(L_i)$  of the sections were calculated. Here

$$\sigma_y(L_i) = [\Delta R(L_i)/\Delta R_f(L_i)]\Delta L_i(R_f S^0)^{-1}$$

Based on these, the function  $f(r)$  was determined using the methods described in §6.2.

**Stage 3.** The solution was injected from the bottom side, and it flowed through the medium for 5 to 15 days until the production rate  $Q$  steadied. After that, as at stage 1, the quantities  $R'_f(L_i)$  were determined (dash indicates the values after

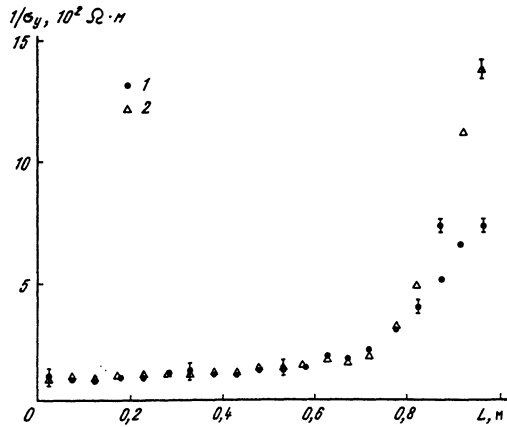


Figure 59: Typical dependence  $1/\sigma_y = f(L)$  in the electric porometry experiments; 1, 2 – measurements were taken before and after electric treatment with impulse current, respectively

treatment) and compared to the initial  $R_f(L_i)$ . In the majority of cases these values did not differ by more than 5%.

**Stage 4.** Electric treatment of the rock with current of density  $j_0$ , greater than the hypothetical threshold value  $j_c$ , was carried out for a certain period. Permeability of the specimen was being measured throughout the whole treatment. Furthermore after the electric treatment was terminated, these measurements were being taken for 2 to 7 more days, until the value of permeability steadied.

**Stage 5.** As at stage 2, the values of  $\sigma'_y(L_i)$  and, correspondingly,  $f'(r)$ , were determined. The results of the electric treatment of a sandy-argillaceous rock specimen (see table 9.1, series I) with impulse current are presented in figs. 59, 60.

It is clear from fig. 59 that the electric conductivity falls rapidly with the increase of height. Moreover after the electric treatment, the total conductivity of the column increases during the steady state flow through it and  $\sigma'_y(L)$  falls more sharply with the increase of height  $L$  than does  $\sigma_y(L)$ .

Comparison of the curves  $f(r)$  and  $f'(r)$  presented in fig. 60, *a*, and marked by numbers 1 and 2 shows that after electric treatment the number of thin capillaries (with radius  $r < 20 \mu\text{m}$ ) decreases, while the number of thick ones (with radius  $r > 20 \mu\text{m}$ ) increases. Such reorganization of the pore space structure causes irreversible increase of the electric conductivity of the specimen by 4 % and of its permeability by 105 % a day after the treatment. In fig. 60, *b*, the curves for the probability density function for capillaries appear, for specimen of rocks from the second series (see table 9.1). It is evident that a rock from the second series is more heterogeneous than one from the first series. In this case irreversible change

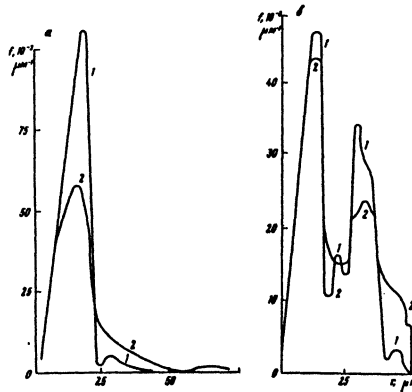


Figure 60: Plots of the radius probability density function for capillaries for a sandy-argillaceous medium obtained using the specimen of series I (a) and II (b) before (1) and after (2) electric treatment

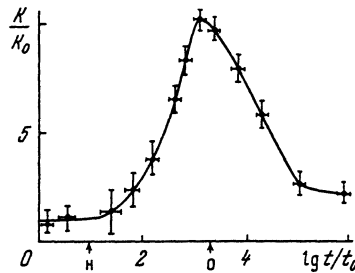


Figure 61: Typical dependence of permeability for a sandy-argillaceous medium on the duration of electric treatment. The beginning and end of the treatment are specified by letters "b" and "e," respectively

of the electric conductivity reached 12% and of permeability, 85 % a day after the treatment. The data presented in figs. 60, a, b, demonstrate the fact that for both types of rocks, the decrease of the fraction of thin capillaries is significant.

The plot of the permeability change during the treatment and the day after it is presented in fig. 61. It shows that during the electric treatment the permeability grows sharply (ten-fold), and when the current is switched off it drops by four times during 2 hours (i.e., it exceeds the initial value  $K_0$  by 2.5 times). Such sharp increase of the permeability during the treatment occurs because of both the partial clearing of the thin non-conducting capillaries plugged up with clay stoppers and the separation of the bounded water in the thin capillaries. The decrease of permeability after the termination of the treatment is due to the re-establishment of the bounded fluid layers in the thin capillaries (this happens fairly quickly) and to the re-precipitation of clay ejected from the thin capillaries on the surface of the thicker capillaries (this is a slower process). Irreversible increase of

the permeability 5 days later made up 2.25 times for the rocks from the first series and 1.95 for those from the second series.

### 9.3 Research on Irreversible Change of Conductivities for Sandy-Argillaceous Media after Electric Treatment

Experiments were conducted to find the values of thresholds  $E'(\tau)$  for the electric treatment with impulse current and  $t'(E_0)$  for the electric treatment with alternating current, and also to determine the nature of the permeability and the electric conductivity change for two sandy-argillaceous media whose characteristics were presented in §9.1. Part of the studied medium was used to determine  $f(\tau)$  according to the methods outlined in §9.2.

The experiment studying comparative effectiveness of electric treatment with impulse and alternating current consisted of several stages. At the first stage, successive packing of three tubes with rock was carried out (the diameter of each tube  $D_t = 1.6$  cm, height  $L = 10$  cm). Filling of the tubes and ramming of the rock there was done gradually with a dilute solution of  $\text{CaCl}_2$  being injected from the bottom side of the tube. This allowed to displace air out of the tube and the rock. At the second stage, long-lasting (around 5 days) flow of the solution through the rock took place, until the production rate steadied. A significant drop in permeability was observed at this stage. At the third stage, electric treatment of the first and the second tubes with a given value of energy input  $w$  per unit mass was carried out. The third tube was kept for references. The first tube was treated with alternating current. Energy input was calculated using the formula

$$w = \frac{1}{2} E_{0p}^2 \int_0^{t_p} \sigma(t) dt$$

Here  $E_{0p}$  is the amplitude of the intensity of the alternating current field,  $t_p$  is the duration of the electric treatment. The second tube was treated with impulse current. Energy consumption was determined using the formula

$$w = \frac{1}{2} \tau \theta_0^{-1} E_{0u} \int_0^{t_u} \Sigma(t) dt$$

Here  $E_{0u}$  is the amplitude of impulse current,  $t_u$  is the duration of the impulse electric treatment. At the fourth stage, durable flow of the solution in the tubes took place until the production rate of the latter steadied (3 to 5 days). Then the

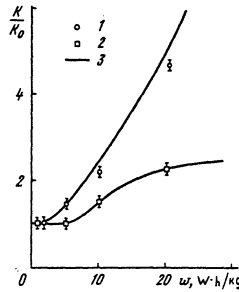


Figure 62: The energy input dependence of the irreversible change of the permeability: 1, 2 – results given by measurements taken after electric treatment of a sandy-argillaceous medium with impulse and alternating current; 3 – results of the theoretical calculations

value of  $w$  was increased, and the third and the fourth stages were conducted for the first and the second tubes.

The results of electric treatment showed that for  $w \leq 0.002$  kilowatt-hours per kilogram, irreversible changes of permeability of the first and the second tubes were not observed. The production rate of the third tube dropped insignificantly (10%). For  $w = 0.005$  kilowatt-hours per kilogram, electric treatment with alternating current did not yield any change in the production rate. At the same time, electric treatment with impulse current 1 hour after it was terminated made the production rate grow by 25% ( $K/K_0 = 1.25$ ). With the flow that followed (stage 4), after 3 days the increase of the production rate reached 50%. For  $w = 0.01$  kilowatt-hours per kilogram, immediately after the electric treatment the production rate in the first two tubes increased; however, 5 days later the augmentation of the production rate for the treatment with alternating current made up 50% and impulse current, 120%. For  $w = 0.02$  kilowatt-hours per kilogram, after the electric treatment the production rate in tubes 1 and 2 fell almost down to zero (3 - 5% from its initial value). However 2 hours after the treatment the augmentation of the production rate reached 100% for tube 1 and 150% for tube 2 ( $K/K_0 = 2.5$ ). A day later the production rates of both tubes grew. For the first tube, the increase reached 130% ( $K/K_0 = 2.3$ ) and for the second tube, 470% ( $K/K_0 = 5.7$ ). Three days later the production rate of the first tube remained still greater than its initial value by 130%, while for the second tube, the augmentation of  $K$  decreased to 280% ( $K/K_0 = 3.8$ ). Further on (for about 5 days) the production rate of the tubes remained almost steady. Thus for  $w = 0.02$  kilowatt-hours per kilogram, a sharp decrease (almost down to zero) of the production rate immediately after the electric treatment and its substantial increase ( $K/K_0 = 3 \div 5$ ) 3 - 5 days later, was observed.

Ejection of substance (clay and fine sand) during the electric treatment was observed in both cases. Fig. 62 illustrates the dependence of the value of the irreversible change in the permeability on the energy consumption. Continuous lines represent the results of the calculations for impulse current according to §8.2 and for alternating current according to §8.4. It can be seen from fig. 62 that the calculations for alternating current agree with experiment satisfactorily (within the error of experiment). Calculations for impulse current yield somewhat overestimated values, as compared to experiment. Apparently, this fact is due to the cement destroyed by impulse current, the cement that was moving slowly (compared to the duration of treatment) with the flowing fluid. It also gradually precipitated on the surface of the capillaries, a fact that was not taken into account in §8.2. Good agreement of the calculated and the experimental data for electric treatment with alternating current is caused by the fact that such treatment lasts longer, and the cement precipitating in thin capillaries does not have time to "settle," since the electric treatment destroying it keeps going. As a result, the destroyed cement reaches the side of the tube with the flow and leaves the rock.

Comparison of the efficiency of the electric treatment with impulse and alternating current proves the conclusion made in chapter 8, which states that electric treatment with impulse current is much more effective than treatment with alternating current.

The following conclusions can be drawn.

1. Passage of the electric current is capable of substantially increasing the conductivities of sandy-argillaceous rocks. Experimental dependence of the reversible changes in the permeability of sandy-argillaceous media on the value of the electric energy put in a unit mass of the medium, was obtained.

2. The threshold nature of the irreversible changes in the permeability of sandy-argillaceous media was confirmed experimentally. It was shown that these changes can be accompanied by the ejection of a suspension of the destroyed cement. They are caused primarily by the notable changes in the pore space structure of the medium, with relatively small variations of the average effective radius of the capillaries.

3. The theoretical conclusion about the efficiency of electric treatment with impulse current being much greater than that of electric treatment with alternating current with industrial frequency, was proved experimentally.



## Chapter 10

# Changing Well Production with Electric Treatment

### 10.1 Calculation of Change in Well Production after Electric Treatment

The relationships describing the changes in the permeability and the electric conductivity of a medium in time for a given amplitude of the electric field intensity (§8.2, 8.4) allow to determine the change of the well production after electric treatment [86].

The result of the electric treatment depends substantially on the diagram of electric energy supply to the medium. Three most widespread diagrams are presented in fig. 63. Further calculations are carried out for diagram *III*, and the conversion factors are given for the other two.

In this diagram, the first power electrode is a casing column with a metal filter (the filter column) with the total length  $H_w$ . The second power electrode is at a distance of  $H_l$ , much greater than the depth of the well, and is grounded. The equation describing the steady state current flow in the general case has the following form,

$$\operatorname{div} j = 0 \quad (10.1)$$

$$j = \Sigma E \quad (10.2)$$

$$E = -\nabla\phi_e \quad (10.3)$$

Here  $j$  is the current density vector,  $E(r, t)$  is the field intensity vector, which depends on the radius-vector  $r$  and time  $t$ ,  $\phi_e$  is the electric field potential and  $\Sigma$  is the electric conductivity of the medium.

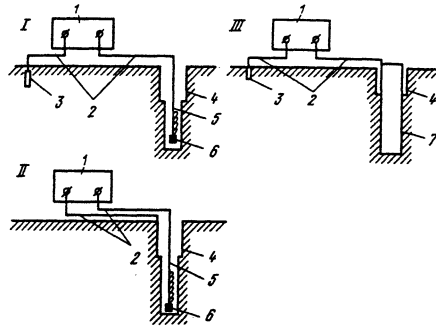


Figure 63: Hook-up diagrams for the electric treatment of solitary wells: 1 – electric energy source; 2 – electric cable; 3 – grounding electrode; 4 – open shaft; 5 – electrode inside the well; 6 – guiding load; 7 – filtering station

The boundary and initial conditions for the considered problem are

$$j|_{r \rightarrow \infty} \approx \frac{I}{2\pi r^2}, \quad j|_{r \rightarrow r_w} \approx \frac{I}{2\pi r H_w} \quad (10.4)$$

where  $r \equiv |r| = r_w$  is the radius of the well;

$$\phi_e|_{r_w} = U, \quad \phi_e|_{r \rightarrow \infty} = 0, \quad (10.5)$$

$$\Sigma(E(r, 0), 0) = \Sigma_0 \quad (10.6)$$

Assume that the electric current is switched on instantly. In the equations above,  $U$  is the voltage supplied to the casing column,  $I = U/R_0$  is the current in the circuit,  $R_0$  is the apparent resistance of the medium. It is taken into account in (10.4) that in the interval  $H_w \gg r \gg r_w$  the problem has cylindrical symmetry, and in the interval  $r \gg H_w$ , spherical symmetry. The component of the electric current vector perpendicular to the surface of the ground vanishes.

Taking account of the time dependencies of  $\Sigma$  and  $E$  does not cause any change to the equations (10.1) - (10.3) and the conditions (10.4) - (10.6), since the characteristic times of variation for  $\Sigma$  and  $E$  are no less than several tens of minutes, and therefore the contribution of the non-steady state terms is negligible. Therefore time can be treated as a parameter in this problem, and the problem itself becomes quasi-stationary. Using the asymptotics (10.4), we can propose a uniform relationship for the current density

$$j(r, t) \approx I(t)/S^0(r) \quad (10.7)$$

where  $S^0(r) \approx 2\pi r H_w (1 + r/H_w)$ .

In this case the apparent resistance of the medium is

$$R_0(t) \cong \int_{r_w}^{\infty} [\Sigma(r, t) S^0(r)]^{-1} dr \quad (10.8)$$

Having divided (10.2) by  $\Sigma(r, t)$  and after integrating with respect to  $r$  from  $r_w$  to  $\infty$ , with regard to (10.8), we obtain

$$I(t) = U/R_0(t), \quad E(r, t) = I(t)[\Sigma(r, t)S^0(r)]^{-1} \quad (10.9)$$

After adding the initial condition

$$\Sigma(r, 0) = \Sigma_0 \quad (10.10)$$

we obtain the following from (10.9) - (10.10)

$$\begin{aligned} R(0) &= R_0, \quad I(0) = I_0 = U/R_0, \\ E(r, 0) &= I_0[\Sigma_0 S^0(r)]^{-1} \end{aligned} \quad (10.11)$$

The expressions (10.7) - (10.11) represent a closed system of equations for the determination of the field intensity distribution  $E(r, t)$ , if the dependence of the specific electric conductivity on  $r$  and  $t$  is known.

To determine the change in the well production after electric treatment, we will use the equations of steady state flow of an incompressible fluid in a porous medium

$$\operatorname{div} \nu = 0, \quad (10.12)$$

$$\nu = -K\mu^{-1}\nabla p \quad (10.13)$$

where  $\nu$  is the flow velocity vector.

Under the assumption the fluid flows at a constant depth, the initial and boundary conditions, have the following form

$$\begin{aligned} p(r, 0) &= p_0, \quad p(r_w, t) = p_w, \quad p(R_{aq}, t) = p_0, \\ K(r, 0) &= K_0(r) \cong K(R_{aq}, t) \end{aligned} \quad (10.14)$$

Here, as in (10.1) - (10.3), the quasi-stationary nature of the process is proposed, and therefore time  $t$  in (10.12) - (10.14) can be treated as a parameter. In (10.14)  $p_w$  is the pressure of the fluid in the well,  $p_0$  is the pressure at the supply line  $R_{aq} \gg r_w$ , where the permeability  $K_0$  does not change and is equal to its initial value. The initial layer pressure is also equal to  $p_0$ .

Since the well production

$$Q \sim \nu(r, t)S^0(r),$$

it can be easily shown that its growth with respect to the initial production is determined by the relationship

$$Q(t)/Q_0 = \int_{r_w}^{R_{a0}} \frac{dr}{K_0(r)S^0(r)} \bigg/ \int_{r_w}^{R_{a0}} \frac{dr}{K(r,t)S^0(r)} \quad (10.15)$$

The absolute value of well production is determined by the expression

$$Q(t) = \frac{p_0 - p_w}{\mu} \bigg/ \int_{r_w}^{R_{a0}} \frac{dr}{K(r,t)S^0(r)} \quad (10.16)$$

which also allows to establish the production rate of an initially non-conducting well ( $K(r_w, 0) = K(r_w) = 0$ ,  $Q_0(0) = 0$ ).

To determine the threshold voltage on the power electrodes during the electric treatment with impulse current (with duration of impulse  $\tau$ ), it is necessary to set  $t = 0$ ,  $r = r_w$   $E = E'(\tau)$  in (10.8), (10.9).

Thus we obtain

$$U'(\tau) = E'(\tau)R_0\Sigma(r_w, 0)S^0(r_w)$$

In the special case of

$$\Sigma(r, 0) = \Sigma_0 = \text{const}$$

we have

$$U'(\tau) \approx E'(\tau)r_w \ln \left[ \frac{H_l(r_w + H_w)}{(H_l + H_w)r_w} \right] \left( 1 + \frac{r_w}{H_w} \right) \quad (10.17)$$

Since  $H_l \gg H_w \gg r_w$ , the expression (10.17) can be simplified some more:

$$U'(\tau) \approx E'(\tau)r_w \ln(H_w/r_w) \quad (10.18)$$

In the case of electric treatment with alternating current the starting point  $t'(E_0)$  for the irreversible changes of permeability in the critical zone of the well can be found by substituting the value of field intensity  $E(r_w)$  in the well into (8.26) and by using the calculated curve depicted in fig. 56.

According to the results of chapter 8, the field intensity distribution (10.9) allows to find the change in the electric conductivity as a function of the distance from the well at any instant that follows (see fig. 56). The latter, in its turn, permits to calculate the new resistance of the medium using (10.8) and the change of the well production using (10.15). Then the procedure is to be repeated. The outlined algorithm for the determination of the field intensity distribution as a function of time and the corresponding changes of the electric conductivity and the permeability distributions, as well as the time dependencies of the current and the production rate, was realized on a computer.

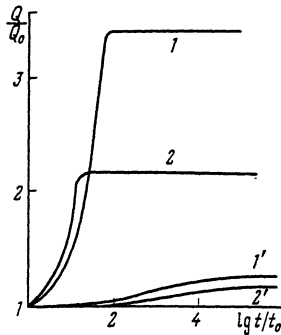


Figure 64: Relation for the irreversible change of well production when it is treated with alternating ( $1'$ ,  $2'$ ) and impulse ( $1$ ,  $2$ ) current

In fig. 64, the dependencies of the well production change for a homogeneous and a heterogeneous media are presented. The parameters of these dependencies are the same as in §8.2, 8.4. Calculations involving  $f(r)$  of the form (8.19) with  $i = 1, j = 2$  and  $i = 5, j = 10$  correspond to the numbers 1, 2, respectively.

Duration of the electric treatment is plotted on the  $x$ -axis and is uniquely related to the total energy consumption

$$w_e = U^2 \int_0^t dt / R_0(t)$$

Here  $t_0$  is the time for the input of an energy unit  $w_{e0}$ , for example, of 1 kilojoule.

## 10.2 Reversible Change of Permeability. Determination of Optimal Regime for Electric Treatment

In chapter 9, it was shown how the dependence of the effective permeability on the amount of electric energy put in the medium (or on the current density and the duration of treatment) can be determined using the data of a laboratory experiment. If the heat capacity and the density of the medium are known, these dependencies can be transformed into a temperature dependence of the permeability.

Consider the problem of steady state flow of a conducting fluid in a micro-heterogeneous medium as current  $I$  passes through it, and the increase of the permeability is reversible.

Suppose that the fluid is recovered from a well with radius  $r_w$ , kept at the constant pressure  $p_w$ . Let the regions of current and fluid flow coincide and be

cylindrically (flow at the depth  $H$ ) or spherically symmetric.

For steady state flow, the temperatures of the fluid and the skeleton are locally equal. Estimates show that in the critical zone, the effect of heat conductance is negligible compared to the convective heat transfer for actual wells and actual conditions of the recovery. In this case the stationary heat equation has the following form

$$c_f \rho_f \nu \nabla T + \rho_e j^2 = 0 \quad (10.19)$$

Here  $c_f$ ,  $\rho_f$ , and  $\rho_e$  are the specific heat and the density of the fluid and the specific electric resistance of the medium, respectively. Furthermore

$$\nu(r) = -\frac{Q}{S^0(r)} \frac{\mathbf{r}}{r}, \quad j(r) = \frac{I}{S^0(r)} \quad (10.20)$$

where

$$S^0(r) = \begin{cases} 2\pi r H, & i = 1, \\ 4\pi r^2, & i = 2 \end{cases} \quad (10.21)$$

In this section, the case of cylindrical symmetry is denoted by index  $i = 1$  and the case of spherical symmetry, by index  $i = 2$ .

After substituting (10.20), (10.21) into (10.19), taking into account the fact that  $\nabla T = \partial T / \partial r (\mathbf{r}/r)$ , and integrating with respect to  $r$  from  $r$  to  $R_{aq}$ , we obtain the radius distribution of temperature

$$T(r) - T(R_{aq}) = \frac{\rho_e I^2}{\rho_f c_f Q} \begin{cases} \frac{\ln(R_{aq}/r)}{2\pi H}, & i = 1, \\ \frac{1}{4\pi} \left( \frac{1}{r} - \frac{1}{R_{aq}} \right), & i = 2 \end{cases} \quad (10.22)$$

The rate of the joule heat release in the medium is

$$w_e = \int_{r_w}^{R_{aq}} \rho_e j^2(r) S^0(r) dr = \frac{\rho_e I^2}{4\pi} \begin{cases} \frac{2 \ln(R_{aq}/r_w)^2}{H}, & i = 1, \\ (1/r_w - 1/R_{aq}), & i = 2 \end{cases} \quad (10.23)$$

If the temperature dependence of the permeability of a micro volume

$$K = K(T) \quad (10.24)$$

is known, then using (10.22), we obtain

$$K = K(r)$$

The well production rate before the electric treatment is determined from (10.16), if we set  $K = K_0 = \text{const}$ ,  $r = R_{aq}$

$$Q_0 = \frac{p_0 - p_w}{\mu} K_0 \begin{cases} 2\pi H / \ln(R_{aq}/r_w), & i = 1, \\ 4\pi / (r_w^{-1} - R_{aq}^{-1}), & i = 2 \end{cases} \quad (10.25)$$

Introduce the following notation

$$x = \begin{cases} \ln(R_{aq}/r)/\ln(R_{aq}/r_w), & i = 1 \\ (r^{-1} - R_{aq}^{-1})/(r_w^{-1} - R_{aq}^{-1}), & i = 2 \end{cases} \quad (10.26)$$

Using (10.16) and (10.23), we transform (10.22) to get

$$T(x) = w_e(c_f \rho_f Q)^{-1} x + T(R_{aq}) \quad (10.27)$$

Further, based on (10.24), (10.25), and (10.27), we obtain a universal equation for both problems

$$\frac{Q_0}{Q} = K_0 \int_0^1 \frac{dx}{K[w_e(c_f \rho_f Q)^{-1} x + T(R_{aq})]} \quad (10.28)$$

If we assume that at a distance  $R_{aq}$ , the temperature of the medium is close to its initial value  $T(R_{aq}) \approx T_0$ ,  $K(T(R_{aq})) = K(T_0) \approx K_0$ , for a specific dependence (10.24), the relationship (10.28) is an equation for  $Q$  with a fixed  $w_e$ .

The relationship (10.24) was obtained experimentally for sandy-argillaceous rocks described in chapter 9 and has the following form

$$K(T) = \begin{cases} K_0 + B''(T - T_0), & T < T_c \\ K_0 + B''(T - T_0) + D''(T - T_c)^2, & T > T_c \end{cases} \quad (10.29)$$

Here  $K_0$  is the permeability at the initial temperature  $T_0$ ;  $B''$ ,  $D''$  are the parameters to be determined from experiment;  $T_c$  is the critical temperature, starting from which the dependence  $K(T)$  becomes nonlinear. After substituting (10.29) in (10.28) and integrating, we obtain a transcendental equation that relates the production rate  $Q$  to the power of energy release  $w_e$

$$\frac{Q_0 w_e}{Q^2 E''} = \begin{cases} \ln[1 + w_e/(E''Q)], & w_e < w_c \\ \ln(1 + L'') + \frac{2}{F''} \arctan \left[ \frac{(w_e - L''E''Q)F''}{(2 + L'')E''Q + w_e} \right], & w_e > w_c \end{cases} \quad (10.30)$$

where

$$L'' = (T_c - T_0)B''K_0^{-1}; \quad F'' = \sqrt{\frac{4E''^2 D''}{c_f^2 \rho_f^2 K_0} (1 + L'') - 1};$$

$$w_c = Q_0 E'' L''^2 \ln^{-1}(1 + L''), \quad E'' = K_0 c_f \rho_f / B''$$

The experimental dependence (10.29) is a good approximation for describing the dependence  $K(T)$  in a large temperature range (from several degrees Celsius to the boiling point of the fluid). After determining the parameters  $T_c$ ,  $K_0$ ,  $B''$ ,

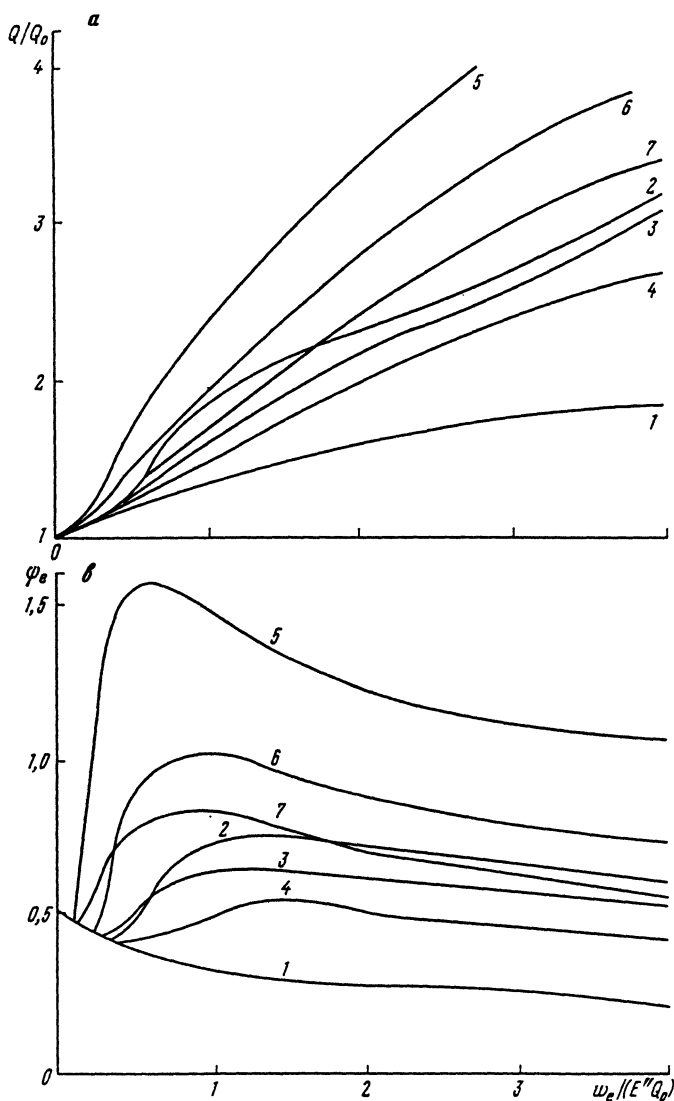


Figure 65: Dependencies of the reversible change in well production (a) and efficiency of electric treatment (b) on the energy release rate in the medium



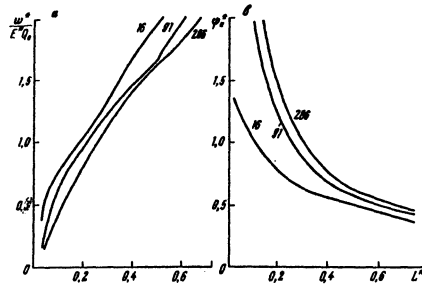


Figure 66: Dependencies of the optimal energy input rate in the medium (a) and the maximal efficiency of the electric treatment (b) of the critical zone of the well on the parameter  $L''$ . Curve code –  $F''$

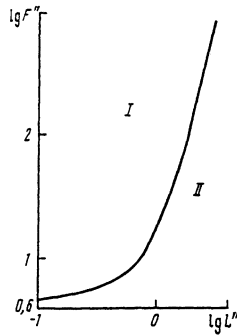


Figure 67: Ranges of  $L''$  and  $F''$  for different modes of electric treatment of the critical zone of the well

$D''$  from experiment, one can construct the dependence  $Q(w_e)$  for the given rock based on (10.30).

The relations  $Q/Q_0(w_e/(E''Q_0))$ ,  $\psi_e(w_e/(E''Q_0)) = (Q - Q_0)E''/w_e$  for some media are presented in fig. 65. The function  $\psi_e$  defines the additional volume of the solution obtained per unit energy consumption rate. Those curves in fig. 65 marked with index 1 correspond to the case of the linear dependence  $K(T)$  in the whole temperature range ( $T_c = \infty$ ). The results of the calculations with parameters  $F'' = 10$ ,  $L'' = 0.1; 0.2; 0.3$ , are denoted by indices 2 - 4, respectively, and the results of the calculations with  $F'' = 40$  and the same  $L''$ , by indices 5 - 7.

It can be seen in fig. 65, b, that the function  $\psi_e$  has a maximum for certain values of  $L''$  and  $F''$ . It corresponds to the minimal energy consumption needed to obtain additional recovered volumes of fluid, and therefore corresponds to the optimal electric treatment regime. Take  $w_e^*/(E''Q_0)$  and  $\psi_e^*$  as the point of maximum for the function  $\psi_e$  and its value  $\psi_e(w_e)$  there. In fig. 66, a, the  $L''$  dependencies

of  $w_e^*/(E''Q_0)$  are presented, and  $\psi_e^*(L'')$  are presented in fig. 66, b.

It is clear from these plots that  $w_e^*/(E''Q_0)$  decreases and  $\psi_e$  increases as  $F''$  grows and  $L''$  diminishes. These dependencies are more sensitive to the changes in the quantity  $L''$  than they are to the changes in  $F''$ . The value  $Q/Q_0$  depends weakly on the parameters of the problem and varies from 1.5 to 2.5.

Two regions are shown in fig. 67 in the plane of the parameters  $F''$  and  $L''$ . The boundaries of those regions, where the optimal electric treatment regime is possible, form region *I*. The boundaries of those regions, where the maximum of  $\psi_e$  does not exist, and consequently the treatment regime with small currents ( $w_e < w_c$ ) is optimal as far as the energy consumption costs are concerned, form region *II*.

Therefore depending on the values of the parameters  $L''$  and  $F''$  determined from the plot of  $K(T)$ , both the presence and the absence of an extremum of the function  $\psi_e$  are possible. In principle, the optimal electric treatment regime can be determined based on the calculated data (see figs. 65 - 67) and the economic calculations. For an arbitrary form of the  $K(T)$  dependence, the optimal electric treatment regime is determined similarly from the solution to the equation (10.28). Note that even when the electric treatment is carried out in non-optimal regimes, the economic effect is positive. This is due to the fact that the time of maintenance of the wells, necessary for the development of a deposit (i.e., for reaching the established level of the recovery of the useful component), is made less.

### 10.3 Results of Field Studies

Typical diagrams of electric energy supply to the reservoir, which have already been tested, are presented in fig. 63 for the case of a single well. In diagram *III* voltage is supplied from the source directly to the casing column. In this case it is not necessary to immerse an electrode into the well. This diagram is rather simple and efficient, but if the reservoir lies more than 300 meters deep, then the electric energy consumption due to the current flow through the lateral area of the wells becomes very large. In this case it is advisable to use a different diagram of energy supply. Experimental work done with objects of various geological types in different regions (over 80 places) showed that the well production rates can increase by 2 to 20 times (at an average of 1.5 to 2 times) after electric treatment.

Experiments showed that well production rates keep stable for two to three years after the electric treatment. A positive effect is observed for electric treatment of different types of rocks, e.g. sandy-argillaceous, carbonate, or fractured ones. The studies involving observation wells showed that the changes of permeability after the electric treatment are registered at distances up to 10 m (fig. 68). A typical correlation for the modification of a hydrogeological well production rate

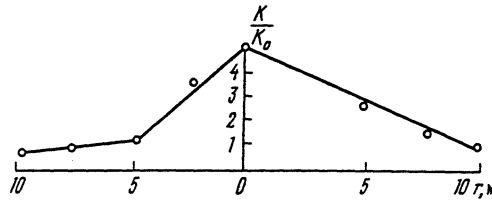


Figure 68: Distribution of the presented permeability factor near the well after electric treatment

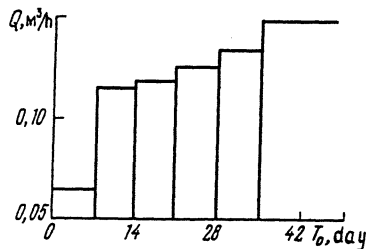


Figure 69: Histogram for a typical dependence  $Q = f(T_0)$  for a well under electric treatment

after electric treatment is presented in fig. 69.  $T_0$  is the duration of a unit cycle of electric treatment.

The results of the electric treatment only weakly depend on the location of the second electrode, since the resistance between the electrodes is a logarithm function of the distance between them. The resistance  $R_e$  and consequently, the current supplied to the reservoir depend more significantly on the lengths of the electrodes.

Thus the results of the field experiments show that the electric treatment of wells is an ecologically pure, very effective, and efficient means of the well production increase.

Electric treatment of wells with "high-density" currents can be used to increase the production rates, purify the well filter, de-mud the critical zone of a well after drilling.

To study the possibility of the pore space structure reconstruction in rocks (underground leaching), an experiment on a fractured low-permeable ore strata in Khodgent was conducted. The region is situated in the piedmont part of a crest composed from granitoid rocks of several phases of magmatism. The most ancient of these rocks, those dating back to the Upper Carboniferous, are represented by the fine-grained leucocratic granites, the segments of a porphyritic structure. Porphyry granites and aplite-like granites of the Lower Permian are examples of the younger ones. The fractures are covered with attrition clay, quartz, or carbonate.

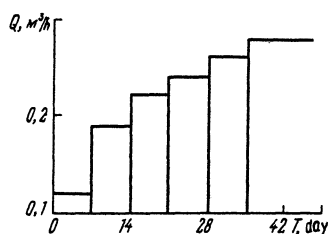


Figure 70: The averaged result of action upon a bulk of fractured granite after five cycles of electric treatment

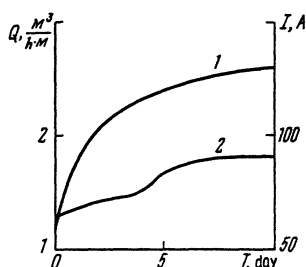


Figure 71: Curves representing the variation of the production rate 1 and the current 2 as the duration of electric treatment goes up

Five cycles of electric treatment were conducted. The results are presented in fig. 70. Observation of the drainage well production demonstrates its steady increase throughout all five cycles of the energy supply to the bulk.

Plots of typical correlations obtained during the electric treatment of a water-bearing well are shown in fig. 71. The reservoir rock was a highly permeable fractured limestone. It is clear from fig. 71 that the increase of the well production (curve 1) was accompanied by the increase of the current in the rock (up to 30%). The well production increased by 130% after electric treatment was stopped. Measurements of the well production seven months after the electric treatment showed that the production rates increased by additional 20%, so that the total increase in the production reached 150% (or 2.5 times the initial value). Similar results were obtained for other analogous wells (a total of 11 wells). The average increase in the production equaled 185%; the range of values was 100 to 200%.

Typical results of the electric treatment of hydrogeological and oil wells are presented in table 10.1. The drop in the inundation of the oil wells after electric treatment is due to the development of gas colmatation described in the next chapter. This effect is reversible and disappears several months after the well has been treated.

Table 10.1:

Well type (rock type)	Number of wells	Depth of wells, m	Change of well rate ( $q/q_0$ )	Drop in inundation
Hydro- geological (sandstones)	167	50 - 200	2.5	—
Hydro- geological (limestones)	92	100 - 250	2.5	—
Hydro- geological (sandy- argillaceous)	143	130 - 300	2 - 3	—
Technological (granite)	42	20 - 150	2.7	—
Oil (limestones)	83	2000 - 2300	2.3	10 - 30%

## Chapter 11

# Gas Colmatation Effect during Electric Action on Saturated Porous Media

Under certain conditions, the temperature of the saturating fluid can reach the critical value, i.e., the boiling point, and the liquid can transform to the gas phase. In this case the capillaries shut off with bubbles of gas are no longer permeable to the liquid phase. The gas colmatation effect develops and causes the decrease in the permeability of media to the flowing liquid. Thus the total effect of electric action is determined by two fundamental competing factors: the increase of permeability due to the change of the pore space structure (cross-section increase in the conducting capillaries) and the decrease of permeability when some of the conducting capillaries are cut off from the flow of the liquid phase (being filled with the gas phase). Domination of either of the outlined trends over the other is determined by the parameters of the medium and of the treatment, or, when these parameters are fixed, by the duration of electric treatment.

Colmatation can not only diminish the desired positive effect of electric treatment, but also cause an altogether negative result. Therefore we shall consider this effect in more detail and carry out theoretical analysis at the micro level and laboratory modelling of the process.

## 11.1 Temperature Effects in Capillaries Caused by Electric Current

We shall begin with the description for the distribution of the electric current flowing in a micro heterogeneous medium. Using the notation (3.1) already introduced, write the expression for the amplitude  $I_0$  of the current flowing through an arbitrary  $r_1$ -chain

$$I_0(r_1) = E_0 \sigma' r_1^2 \phi(r_1) \quad (11.1)$$

where the so-called heterogeneity factor of the medium is

$$\phi(r_1) = [r_1^2 < r_1, r^{-2}, a^* >]^{-1}$$

It is clear from (11.1) that the amplitude of the current flowing through an  $r_1$ -chain depends only on the amplitude of the field intensity  $E_0$ , the electric conductivity  $\sigma'$  of the fluid that fills the pore space, and the heterogeneity factor  $\phi(r_1)$  of the medium.

According to the results of §1.2, the total current flowing in the medium is determined by the expression

$$J_0 = \int_{a^*}^{r_c} I_0(r_1) dn(r_1)$$

Hydraulic conductivity of the  $r_1$ -chain (for Poiseuille flow in capillaries) can be found from an expression similar to (11.1)

$$k(r_1) = (\pi/8)r_1^4 \psi(r_1), \quad \psi(r_1) = [r_1^4 < r_1, r^{-4}, a^* >]^{-1}$$

Permeability of the medium in this case is

$$K = \int_{a^*}^{r_c} k(r_1) dn(r_1)$$

It can be shown that the functions  $\phi(r_1)$  and  $\psi(r_1)$  increase as the degree of heterogeneity of the medium (the variance of  $f(r)$ ) decreases.

The energy release density in an  $r$ -capillary ( $r_1 \leq r \leq a^*$ ) of an  $r_1$ -chain is

$$q_0(r, r_1) = I_0^2(r_1) [\sigma' \pi^2 r^4]^{-1} = E_0^2 \sigma' (r_1/r)^4 \phi^2(r_1) \quad (11.2)$$

It follows that  $q_0(r, r_1)$  goes up as  $r$  decreases and is maximal in the  $r_1$ -capillary.

For exponential distribution functions of the form

$$f(r) = a/r^i \quad (11.3)$$

$a$  is determined from the normalization condition for  $f(r)$ .

For  $a^* \gg a_*$  we have

$$\begin{aligned} a &= (i - 1)a_*^{i-1}, \quad r_c = a_*\xi_c^{-1/(i-1)} \\ \phi(r_1) &= (i + 1)/(i - 1) = \phi_0, \quad \psi(r_1) = (i + 3)/(i - 1) = \psi_0 \\ dn(r_1)/dr_1 &= n_0(a_*/r_1)^i[(a_*/r_1)^{i-1} - (a_*/r_c)^{i-1}] \\ I_0(r_1) &= E_0\sigma'\phi_0\pi r_1^2, \quad k(r_1) = (\pi/8)r_1^4\psi_0 \\ q(r, r_1) &= E_0^2\sigma'(r_1/r)^4\phi_0^2 \end{aligned} \tag{11.4}$$

We shall now use the solution to the problem (8.2) presented in §8.1. This problem deals with the temperature distribution in a long cylindrical capillary with radius  $r$  in a boundless medium (with temperature conductivity the same as that of the fluid in the capillary) as electric current  $I(t) = I_0i(t)$  passes through it. After determining  $q_0$  according to (11.2) and substituting the obtained expression in the relationship (8.3) for  $q(t')$ , after transformations we obtain the following

$$\begin{aligned} T(t, z) &= 1/2 + \int_0^1 q_0(xt)\{1 - \exp[(-y'(1-x))^{-1}]\} \\ &\quad \times \{1 + \Phi[zr^{-1}(y'(1-x))^{-1/2}]\}dx \end{aligned} \tag{11.5}$$

Here  $y'$  is determined according to (8.4),  $x$  is a dummy integration variable, and  $\Phi(\cdot)$  is the error integral defined as

$$\Phi(x) = \frac{2}{\sqrt{\pi}} \int_0^x \exp(-\xi^2)d\xi \tag{11.6}$$

After differentiating (11.5) with respect to  $z$  and  $t$ , we obtain, respectively, the temperature gradient along the capillary

$$\begin{aligned} T'_z(t, z) &= \sqrt{\frac{t}{4\pi\kappa t}} \int_0^1 q_0(xt)\{1 - \exp[(-y'(1-x))^{-1}]\} \\ &\quad \times \exp\{-z^2[r^2y'(1-x)]^{-1}\}(1-x)^{-1/2}dx \end{aligned} \tag{11.7}$$

and the rate of the temperature change in the capillary

$$\dot{T}(t, \infty) = q_0(t) - \frac{1}{y'} \int_0^1 q_0(x, t) \exp\{[-y'(1-x)^{-1}]\}(1-x)^{-2}dx \tag{11.8}$$

When  $q_0 = q_p = \text{const}$ , where  $q_p = I_0^2/(c_i\rho_i\sigma'\pi^2r^4)$  is the current density amplitude, it follows from that (11.5) - (11.8) that

$$T(t, \infty) = q_p t \{1 - \exp[-(y')^{-1}] - y'^{-1} \text{Ei}[-(y')^{-1}]\} \tag{11.9}$$



$$\dot{T}(t, \infty) = q_p \{1 - \exp[-(y')^{-1}]\} \quad (11.10)$$

$$T'_z(t, z) = q_p \sqrt{t/(4\pi\kappa t)} [\Lambda(\gamma_0) - \Lambda(\gamma_0 + \Delta)] \quad (11.11)$$

$$\Lambda(\gamma_0) = 2e^{-\gamma_0} - 2\sqrt{\pi\gamma_0} [1 - \Phi(\sqrt{\gamma_0})], \quad \gamma_0 = z^2/(r^2 y'), \quad \Delta = 1/y'$$

The integral exponential function is

$$\text{Ei}(-x) = \int_{\infty}^x \xi^{-1} e^{-\xi} d\xi \quad (11.12)$$

Using the asymptotics for the functions (11.6) and (11.12), the following asymptotics for  $T$ ,  $\dot{T}$ , and  $T'$  can be obtained based on (11.9) - (11.11)

$$T(t) = q_p(t) \begin{cases} 1 - (\tau_0/t) \exp(-\tau_0/t), & t \ll \tau_0, y' \ll 1 \\ (\tau_0/t) \ln[et/(\gamma\tau_0)] - \tau_0/t, & t \gg \tau_0, y' \gg 1 \end{cases}$$

where  $\gamma = 1.78$  is the Euler - Masceroni number;  $\tau_0 = r^2/(4\kappa t)$ ;

$$\begin{aligned} \dot{T}(t) &\approx q_p(t) \begin{cases} 1 - e^{-1/y'}, & y' \ll 1, t \ll \tau_0 \\ 1/y' - 1/(2y'^2), & y' \gg 1, t \gg \tau_0 \end{cases} \\ T'(t) &\approx \frac{q_0(t)r}{\kappa t} \begin{cases} \frac{r^2}{4z^2} \sqrt{\frac{y'}{\pi}} \exp(-z^2/r^2 y') \left(1 - \frac{r^2 y'}{2z^2}\right), & 1 \ll y' \ll (z/r)^2 \\ \frac{r}{4z} \left(1 - \frac{2}{\sqrt{\pi y'}} \exp(-z^2/r^2 y')\right), & 1 \ll (z/r)^2 \ll y' \end{cases} \end{aligned}$$

It follows from (11.10) and (11.2) that

$$\partial T/\partial r < 0; \quad \partial \dot{T}/\partial r_1 > 0 \quad (11.13)$$

We thus conclude that the greatest rate of the temperature change is assumed in the thinnest  $r_1$ -capillary of the  $r_1$ -chain. Also, the capillaries with radii equal to  $r$  have greater values of  $\dot{T}$  in the larger  $r_1$ -chains. Therefore the greatest rate of the temperature change in the medium is observed in the thinnest capillaries of the thickest  $r_1$ -chains, i.e., in the  $r_c$ -capillaries of the  $r_c$ -chains.

## 11.2 Movement and Growth of Bubbles in Capillaries

Inequalities (11.13) imply that in the thin capillaries of all  $r_1$ -chains the temperature grows faster than in the thick capillaries of the same chains. If we take into account the temperature dependence  $\chi(T)$  of the interfacial tension, we can state that the thin ("hot") capillaries become stable attraction centers for the bubbles coming from thicker ("cold") capillaries.

Estimate the velocity of a bubble with radius  $a_0$  as it moves from a pore of size  $\sim a^*$  to a capillary of radius  $r \ll a^*$ . Consider the movement of the bubble as though the fluid were flowing past it. The mass of the former,  $m^0$ , is of the order of mass of the fluid displaced by the bubble

$$m^0 \approx \rho_f (4/3) \pi a_0^3$$

When the velocity of the bubble  $\nu_0 \ll \mu a_0^{-1} \rho_f^{-1}$  ( $a_0 \lesssim 10^{-4}$  m), the resistance to the movement of the bubble is adequately described by Stokes's formula

$$F_c = 6\pi\mu\nu_0 a_0$$

The force that causes the movement of the bubbles for small temperature gradients  $T'$  is determined by the following relationship [87, 88]

$$F_g = -\chi' T' \pi a_0^2, \quad \chi' = d\chi/dT$$

As the bubble comes closer to a thinner capillary, both the temperature gradient and the velocity go up.

The steady state velocity of the bubble is determined from the condition  $F_c = F_g$

$$\nu_0 = -\chi' T' a_0 \mu^{-1} / 6 \quad (11.14)$$

The transient period for the velocity of the bubble is

$$\tau_y \sim \frac{m^0}{6\pi\mu a_0} = \frac{2}{9} \frac{\rho_f}{\mu} a_0^2 \quad (11.15)$$

and is usually much less than the time  $\tau_g$  needed for a bubble to reach the capillary from the pore. This fact permits to consider the movement of the bubble to be quasi-uniform with velocity determined by (11.14) and  $T'$  determined according to (11.11) or the corresponding asymptotics. For example, when  $T'$  grows slowly (when  $t \gg a^{*2}/(4\kappa_t)$ ), using the asymptotics of the expression (11.11), we obtain the duration of the movement for the bubble

$$\tau_g \approx \frac{48\mu\kappa_t}{(-\chi')q_p} \frac{1}{a_0} \left( \frac{a^*}{r} \right)^2 \quad (11.16)$$

From the condition  $\tau_y/\tau_g \ll 1$ , the following relationship results,

$$q_p \ll \frac{216\mu^2\kappa_t}{(-\chi')\rho_f} \frac{1}{a_0^3} \left( \frac{a^*}{r} \right)^2$$

For the period of  $\sim \tau_g$  the bubbles move within a large capillary towards its boundary. This results in the bubbles situated in the pores that surround the "hot" capillary concentrating inside it  $\sim \tau_g$  seconds after the current is turned on.

The bubbles can merge at this stage of the process due to the attraction forces that act when the distance between the bubbles is of the order of two to three times their radius. Attraction between the bubbles is caused by the overlap of the low-pressure domains in the surrounding fluid. These domains are formed once the balance between the surface tension and the vapor and gas pressure inside a bubble is established. When  $a_0 < 10^{-7}$  m attraction forces can be significant, since the pressure outside the bubbles becomes negative.

It is evident from (11.2) and (11.6) that the first to be filled with bubbles are the thinnest  $r_1$ -capillaries in  $r_1$ -chains. For probability density functions of the form (11.3), we have the following, with regard to (11.4)

$$\tau_g = \frac{48\mu\kappa_t}{(-\chi')E_0^2\sigma'\phi_0^2} \frac{1}{a_0} \left(\frac{a^*}{r_1}\right)^2 \quad (11.17)$$

Note that during the period of  $\sim \tau_g$ , the density of bubbles in the thin capillaries increases from the initial value  $n_*$  to  $n_0 \approx n_*(a^*/r)^2$ , since a thin capillary is most likely to borrow almost all capillaries from the adjacent pore. However, adjacent capillaries separated by a pore are not likely to compete in the future, since an own "warm" capillary is more attractive for any bubble than perhaps a "hotter" one, but separated from it by a big "cold" pore.

For a bubble in the fluid being heated by the electric current, two essentially different phases of growth can be specified.

At the first stage, when the temperature of the fluid  $T < T_b(p_\infty)$ , where  $p_\infty$  is the fluid pressure at a large distance from the bubbles,  $T_b$  is the boiling point which corresponds to the pressure  $p_\infty$ , the bubble is in the quasi-steady state. At the second stage, when  $T = T_b(p_\infty)$ , the bubble is not in a steady state, and its limitless growth begins. The rate of this growth is determined only by the rate of the energy supply to the bubble.

Estimates show that for the actually achievable values  $q_0$  of the energy release rate in micro capillaries in different media, the pattern of a homogeneous steady state vapor bubble can be used. In this pattern, the velocities of the radial motion of the phases and the surfaces of the bubbles are considered much less than the velocities of the molecular thermal motion or the velocity of sound.

At the vapor-liquid surface, there is a thin boundary layer, where the phase transitions to and from vapor take place. For a balanced system, it is assumed that the temperature  $T_p$  inside the bubble near the boundary layer, the temperature  $T_\psi$  in the boundary layer, and the temperature  $T_a$  in the fluid near the boundary layer are all equal

$$T_p = T_\psi = T_a$$

The vapor temperature conductivity  $\kappa_p$  is much greater than that of the liquid  $\kappa_t$ , and therefore the time for establishing the temperature balance outside the

sphere is much greater than inside it. Thus we can consider the temperature of vapor inside the bubble to be constant and equal to the temperature  $T_s$  of the saturated vapor which corresponds to the vapor pressure  $p_p$  inside the bubble

$$T_p = T_s(p_p) \quad (11.18)$$

Thus we can consider the properties of the vapor to be observed only by changing its pressure.

According to the first law of thermodynamics, we have

$$\delta Q_p = du_p + p_p d(1/\rho_p) \quad (11.19)$$

where  $\delta Q_p$ ,  $du_p$  are, respectively, the amount of heat absorbed by and the change of the internal energy of, a unit mass of vapor in the bubble. The correlation between the heat flow  $q'_p$  through the surface of the boundary layer and the quantity  $\delta Q_p$  is determined by the following equations

$$\begin{aligned} \frac{4}{3}\pi a^3 \rho_p \delta Q_p &= q'_p dt \\ q'_p &= -k_p (\partial T_p / \partial r_p) \Big|_{r_p=a-0} \cdot 4\pi a^2 \end{aligned} \quad (11.20)$$

The equation of state for vapor is

$$p_p = \rho_p R_p T_p, \quad R_p = R/\mu_p \quad (11.21)$$

In the above,  $R = 8.31 \cdot 10^3$  kilojoule per mole-kelvin is the universal molar gas constant;  $\mu_p$  is the mass of one mole of vapor;  $k_p$  is the heat conductivity of the vapor;  $r_p$  is the radial coordinate with the origin in the center of the bubble; and  $a(t)$  is the current value of the latter's radius. Total internal energy of the vapor is

$$u_p = C_V^p T_p + u_{p0}$$

where  $u_{p0}$  is the initial energy of the vapor and  $C_V^p$  is the specific heat of the vapor at a constant volume. It follows from (11.18) that  $dT_s = dT_p$ , and finally we obtain the following

$$du_p = (C_p^p/\gamma_p) dT_s = (C_p^p/\gamma_p) (dT_s/dp_p) dp_p \quad (11.22)$$

where  $C_p^p$  is the specific heat of the vapor at a constant pressure and  $\gamma_p$  is the isentropic exponent for the vapor.

After differentiating the equation of state (11.21) with respect to  $T_p$ , we obtain

$$d\rho_p/\rho_p = (1 - R_p \rho_p dT_s/dp_p) dp_p/p_p \quad (11.23)$$

Using the Clausius-Clapeyron equation with  $p_p = p_s$

$$dT_s/dp_s = (T_s/L_p)[1/\rho_p(T_s) - 1/\rho_f(T_s)]$$

where  $L_p$  is the specific heat of liquid evaporation, we obtain

$$R_p \rho_p \frac{dT_s}{dp_p} = \frac{1 - \rho_p(p_p)/\rho_f(p_p)}{\gamma_p L^*(p_p)} \quad (11.24)$$

$$L^* = \frac{L_p(p_p)}{\gamma_p R_p T_s(p_p)}, \quad \gamma_p = \frac{C_p^p}{C_V^p} = \frac{C_p^p}{C_p^p - R_p} \quad (11.25)$$

After substituting (11.24) in (11.22) and (11.19) and taking into account (11.23), we obtain the correlation between  $Q'_p$  and the change of pressure

$$q'_p = (4/3)\pi a^3 (\Gamma_*^{-1}) dp_p/dt \quad (11.26)$$

$$\Gamma_* = (\gamma_p - 1)L^*(1 - \rho_p/\rho_f)^{-1}$$

Since along the vapor isentrope (the entropy of the vapor is  $S_p = \text{const}$ )

$$(\partial T_p/\partial p_p)_{S_p} = (\gamma_p - 1)/\gamma_p (T_p/p_p)$$

and along the saturation line of the vapor, according to (11.24), (11.25),

$$(\partial T_p/\partial p_p)_S = (1 - \rho_p/\rho_f)[\gamma_p L^*(p_p)]^{-1} (T_p/p_p)$$

it follows that the quantity  $\Gamma_*$  shows how close to isentropic is the behavior of the vapor, since

$$\Gamma_* = \left( \frac{\partial T_p}{\partial p_p} \right)_{S_p} / \left( \frac{\partial T_p}{\partial p_p} \right)_S$$

When  $\Gamma_* > 1$  and  $dp_p/dt < 0$ , it follows from (11.26) that  $q'_p > 0$  and from (11.20) that  $\delta Q_p > 0$ . This means that the vapor is receiving heat, while the pressure in the bubble grows. At the same time, the temperature gradient  $\partial T_p/\partial r < 0$ , and therefore the temperature is higher in the center of the bubble than on its surface. The latter fact demonstrates the stability of the bubble growth.

If we differentiate the mass conservation equation for the bubble

$$m_p = (4/3)\pi a^3 \rho_p$$

and take into account the relationship

$$dm_p/dt = 4\pi a^2 \xi_{12}$$

where  $\xi_{12}$  is the mass flow of the bubble due to the phase transition in the boundary layer through a unit surface area, we obtain

$$\frac{\dot{\rho}_p}{\rho_p} = -3\frac{\dot{a}}{a} + \frac{3}{a} \frac{\xi_{12}}{\rho_p} \quad (11.27)$$

On the other hand, conservation of the total energy of the phases yields

$$\begin{aligned} L_p dm_p + (q'_p + q_f) dt &= 0 & (11.28) \\ q_f &= -q_f^0 - q'_f \\ q'_f &= -k_f (\partial T_p / \partial r_p) \Big|_{r_p=a+0} \cdot 4\pi a^2 \end{aligned}$$

where  $q_f$  is the heat flow through the boundary of the liquid phase;  $q_f^0$  is an additional heat flow due to the release of the joule heat in the fluid as the electric current passes through it.

Since the heat conductivity of vapor  $k_p$  is much less than the heat conductivity of liquid  $k_f$ , it follows that  $|q_f| \gg |q_p|$ .

Transform (11.28) to get

$$4\pi a^2 L_p \xi_{12} = -q_f - q_p \quad (11.29)$$

After substituting  $\xi_{12}$  from (11.29) into (11.27) and changing  $\dot{\rho}_p / \rho_p$  for (11.23) with regard to (11.24) and  $q_p$  for (11.26) with regard to (11.25), we obtain

$$\begin{aligned} \frac{\dot{p}_p}{p_p} &= -\chi_0 \left[ 3 \frac{\dot{a}}{a} + \frac{3q_f}{4\pi a^3 L_p \rho_p} \right] & (11.30) \\ \chi_0 &= \gamma_p [1 + (\gamma_p - 1)(1 - 1/\Gamma_*)^2]^{-1} \end{aligned}$$

The movement of the bubble boundary is described by the Rayleigh-Lamb equation [89, 90]

$$\begin{aligned} a \frac{d}{dt} (\dot{a} - \xi_{12}/\rho_f) + \frac{3}{2} (\dot{a} - \xi_{12}/\rho_f)^2 \\ = (p_p - p_f - 2\chi/a)/\rho_f - 4\mu(\dot{a} - \xi_{12}/\rho_f)/(a\rho_f) \end{aligned} \quad (11.31)$$

Due to the fact that the liquid is virtually incompressible, and its radial velocity is relatively small, we can set  $p_f = p_\infty$ .

The heat flow  $q_f$  must be determined from the solution of the exterior heat conductance problem for  $r_p > 0$  using the initial and boundary conditions

$$\begin{aligned} C_f \rho_f \left\{ \frac{\partial T}{\partial t} + \left[ \left( \frac{\dot{a}}{a} - \frac{\xi_{12}}{a\rho_f} \right) \frac{1}{r^2} - r \frac{\dot{a}}{a} \right] \frac{\partial T}{\partial t} \right\} \\ = \frac{1}{a^2 r^2} \frac{\partial}{\partial r} \left( k_f r^2 \frac{\partial T}{\partial r} \right) + \epsilon(t) & (11.32) \\ T \Big|_{r=a+0} = T_s(p_p), \quad T(r) \Big|_{t=0} = T_0 \end{aligned}$$

Here the effective temperature growth rate  $\dot{T}$  in a capillary, defined by the expression (11.10), can be taken as  $\epsilon(t)$

$$\delta(t) = q_p [1 - \exp(-r^2/(4\kappa_t t))] \quad (11.33)$$

The equations (11.31), (11.32) are good for describing the growth of a single bubble in a boundless medium. However there may be many bubbles in a capillary and the average distance between them may be relatively small compared to their size ( $l_a \approx (10 - 10^3)a$ ). Therefore it is necessary to take into account the interaction of thermal fields of the bubbles.

Suppose that at the time  $dt$ , an amount of energy equal to  $\pi r^2 l \epsilon(t)$  was released in a capillary. (In the general case, heat losses caused by the outflow through the capillary surface must be taken into account in  $\epsilon(t)$ .) Furthermore, suppose that this amount of energy was distributed uniformly among  $\pi r^2 l n_0$  bubbles in the capillary. Now, taking into account  $q_f \gg q_p$ , we obtain

$$q_f \simeq q_f^0 \simeq \epsilon(t)/n_0 \quad (11.34)$$

If we assume that not all, but only a part of the energy  $\epsilon(t)$  was used for supplying heat to the bubbles, then the rest of the energy will be used for the fluid overheating. The latter will make heat losses through the capillary surface larger, and therefore will decrease  $\epsilon(t)$ . In its turn, this will create an additional flow  $q'_f$  in (11.28), which is going to partially comensate the mentioned loss, and therefore is likely to make the quantity  $q_f$  closer to  $\epsilon(t)/n_0$  in its value. It is possible to estimate the additional flow  $q'_f$ , which may cause deviation from equality (11.34), as follows. If there is no heat discharge, the temperature at a distance  $\sim l_a$  from a bubble must grow by approximately  $\Delta T = \epsilon(t)\tau_k/(C_T^f \rho_f)$  in a characteristic period of temperature equalizing

$$\tau_k = l_a^2/\kappa_t$$

Therefore  $q'_f \approx k_f \Delta T l_a^{-1} 4\pi a^2 \approx 10a^2 l_a \epsilon(t)$ .

In this case the ratio

$$q'_f/q_f^0 \approx 10(a/l_a)^2 \ll 1 \quad (11.35)$$

since  $(a/l_a) \ll 1$ .

Initial conditions

$$a(0) = a_0, \quad p_p(0) = p_f + 2\chi/a_0$$

and the equations (11.27), (11.26), (11.31), (11.33), (11.34) define the relations  $a(t)$  and  $p_p(t)$  completely.

Introduce the notations

$$\Lambda_0 = n_0(4/3)\pi a_0^3, \quad \Lambda = \Lambda_0(n_0/n_*), \quad X = q_p/(p_f L_p), \\ H = \chi_0 R_p T_p p_f p_\infty^{-1}, \quad Z = 2\chi/(a_0 p_\infty)$$

and the dimensionless variables

$$\theta_* = Xt, \quad \omega_* = a/a_0, \quad G_* = p_p/p_\infty$$

Derivatives with respect to  $\theta_*$  will be denoted by a prime.

In this case the equations (11.30), (11.31) and the initial conditions can be represented in the following form, which is convenient for the further investigation,

$$G'_*/G_* + 3\chi_0\omega'_*/\omega_* = DH\Lambda^{-1}G_*^{-1}\omega_*^{-3}; \quad (11.36)$$

$$\omega_*(\omega'_*Y)' + 3/2(\omega'_* - Y)^2 = (G_* - 1 - Z/\omega_*)M \\ - (\omega'_*/\omega_* - Y)N; \quad (11.37)$$

$$G_*(0) = 1 + Z, \quad \omega_*(0) = 1 \quad (11.38)$$

where  $M = p_\infty/(\rho_f a_0^2 X^2)$ ,  $N = 4\mu/(\rho_f a_0^2 X)$ ,  $Y = \xi_{12}/(a\rho_f X)$ ,  $L_0 = p_\infty(3L_p\rho_f)^{-1}(1 - \Gamma_*^{-1})$ ,  $D = 3\Lambda\omega_*^3(Y + L_0G'_*)$ .

Note that as the liquid reaches its boiling point  $T_s(p_\infty) = T_b$ , the temperature inside the bubble  $T_s(p_p)$  can be substantially higher if the size of the latter is sufficiently small ( $Z > 1$ ). Moreover, if the conditions (11.35) are met, then it is possible to assume that the temperature outside the bubble undergoes little change. Therefore (for  $T < 0.8T_b$ ) the parameters of the liquid can be considered practically constant, whereas the parameters of the vapor can change significantly.

In the general case, a solution to a system of nonlinear equations (11.36) - (11.37) with conditions (11.38) can be obtained only numerically.

To obtain a qualitative dependence  $\omega_*(\theta_*)$ , transform (11.36) to

$$(G_*\omega_*^{3\chi_0})' = (H/\Lambda)\omega_*^{3(\chi_0-1)} \quad (11.39)$$

Since  $Y \sim X$ ,  $M \sim X^{-2}$ ,  $N \sim X^{-1}$ , it follows that as  $q_0 \sim X$  goes down, the term  $\sim M$  becomes the principal term in the equation (11.36). (This follows from the obvious fact that  $\omega'_*$  and  $\omega''_*$  decrease as  $X$  goes down.) In this case we have

$$G_* \approx 1 + Z/\omega_* \quad (11.40)$$

After substituting (11.40) in (11.39), integrating, and taking into account the initial value (11.38), we obtain

$$\omega_*^3 + Z(3\chi_0 - 1)(2\chi_0)^{-1}\omega_*^2 = \xi(\theta_*), \\ \xi(\theta_*) = \xi(0) + (\Lambda\chi_0)^{-1} \int_0^{\theta_*} D d\theta_*, \quad \xi(0) = 1 + Z(3\chi_0 - 1)(2\chi_0)^{-1} \quad (11.41)$$

The following facts are taken into account in (11.41).  $Z$  depends on the temperature of the fluid  $T_f$  and changes little in time.  $H \sim T(p_p)$  and depends on  $G_*$ ; however, this dependence is weak  $\sim \ln G_*$ . The second term in (11.41) can be significant only for very small bubbles ( $Z \gg 1$ ) at the initial stage of the movement  $\omega_* \gtrsim 1$ , when it can be approximately taken that

$$\omega_*^3 \approx (2\chi_0\xi(\theta_*)/\theta_*)[Z(3\chi_0 - 1)]^{-3/2} \ll \xi^{2/3}(\theta_*)$$



When

$$\omega_* \gg Z(3\chi_0 - 1)(2\chi_0)^{-1}, \quad H\theta_*\Lambda^{-1}\chi_0^{-1} \ll \xi(\theta_*) \quad (11.42)$$

we have

$$\omega_*^3 \approx \xi(\theta_*) \quad (11.43)$$

Using the solution of the problem (11.41) under the condition (11.33), it is possible to show that after integrating in (11.41), the relationship (11.43) gets the following form

$$\begin{aligned} \omega_*^3 &= H\theta_*\lambda_0(\theta^*)\Lambda^{-1}\chi_0^{-1}, \\ \lambda_0(\theta^*) &= 1 - \exp(-1/\theta^*) - (1/\theta^*)\text{Ei}(1/\theta^*), \quad \theta^* = t/\tau_0 \end{aligned} \quad (11.44)$$

Using the asymptotics for the functions (11.12), the given relation can be represented in the form of the following approximate ones

$$\omega_*^3 = \frac{H\theta_*}{\Lambda\chi_0} \begin{cases} 1 - (1/\theta^*)\exp(-1/\theta^*), & \theta^* \ll 1, \\ (1/\theta^*)[1 + \ln(\theta^*/\gamma_p) + \theta^*/2], & \theta^* \gg 1 \end{cases} \quad (11.45)$$

or

$$\omega_*^3 = \begin{cases} \frac{HXt}{\Lambda\chi_0}, & t \ll \tau_0, \\ \frac{X}{\Lambda\psi^0}\tau_0 \ln[(e/\gamma_p)(t/\tau_0)], & t \gg \tau_0 \end{cases} \quad (11.46)$$

However when  $t \gg a^2(4\kappa_t)$ , intensive heat transfer to the skeleton of the medium decreases, and the whole medium begins to get heat. In this case it is possible to take

$$\xi(\theta_*) \approx \xi(0) + \frac{H\theta_*}{\Lambda\chi_0} \quad (11.47)$$

It is evident that the upper expression in (11.46) coincides with the condition (11.42), since both of the expressions reflect the case when the volume of the bubbles is small compared to the volume of the surrounding water.

### 11.3 Permeability Change under Electric Field

It was shown in §§11.1, 11.2 that as electric current passes through a micro heterogeneous medium, bubbles of liquid migrate towards thin "hot" capillaries of the medium. This is caused by the temperature gradients and the temperature dependence of the surface tension in the liquid. In the thin capillaries, the bubbles grow due to the inflow of the heat released by the electric current. The growing bubbles shut the capillary cross-sections; this causes the permeability and the electric conductivity of the medium to drop.

The shut-off of a capillary cross-section can happen in two ways. First of all, it can be caused by merging of the bubbles when their densities become sufficiently large and the distance between them becomes of the order of their radii

$$l_a \sim n_0^{-1/3} \approx 2a, \quad 10\Lambda\omega_*^3 \approx 1 \quad (11.48)$$

Second of all, the capillaries can be shut by solitary growing bubbles, i.e., when

$$a \approx r, \quad \Lambda\omega_*^3 \approx \Lambda_0 l^2 r \quad (11.49)$$

Consider the case when the initial radii of all bubbles in the fluid are the same and equal to  $a_0$ ; we shall also neglect the changes of these initial radii during the bubble's movement from a pore to a capillary. Furthermore, we shall neglect the change of the current density, as the growing bubbles shut the cross-section of the capillary. Estimates show that it drops not more than by a factor of two up till an all but total shut-off of the capillary by the growing bubble.

According to (11.13)

$$\partial\epsilon(t)/\partial r < 0, \quad \partial\epsilon(t)/\partial r_1 > 0$$

Therefore the greatest rates the bubble growth are to be observed in the thinnest  $r_1$ -capillaries of the largest  $r_1$ -chains. This, however, does not mean that the cross-sections of these capillaries are going to be the first to be shut off.

The condition of a capillary shut-off due to the merging of the bubbles (11.48), with regard to (11.44), has the following form

$$H\theta_*\Lambda_0\chi_0^{-1}[t/\tau_0(r)] \approx 0.1 \quad (11.50)$$

When (11.49) is satisfied we have

$$H\theta_*\Lambda_0\chi_0^{-1}[t/\tau_0(r)] \approx 4n_*r^3 \quad (11.51)$$

After taking into account the change of the density for bubbles, we obtain

$$\Lambda = n_*(4/3)\pi a_0^3(l/r)^2, \quad A_e = E_0^2\sigma'\rho_f^{-1}l^{-1}$$

It is possible to calculate the time dependence for the permeability of the medium by changing order relationships with equalities in (11.51), (11.52) and solving them with respect to  $t(r, r_1)$ , which is the period of shut-off for a capillary of radius  $r$  in an  $r_1$ -chain. For small (11.47) and large (the lower expression in (11.45)) heat losses, respectively, we obtain the following explicit relationships for  $t(r, r_1)$ ,

$$t(r, r_1) \approx \chi_0/(10HA_e\phi^2(r_1))(r/r_1)^4, \quad t \ll \tau_0 \quad (11.52)$$

$$t(r, r_1) \approx \gamma_p r^2/(4e\kappa_t) \exp\left[\frac{4\kappa_t\chi_0}{10A_e\phi^2(r_1)}(r/r_1)^4 r^{-2}\right], \quad t \gg \tau_0,$$

when the bubbles merge in the case described by (11.48). When the bubbles grow in the case described by (11.49), the relationships are as follows

$$t(r, r_1) \approx \frac{\Lambda_0 \chi_0}{H A_e} \frac{(l/a_0)^3}{\phi^2(r_1)} \left( \frac{r}{r_1} \right)^4 \frac{r}{l}, \quad t \ll \tau_0 \quad (11.53)$$

$$t(r, r_1) \approx \frac{\gamma_p r^2}{4e\kappa_t} \exp \left[ \frac{4\kappa_t \Lambda_0 (l/a_0)^3}{A_e \phi^2(r_1) l} \left( \frac{r}{r_1} \right)^4 \frac{1}{r^2} \right], \quad t \gg \tau_0$$

It is clear from the expressions presented above that the shut-off time for a capillary goes up sharply as its radius goes up and  $r_1$  decreases. This phenomenon is especially notable when the intensive heat outflow to the skeleton of the medium takes place (the lower expressions in (11.52), (11.53)). When  $r = r_1$  and the bubbles merge we have

$$t(r_1) \approx \begin{cases} \chi_0 [10 H A_e \phi^2(r_1)]^{-1}, & t \ll \tau_0 \\ \gamma_p r_1^2 / (4e\kappa_t) \exp\{4\kappa_t \chi_0 [10 A_e \phi^2(r_1) r_1^2]^{-1}\}, & t \gg \tau_0; \end{cases} \quad (11.54)$$

when the bubbles grow we have

$$t(r_1) \approx \begin{cases} \Lambda_0 \chi_0 H^{-1} A_e^{-1} (l/a_0)^3 \phi^{-2}(r_1) (r_1/l), & t \ll \tau_0 \\ \gamma_p r_1^2 / (4e\kappa_t) \exp[4\kappa_t \Lambda_0 (l/a_0)^3 A_e^{-1} \phi^{-2}(r_1) l^{-1} r_1^{-1}], & t \gg \tau_0 \end{cases} \quad (11.55)$$

The lower expressions in (11.48), (11.55) imply that when intensive heat exchange takes place  $t(r_1)$  is minimal in the large  $r_1$ -chains. As some of the ways for the fluid and current flow are shut off in these chains, a considerable rearrangement of the current in the medium takes place there, and the study of the further development of colmatation becomes substantially more difficult. Therefore we shall confine ourselves to the case of the steady-state heat exchange (11.47), when the medium receives heat as a whole. In this case, according to the upper expressions in (11.54), (11.55), if the heat exchange with the skeleton of the rock is not too intensive, the values of  $t(r_1)$  either decrease as  $r_1$  goes up, or undergo little change. This corresponds to the shut-off of the thinnest  $r_1$ -chains by the bubbles. However no notable increase of the current in the large  $r_1$ -chains is likely to be detected, and the hierarchy of the  $r_1$ -chains with respect to their conductivities is preserved. Conductivities of those  $r_1$ -chains, for which  $t \lesssim t(r_1)$ , is determined primarily by the conductivities of the  $r_1$ -capillaries, since the shut-off periods for other capillaries in the  $r_1$ -chain are much greater than  $t(r_1)$ . After the  $r_1$ -capillary is shut off, the current in the chain vanishes, and further heating of the capillaries in the chain (and consequently, growth of bubbles there) stops. Actually, a certain heat exchange with the medium does take place. The  $r_1$ -capillaries shut off by the bubbles gradually (over a period of  $\tau_0(r_1) \approx r_1^2/4\kappa_t$ ) cool down; part of the vapor in the bubbles condenses; the bubbles diminish in size; and the  $r_1$ -capillary

resumes to conduct current. Consequently the fluid gets heated again, then the bubbles grow, and the capillary is shut off. Thus, as electric current passes through the medium, colmatation effects are cyclic. This is also confirmed by experimental studies of cores saturated with a conducting leaching solution. The results of these studies will be discussed in detail below.

According to the upper expression in (11.54), when the losses due to the heating of the skeleton of the medium are not too intensive (for instance, in micro grained media) and the liquid contains a good deal of gas (i.e., when the density of the bubble germs  $n_*$  is large), merging of the vapor bubbles in the thin capillaries dominates in the colmatation of the medium. Furthermore colmatation will take place almost at the same time in all  $r_1$ -chains of the rock. This must have a visual impression of abrupt termination of the fluid flow in the rock. As for the time dependencies of the permeability and the electric current flowing through the medium, they must have a typical form of the percolation relations near the percolation threshold

$$\begin{aligned} K(t) &\approx K(0)(1 - t/t_p)^{\alpha_t}, \\ I(t) &\approx I(0)(1 - t/t_p)^{\beta_t}, \\ t_p &= \langle a_*, t(r_1), r_c \rangle \end{aligned}$$

where the exponents  $\alpha_t$  and  $\beta_t$  must be of the order of unity (less than one).

If the density of the bubble germs is relatively small, then the merging of the bubbles and their independent growth may rival in some chains. When the heat exchange between the liquid and the skeleton takes place (this happens when the specific heat of the rock is large, as in fractured media), colmatation can be long-lasting. It is also possible in this case that a complete colmatation of the medium is not achieved.

We shall now compare the obtained results to those of an experimental study of electric treatment of a sandy-argillaceous medium saturated with a leaching solution. The parameters of the medium, the liquid, and the electric treatment are to be set to equal those in the experiment, i.e., the specific electric conductivity of the fluid,  $\sigma' = 1.7 \Omega^{-1} \text{m}^{-1}$ ; the characteristic size of a pore and a grain,  $l = 2 \cdot 10^{-4}$  m; the cross-section of the experimental tubes (see §9.2),  $S^0 = 9 \cdot 10^{-4} \text{m}^2$ ; the number of conducting channels, in order of magnitude,  $N_0 \approx S^0/l^2 = 2.3 \cdot 10^4$ ; the average capillary radius,  $r \approx 8 \cdot 10^{-5}$  m; the amplitude of the alternating electric field intensity,  $E_0 = 180 \text{V/m}$ ; the energy input density,  $q_p \approx 5.5 \cdot 10^4$  watt per  $\text{m}^3$ . Typical values of bubble radii and densities at NTP ( $p = 0.1 \text{MPa}$ ,  $T_0 = 293 \text{K}$  ( $20^\circ \text{C}$ ),  $T_b = 373 \text{K}$  ( $100^\circ \text{C}$ )) are  $a_0 = 10^{-6} \text{m}$ ,  $n_* \approx 10^{13} \text{m}^{-3}$ .

It follows from (11.15) and (11.17) for the parameters specified and for the viscosity  $\mu = 10^{-3} \text{Pa} \cdot \text{s}$ , that the time for establishing of a steady state movement,  $\tau_y \sim 10^{-7}$  seconds, is much less than the characteristic time of movement for a

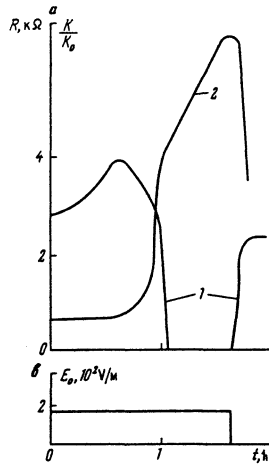


Figure 72: Plots for the time dependencies of the permeability 1, the electric resistance 2 of the medium (a) and the electric field intensity (b) in experiments on electric treatment of media saturated with leaching solutions

bubble in the temperature field,  $\tau_g \sim 10^4$  seconds. This fact confirms the validity of the speculation on the movement of bubbles being quasi-uniform. Experimental data (fig.72) yield  $\tau_g \approx 1.5$  hours ( $5 \cdot 10^3$  seconds). The overestimated calculated value of  $\tau_g$  was obtained because an overestimated value of  $\mu$  and an underestimated value of  $\chi'$  were used in substituting in the formula (11.17). (When the temperature grows from  $20^\circ$  C to  $100^\circ$  C, the viscosity drops by a factor of three, and  $\chi'$  increases by more than 20%.) In the estimates, the constant values of  $\mu$  and  $\chi'$  were used, which correspond to  $T = 20^\circ$  C. Taking account of the changes in these quantities as the temperature of the liquid grows, yields a result which is much closer to the experimental one,  $\tau_g \approx 1.1$  hours ( $4 \cdot 10^3$  seconds).

Having got inside the capillary, the bubbles begin to grow. The first stage of the growth takes place for  $T < T_b$ . For the specified parameters of the field, medium, and liquid, the temperature in the liquid inside the capillary reaches  $T_b$  after  $t \approx 1.6$  hours. This result agrees adequately with the experiment, where a sharp drop of the electric conductivity occurs at the time  $t = 1.5$  hours. An earlier termination of the flow (see fig. 72) is due to the fact that the grown bubbles impede the fluid flow to a greater extent than they impede the current flow in the medium. Up to the instant of merging, the growth of the bubbles is described by equations (11.36) - (11.38).

The parameters defined in deducing these equations have the following values,  $\Lambda = 2.5 \cdot 10^{-4}$ ,  $\Lambda_0 = 4 \cdot 10^{-5}$ ,  $X = 2.54 \cdot 10^{-5} \text{ s}^{-1}$ . The quantities  $H$  and  $Z$  depend on the temperature inside the bubble and vary within the following ranges,  $H = (2.14 \div 1.44) \cdot 10^3$ ,  $Z = 1.45 \div 1.18$ .

Suppose that the relationships (11.40) and (11.47) hold, i.e., we neglect the outlined variations of  $H$  and  $Z$ . In this case, according to (11.34),  $\xi(0) \approx 2.5$ , and the condition (11.42) holds for  $a/a_0 > 1.5$ . It follows accordingly that

$$\omega_*^3 \approx \frac{H\theta_*}{\Lambda\chi_0} \approx 1.8 \cdot 10^2 t \quad (11.56)$$

This implies that  $a/a_0 \sim 10$  when  $t \sim 10$  seconds.

If, however, we suppose that the capillary is shut off for  $a \sim r = 8 \cdot 10^5$  m, then  $t \approx 0.8$  hours.

(11.56) implies that

$$\omega_*' = (H/3)(\Lambda\chi_0)^{-1}\omega_*^{-2}$$

Therefore

$$\omega_*' \gg Y, \quad \omega_*'/\omega_* \gg Y$$

and the left side of (11.36) is of the order of

$$\omega_*\omega_*'' + 3/2(\omega_*')^2 \approx -(4 \cdot 10^{11} \div 2 \cdot 10^8)$$

The term in the right side of the equation is of the order of

$$M \approx 1.6 \cdot 10^{23}, \quad N \approx 4.8 \cdot 10^{10}, \quad (\omega_*'/\omega_*)N \approx 6.3 \cdot 10^{13} \div 1.0 \cdot 10^{17}$$

It follows that for the given characteristic parameters, the dynamic terms in the Rayleigh-Lamb equation may indeed be neglected. Thus this equation assumes the form (11.40), and the dynamics of the bubble growth is taken into account in the equation (11.35).

Thus the following stages of the reversible change of the permeability for a micro heterogeneous medium as the electric current passes through it can be outlined, based on the theoretical analysis and the obtained experimental data.

1. Increase of the electric conductivity and the permeability of the medium caused by the destruction of the bounded fluid on the surface of capillaries and by the decrease of its viscosity. At the same stage, the migration of bubbles of fluid towards the thin capillaries of the medium, which are heat sources, takes place.
2. Termination of the growth of the electric conductivity and the permeability and the formation of a "platform" in  $K(t)$  and  $\Sigma(t)$  coordinates. At this stage, the growth of bubbles of vapor takes place at a temperature less than the boiling point. These bubbles shut off the capillaries and make up for the increase of the electric conductivity and the permeability of the fluid caused by the increase of the capillary cross-sections.

3. The stage of colmatation in the strict sense of the word. The bubbles shut off the capillaries completely, and a sharp drop of the permeability (down to zero) and a substantial decrease of the electric conductivity (by several tens of times) occurs. Compared to the two previous ones, this stage is several hundreds of times shorter.

In some cases (e.g., in the media with a specific heat of the solid part of the rock much greater than that of the saturating fluid), complete colmatation of the medium might be impossible for actual values of the energy release density provided by customary sources of electric energy.

## Chapter 12

# Effects of Acoustic Waves on Irreversible Change of Permeability of a Saturated Porous Medium

Along with the electromagnetic fields, the acoustic fields are extensively used for managing the conducting properties of reservoir rocks. Some properties of acoustic treatment make it essentially different from electric treatment. We shall consider the main features in the behavior of saturated porous media in an acoustic field.

The following mechanisms of interaction between the acoustic field and a saturated porous medium, which cause irreversible changes in the permeability of the latter, are possible.

1. Dissipation of the energy of a viscous Poiseuille flow in the case of mutual displacement of the liquid and solid phases. Increase of the temperature in the liquid results in the increase of its pressure and in the corresponding increase of the pore channel radii, for example, because of the destruction of the cement in the thin capillaries or on the surface of the capillaries.
2. Destruction of the surface layer of pore channels under tangential stress generated at the interface of the solid and the viscous liquid phases during the flow of the latter.
3. Cavitation in the pore channels as the acoustic wave passes through the medium. The small "cumulative" jets formed when the cavitation bubbles collapse, destroy the surfaces of pore channels and thus increase their radii.



4. Dissipation of the acoustic field energy due to the "flowless" movement of the fluid in the pore channels, when the total displacement of the fluid in any physically small volume vanishes. Temperature increase causes the same effects as those stated in 1.

Analyze the probabilities and the nature of realization of each of the mentioned mechanisms in the process of acoustic treatment of the medium in reservoir setting, for the parameters of an ultrasonic wave source.

## 12.1 Dissipation of Energy in Viscous Poiseuille Flow

If a total flow  $Q$  develops due to the displacement of the fluid with respect to the solid skeleton, Poiseuille flow directed along the gradient of the external pressure  $\nabla p$ , takes place in the chains of the IC skeleton.

However the existence of such flow is possible only for the frequencies lower than a certain value, called the characteristic frequency:

$$\nu_{0c} = (\pi/16)\mu\rho_f^{-1} < r >^{-2} \quad (12.1)$$

The first to obtain this result was M. A. Biot (1956) [97], who got it studying the solutions to the equation for the non-steady state fluid flow in porous media

$$\rho_f d\nu/dt = -m\nabla p + F - (\mu/K)\nu$$

in the interval of relatively low frequencies ( $\nu_0 \lesssim 10^5$  Hz). For frequencies higher than  $\nu_{0c}$ , the relative displacement of the fluid and the skeleton of the rock does not take place, i.e., the solid and the liquid phases move in phase. Estimate the value of  $\nu_{0c}$ . Take  $\mu \sim 10^{-3}$  Pa·s,  $\rho_f \sim 10^{-3}$  kg·m<sup>-3</sup> and the averaged radius of the capillary chain to be  $< r >$ .

To calculate  $< r >$ , use the model function (4.9) which reflects the qualitative behavior of actual  $f(r)$  well. In this case  $< r > = a_* a^* (a^* - a_*)^{-1} \ln(a^*/a_*)$ . We assume, as usual, that  $a^* \gg a_*$  and set  $a^*/a_* \sim 10^3 \div 10^4 \sim e^7 \div e^{10}$  and therefore  $< r > \sim 10a_*$ . Since  $a_* \sim 10^{-6}$  m can be taken as the minimal radius of the conducting capillaries where Poiseuille flow is still realized [88], we have

$$< r > \sim 10^{-5} \text{ m} \quad (12.2)$$

After substituting the above-mentioned values of  $\mu$ ,  $\rho_f$ , and  $< r >$  in (12.1), we obtain  $\nu_{0c} \sim 10^4$  Hz. It can be thus inferred that for Poiseuille flow to take place in the medium and for the "first" mechanism of the acoustic energy transfer to be realized, the frequency of the treatment must be lower than  $\nu_0 \sim 10^4$  Hz. Since

ultrasound, i.e., the oscillations with frequency no less than  $\nu_0 \cong (1.5 \div 2.0) \cdot 10^4$  Hz, is going to be used, the obtained estimate does not allow to decide whether the considered mechanism is or is not going to work at this frequency.

Therefore we will analyze the possibility of its realization more closely. The velocity profile in a capillary for Poiseuille flow is described by the following relationship [89],

$$\nu = (1/4\mu)(r^2 - r_0^2)\nabla p \quad (12.3)$$

where  $r$  is the capillary radius,  $r_0$  is the distance from the axis of the capillary, and  $\nabla p$  is the local pressure gradient in the given capillary. In this case the average velocity in the capillary is

$$\langle \nu \rangle = (1/8\mu)r^2\nabla p \quad (12.4)$$

and the flow is

$$q = (\pi/8\mu)r^4\nabla p$$

Since for each marked chain we have  $q = \text{const}$ , it follows that

$$\nabla p \sim r^{-4}$$

Therefore

$$\nu(r_0) \sim r_0^2/r^4, \quad \partial\nu/\partial r_0 \sim 2r_0/r^4$$

and the release of energy per unit time per unit length of a capillary is

$$E' \sim \int_0^r (\partial\nu/\partial r_0)^2 r_0 dr_0 \sim r^{-4}$$

i.e., when there exist non-vanishing total flows under the action of the acoustic wave one could expect localization of the dissipated energy release in the thinnest capillaries. However it is clear that in the considered case of the acoustic wave propagation, no integral displacement of the fluid in the capillary chain is observed when a fixed cross-section of the fluid passes through several capillaries of the chain.

The average velocity of Poiseuille flow in a capillary with a variable cross-section can be estimated using the relationship (12.4), with the average capillary radius substituted for radius.

After substituting (12.2) in (12.4), we obtain the characteristic velocity  $\langle \nu \rangle \cong 2.5 \cdot 10^{-2}$  m/s.

At the frequency  $\nu_0 = 20$  kHz, the period of the directed motion is  $\tau/2 = \nu_0^{-1}/2 = (1/4)10^{-4}$  s and the displacement during this period is  $\Delta l = \langle \nu \rangle \tau/2 \sim 10^{-6} \div 10^{-7}$  m. This value is substantially less than the characteristic length of a capillary in the chain, since it is assumed that the lengths of

capillaries exceed their cross-sections, and therefore characteristic capillary length is  $l \gg 10^{-6}$  m.

The presented estimate shows that under acoustic treatment with frequency within the kilohertz range, the release of energy due to the dissipation during the directed flow of a viscous fluid is not observed. Consequently, unlike in the case of electric action, the effect of localization of the energy release in the thinnest capillaries, which limit the hydraulic conductivity of the medium, does not appear, either.

## 12.2 Destruction of Surface Layer in Pore Channels under Tangential Stress

When the surface of the pore channels, or at least a part of it, is covered with a cementing clayey solution drift (or, as in the pre-filter zone of the well, with mud drift) which has low shear strength, the shear stress developing at the phase interface during the fluid flow can cause destruction and further hydrodynamic entrainment of the solid particles from the boundary layer. Consequently the radius of the conducting capillaries increases by the value of thickness of the entrained low-strength boundary layer. This results in the increase of the permeability of the medium.

Investigate the reality of this effect appearing in the medium, given the characteristic values of the corresponding parameters. Calculate the tangential force  $F_\tau$  with which the fluid acts on a unit length of a cylindrical circular capillary [89]. From the momentum equation for a liquid cylinder of radius  $r$  we have

$$F_\tau = (\Delta p/l)\pi r^2 \quad (12.5)$$

where  $\Delta p$  is the pressure difference at a distance  $l$ . The tangential stress acting on the surface of the channel by Navier - Stokes law equals

$$\tau_s = -\mu \left. \frac{\partial v}{\partial r_0} \right|_{r_0=r} = \frac{\Delta p}{l} \frac{r}{2} \quad (12.6)$$

The Hagen - Poiseuille formula (12.3) for the profile of velocities for the fluid in the capillaries was used in deriving the resultant expression (12.6). After expressing  $\Delta p/l$  in terms of the stress  $\tau_s$  from (12.6) and substituting the obtained relation in (12.5), we find the value of the applied tangential force per unit length of a capillary in the following form

$$F_\tau = 2\pi r \tau_s$$

To obtain the critical value of the shear force, when the removal of the layer from the surface takes place, we substitute the quantity  $\tau_s$  with the shear strength

of the surface layer  $\sigma_*$ :  $F_\tau = 2\pi r\sigma_*$ . Furthermore introduce the parameter

$$\Gamma_\tau = 0.5\rho_f \langle \nu \rangle^2 \beta'^{-1}$$

where  $\beta' = F_\tau/S'$  and  $S' = 2\pi r$  is the area of a unit surface of the capillary to which the shear force  $F_\tau$  is applied. The parameter  $\Gamma_\tau$  characterizes the ratio of the hydrodynamic head  $\rho_f \langle \nu \rangle^2 / 2$  to the critical shear stress  $\beta'$  that can be endured by the capillary surface without destruction. Obviously  $\beta' = \sigma_*$ , and therefore finally

$$\Gamma_\tau = \rho_f \langle \nu \rangle^2 \sigma_*^{-1} / 2$$

Fulfillment of the condition

$$\Gamma_\tau \gtrsim 1 \quad (12.7)$$

is the criterion for the destruction and entrainment of the surface layer from the capillary surface by the flow.

Estimate the quantity  $\Gamma_\tau$  and verify the fulfillment of the condition (12.7). Taking account of the velocity profile  $\nu(r_0)$  in a capillary, we obtain

$$\langle \nu \rangle = \frac{1}{\pi r^2} \int_0^r 2\pi\nu(r_0)r_0 dr_0 = \frac{1}{8\mu} r^2 \nabla p$$

where  $\nabla p$  is the pressure gradient in the considered volume of the medium. Estimate  $\nabla p$  using the characteristic values for the parameters of acoustic action. Wavelength  $\lambda$  is of the order  $10^{-1}$  m, and the amplitude of the pressure wave is  $p_a \sim 10$  Pa; therefore, the characteristic value of  $\nabla p \sim p_a/\lambda = 10^5$  Pa/m. The average value of the pore channel radius for a reservoir rock is of the order of  $10^{-5}$  m, as can be seen from (12.2) as well as [48]. For our estimates, take the capillaries that are thicker by one order, i.e., those with radii  $r \sim 10^{-4}$  m. In this case  $\langle \nu \rangle \sim 10^{-1}$  m/s,  $\langle \nu \rangle^2 \sim 10^{-2}$  m<sup>2</sup>/s<sup>2</sup>, and  $\rho_f \langle \nu \rangle^2 / 2 \sim 1/2 \cdot 10$  Pa. Since the shear strength of clay is no less than  $10^3$  Pa, while this value for mud is as a rule no less than  $10 - 10^2$  Pa [84], it can be seen from the presented estimate that the "shear stress mechanism" can work only for very large capillaries. However in such capillaries, where maximal flow rates are realized, visible clay depositions can hardly be found. Thus the given mechanism is unable to substantially change both the radii of thick capillaries (since the layer of depositions on their surface is minor) and the radii of thin capillaries, where the hydraulic head is too small.

## 12.3 Cavitation in Pore Channels under Acoustic Action

As an acoustic wave passes through a saturated porous medium, the effect of cavitation may appear, if negative pressures exceeding the tensile strength of the fluid

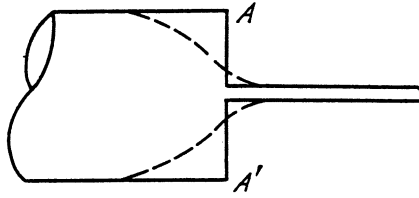


Figure 73: A sketch of a capillary junction element for capillaries with different radii

in the absolute value develop at the relief stage. Consider two possible mechanisms for the development of negative pressure during ultrasonic action. This can happen at the junctions of capillaries with different radii during the flow from the thicker to the thinner one and at the relief stage of the traveling pressure wave in the fluid.

1. Suppose two capillaries in a chain form a junction of the type presented in fig. 73. As was shown by the estimates presented above, the displacement of the fluid during a half-period of the wave in a capillary chain is rather small ( $\sim 10^{-7}$  m); however, in the immediate vicinity of the junction, as the fluid passes from the thick capillary to the thin one, the increase of the flow rate and the pressure drop take place. We will estimate this pressure drop using Bernoulli's integral along a horizontal flow tube, when the  $z$ -coordinate is constant. In this case the  $gz$  term can be included in the general constant, so that the following equality can be written

$$p_0 + \rho_0 \nu_0^2 / 2 = p + \rho \nu^2 / 2 \quad (12.8)$$

The quantities marked with index "0" correspond to the thick capillary, and those without an index, to the thin one. From the mass conservation equation we have  $\rho \nu S_k = \text{const}$ , where  $S_k$  is the area of the cross-section of the capillary, and we obtain

$$\nu_0 / \nu = (r / r^0)^2 \quad (12.9)$$

where  $r$  and  $r^0$  are the radii of the corresponding capillaries. After substituting (12.9) in (12,8), we obtain

$$p = p_0 - 0.5 \rho_0 \nu^2 [1 - (r / r^0)^4] \approx p_0 - 0.5 \rho_0 \nu^2 \quad (12.10)$$

since we are discussing the case when  $(r / r^0)^4 \ll 1$ .

The average velocity  $\langle \nu \rangle$  of Poiseuille flow along a chain in the high pressure phase can be estimated using the average radius  $\langle r \rangle$  of a capillary chain for a given function  $f(r)$ . In this case

$$\langle \nu \rangle \sim \langle r \rangle^2 p_a / \lambda \quad (12.11)$$

On the other hand [85], the mass velocity is

$$\tilde{\nu} \cong p_a \rho_f^{-1} C_f^{-1} \quad (12.12)$$

where  $C_f$  is the velocity of sound in the fluid. In this case, as in (12.9), after taking into account (12.11) we obtain

$$\nu / \langle \nu \rangle \sim (\langle r \rangle / r)^2$$

and using (12.12) and the fact that  $\langle \nu \rangle \sim \tilde{\nu}$ ,

$$\nu \cong \frac{p_a}{\rho_f C_f} \left( \frac{\langle r \rangle}{r} \right)^2$$

After substituting this value of  $\nu$  in (12.10), we finally obtain the formula for the pressure difference when the fluid passes from a thick capillary to a thin one:

$$p = p_0 - \frac{1}{2} \frac{p_a^2}{\rho_f C_f^2} \left( \frac{\langle r \rangle}{r} \right)^4 \quad (12.13)$$

For a fluid,  $\rho_f C_f^2 \sim 1$  GPa;  $p_a \sim 0.01 - 0.1$  MPa for the considered phenomena. As it was demonstrated above, one can take  $\langle r \rangle \sim 10^{-5}$  m and the minimal value of radius  $r \sim 10^{-6}$  m. In this case  $\langle r \rangle / r \sim 10$ ,  $(\langle r \rangle / r)^4 \sim 10^4$ , and if the background pressure of the order 10 MPa is taken as  $p_0$ , we obtain from (12.13) that  $p \sim 10^7 - (1/2) \cdot 10^{-4} \cdot 10^4 \sim 10^7 - (1 \div 0.1) \sim 10^7$  Pa. This means that in a reasonable range of radii of the joining capillaries ( $r/r^0 \lesssim 10$ ), the pressure difference, as fluid passes from a thick capillary to a thin one, is of the order of the wave amplitude  $p_a$ , and therefore no negative pressure develops with respect to the high reservoir pressure  $p_0$ .

If we take an "exotic" case  $\langle r \rangle / r \sim 10^2$ , i.e.,  $r \sim 10^{-7}$  m, then  $(\langle r \rangle / r)^4 \sim 10^8$  and  $p \sim -1$  GPa. At such values of negative pressure one can expect the effect of cavitation to work. For the mentioned rarefaction pressure, the existing hydrodynamic pressure, and the given frequency of action, estimate the range of radii of the cavitating gas bubbles.

Suppose that due to some reasons, the so-called germs, i.e., bubbles of gas, exist inside the fluid. Formed inside the cone of depression during the evolution of gas because of the local temperature, concentration and other fluctuations, these germs can oscillate in the pressure wave and collapse with the formation of cumulative jets directed towards the interface of the fluid and the solid capillary surface [89, 90]. As in the approach [91], consider the variation of the initial pressure  $p_0$  in the fluid in the vicinity of the oscillating bubble with initial radius  $a_0$ . If we neglect the elasticity of vapor, the pressure of the gas inside the bubble is

$$p_n = p_0 + 2\chi/a_0$$

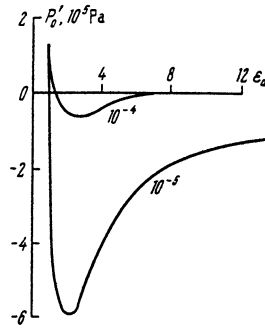


Figure 74: Relation between the pressure in the fluid around the bubble and the extent of its growth (plotted according to the data of L. K. Zaremba and V. A. Krasilnikov) Code of the curves -  $a_0, m$

As the pressure around the bubble drops, its radius increases by  $\epsilon_a$  times. Suppose that the expansion of the bubble is isothermal and that the mass of gas inside the bubble does not change. In this case the external compensating pressure is

$$p'_0 = (p_0 + 2\chi/a_0)\epsilon_a^{-3} - 2\chi/(\epsilon_a a_0) \quad (12.14)$$

Use (12.14) to estimate the maximal negative pressure that can be endured by a fluid with identical bubbles of initial radius  $a_0$ . Consider the derivative  $dp'_0/d\epsilon_a$ . Rupture of the fluid takes place only when the curve  $p'_0(\epsilon_a)$  has an extremum, since after the curve passes its extremum, the expansion of bubbles continues with the pressure going up. Typical  $p'_0(\epsilon_a)$  curves are represented in fig. 74 for two different values of the parameter  $a_0$ . After setting the derivative  $dp'_0/d\epsilon_a$  to zero, we obtain the following from (12.14) for the critical value of the variable,

$$\epsilon_a^* = \sqrt{\frac{3}{2} \frac{a_0}{\chi} \left( p_0 + \frac{2\chi}{a_0} \right)}$$

The minimal size of the cavitating germ can be estimated from the condition of the fluid rupture. This condition implies that the total pressure must be negative and must exceed in absolute value the critical pressure  $p_{0c}$ , which corresponds to  $\epsilon_a^*$ ,

$$|p + p_0| \gtrsim |p'_0(\epsilon_a^*)| = \frac{2}{3} \sqrt{\frac{(2\chi/a_0)^3}{3(p_0 + 2\chi/a_0)}} \quad (12.15)$$

For the value  $p \sim -1$  GPa when  $p_0 \sim 10$  MPa,  $|p/p_0| \gg 1$ , and the equation (12.15) can be rewritten in the form

$$7p^2 p_0 (a_0/2\chi)^3 = 1 - 7p^2 (a_0/2\chi)^2$$

After assuming that  $\chi \sim 7 \cdot 10^{-2}$  newtons per meter, we obtain

$$7 \cdot 10^{28} a_0^3 = 1 - 7 \cdot 10^{20} a_0^2 \quad (12.16)$$

where  $a_0$  is measured in meters. For the expression (12.16) to have physical sense, i.e., for  $a_0$  to be greater than zero, it is necessary that  $a_0 \lesssim 10^{-11}$  m, as it can be seen from the right side of (12.16). In this case we obtain  $a_0 \lesssim 10^{-10} \div 10^{-9}$  m. That is, if we choose the minimal value of  $a_0$  of the mentioned, we obtain  $a_{\min} \sim 10^{-11}$  m, or  $10^{-2}$  nm, a value that is less than the characteristic size of the atom by an order of magnitude.

The maximal size of a cavitating bubble can be estimated using the relation for the resonance frequency of small oscillations

$$\nu_r = \frac{1}{a_0} \sqrt{\frac{3\gamma_p(p_0 + 2\chi/a_0)}{\rho_f}} \quad (12.17)$$

where  $\gamma_p$  is the isentropic exponent for vapor.

Since the germs with  $a$  less than the resonance radius  $a_0$  oscillate with a bigger amplitude, which causes the rupture of the fluid, these germs cavitate. After representing (12.17) in the form

$$\nu_r^2 a_{\max} = (3\gamma_p/\rho_f)(p_0 + 2\chi/a_{\max})$$

and transforming it into the equation

$$[\rho_f \nu_r^2 / (6\gamma_p \chi)] a_{\max}^3 = 1 + 0.5(p_0/\chi) a_{\max}$$

we obtain that for  $p_0 \sim 10$  MPa,  $\gamma_p = 1.4$ ,  $\chi = 7 \cdot 10^{-2}$  newtons per meter,  $\rho_f = 10^3$  kg/m<sup>3</sup>,  $\nu_r = 2 \cdot 10^4$  s<sup>-1</sup>,  $a_{\max} \sim 10^{-2}$  m.

Since all germs of the initial size  $a_{\min} < a < a_{\max}$  must cavitate, it follows that for the given negative pressure, germs of virtually any size can cavitate in capillaries of all radii. However, due to the fact that the presented investigation is valid only for  $r \lesssim 10^{-7}$  m, where there is no Poiseuille flow, and therefore for those capillaries which do not contribute to the permeability of the medium, the cavitation effect cannot appear in any significant quantities. If we also take into account the fact that we considered a rather improbable case of capillary junction, when  $r/r^0 \sim 10^2$  and the boundary between them is very sharp (see fig. 73, AA'-plane), whereas the cross-sectional views of actual reservoir rocks demonstrate a more gradual change of radii of the capillary chains (see fig. 73, dotted line), and the fact that the cavitation destruction in any case takes place only in the closest vicinity of the plane of contact of the capillaries, we should admit that for the given parameters of the process, i.e.,  $p_0 \sim 10$  MPa,  $p_a \sim 0.1$  MPa, the cavitation effect may be neglected.



2. Directly at the unloading stage of the traveling wave, for the given  $p_0$  and  $p_a$ , cavitation in the fluid cannot develop, either. This follows clearly from the relationship (12.15), which shows that after the value  $p_a$  is substituted for  $p$  in this expression, the sum  $(p_a + p_0)$  never becomes negative, and cavitation is therefore impossible in principle. In [92] an interval  $p_0^* \pm \Delta p_h$  of pressures, called the metastable zone, was established experimentally. Supposedly, outgassing and cavitation take place for low intensity of the acoustic field, if the difference between the reservoir pressure  $p_0$  and the saturation pressure of the fluid with the gas lies in the mentioned interval. However the presented data, concerning the change of the velocity of sound in the saturated medium and the volume of the released gas, do not permit to make any definite conclusions on the physical picture of the processes that take place here (in particular, the development of cavitation), let alone the quantitative parameters of these phenomena. Therefore there is no reason to think that at the given amplitude and intensity of the acoustic action and such high reservoir pressure cavitation may develop in the pore space filled with the fluid.

## 12.4 Dissipation of Acoustic Energy Due to Thermal Slide

It was established in §12.1 that when there is no integral flow in a chain, the mechanism of the acoustic energy dissipation due to thermal slide is possible. The characteristic feature of this mechanism is the vanishing of the total flow of the fluid, even within a single capillary.

Since the capillary length is assumed to be much greater than the radius, a capillary can be considered having infinite length, so that boundary effects on the capillary junctions can be neglected. Consider the fluid movement in a capillary under the outlined condition and under the action of a pressure wave with amplitude  $p_a$  and frequency  $\nu_0$

$$p = p_a \cos[2\pi(\nu_0 t - x/\lambda)] \quad (12.18)$$

where  $\lambda$  is the wavelength, whose correlation with the frequency is expressed by the well-known formula  $\lambda\nu_0 = C_m$  ( $C_m$  is the velocity of sound in the medium). In writing out the relationship (12.18), it was supposed that the wave propagates in the direction of the  $x$ -axis, which coincides with the axis of the capillary. For such relative location of the wave vector  $k$  and the capillary axis, the action upon the fluid of a longitudinal simple harmonic wave in the capillary is maximal. The closer  $(k, x)$  to zero, the less the components of pressure and the corresponding velocity of the movement along the capillary, and therefore the less the considered effect. The point is that the velocity of thermal slide is proportional to the gradient of

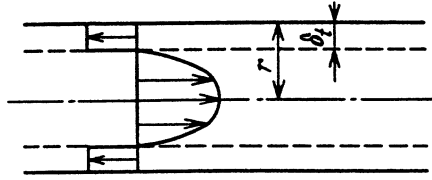


Figure 75: Profile of velocities of the fluid in a capillary for the thermal slide

the developing temperature profile [93]. The given temperature profile is caused by different degrees of compression of the medium by the propagating pressure wave. Since the temperature of the medium is proportional to pressure (8.17), and consequently the gradient of temperature is proportional to the gradient of pressure  $\nabla T \sim \nabla p$ , it follows that the maximal velocity of thermal slide compensating Poiseuille flow is directed as  $\nabla p$ , i.e., as  $k$ . Under the outlined assumptions, the presence of thermal slide along the capillary surface results in the velocity profile represented schematically in fig. 75. This profile can be described by the relationship

$$\nu(r_0) = -(1/4\mu)\nabla p[(r - \delta_t)^2 - r_0^2] + \gamma_T \nabla T \eta[r_0 - (r - \delta_t)] \quad (12.19)$$

where  $\delta_t$  is the thickness of the thermal flow layer, which has the order of the diffusion layer thickness [93] (the latter is equal to several times the free path for molecules of the fluid);  $\gamma_T$  is the proportionality factor in the expression for the velocity of thermal slide [93]  $\nu_T = \gamma_T \nabla T$ ;  $\eta(\cdot)$  is Heavyside's function. Using (12.19), compute the flow of fluid in a capillary

$$q = 2\pi\rho_f \int_0^r \nu(r_0) r_0 dr_0$$

Having set it to zero, we obtain the correlation between the gradients of pressure and temperature

$$\gamma_T \nabla T = \frac{1}{16\mu} \frac{r^3}{\delta_t} \nabla p \quad (12.20)$$

Dissipation of energy due to the internal friction for Poiseuille flow (per unit length of a capillary) equals

$$E_1 = 2\pi\mu \int_0^r (\partial\nu/\partial r_0)^2 r_0 dr_0 \quad (12.21)$$

The corresponding heating of the fluid with specific heat  $c_T$  by  $\Delta T$  degrees absorbs the energy equal to

$$E_2 = \pi r^2 \rho_f c_T \Delta T$$

Although the heat conductivity of water and the surrounding rock are of the same order ( $\sim 1$  watt per meter-Kelvin), we shall neglect the heat transfer from the fluid to the solid skeleton in the zero approximation. In this case we obtain the condition

$$E_1 = E_2$$

Using this condition and relationships (12.19) - (12.21), we obtain

$$\Delta T = \frac{(\nabla p)^2}{8\mu} \frac{1}{\rho_f c_T} \frac{r^3}{\delta_t}$$

For a simple harmonic wave (12.18) we have

$$\Delta T = \pi^2 r^3 p_a^2 (2\mu \rho_f c_T \lambda^2 \delta_t)^{-1} \sin^2 [2\pi(\nu_0 t - x/\lambda)] \quad (12.22)$$

After averaging (12.22) over the wave period

$$\langle \Delta T \rangle = \nu_0 \int_0^{1/\nu_0} \Delta T dt$$

we obtain an expression for the temperature increase in a capillary with radius  $r$  after a period of  $\tau_\nu$  of action of a simple harmonic wave source with frequency  $\nu_0$  and intensity  $I'_0$ :

$$\Delta T = \pi^2 q_p r^3 (4\mu c_T C_m \delta_t)^{-1} \nu_0^2 I'_0 \tau_\nu \quad (12.23)$$

where  $q_p$  is the coefficient of transmission showing the extent to which the ultrasonic wave is reduced as it passes from the source through the liquid filling the well and through the partition of the well into the rock.

The obtained relationship (12.23) shows that the considered thermal slide mechanism permits to qualitatively explain and quantitatively estimate the consequences of acoustic action upon a saturated porous medium. If the process does not cause phase transitions in the liquid phase, then the formula (12.23) shows how the temperature and the pressure increases in the fluid depend on the ratio of the parameters of the fluid and the medium and on the operating conditions. The effect of phase transitions (here, the gas release) can be estimated, at least qualitatively, by taking into account the relations  $\mu(\Gamma')$ ,  $c_T(\Gamma')$ ,  $C_m(\Gamma')$ , where  $\Gamma'$  is the parameter that characterizes gas release, e.g., volumetric or mass concentration of gas bubbles in the liquid.

## 12.5 Gas Colmatation During Acoustic Action on Porous Media

As in the case of electric action (see chapter 11), gas colmatation of a fluid-containing rock, as the fluid gets heated due to the dissipation of acoustic energy,

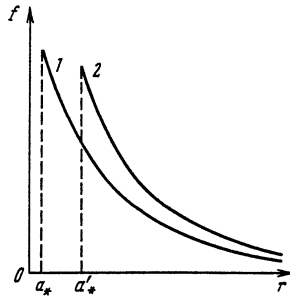


Figure 76: Qualitative picture of the change in the porometric curve of the form  $a_*/r^2$  (1) after electric treatment (2)

is a mechanism that competes in its consequences with the four already analyzed. If we consider the movement of bubbles in a micro heterogeneous medium saturated with a fluid in an acoustic field, as in §11.2 for an electric field, we can infer from (12.23) that the situation here is opposite to the one discussed in §11.2 for electric current. That is, in the thinner capillaries, the temperature increases slower than in the thicker ones. If we take into account the relation between the surface tension and the temperature, we come to the conclusion that the thick ("hot") capillaries thus become the stable centers of attraction for the bubbles from the thinner ("cold") capillaries.

Even a rough preliminary estimate shows, as in the case of electric action (chapter 11), that the characteristic period  $\tau^*$  of colmatation coincides in order of magnitude with the characteristic period  $\tau_*$  of attaining the critical temperature  $T_k$ .

To carry out this estimate, we shall use the simplest, but also the most typical form of the function  $f(r)$ ,  $f(r) = a_*/r^2$ . It can be easily shown using the results of §1.2 that

$$K/K_0 \cong (a'_*/a_*)^4 \quad (12.24)$$

where  $a'_*$  is the minimal capillary radius after treatment (fig. 76). This means that the change of the permeability  $K$  with respect to the initial coefficient  $K_0$  is caused primarily by the right shift of the left limit of the function  $f(r)$ . Deformation of the form of the curve  $f(r)$  in itself affects the behavior of  $K$  to a substantially smaller extent. Therefore to determine the permeability change, it is necessary to estimate the change of the minimal radius in the distribution  $f(r)$ .

As many times before, take  $a_* \approx 10^{-6}$  m, and let the depositions on the surface of the capillaries be represented by a widespread type of cement (see §8.1) with a range of strength  $10^{-1}$  - 10 MPa [84]. For our estimates, we shall use the largest value of the crushing strength of the cement  $\sigma^* \sim 10$  MPa and determine the characteristic period  $\tau_*$  of heating necessary to increase the pressure in the fluid

up to  $p \sim \sigma^* \sim 10$  MPa.

We have already mentioned that the correlation between temperature and pressure is established by the expression (8.17). For water we have  $\alpha_T \approx 0.2 \cdot 10^{-3} \text{ K}^{-1}$ ,  $\beta_T \approx 5 \text{ Pa}^{-1}$ , and for oil,  $\alpha_T \approx 10^{-3} \text{ K}^{-1}$ ,  $\beta_T \approx 10 \text{ Pa}^{-1}$ . The ratio of proportionality factors  $\alpha_T/\beta_T$  equals 2.5 in both cases. Therefore the lengths of the critical temperature intervals  $\Delta T_*$ , for which the pressure increase is  $\Delta p \sim \sigma^*$ , coincide in order of magnitude:  $\Delta T_* \sim 10 \text{ K}$ . In this case it follows from (12.23) that the minimal duration  $\tau_*$  of the thermo-acoustic action on the capillaries with  $r \sim 10^{-6} \text{ m}$  for  $\nu_0 = 20 \text{ kHz}$ ,  $I'_0 = 2 \text{ watt per cm}^2$ , and  $q_p = 10^{-1}$  is approximately equal to  $5 \cdot 10^3$  seconds.

We will use the formula (11.14) to find  $\tau^*$  after estimating the temperature gradient  $\nabla T$  appearing at the micro level. The following points will be taken into consideration. Although the thick capillaries with  $r \gtrsim 10^{-4} \text{ m}$  are the first to get heat, and therefore, the first to colmatate, they make a very small contribution to permeability. Therefore cutting the function  $f(r)$  in the interval of large  $r$  virtually does not affect the change of  $K$ , while the principal interest is with the range  $(10^{-6} \lesssim r \lesssim 10^{-5}) \text{ m}$ . Since we have supposed that the capillary length  $l \gg r$ , we will take  $l \sim 10^{-3} \text{ m}$  as the characteristic length. To analyze the temperature regimes in adjacent capillaries of different radii, return to the model representation of a capillary junction (see fig. 73).

Let the ratio of radii of the joining capillaries be maximal, i.e., of the order 10, and consequently, the radius of the larger capillary be  $r \sim 10^{-5} \text{ m}$ . The characteristic longitudinal size in the chain is  $\sim l$  (capillary length); therefore, the time of the temperature equalization after its difference occurs between different points in the capillary chain is

$$\tau' \sim l^2/(4\kappa_t) \quad (12.25)$$

For example,  $\kappa_t^{(o)} \sim 0.4 \cdot 10^{-6} \text{ m}^2/\text{s}$  for oil, and from (12.25) we have  $\tau'_n$  of the order of several seconds. The temperature difference between the capillaries of different radii develops during the specified period of establishment (12.25), since for larger periods, equalization of the temperatures will take place caused by both the heat transfer in the fluid and by the backflow of heat into the skeleton of the rock. Note that both of the mentioned processes are identical in terms of the characteristic time intervals, since the coefficients of temperature conductivity for oil and sandstone differ only by a factor of two, i.e., have the same order of magnitude ( $\kappa_t^{(o)} \approx 0.4 \cdot 10^{-6} \text{ m}^2/\text{s}$ ,  $\kappa_t^{(s)} \approx 0.8 \cdot 10^{-6} \text{ m}^2/\text{s}$ ), while the characteristic size of a grain in the rock and characteristic capillary length in a grained medium obviously coincide ( $l \sim 10^{-3} \text{ m}$ ).

In this case we have

$$\Delta T = T(r^0, \tau') - T(r, \tau') = -\frac{\pi^4}{4} \frac{q_p}{\mu c_T C_m} \frac{r^3}{\delta_t} \left[ 1 - \left( \frac{r^0}{r} \right)^3 \right] \nu_0^2 I'_0 \tau'$$

It follows that for  $r \sim 10^{-5}$  m,  $r^0/r \sim 10^{-1}$ ,  $\nu_0 = 20$  kHz,  $I'_0 = 2$  watt per  $\text{cm}^2$ ,  $q_p = 10^{-1}$ , we get  $\Delta T \sim -1$  K. Consequently the temperature gradient is of the order of  $\Delta T/l \sim -10^3$  K/m.

As a matter of fact, since actual cross-sections of the pore channels change gradually, i.e., in the vicinity of the considered section the ratio  $r/r^0 \neq 10$ , but is substantially smaller (approximately, 1 - 2), so that we should take an average value from the considered interval ( $10^{-6}$  -  $10^{-5}$ ) m as  $r$ , the estimate of the quantity  $\nabla T$  should be decreased by a factor of 10, which yields  $\nabla T/e \sim -10^2$  K/m.

After taking  $\chi' = 0.11 \cdot 10^{-3}$  J/( $\text{m}^2 \cdot \text{K}$ ) for oil [87], from (11.14) we find the velocity of steady state movement of bubbles from the capillaries with  $r \sim 10^{-6}$  m to the larger ones. (We set the characteristic size of bubbles able to move freely inside the capillaries with  $r \sim 10^{-6}$  m to equal  $a_0 \sim 10^{-7}$  m.) This velocity is  $\nu \sim (1/6) \cdot 10^{-6}$  m/s. Hence the time necessary for the gas bubbles to accumulate in the "hotter" capillaries from the given range  $r \lesssim 10^{-5}$  m is  $\tau^* \sim l/\nu \approx 6 \cdot 10^3$  seconds.

It follows from (11.15) that the relaxation time for the velocity of bubbles with radii  $a_0 \sim 10^{-7}$  m is  $\tau_y \sim 10^{-8}$  seconds, a value obviously less than  $\tau_g = \tau^*$ , and therefore the assumption about the quasi-uniform nature of the movement of bubbles is justified in the considered case as well.

So during the period  $\sim \tau^*$  the gas bubbles move from the thinnest capillaries to the closest thickest ones and accumulate in the latter.

It should be added that during such migration from the "cold" capillaries to the "hot" ones, as well as after it is finished and the bubbles accumulate in the "hot" capillaries, the bubbles grow due to the inflow of heat (see §11.2) released as the acoustic wave passes through the medium. The growing bubbles cut off the cross-section of the capillaries, so that the whole chain is "shut off," and the permeability of the medium drops.

The mentioned processes causes gas colmatation of the volume of the medium in the acoustic field. If we compare the two periods  $\tau_* \approx 5 \cdot 10^3$  s and  $\tau^* \approx 6 \cdot 10^3$  s, we can see that the characteristic times of the two competing effects are very close. At the same time, the period of migration  $\tau^*$  somewhat exceeds (approximately, by 20%) the time of attaining the maximal permeability.

## Chapter 13

# Effect of Acoustic Action on Well Production

Estimates and calculations presented in chapter 12 show that when a medium undergoes acoustic treatment at the most common frequency of  $\sim 10^4$  Hz, the mechanism of the acoustic energy dissipation due to the development of the so-called "thermal slide," a "flowless" motion of fluid, plays the principal part in the alteration of conducting properties of the medium. The dissipative character of the energy release in separate capillary groups permits to explain the feature of the acoustic treatment of reservoirs caused by the cumulativity of this treatment. Localization of the energy release in separate capillary groups causes the destruction of the cementing substance (clay, biotite, etc.) and its being carried away from the group. This substance is weak, and therefore the thermoelastic stress developing in the medium is sufficient to destroy it.

Since permeability is proportional to  $r^4$ , where  $r$  is the capillary radius, even a small change of the effective capillary radius suffices to alter its conducting properties, and consequently to alter the effective permeability of the whole medium.

At the same time, as the duration of acoustic treatment goes up, one can run across a substantial local increase of temperature in some groups of micro capillaries (12.23). This phenomenon can cause the release of gas phase in such capillaries. As a result, gas colmatation can develop, and the permeability of the medium can drop sharply to as low as zero. The given effect causes natural limitations of either the duration or the intensity of acoustic treatment.

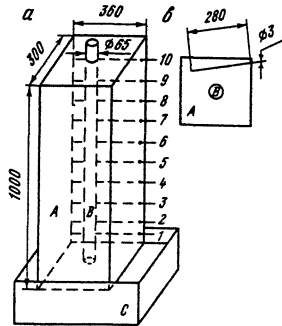


Figure 77: Plan of a laboratory facility used to determine the change of the permeability of a medium after acoustic treatment: *a* - general view; *b* - top view

### 13.1 Laboratory Research on Permeability of Media after Acoustic Treatment

An experiment was conducted, using the method described in chapter 6, to determine the change of the conducting properties of an artificial medium simulating a natural reservoir, under ultrasonic treatment.

**Experimental set-up.** The facility used for the experiment is presented in fig. 77. The artificial medium was a homogeneous blend of Lubertsy sand and clay in the 9:1 ratio. The given blend, if packed tightly, corresponds in its basic geophysical and physicommechanical properties to the dense sedimentary sandstone-type rocks.

Having been mixed thoroughly, with some water added to avoid the restraint of air, the artificial medium was placed in layers in the container *A* around the well *B*. Every layer placed was tramped, after which the next one was placed over it, and so on, until the whole volume *A* was filled. On levels 1 - 10 in the medium, electrodes were set. The character of their setting in the plan is shown in fig. 77, *b*. Electrodes 2 - 10 were set at equal distances  $\Delta L = 10^{-1}$  m from each other. The distance from the bottom of the model to electrode 1 was  $4 \cdot 10^{-2}$  m, and between electrodes 1 and 2,  $6 \cdot 10^{-2}$  m. The bottom part of volume *A* was made of a permeable material and touched the surface of the fluid filling the container *C*.

At the first stage of the experiment the medium was kept at the atmospheric pressure for 24 hours, for the height distribution of saturation to develop, corresponding to the radii distribution of pore channels. Resistances between the first and all successive electrodes were then measured.

At the preliminary stage, a series of such measurements was taken in order to find the characteristic value of the experimental error caused by the unsteady



conditions of the environment, such as the change of humidity and external temperature, atmospheric pressure, possible variations in the mineralization of water, etc.

At the second stage acoustic action upon a saturated layer composed of the sandstone-type rocks was simulated. Container *A* was filled with water poured from the above for complete saturation of the medium to be achieved. After the medium was saturated, an ultrasonic wave source was placed in the well *B*, which was also filled with water, and the medium was treated with acoustic waves for 1 hour. Then the source was taken out of well *B*. The third stage was the same as the first one: the medium stayed at the atmospheric pressure for 24 hours, after which measurements of the resistances between the electrodes were taken.

**Experimental data processing.** Results of the direct processing of the obtained data according to the technique described in §6.2 did not reveal any notable change in the permeability after the acoustic treatment. This can be explained by the fact that the given experimental design does not permit one to advance into the region of the probability density function for capillaries containing the thin capillaries. The least radius that can "take part" in the experiment is

$$r^0 = 2\chi \cos \theta / (\rho_f g L)$$

If we assume complete wettability ( $\cos \theta = 1$ ) and take for the water-air contact,  $\chi = 73 \cdot 10^{-3}$  newtons per meter, we obtain for  $L = 1$  m  $r^0 \approx 15 \mu\text{m}$ . At the same time, according to [48], the characteristic value of the minimal capillary radius in cemented sandstone is  $a_* \sim 1 \mu\text{m}$ , which is less by an order of magnitude.

Estimate the effect of the region of the small capillary radii in the function  $f(r)$  on the permeability  $K$  in the developed percolational approach. The model for the permeability of a grained medium is most adequate for the considered medium; therefore, we will use the results of §2.1. Take the most simple typical exponential function

$$f(r) = a_*/r^2, \quad r \geq a_*$$

In this case, after setting  $\nu = 1$  to make the calculations easier, we obtain

$$K \sim a_*^4$$

Thus the permeability of the medium is determined primarily by the quantity  $a_*$  and not by the average value of radius  $\langle r \rangle$ . Therefore for a constant value of  $a_*$ , the value of the permeability coefficient  $K$  is constant, too.

To observe the variation of the function  $f(r)$  in the interval of small radii ( $1 \lesssim r \lesssim 10$ )  $\mu\text{m}$ , it is necessary to either increase the height of the volume *A* by an order of magnitude, i.e., make it 10 m, or decrease the coefficient of surface tension  $\chi$ , or, more exactly, the value of the product  $\chi \cos \theta$ , by an order of magnitude, for example, by adding a surface-active substance to the fluid.

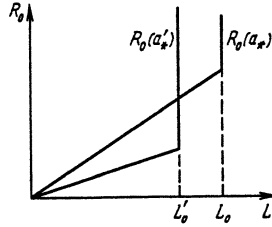


Figure 78: Nature of the change in the total resistance of the medium with height (for the facility presented in fig. 77)

However the obtained data do permit to carry out a qualitative analysis to estimate the order of the change to the permeability  $K$ . Assume that the medium is sufficiently homogeneous and the distribution  $f(r)$  is close to delta-like in the vicinity of the minimal radius  $a_*$ , determining the permeability of the medium. For the network model (with period  $l$ ), the specific electric conductivity is equal to

$$\sigma_y \cong \pi(a_*/l)^2 \sigma' \quad (13.1)$$

and the coefficient of permeability is equal to

$$K = (\pi/8)(a_*/l)^4 l^2$$

The change in the total resistance of the medium with height  $R_0(L) = \sigma_y^{-1}(L/S^0)$ , where  $S^0$  is the cross-section of the specimen, can be represented graphically in this case, as in fig. 78, where  $L_0$  is the static height of the capillary rise [94]. In the experiment conducted, the height of the specimen is less than  $L_0$ , but one can notice that as the point of inflection of the curve  $R_0(L)$  shifts along the  $L$ -axis, the slope of its linear segment changes. It follows from the expression for  $R_0(L)$  and from (13.1) that

$$R_0(L, a'_*)/R_0(L, a_*) = (a_*/a'_*)^2$$

Comparison of the relations for  $K$  and  $R_0(L)$  shows that

$$K(a'_*)/K(a_*) = [R_0(L, a_*)/R_0(L, a'_*)]^2$$

Hence even the linear segments of relations  $R_0(L)$  permit to estimate the permeability change. The results of the measurements of resistances in the volume between the first and the successive electrodes are given in fig. 79, together with the characteristic systematic error of the experiment. Straight lines represent the interpolation of the points obtained, carried out with regard to the fact

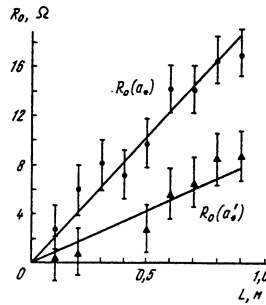


Figure 79: Results of experimental study of the change in the total resistance of the medium with height (facility presented in fig. 77)

that the curve  $R_0(L)$  can be only increasing, and is close to linear in the considered case of a delta-like function  $f(r)$ . From the plots in fig. 79 we obtain that  $R_0(L, a_*)/R_0(L, a'_*) \cong 2.5$ ; therefore,  $K(a'_*)/K(a_*) \sim 6$ . Thus we conclude that as a result of acoustic action, the permeability of the studied volume has increased by approximately an order of magnitude.

Equivalent studies were conducted in volume  $A$  filled with an ordinary bulk (not cemented) sand, a rock which corresponds to the water-bearing horizons that occur at small depths.

However in this case, no notable changes in the electric conductivity and therefore, in the permeability after ultrasonic treatment were observed. This can be explained by the fact that a bulk material does not contain cement. The cement binds the grains of the medium, and its strength is substantially less than that of the grains; at the same time, it fills the pore channels due to its plasticity and thus reduces its hydraulic conductivity. Acoustic action causes destruction of the cementing layer in channels and its further entrainment by the fluid flow. This results in the increase of the permeability. The described mechanism works in cemented rocks. In the non-cemented ones it is impossible, and acoustic treatment is thus ineffective.

Theoretically, a certain increase of the hydraulic radius of the conducting capillaries is possible in the non-cemented rocks, if the double electric layer is made thinner. Acoustic action causes destruction of the adsorptive part of the double electric layer. Some of the ions from the adsorptive part of the double electric layer pass into the solution, and the concentration  $C_i$  of ions there grows. Since the thickness of the double electric layer connected with the surface of capillaries [87] is

$$\lambda_e \sim \sqrt{T/C_i}$$

it follows that as  $C_i$  goes up,  $\lambda_e$  goes down.

However at the same time, temperature  $T$  goes up during acoustic action, too.

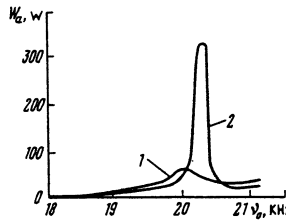


Figure 80: Frequency dependence of the power transferred to the medium by a magnetostrictive oscillator (data of Zh. M. Bulatov, 1970). Curves 1 and 2 were obtained for water and air, respectively

Still, in the thin capillaries, which determine the value of  $K$ , it grows slowly, so that the resultant effect may be the decrease of  $\lambda_e$ .

In any case, the mentioned effect is reversible and can take place only during acoustic treatment. Irreversible effect of the permeability increase in unbound soils is impossible for the considered intensity of acoustic action. This is pointed out by experimental research carried out in laboratories at the atmospheric pressure. This will be the more valid for the litho-static pressure of  $\sim 10^7$  Pa in reservoirs, when dilatant effects [95, 96], which can cause reconstruction of the grain packing structure, will not, obviously, be observed at the intensity of acoustic action used.

## 13.2 Determination of Size for the Acoustic Action Zone

A series of experimental, as well as theoretical works is devoted to the direct research on the acoustic wave attenuation in saturated porous media.

In studying the effects of acoustic action from an ultrasonic source on a saturated porous medium, it is most important to determine the size of the attenuation zone of an ultrasonic wave in the vicinity of the well. It is in this zone only that the modifications in the pore space structure, which affect the fluid flow in the medium, can take place.

It is known that the attenuation factor  $\alpha_\omega(\nu_0)$  increases with frequency  $\nu_0$ . Although at low frequencies,  $\alpha_\omega(\nu_0) \sim \nu_0^2$ , and at high frequencies,  $\alpha_\omega(\nu_0) \sim \nu_0^{1/2}$ , i.e., the growth of  $\alpha_\omega(\nu_0)$  slows down with the increase of frequency, it is still evident that there is no use in carrying out acoustic treatment of the medium at high frequencies. No expansion of the treated portion will be observed in this case to make up for the increase of the labor intensity.

Furthermore the resonance curve of the magnetostrictive oscillator (fig. 80) shows the energy resonance in the neighborhood of  $\nu_0 = 20$  kHz for the energy

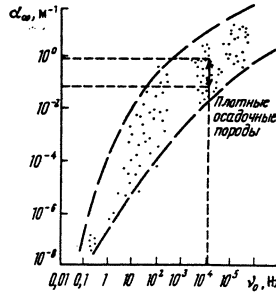


Figure 81: Frequency dependence of the attenuation factor of acoustic waves in actual media (data of Zh. M. Bulatov, 1970)

transfer from the oscillator to the medium for water. It can be inferred that during the acoustic treatment of media saturated with liquid, as well as when liquid is used as a go-between for the source and the medium, it is reasonable to use the low-frequency ultrasound ( $\nu_0 = 20$  kHz). Estimate the characteristic size  $L_\omega$  of the wave attenuation zone in the corresponding range of ultrasonic frequencies.

Within the framework of Biot's theory [97], absorption of ultrasonic waves in the low-frequency range is determined by the attenuation factors for the longitudinal  $\alpha_P$  and the transverse  $\alpha_S$  waves, respectively,

$$\alpha_P = \frac{2\pi^2}{C_P} \frac{\rho_f}{\rho} \frac{K\rho_f}{\mu} \left( 1 - \frac{\rho}{\rho_f} \frac{\beta_s}{E} \frac{1 - \beta_m/\beta_s}{1 - \Phi + \Phi\beta_s/\beta_f - \beta_m/\beta_s} \right) \nu_0^2, \quad (13.2)$$

$$\alpha_S = \frac{2\pi^2}{C_S} \frac{\rho_f}{\rho} \frac{K\rho_f}{\mu} \nu_0^2$$

where  $C_P$ ,  $C_S$  are the velocities of the longitudinal and the transverse waves, respectively,  $E$  is Young's elasticity modulus of the medium,  $K$  is the coefficient of permeability of the medium,  $\rho$  is the density of the medium,  $\rho_f$  is the density of the fluid,  $\mu$  is the viscosity of the fluid,  $\Phi$  is the porosity of the medium,  $\beta_m$  is the compressibility of the medium,  $\beta_s$  is the compressibility of the material of the skeleton,  $\beta_f$  is the compressibility of the fluid. For the typical water-saturated sandstones we obtain the following values (in the units of  $s^2/m$ ) using (13.2)

$$\alpha_P \cong 10^{-9} \nu_0^2, \quad \alpha_S \cong 0.5 \cdot 10^{-8} \nu_0^2 \quad (13.3)$$

Consequently when  $\nu_0 = 20$  kHz, for the longitudinal waves, we have  $\alpha_P \approx 0.4$   $m^{-1}$ , and for the transverse waves,  $\alpha_S \approx 2$   $m^{-1}$ . Since the longitudinal waves attenuate substantially slower, by "acoustic wave" we will further mean the longitudinal wave.

The models used for the theoretical calculation of the parameters of heterogeneous media cannot take into account all of the medium's heterogeneous properties,

as well as the features of the phase distribution in a saturated medium with regard to the phase transitions. Therefore a series of experimental studies [93, 98-100] was performed to improve the calculated results (13.3). Outcomes of these studies were usually presented either as empirical, or as graphical relations. For example, the following empirical relation [101] is known

$$\alpha_\omega = 4.53 \cdot 10^{-5} \nu_0 \quad (13.4)$$

(in the units of s/m). In [98],

$$\alpha_\omega = (3.2 \div 8.6) \cdot 10^{-5} \nu_0 \quad (13.5)$$

(in the same units). This points to the fact that the  $\alpha_\omega(\nu_0)$  relation is approximately linear up to the frequencies  $\nu_0 \sim 10^6 \div 10^7$  Hz. For the values  $\nu_0 \cong 20$  kHz, the expressions (13.4) and (13.5) give an estimate  $\alpha_\omega \sim 1 \text{ m}^{-1}$ , which agrees satisfactorily with the results of the model calculations (13.3). After numerous experiments, the dependencies of attenuation factors on frequency for different media were obtained (fig. 81). On the whole, the nature of  $\alpha_\omega(\nu_0)$  corresponds to the one predicted theoretically ( $\alpha_\omega \sim \nu_0^2$  for  $\nu_0 \lesssim 10^3$  Hz and  $\alpha_\omega \sim \nu_0^{1/2}$  for  $\nu_0 \gtrsim 10^6$  Hz). In the figure presented, the interval of spread for the data on the determination of the quantity  $\alpha_\omega$  for  $\nu_0 = 20$  kHz in dense sedimentary rocks is marked. It can be seen that  $\alpha_\omega \approx 1 \div 10^{-1} \text{ m}^{-1}$ . Thus both the theoretical calculations and the experimental data indicate that  $\alpha_\omega$  is of the order of  $1 - 10^{-1} \text{ m}^{-1}$ , a range that corresponds to the attenuation length of the order of several meters. However the presented results were obtained for a planar wave. In the case of a cylindrical wave, attenuation due to the geometric divergence of the wave should be taken into account [102]

$$I'_0(r_\xi) = I'_\Pi \frac{\exp[-a(r_\xi - r_W)]}{r_\xi/r_W}$$

where  $I'_0(r_\xi)$  is the acoustic wave intensity at a distance  $r_\xi$  from the axis of the well,  $I'_\Pi$  is the intensity in the rock at the wall of the well (at a distance  $r_W$ ). Since  $r_W \sim 0.1$  m, taking account of the geometric divergence of the wave decreases its intensity by an order of magnitude at a distance of about 1 m. Therefore in the vicinity of the well, the typical attenuation distance for a wave with a frequency 20 kHz in sandstone-type rocks is around several tens of centimeters.

This implies that the radius  $L_\omega$  of the zone where the acoustic source is actually "felt" is a magnitude of the order of  $10^{-1}$  m, or  $r_W \leq L_\omega \lesssim (2 \div 5)r_W$ .

### 13.3 Calculation of Well Rate after Acoustic Action and Results of Field Experiments

For clarity, consider the most simple case of a perfect well in an infinitely long reservoir. In this case the production rate of the well per unit power of the filter is determined from Dupui's formula [94]

$$Q = \frac{2\pi K \Delta p}{\mu \log(R_{\text{aq}}/r_W)} \quad (13.6)$$

where  $\Delta p = p(R_{\text{aq}}) - p(r_W)$ .

Now use the relationship (12.24) obtained for the typical function  $f(r)$ ,  $f(r) = a_*/r^2$  (see fig. 76), and the results yielded by studying the pressure growth in the fluid by  $\Delta p \sim \sigma^*$  in capillaries of different radii (these results were presented in §12.5). The mentioned analysis showed that after acoustic action is performed for  $\tau_* \approx 1$  hour, the capillaries of radii  $r \sim 10^{-6}$  m are destroyed, and the products of this destruction are carried away by the fluid when the flow resumes. Capillary radii close to  $a_*$  increase by 1.5 to 2 times.

In this case, according to (12.24), the permeability of the medium must increase by a factor of 5 or 10. On the whole, this agrees with the results of the experimental studies in §13.1. These studies showed that after a model medium with clay cement underwent acoustic treatment, its permeability  $K$  did increase in the above-mentioned ratio.

Given such significant growth of the permeability in the vicinity of the well, the following method for estimating the change of  $Q$  appears more convenient. Suppose that the region of the sharp permeability increase near the well brings about some kind of new effective radius of the well. Permeability of the reservoir beyond this radius can be considered constant. In this case the change in the well production rate can be estimated as follows (according to (13.6))

$$\frac{Q}{Q_0} = \frac{\ln(R_{\text{aq}}/r_W)}{\ln(R_{\text{aq}}/r_{\text{eff}W})} \quad (13.7)$$

In §13.2 it was established that the size of the attenuation zone for an ultrasonic wave makes up several tens of cm (up to a meter). Take the typical value  $r_W \approx 10^{-1}$  m as the radius of a production well. Note that the major change in the pore space structure takes place near the well, while closer to the boundary of the attenuation zone the effectiveness of action drops down to zero. In this case we can take the effective radius of the well after acoustic treatment to equal

$$r_{\text{eff}W} \cong (2 \div 3)r_W$$

If we take  $R_{\text{aq}} \sim 10^2 \div 10^3$  m for the considered case of a single well, the

Table 13.1:

Number of Well	$Q_0$ , tns./day	$Q$ , tns./day	$\Delta Q$ , tns./day	$\tau_{\text{work}}$ , months
1980	82.9	85.3	-17.6	0
3356	39.5	45.7	6.2	1
2031	77.9	110.9	13.0	2
2023	33.6	76.5	42.9	3
2661	93.6	107.0	13.4	5
3246	111.3	130.4	19.1	4
3126	51.2	62.1	10.9	2
3829	14.6	41.5	26.9	5
1963	47.7	55.0	7.3	7
2693	81.0	32.9	-48.1	0
1662	77.0	77.2	-0.6	0
1663	47.6	25.7	-21.9	0
1682	6.6	8.7	2.1	5
3330	58.7	79.0	20.3	6
3329	81.1	62.9	-18.2	0
1940	4.3	9.1	4.0	4
1967	57.0	74.0	17.0	4
2650	46.5	98.6	52.1	4
2612	83.0	94.8	11.8	2
3543	12.4	22.4	10.0	5
3044	17.0	29.3	12.3	5
7240	92.7	118.7	26.0	5
7241	34.0	18.3	-15.7	0
7144	57.0	84.0	27.0	5
1966	17.0	20.3	3.3	3
3530	34.3	25.6	-8.7	0
1683	2.9	8.6	5.7	4
2269	43.2	47.0	3.8	1
3242	98.9	72.3	-26.6	0
3243	92.8	44.9	-47.9	0
2634	34.0	18.9	-15.0	1
2652	31.2	87.9	56.7	6
3036	51.9	58.0	5.7	2.8
Std. Devtn. 1507	31.1	34.9	22.7	2.3
Minimum 1662	2.9	8.6	-48.1	0
Maximum 7241	111.3	130.4	52.1	7
Range 5579	108.4	121.8	100.2	7



relationship (13.7) yields the estimate

$$Q/Q_0 \approx 1.10 \div 1.15$$

If the zone of the sharp permeability increase is large, e.g.,  $r_{effW} \approx 5r_W$ , then the ratio  $Q/Q_0 = 1.2$ .

Thus the following conclusion can be made for the sandstone-type grained media with a typical radius probability density function for capillaries  $f(r) \sim r^{-2}$  and a typical value of strength of the cementing substance  $\sigma^* \sim 10$  MPa. After acoustic treatment with parameters  $\nu_0 = 2 \cdot 10^4$  Hz and  $p_a = 1.7 \cdot 10^5$  Pa during no less than 1 hour, the production rate of an oil or water well must go up by approximately 10 to 15 %. This effect is irreversible, since it is associated with the reconstruction of the pore space structure. The obtained conclusion agrees adequately with numerous results of field and industrial tests carried out in the Tumen' district (see table 13.1). These results show a steady increase of the rates in production wells  $\Delta Q$  by an average of 12% after 1-hour acoustic treatment.

## 13.4 Optimization of Acoustic Treatment of Porous Media

Dupui's formula used in §13.3 shows that the parameters determining the well production rate  $Q$  can change under the action of an acoustic field. These parameters are the permeability  $K$  and the viscosity  $\mu$ . The change of the latter is reversible, takes place only during the acoustic treatment, and disappears after the treatment is stopped. Therefore the behavior of  $\mu(\nu_0)$  is not analyzed in this study, since we investigate the long-term change of  $Q$  and its possible causes. Thus the principal cause for the alteration of  $Q$  is the change of the permeability  $K$  near the well filter.

Results of research (see chapters 1, 2) show that the permeability of a medium is primarily determined by such a characteristic of the pore space as  $f(r)$ . Therefore to find the change of the permeability  $K$ , it is necessary to determine how the function  $f(r)$  changes under acoustic action.

It was established in chapter 12 that the main mechanism for the energy transfer from the acoustic field to the fluid saturating the rock is the "thermal slide" in the layers adjacent to the surface of pore channels. The increase of the temperature  $\Delta T$  in a capillary of radius  $r$ , as a source of simple harmonic waves with frequency  $\nu_0$  and intensity  $I'_0$  works for a period of  $\tau_\nu$ , is determined by the formula (12.23). In this relationship  $q_p$  is the coefficient of transmission for a source immersed in the well, when the fluid filling the well is used as a binding medium [102, 100].

After taking into account the pressure  $p$  – temperature  $T$  correlation (8.17) and the strength  $\sigma^*$  of the cementing material filling the thinnest capillaries, according

to (12.23), as it was mentioned in §12.5, we obtain that the minimal time  $\tau_*$  of the thermo-acoustic action on the capillaries with  $r \sim 10^{-6}$  m for  $\nu_0 = 20$  kHz,  $I'_0 = 2$  watt per  $\text{cm}^2$ , and  $q_p = 10^{-1}$  is  $\approx 5 \cdot 10^3$  seconds, or  $\tau_* \approx 1.25$  hours.

Thus after the time  $\tau_*$  elapses, a substantial increase in the radii of the conducting capillaries will have taken place. This causes the increase of permeability according to (12.24). The obtained theoretical estimate adequately agrees with experimental data (see §13.1).

Sharp increase of the permeability takes place in the attenuation zone of acoustic waves. The characteristic size of this zone is  $L_\omega \lesssim \alpha_\omega^{-1}$ , where  $\alpha_\omega$  is the attenuation factor of the wave in a dissipative medium. According to the results of §13.3, we can take the effective radius of the well after acoustic treatment to equal

$$r_{effW} \cong (2 \div 3)r_W$$

where  $r_W \simeq 10^{-1}$  m is the standard radius of a production well.

Thus the effectiveness of treatment can be increased by means of the increase in the permeability  $K$  or the size  $L_\omega$  of the zone where  $K$  grows. Since the behavior of the first of the mentioned factors is related to the temperature change  $\Delta T$ , it follows from (12.23) that to increase the efficiency of the source, one should increase the values of the quantities  $q_p$ ,  $\nu_0$ ,  $I'_0$ ,  $\tau_\nu$ .

As for the coefficient of transmission  $q_p$ , it appears obvious that it should be made larger in any case, i.e., the losses occurring during the energy transfer from the source through the fluid filling the well and casing pipes, should be made smaller. The use of fluid as a binding medium is most simple practically, but at the same time is least effective, especially if there is a gas phase present in the extracted fluid [103]. In the mentioned study a way of increasing effectiveness of the acoustic energy transmission to the oil-bearing pool is proposed. The source of acoustic energy is in close contact with walls of the casing pipe. It acts on pipe walls to deform them in the transverse direction and make them oscillate with the natural frequency. Vibrators of a special construction [103], allowing for the automatic preservation of the system "vibrator-column" in resonance, are used for this purpose. In this case the parameter  $q_p$  can be increased by several times.

The remaining parameters of the process, i.e.,  $\nu_0$ ,  $I'_0$ , and  $\tau_\nu$ , must be optimized, since their variation can cause qualitatively different consequences for  $K$ . Besides, they are all interconnected.

Intensity of the source is related to the power  $W_a$  transferred by it into the liquid phase. In its turn,  $W_a$ , as a function of  $\nu_0$ , has a resonance nature (see fig. 80). The peak of the function  $W_a(\nu_0)$  is at the frequency  $\nu_0 \approx 2 \cdot 10^4$  Hz. The value  $I'_0 \approx 1$  watt per  $\text{cm}^2$  corresponds to the resonance value of  $W_a(\nu_0)$ . Therefore it is advantageous to use the most effective values, as far as the energy input is concerned, in operating modes:  $I'_0 \approx 1 \div 2$  watt per  $\text{cm}^2$ ,  $\nu_0 \approx 20$  kHz.

Analysis of the interaction of the two competing processes, the increase of  $\Delta T(\nu_0)$  (and consequently,  $K(\nu_0)$ ) and the decrease of  $L_\omega(\nu_0)$ , with the increase of  $\nu_0$ , results in similar conclusions. The zone where  $K$  increases by an order of magnitude or greater can be included in the so-called effective radius of the well  $r_{effW}$ . Note that it is not all that important by how many orders of magnitude (1 - 4) the coefficient of permeability does in fact increase. More important is the size  $L_\omega$  of the region where this takes place. At the same time, in the 1 kHz frequency range we have  $L_\omega \sim \nu_0^{-2}$  (theoretical result) or no less than the first power of the frequency  $L_\omega \sim \nu_0^{-1}$  (some of the experimental data). Since  $r_{effW} = r_W \div L_\omega$  and the increase of frequency  $\nu_0$  by one order of magnitude causes the size  $L_\omega$  to go down by one or two orders of magnitude, this decreases the effectiveness of the treatment drastically: according to (13.7), the production rate of the well will remain almost unaffected. If we consider  $L_\omega \sim 1$  m a reasonable and acceptable value, we conclude that the optimal frequency of acoustic action is  $\nu_0 \sim 10$  kHz. After taking into account the above-presented reasoning about the relation  $W_a(\nu_0)$ , we obtain the optimal value  $\nu_0 = 20$  kHz again.

When parameters  $I'_0$  and  $\nu_0$  are set, the basic characteristic of the acoustic treatment regime is the duration of treatment  $\tau_*$ . In determining the optimal value of  $\tau_*$ , it is necessary to take into account the development of the competing trends during acoustic action. On the one hand, according to (12.23), for  $|r| < L_\omega$ ,  $\Delta T$  grows proportional to  $\tau_\nu$ , and therefore so does  $K(r)$ . On the other hand, due to the non-uniform heating of capillaries with different radii, migration of the gas bubbles takes place, so that they accumulate in the "hot" capillaries, where they grow and merge. The described phenomenon may result in gas colmatation of the pre-filter zone with further "cut-off" of the well.

If at the beginning of the treatment the effect of the growth of  $K$  prevails and the migration from the thin "cold" to the thick "hot" capillaries has only just started, then as time passes, inflation of separate pores with gas becomes more evident. The number of such pores begins to grow rapidly, and the colmatation effect dominates. As a result, the permeability goes down (if the treatment is continued, the permeability can vanish), and the effect of acoustic action becomes negative.

Theoretical calculations show that the time  $\tau_*$ , after which the greatest increase of the permeability is achieved, is less than the period of colmatation  $\tau^*$ . Therefore  $\tau_*$  can be considered the optimal duration of treatment.

Duration of the treatment  $\tau_*$  can be calculated theoretically based on the expressions presented in the previous sections of the book. However this requires a vast amount of information about the characteristics of the saturated porous medium and also about the variation of these characteristics during acoustic action, depending on the parameters of action. In particular, it is necessary to know the initial radius probability density function for capillaries  $f_0(r)$  and its final form

$f(\tau)$  after treatment. It is also very important to find the frequency dependence of the attenuation factor of the acoustic wave  $\alpha_\omega(\nu_0)$  for the given medium, its (perhaps, two-phase) saturation, and the given conditions in the reservoir. Correct determination of the coefficient of transmission  $q_p$  for the type of equipment used is of special significance. If there is gas release present, the gas factor  $\Gamma'$  (quantity of gas released per unit mass of liquid) dependencies of the velocity of wave  $C_m(\Gamma')$ , the specific heat of the saturating fluid  $c_T(\Gamma')$ , its density  $\rho_f(\Gamma')$  and viscosity  $\mu(\Gamma')$  should be taken into account. It is also necessary to determine the strength of the cementing material  $\sigma_*$ ,  $\sigma^*$ , and some other parameters.

Obtaining the necessary set of data requires a large number of detailed laboratory and field experiments, which can cause substantial technical and organizational difficulties. Therefore it appears more reasonable to conduct a single resultant tune-up experiment (or, perhaps, two – a laboratory and a field one) to determine the time regime of treatment (i.e., the parameter  $\tau_*$ ) for the chosen equipment, i.e., the chosen parameters  $I'_0$ ,  $\nu_0$ , and  $q_p$ . The latter are chosen, as it was stated above, according to the economic benefit. In particular, the frequency is chosen according to the resonance curve  $W_a(\nu_0)$  of the vibrator. The obtained value is compared to the characteristic data on the wave attenuation  $\alpha_\omega(\nu_0)$  for the quantity  $L_\omega$  not to be too small (less than 30 cm.). Further, the acoustic field with  $\nu_{\text{res}}$  and the corresponding intensity  $I'_0(\nu_{\text{res}})$  is used. The parameter  $q_p$  is in any case better to be increased by choosing an adequate binding medium between the vibrator and the reservoir rock. For the specified  $\nu_0$  and  $I'_0$  for the given rock, the saturating fluid, and the external reservoir conditions,  $\tau_*$  is determined from a laboratory and/or field experiment.

For the sources used at present ( $\nu_0 \approx 20$  kHz,  $I'_0 \approx 2$  watt per cm<sup>2</sup>,  $q_p \approx 10^{-1}$ ), in grained sandstone-type media, theoretical calculations of the typical values for the parameters of the medium and the fluid give  $\tau_* \cong 1 \div 1.5$  hours and  $\tau^* \gtrsim 1.7$  hours. Clearly,  $\tau^*$  lies somewhat dangerously close to  $\tau_*$ . Therefore the significance of the high performance of the experiment for plotting the  $K(\tau_\nu)$  curve with the rest of parameters fixed, is obvious. Correct determination of the time  $\tau_*$  permits to conduct the treatment optimally and achieve a 10 to 15% increase of the well production rate. An "overcautious" error – understatement of the duration  $\tau_*$  of treatment – lowers the effectiveness of treatment, since in this case  $K$ , together with the rate  $Q$ , increases to a small extent. Overestimation of  $\tau_*$ , when  $\tau_* \geq \tau^*$ , causes a negative effect: powerful gas colmatation develops in the pre-filter zone, and the well is "cut off."

# Bibliography

- [1] King, P.R., Smith, P.J.: 1988, 'Generation of correlated properties in heterogeneous porous media', *Mathematical Geology*, Vol.20, No.7, pp. 863 – 877.
- [2] King, P.R.: 1987, 'The use of field theoretic method for the study of flow in a heterogeneous porous medium', *J.Phys.A: Math.Gen.* 20, pp. 3935 – 3947.
- [3] King, P.R.: 1988, 'The use of renormalization for calculating effective permeability', *Transport in porous media*, Vol.4, pp. 37 – 58.
- [4] King, P.R.: 1987, 'The fractal nature of viscous fingering in porous media', *J.Phys.A: Math.Gen.* 20, pp. 529 – 534.
- [5] Dullien, F.A.L.: 1991, 'Characterization of porous media - pore level', *Transport in porous media*, No. 6, pp. 581 – 606.
- [6] Ramakrishnan, T.S., Wasan, D.T.: 1986, 'Two-phase distribution in porous media: an application of percolation theory', *Int.J. Multiphase Flow*, Vol. 12, No 3, pp. 357 – 388.
- [7] Paredes, R. and Octavio, M.: 1990, 'Calculation of permeabilities and residual saturation using invasion percolation', *SPE 21079*.
- [8] \*<sup>1</sup> Belikhova, N.V., Danilova, N.A., Entov, V.M. and Chensin, E.: 1977, 'Modeling of non-steady state and nonlinear fluid flow in a capillary network', *Numerical solution of problems in multi-phase compressible fluid flow*, Novosibirsk, pp. 17 – 24.
- [9] Entov, V.M., Zak, S.A. and Chensin, E.: 1984, 'On two-phase flow in a medium with mixed wettability', *Physics – doklady, Gidromekhanika*, Vol.164, No 6. pp.334 – 337, (Transl. from Russian, *Doklady Akademii Nauk*).

---

<sup>1</sup>Here and below: items marked with asterisk (\*) were published in Russian

- [10] Yanuka, M.: 1992, 'Percolation theory approach to transport phenomena in porous media', *Transport in porous media*, **No.7** pp. 265 – 282.
- [11] Yanuka, M., Dullien, F.A.L. and Eelrick, D.E.: 1986, 'Percolation Processes and Porous Media. I.Geometrical and topological model of porous media using a three-dimensional joint pore size distribution', *Journal of Colloid and Interface Science*, **Vol.112, No.1**, pp. 24 – 41.
- [12] Yanuka, M.: 1989, 'Percolation Processes and Porous Media. II.Computer calculations of percolation probabilities and cluster formation', *Journal of Colloid and Interface Science*, **Vol.127, No.1**, pp. 35 – 47.
- [13] Yanuka, M.: 1989, 'Percolation Processes and Porous Media. III.Prediction of the capillary hysteresis loop from geometrical and topological information of pore space', *Journal of Colloid and Interface Science*, **Vol.127, No.1**, pp. 48 – 58.
- [14] Yortsos, Y.C., Satik, C., Bacri, J.-C. and Salin, D.: 1993, 'Large-scale percolation theory of drainage', *Transport in porous media*, **No.10**, pp. 171 – 195.
- [15] Parlar, M. and Yortsos, Y.C.: 1987, 'Percolation theory of stream/water relative permeability', *SPE 16969*.
- [16] Yortsos, Y.C.: 1991, 'Percolation models for boiling and bubble growth in porous media. Topical Report', DOE/BC/14600-9. Distribution category UC-122..
- [17] Lenormand, R.: 1990, 'Visualization techniques in porous media', *Hydrodynamics of dispersed media*, pp. 287 – 294.
- [18] Feder, J., Maloy, K.J. and Jossang, T.: 1990, 'Experiments on diphasic flow: front dynamics in model porous media', *Hydrodynamics of dispersed media*, pp. 231 – 248.
- [19] Clement, E., Baudet, C., Guyon, E. and Hulin, J.P.: 1987, 'Invasion front structure in a 3D model porous medium under a hydrostatic pressure gradient', *J.Phys.D: Appl.Phys.*, **No.20**, pp. 608 – 615.
- [20] Sarma, H.K., Maini, B.B. and Allen, G.: 1992, 'Effect of viscous instability on unsteady-state relative permeability', *Revue de L'Institut Francais du Petrole*, **Vol.47, No.6**, pp. 753 – 770.
- [21] Jerauld, G.R. and Salter, S.J.: 1990, 'The effect of pore-structure on hysteresis in relative permeability and capillary pressure: pore-level modeling', *Transport in porous media*, **No.5**, pp. 103 – 105.

- [22] Lenormand, R., Touboul, E. and Zarcone, C.: 1988, 'Numerical models and experiments on immiscible displacement in porous media', *J.Fluid Mech.*, Vol.189, pp. 165 – 187.
- [23] Ni, L.W., Hornof, V. and Neale, G.: 1986, 'Radial fingering in a porous medium', *Revue de L'Institut Francais du Petrole*, Vol.41, No.2, pp. 217 – 228.
- [24] Host-Madsen, J. and Høgh-Jensen, K.: 1992, 'Laboratory and numerical investigations of immiscible multiphase flow in soil', *Journal of Hydrology*, Vol.135, pp. 13 – 52.
- [25] Shklovsky, B.I. and Efros, A.L.:1975, 'Percolation theory and conductivity of strongly heterogeneous systems', *Physics – Uspekhi*, Vol.97, No.3, pp.15 – 34 (Transl. from Russian, *Uspekhi fizicheskikh nauk*).
- [26] \*Menshikov, M.V., Molchanov, S.A. and Sidorenko, A.F.: 1986, 'Percolation theory with applications', *Itogi nauki I tekhniki. Series: Probability theory. Mathematical statistics. Theoretical cybernetics*, Vol.24, pp. 53 – 110.
- [27] Sokolov, I.M.: 1986, 'Dimensions and other geometrical critical indicators in percolation theory', *Physics – Uspekhi*, Vol.106, No.3, pp. 221 – 255 (Transl. from Russian, *Uspekhi fizicheskikh nauk*).
- [28] Entov, V.M.: 1992, 'Micromechanics of flow in porous media', *Fluid Dynamics*, Vol.28, No.3, pp. 96 – 108 (Transl. from Russian, *Izvestiya Akademii Nauk RF, M.Zh.G.*).
- [29] Kirkpatrick, S.: 1973, 'Percolation and conductivity', *Rev. Mod. Phys.*, V.45, pp. 574 – 588.
- [30] Kesten, Ch.: 1986, 'Percolation theory for mathematicians', *Progress in Probability and Statistics*, Vol. 2, ed. by P.Huber and M.Rosenblatt, Birkhauser.
- [31] Dullien, F.A.L.: 1992, 'Porous media. Fluid transport and pore structure', (2nd ed.), *Academic Press*, New York.
- [32] Gennes, P.G.de: 1983, 'Theory of slow biphasic flows in porous media', *Phys. Chem. Hydrodynam.*, Vol.4, No.2, pp. 175 – 185.
- [33] Stauffer, D. and Aharony, A.: 1992, 'Introduction to percolation theory', *Taylor & Francis*, London.
- [34] Feder, J.: 1988, 'Fractals', *Plenum Press*, New York.

- [35] Cushman, J.H.: 1990, 'Dynamics of Fluids in Hierarchical Porous Media', *Academic Press*, New York.
- [36] Adler, P.M.: 1992, 'Porous media. Geometry and transport', *Academic Press*, New York.
- [37] Kadet, V.V. and Selyakov, V.I.: 1987, 'Percolation model of two-phase flow in porous media', *Fluid Dynamics*, Vol.25, No.1, pp. 38 – 45 (Transl. from Russian, *Izvestiya AN USSR, M.Zh.G.*).
- [38] Kadet, V.V. and Selyakov, V.I.: 1989, 'Percolation model of steady-state three-phase flow in porous media', *Fluid Dynamics*, Vol.27, No.1, pp. 119 – 124 (Transl. from Russian, *Izvestiya AN USSR, M.Zh.G.*).
- [39] Glushko, S.P., Kadet, V.V. and Selyakov, V.I.: 1989, 'Percolation model of two-phase steady-state flow in a medium with mixed wettability', *Fluid Dynamics*, Vol. 27, No.4, pp. 86 – 93 (Transl. from Russian, *Izvestiya AN USSR, M.Zh.G.*).
- [40] Kadet, V.V., Popov, A.E. and Selyakov, V.I.: 1991, 'Effect of plastic properties of fluids on phase permeabilities', *Fluid Dynamics*, Vol. 28, No.1, pp. 138 – 143 (Transl. from Russian, *Izvestiya AN USSR, M.Zh.G.*).
- [41] Kadet, V.V.: 1990, 'Methods of percolation theory in investigations of steady-state multi-phase flow in homogeneous and heterogeneous media', International conference *Development of condensed gas deposits*, proceedings; Krasnodar, 05/29 - 06/02/90.
- [42] Kadet, V.V.: 1992, 'Phase permeabilities in flow of non-Newtonian fluids in porous media', International conference *Flow in porous media*, proceedings; Moscow, 09/21-09/26/92.
- [43] \*Scheinmann, S.M.: 1969, 'Contemporary physical basis of electric geophysical exploration theory', *Nedra Publishers*, Leningrad.
- [44] Collins, R.: 1961, 'Flow of fluids through porous materials', *Chapman & Hall*, New York, Reinhold, London.
- [45] \*Kobranova, V.N.: 1962, 'Physical properties of rocks', *Gostoptechizdat Publishers*, Moscow.
- [46] \*Emelyanov, N.I.: 1962, 'Investigation of accuracy in determination of reservoir properties of field IX at the Ozek-Souat deposit' – in the book 'Estimates of accuracy in determination of parameters for oil and gas deposits', *Nedra Publishers*, Moscow.



- [47] \*Romm, E. S.: 1985, 'Structural models of pore space in rocks', *Nedra Publishers*, Leningrad.
- [48] \*Marmorstein, L. M.: 1975, 'Reservoir and screening properties of sedimentary rocks under different thermodynamic conditions', *Nedra Publishers*, Leningrad.
- [49] \*Krechetova, T. N. and Romm, E. S.: 1981, 'On the use of the nonlinear-elastic fractured-capillary model of a porous medium in research on effects of pressure on physical properties of oil and gas reservoirs', *Voprosy Nelineynoy Geofiziki*, pp. 86 – 101.
- [50] \*Arje, A. G.: 1984, 'Physical basis of underground water flow', *Nedra Publishers*, Moscow.
- [51] \*Kadet, V. V. and Shapiro, A. A.: 1988, 'Determination of inertial and viscous losses in nonlinear fluid flow in porous media', *Fil'tratsia Neodnorodnykh Sistem*, VNIIGAZ, Moscow, pp. 20 – 26.
- [52] Rostovsky, N. S. and Selyakov, V. I.: 1989, 'Effects of microheterogeneity of a medium on laws describing fluid flow', *Fluid Dynamics*, Vol.27, No. 2, pp. 53 – 63 (Transl. from Russian, *Izvestiya AN USSR, M.Zh.G.*).
- [53] \*Altshul', A. D.: 1982, 'Hydraulic resistances', (2 th ed.), *Nedra Publishers*, Moscow.
- [54] \*Zlochevskaya, R.I.: 1969, 'Bound water in argillaceous soil', *MGU Publishers*, Moscow.
- [55] \*Idel'chik, I.E.: 1975, 'A handbook on hidraulic resistances', (2th ed.), *Mashinostroenie Publishers*, Moscow.
- [56] \*Zatsepina, G. N.: 1974, 'Properties and structure of water', *MGU Publishers*, Moscow.
- [57] Barenblatt, G. I., Entov, V. M. and Ryzhik, V. M.: 1991, 'Theory of Fluid Flows through Natural Rocks', *Kluwer Academic Publishers*, Dordrecht, Boston, London.
- [58] \*Shvidler, M.I. and Levi, B.I.: 1970, 'One-dimensional flow of immiscible fluids', *Nedra Publishers*, Moscow.
- [59] \*Entov, V. M., Feldman, A. Ya. and Chen-Sin, E. P.: 1975, 'Program modeling of capillary displacement in a porous medium', *Programmirovanie*, No.3, pp. 71 – 78.

- [60] \*Entov, V. M., Feldman, A. Ya., Yudin, V. A. and Chen-Sin, E. P.:1980, 'Numerical modeling of equilibrium and motion of immiscible fluids in a capillary network on computer', *VINITI*, 04/16/80, No. 3608-80
- [61] \*Manucharyants, E. O., Mishina, A. Yu. and Yudin, V. A.: 1984, 'Modeling of unsteady-state displacement of immiscible fluids in a capillary network on computer,' The All-Union seminar *Contemporary problems and mathematical methods of fluid flow theory*, proceedings; *MING Publishers*, pp. 80 – 82.
- [62] Wilkinson, W.L.: 1960, 'Non-Newtonian fluids. Fluid mechanics, mixing and heat transfer', *Pergamon press*, London.
- [63] \*Basniev, K. S., Vlasov, A. M., Kochina, I. N. et al.: 1986, 'Underground hydraulics', *Nedra Publishers*, Moscow.
- [64] \*Bernadiner, M. G. and Entov, V. M.: 1975, 'Hydrodynamic theory for flow of anomalous fluids', *Nauka Publishers*, Moscow.
- [65] \*Kovalev, A.G. and Peysakhov, S.I.: 1970, 'Relative phase permeabilities in flow of water and gas blends with non-Newtonian oil' in the book 'Application of non-Newtonian systems to oil recovery', *VNIOENG Publishers*, pp. 56 – 61.
- [66] Amyx, J.W., Bass, D.M. and Whiting, R.L.: 1960, 'Petroleum Reservoir Engineering. Physical Properties', *McGraw-Hill Book Co.*, New York, Toronto, London.
- [67] Entov, V.M.: 1980, 'Regarding theory of nonequilibrium effects during flow of heterogeneous fluids', *Fluid Dynamics*, Vol. 21, No. 2, pp. 52 – 57 (Transl. from Russian, *Izvestiya AN USSR, M.Zh.G.*).
- [68] \*Barenblatt, G.I. and Vinichenko, A.P.:1980, 'Nonequilibrium flow of immiscible fluids', *Uspekhi mekhaniki* (Scientific papers), pp. 35 – 50.
- [69] Selyakov, V.I.: 1986, 'Conductivity of grained and cavernous media', *Earth Sciences*, No.12, pp. 44 – 52 (Transl. from Russian, *Izvestiya AN USSR, Fizika Zemli*).
- [70] \*Selyakov, V.I.: 1988-1989, 'Model of forest growth', 9th All-Union seminar *Numerical methods for solution of fluid flow problems. Dynamics of multi-phase media*, Yakutsk - 1988, Novosibirsk - 1989, pp. 201 – 211.
- [71] Kadet, V.V., Musin, R.M. and Selyakov, V.I.: 1994, 'Effect of fluid viscosities and interfacial tension on the development of unsteady two-phase flow in

porous media', *Fluid Dynamics*, **Vol.29, No.1**, pp. 91 – 96 (Transl. from Russian, *Izvestiya RAN, M.Zh.G.*).

- [72] \*Dobrynin, V. M., Kovalev, A. G., Kuznetsov, A. M. and Chernoglazov, V. N.: 1988, 'Phase permeabilities of oil and gas reservoirs', *VNIIOENG Publishers*, Moscow.
- [73] \*Chirkov, Yu. G., Chernenko, A. A.: 1979, 'Regarding interpretation of the mercury porometry data', *Elektrokhimiya*, **Vol.12, No 5**, pp.697 – 685.
- [74] Abdul'manov, I. G., Glushko, S. P., Kadet, V. V. and Selyakov, V. I.: 1988, 'Method of electric porometry for recovering of the radius distribution function of capillaries', *Applied Mechanics and Technical Physics*, **No. 5**, pp. 03 –10 (Transl. from Russian, *Prikladnaya Mekhanika i Tekhnicheskaya Fizika*).
- [75] \*Bedrikovetsky, P.G., Kadet, V.V. and Shapiro, A.A.: 1990, 'Simulation of immiscible fluid displacement in reservoirs with thin pores (application to the mercury porometry method)', *Development and exploiting of deposits in the Caspian region* (Scientific papers), **No.221**.
- [76] \*Tikhonov, A. N. and Arsenin, V. Ya.: 1986, 'Methods for solving the ill-posed problems', *Nauka Publishers*, Moscow.
- [77] \*Kolmogorov, A.N. and Fomin, S.V.: 1976, 'Elements of theory of functions and functional analysis', (4 th ed.) *Nauka Publishers*, Moscow.
- [78] \*Arsenin, V. Ya.: 1984, 'Methods of mathematical physics and special functions', (2 th ed.) *Nauka Publishers*, Moscow.
- [79] Salganik, R. L.: 1974, 'Transfer phenomena in bodies with a large number of fractures', *Journal of Engineering Physics*, **Vol. 27, No. 6**, pp. 1067 – 1079 (Transl. from Russian, *Inzhenerno-Fizicheskiy Zhurnal*).
- [80] Kadet, V. V., Lovetsky, E. E., Selyakov, V. I. and Sirotkin, V. K.: 1981, 'Effects of camouflet explosion on conducting properties of a brittle medium,' *Applied Mechanics and Technical Physics*, **No. 1**, pp. 144 –151 (Transl. from Russian, *Prikladnaya Mekhanika i Tekhnicheskaya Fizika*).
- [81] \*Bagrintseva, K. I.: 1977, 'Carbonate rocks – oil and gas reservoirs', *Nedra Publishers*, Moscow.
- [82] Seaman, L., Curran, D. R. and Grewdson, R. C.: 1978, 'Transformation of observed crack density for fracture calculations', *Journal of Applied Physics*, **Vol. 49, No. 10**, pp. 5221 – 5229.

- [83] Carslow, H.S. and Jaeger, J.C.: 1960, 'Conduction of Heat in Solids', *Clarendon Press*, Oxford.
- [84] \*Osipov, V. I.: 1979, 'Nature of strength and deformation properties of argillaceous rocks', *MGU Publishers*, Moscow.
- [85] Landau, L. D. and Lifshits, E. M.: 1987, 'Fluid Mechanics', ('Course of Theoretical Physics, Vol. 6), 2nd ed., *Pergamon Press*, Oxford.
- [86] Rostovsky, N. S., Selyakov, V. I.: 1989, 'Changes in well rate when electric current passes through it', *Journal of Mining Science*, Vol. 24, No. 4, pp. 37 – 43 (Transl. from Russian *Fiziko-tehnicheskie problemy razrabotki poleznykh iskopaemykh*).
- [87] \*Frolov, Yu. G.: 1982, 'Course of colloid chemistry,' *Khimiya Publishers*, Moscow.
- [88] \*Aksel'rud, G. A. and Altshuler, M. A.: 1983, 'Introduction to capillary chemical technology', *Khimiya Publishers*, Moscow.
- [89] \*Sedov, L. I.: 1976, 'Mechanics of continua', (3 th ed.) *Nauka Publishers*, Moscow, vol. 2.
- [90] Merch, K. A.:1979 'Dynamics of cavitation bubbles and cavitating fluids' , *Erosion* (Edited by Carolyn M. Preese), pp. 331 – 381, *Academic Press*, New-York, San-Francisco, London.
- [91] \*Zaremba, L.K. and Krasilnikov, V.A.: 1966, 'Introduction to nonlinear acoustics', *Nauka Publishers*, Moscow.
- [92] \*Karevsky, V.A.: 1965, 'Some results of research on the kinetics of gas phase formation in gas-liquid systems and reservoir oils', in the book 'Application of ultraacoustics to study of matter', **Iss.21**, pp. 120 – 139.
- [93] \*Surguchev, N. L., Kuznetsov, O. L. and Simkin, E. M.: 1975, 'Hydrodynamic, acoustic, heat cyclic action on oil pools,' *Nedra Publishers*, Moscow.
- [94] Polubarinova-Kochina, P. Ya.: 1962, 'Theory of ground water movement', *Princeton Univ. Press*, Princeton, New York.
- [95] Rice, J.: 1980, 'The mechanics of earthquake rupture' (Proceeding of the International School of Physics "Enrico Fermi", Course 78, 1979, edited by A.M. Dziewonski and E. Boschi, Italian Physical Society, 1980, pp. 555 – 649), Amsterdam.

- [96] Nikolaevsij, V.N.: 1990, 'Mechanics of Porous and Fractured Media', *World Scientific Series in Theoretical and Applied Mechanics*, Vol. 8, World Scientific, Singapore, New Jersey, London, Hong Kong.
- [97] Biot, M.A.: 1956, 'Theory of propagation of elastic waves in a fluid-saturated porous solid, part I, II', *J. Acoust. Soc. Amer.*, Vol. 28, No. 2, pp. 101 – 106.
- [98] White, G.: 1983, 'Underground sound: Application of seismic waves', *Elsevier Publishers - XVI*, Amsterdam etc. (Methods in geochemistry and geophysics; Vol. 18).
- [99] \*Itenberg, S. S. and Dakhkil'gov, T. D.: 1982, 'Geophysical studies in wells', *Nedra Publishers*, Moscow.
- [100] \*Vakhitov, G. G. and Simkin, E. M.: 1985, 'Using physical fields for oil recovery from strata', *Nedra Publishers*, Moscow.
- [101] \*Bulatova, Zh.M., Volkova, E.A. and Dubrov, E.F.: 1970, 'Acoustic logging', *Nedra Publishers*, Leningrad.
- [102] \*Kuznetsov, O. L. and Efimova, S. A.: 1983, 'Application of ultrasound in oil industry', *Nedra Publishers*, Moscow.
- [103] Bodine, Albert G., 'Sonic method and apparatus for augmenting the flow of oil from oil bearing strata', May 11, 1971: *United States Patent*, No. 3, 578, 081, E 21 B 43/25.
- [104] \*Schwidler, M. I.: 1985, 'Statistical Hydrodynamics of Porous Media', *Nedra Publishers*, Moscow.
- [105] Gelhar, L. W.: 1993, 'Stochastic Subsurface Hydrology', *Prentice Hall*, Englewood Cliffs, NJ.
- [106] Dagan, G.: 1989, 'Flow and Transport in Porous Formations', *Springer-Verlag*, Berlin, London, New York.
- [107] Warren, J. E. and Price, H. S.: 1961, 'Flow in Heterogeneous Porous Media', *SPE Journal*, No.1, pp. 153 – 169.
- [108] Holden, L.: 1992, Chapter in: 'Recent Advances in Improved Oil Recovery for North Sea Sandstone Reservoirs', (ed. J. Kleppe, S.M.Skjavelend), Norway.
- [109] McCarthy, J. F.: 1991, 'Analytical Models of the Effective Permeability of Sand-Shale Reservoirs', *Geophys. J. Int.*, Vol. 105, pp. 513 – 527.

- [110] Holden, L., Hoiberg, J. and Lia, O.: 1990, 'An Estimator for Effective Permeability', *2nd European Conference on Mathematics of Oil Recovery*, Paris, pp. 287 – 290.
- [111] Durlofsky, L. J., Jones, R. C. and Milliken, W. J.: 1994, 'A New Method for the Scale Up of Displacement Processes in Heterogeneous Reservoirs', *4th European Conference on the Mathematics of Oil Recovery*, Roros, Norway, June 7 – 10.
- [112] Muggeridge, A. H.: 1991, 'Generation of Effective Relative Permeability from Detailed Simulation of Flow in Heterogeneous Porous Media', in: 'Reservoir Characterization II' (ed. L.W. Lake et al), *Academic Press*, New York, pp. 197 – 225.
- [113] Bedrikovetsky, P. G. and Bruining, J.: 1995, 'A Percolation Based Analytical Technique for Viscous Force Dominated Waterflooding in Uncorrelated Heterogeneous Reservoirs', *VIII European Symposium on Improved Oil Recovery*, Vienna, May 15 – 17, pp. 316 – 327.
- [114] Bedrikovetsky, P. G.: 1993, 'Mathematical Theory of Oil and Gas Recovery', *Kluwer Academic Publishers*, London, Boston.
- [115] Heiba, A. A.: 1982, 'Percolation Theory of Two-Phase Relative Permeability', *SPE RE*, September, p. 123.
- [116] Bryant, S. and Blunt, M.: 1992, 'Prediction of Relative Permeability in Simple Porous Media', *Phys. Rev. A.*, **Vol. 46**, **No. 4** , p. 2004.
- [117] Chandler, R. et al: 1982, 'Capillary Displacement and Percolation in Porous Media', *J. Fluid Mech.*, **Vol. 119**, p. 249.
- [118] Wilkinson, D. and Willemsen, J. F.: 1983, 'Invasion Percolation: A New Form of Percolation', *J. Phys. A. (October)*, **Vol. 16**, p. 3365.

# Index

- Acoustic treatment 189, 194, 200, 209
  - in cemented rocks 189, 192, 205, 208
  - in non-cemented rocks 208
- Attenuation factor for acoustic wave 209, 214
- Binghamian plastic 65
- Capillary pressure curve 87
- Cavitation in pore channels under acoustic action 190, 194
- Cluster 10, 27, 42, 58, 60, 70, 89, 96, 102, 105
- Coefficient of permeability 9, 22, 26, 29, 33, 38, 44, 65, 101, 123, 144, 148, 156, 163, 188, 201, 207, 212, 214
  - correlation with porosity 28
  - correlation with strained state 35
  - of transmission for a source 200, 214, 216
- Comparison of analytical and numerical calculations 19, 22, 62
- Concentration of fractures 32, 124, 131
  - of fracture traces 125
- Coordination number of network 79, 80
- Correlation radius of infinite cluster 12, 30, 91
  - index 11, 12, 82, 90, 100
- Criterion for tree blocking 91
- Current flow in heterogeneous media 20, 26, 109, 137, 142, 146, 151, 161, 172, 183
- Density of infinite cluster 10, 14
- Destruction of natural cement
  - "gradient" mechanism 138, 141, 146
  - "temperature" mechanism 138, 146, 148
- Diagram of electric energy supply to the well 161, 168
- Dilatant fluids 67
- Endpoint effect in two-phase flow 64
- Electric treatment
  - with alternating current 152, 153, 156-158, 164
  - with impulse current 137, 138, 144-145, 152, 155-158, 164
- Expansion of porometric curve in series 61, 113
- Experimental data processing 115, 118, 120, 130, 158, 206
  - technique 115, 120, 130
  - results 106, 118
- Fundamental relationship in percolation model of conductivity 16
- Gas colmatation

- during acoustic action 200
- during electric action 171
- Infinite cluster (IC) 26, 29, 58, 78, 88, 94, 97, 100, 102, 105, 115, 142, 190
- Integral equation
  - first type 113, 128
  - Schlömilch 128
- Laws describing fluid flow
  - local 41, 44
    - laminar regime 41, 45
    - transient regime 41, 45
    - turbulent regime 41, 46
  - macroscopic 47
    - laminar flow under large pressure gradients 50
    - laminar flow under very small pressure gradients 52
    - laminar regime 50
    - transient-laminar regime 50
    - transient regime 49
    - turbulent regime 48
    - turbulent-transient regime 48
    - turbulent-transient-laminar regime 49
- Length distribution
  - of fractures 126, 129
  - of fracture traces 129, 131
- Leverett's function 61, 87
- Mechanism of growth of vapor bubbles in liquid 174, 180, 196
- Medium with mixed wettability 69
- Method of electric porometry 107
  - of mercury porometry (injection) 102, 106
  - of mercury electric porometry (combined) 114
  - of regularization 113, 118
- Model
  - I and II for calculation of saturation 60
  - of "effective medium" 111, 114, 118
  - of "forest growth" 88
  - of Shklovsky - de Gennes 12, 96
  - for three-phase steady state fluid flow 77
  - for two-phase steady state fluid flow 58
- Non-Newtonian fluids 69
- Numerical experiment on a network of random links 54, 97, 100, 118
- Optimal regime of acoustic treatment 214
  - of electric treatment 165
- Percolation
  - model of cavernous medium 30
  - of fractured medium 32
  - of grained medium 25
  - theory 25, 29, 102, 112
  - threshold 28, 35, 58, 79, 89, 104, 111, 114, 186
- Probability density function
  - for links with respect to conductivities 20, 21, 58, 61, 111
  - for capillaries with respect to radii 54, 59, 65, 82, 89, 97, 109, 111, 119, 121, 176, 207, 212
- Pseudo-plastic fluids 67
- Rayleigh-Lamb equations 179
- Relative phase permeabilities 59, 70, 80, 95
- Relaxation of the value of residual saturation 88
- Residual saturation 88, 94



- Shear destruction during acoustic treatment 192
- Size of acoustic action zone 209, 214
- Stability of percolation methods for calculations 82
  
- Temperature increase caused by electric current 137
  - during Poiseuille flow 189, 200
- Thermal slide in pore channels during acoustic treatment 198, 205, 214
- Threshold values of field intensity during electric treatment 142, 156
  - temperature during electric treatment 138, 146
  - gradient during electric treatment 138, 142, 146
- Triangular diagram for three-phase flow 79
  
- Velocity of phase interface 89, 93
  
- Well production rate
  - after acoustic treatment 205, 211
  - after electric treatment 161, 168

# Theory and Applications of Transport in Porous Media

---

*Series Editor:*

Jacob Bear, Technion – Israel Institute of Technology, Haifa, Israel

---

1. H.I. Ene and D. Poliševski: *Thermal Flow in Porous Media*. 1987  
ISBN 90-277-2225-0
2. J. Bear and A. Verruijt: *Modeling Groundwater Flow and Pollution*. With Computer Programs for Sample Cases. 1987 ISBN 1-55608-014-X; Pb 1-55608-015-8
3. G.I. Barenblatt, V.M. Entov and V.M. Ryzhik: *Theory of Fluid Flows Through Natural Rocks*. 1990  
ISBN 0-7923-0167-6
4. J. Bear and Y. Bachmat: *Introduction to Modeling of Transport Phenomena in Porous Media*. 1990  
ISBN 0-7923-0557-4; Pb (1991) 0-7923-1106-X
5. J. Bear and J-M. Buchlin (eds.): *Modelling and Applications of Transport Phenomena in Porous Media*. 1991  
ISBN 0-7923-1443-3
6. Ne-Zheng Sun: *Inverse Problems in Groundwater Modeling*. 1994  
ISBN 0-7923-2987-2
7. A. Verruijt: *Computational Geomechanics*. 1995  
ISBN 0-7923-3407-8
8. V.N. Nikolaevskiy: *Geomechanics and Fluidodynamics*. With Applications to Reservoir Engineering. 1996  
ISBN 0-7923-3793-X
9. V.I. Selyakov and V.V. Kadet: *Percolation Models for Transport in Porous Media*. With Applications to Reservoir Engineering. 1996  
ISBN 0-7923-4322-0